INVESTIGATIONS ON MACHINING CHARACTERISTICS OF CRYOTREATED TITANIUM ALLOYS AND ELECTRODES USING EDM

A THESIS

Submitted in fulfillment of the requirements

for the award of the degree

of

DOCTOR OF PHILOSOPHY

in

MECHANICAL ENGINEERING

By

SANJEEV KUMAR

(Reg. No. 950808005)

DEPARTMENT OF MECHANICAL ENGINEERING

THAPAR UNIVERSITY

PATIALA–147004 (INDIA)

June, 2016

PREFACE

This research work was carried out by the author under the supervision of **Dr. Ajay Batish**, Professor, Department of Mechanical Engineering, Thapar University, Patiala, Punjab, India, **Dr. Rupinder Singh**, Professor, Department of Production Engineering, Ludhiana (Punjab) and **Dr. T.P. Singh**, Professor and Director, Symbiosis Institute of Technology, Pune (Maharashtra).

During this research work, three grades of titanium alloys (ASTM grade II, V and VI) were machined using three types of electrode materials, namely copper, copper-chromium and copper-tungsten in the presence of manganese and tungsten powder mixed dielectric fluid with the help of an electric discharge machine (EDM). Three parameters such as peak current, pulse-on-time and pulse-off-time were varied during the experimentation to explore their effects on machining performance. The effect of cryogenic treatment of both workpiece and electrode was also studied. Several measuring instruments, namely weighing machine, surface roughness tester, micro-hardness tester, stop watch were used to measure the material removal rate (MRR), tool wear rate (TWR), surface roughness (SR) and micro-hardness (MH). For conducting the metallographic analysis of the machined samples, Scanning Electron Microscope (SEM), Energy Dispersive X-ray analysis (EDX) and X-ray Diffraction (XRD) equipments were used available at Indian Institute of Technology (I.I.T.), Ropar, Punjab.

Some research papers based on the present research work have already been published in the various reputed journals and conference.

The list of Journals/Conferences in which the papers find place is given below:

Journals:

1) Sanjeev Kumar, Ajay Batish, Rupinder Singh, Tejinder P Singh," **A mathematical model to predict material removal rate during electric discharge machining of cryogenically treated titanium alloys"**, *Proceedings of Institutions of Mechanical Engineering, Part B: Journal of Engineering Manufacture*, Vol. 229 (2), 2015, 214-228.
   (SCI-Indexed; Thomson Reuters) Impact Factor: 0.954 (*SAGE Publication*)

2) Sanjeev Kumar, Ajay Batish, Rupinder Singh and T. P. Singh," **A hybrid Taguchi–artificial neural network approach to predict surface roughness during electric discharge machining of titanium alloys**," *Journal of Mechanical Science and Technology*, Vol. 28, Issue7, 2014,2831-2844.
(SCI-Indexed; Thomson Reuters) Impact Factor: 0.838 (*KSME & Springer*)

3) Sanjeev Kumar, Rupinder Singh, Ajay Batish, and T. P. Singh, "**Modeling the tool wear rate in powder mixed electro-discharge machining process using dimensional analysis of cryogenically treated electrodes"** *Proceedings of Institutions of Mechanical Engineering, Part E: Journal of Process Mechanical Engineering.* DOI: 10.1177/0954408915593875
(SCI-Indexed; Thomson Reuters) Impact Factor: 0.547 (*SAGE Publication*)

4) Sanjeev Kumar, Ajay Batish, Rupinder Singh, T.P.Singh**,"Machining Performance of Cryogenically Treated Ti-5Al-2.5Sn Titanium Alloy in Electric Discharge Machining: A Comparative Study,** *Proceedings of Institutions of Mechanical Engineering, Part C: Journal of Mechanical Engineering Science***.** DOI: 10.1177/0954406215628030
(SCI-Indexed; Thomson Reuters) Impact Factor: 0.560 (*SAGE Publication*)

5) Sanjeev Kumar, Rupinder Singh, Ajay Batish, T.P. Singh, "**Study the Surface Characteristics of Cryogenically Treated Tool-Electrodes in Powder Mixed Electric Discharge Machining Process**", *Materials science forum*, Vol. 808, 2015, 19-33.

6) Sanjeev Kumar, Rupinder Singh, Ajay Batish, T.P. Singh, "**Investigations on Effect of Electrode Polarity on Machining Performance of Ti-5Al-2.5Sn Alloy using Electric Discharge Machining Process** ", *Materials science forum (Accepted)*

7) Sanjeev Kumar, Rupinder Singh, Ajay Batish, T.P. Singh, "**Electric discharge machining of titanium and its alloys: a review**", *International Journal of Machining and Machinability of Materials*, Vol. 11, Issue1, 2012, 84-111. (Inderscience Publisher)

8) Sanjeev Kumar, Rupinder Singh, Ajay Batish, and T. P. Singh**, "Study the effect of black layer on electrode wear ratio in powder mixed electric discharge machining of titanium alloys",** *International Journal of Machining and Machinability of Materials*,Vol.18, Nos. 1/2, 2016,18-35. (Inderscience Publisher)

Conference:

1) Sanjeev Kumar, Ajay Batish, Rupinder Singh, T.P.Singh**, "Research Developments in Powder Mixed Dielectric Electric Discharge Machining (PMEDM): A review",** 2nd International Conference on Production and Industrial Engineering. CPIE-2010, NIT, Jalandhar, 2010, 702-713.

The list of Journals in which the papers are communicated is given below:

1. Sanjeev Kumar, Ajay Batish, Rupinder Singh and T. P. Singh, **"Investigating surface properties of cryogenically treated titanium alloys in powder mixed electric discharge machining"** *Journal of Brazilian Society of Mechanical Sciences and Engineering* **(Springer, SCI Listed).**
2. Sanjeev Kumar, Rupinder Singh, Ajay Batish, T.P. Singh, "**Optimization of the process parameters for powder mixed electric discharge machining of deep cryogenically treated pure titanium with cryogenically treated (shallow and deep) electrodes using Grey-Taguchi approach"** *Proceedings of the IMeche,Part E:Journal of Process Mechanical Engineering,* **(SCI-Indexed; Thomson Reuters) (*SAGE Publication*).**
3. Sanjeev Kumar, Rupinder Singh, Ajay Batish, T.P. Singh, **"Multi-objective parametric optimization using Grey-Taguchi approach for powder mixed electric discharge machining of grade-II titanium alloy with cryogenically treated electrodes"** *Indian Journal of Engineering and Materials Sciences (IJEMS),* **(SCI-Indexed; Thomson Reuters)**

(Sanjeev Kumar)

CERTIFICATE

This is to certify that the thesis entitled "**INVESTIGATIONS ON MACHINING CHARACTERISTICS OF CRYOTREATED TITANIUM ALLOYS AND ELECTRODES USING EDM"** which is being submitted by Mr. Sanjeev Kumar to Department of Mechanical Engineering, Thapar University, Patiala in fulfillment of the requirements for the award of the degree of Doctor of Philosophy, is an authentic record of research work carried out by him under our guidance. The matter presented in this thesis work has not been submitted elsewhere for the award of any other degree.

Date: 06-06-2016

Place: Patiala

Dr. Ajay Batish	Dr. Rupinder Singh	Dr. T.P.Singh
Professor	Professor	Director
Department of Mechanical Engineering,	Department of Production Engineering,	Symbiosis Institute of Technology,
Thapar University,	Guru Nanak Dev	Pune, Maharashtra, India
Patiala	Engineering College,	
Punjab, India	Ludhiana, Punjab, India	
Supervisor	Supervisor	Supervisor

ACKNOWLEDGEMENT

In the name of God, the Most Gracious and Most Compassionate

All praise to God Almightily, whose ultimate guidance, giving me strength and health to complete this thesis successfully. I take the opportunity to express my heartfelt adulation and gratitude to my supervisors, **Dr. Ajay Batish**, Professor, Department of Mechanical Engineering and Dean, Partnerships and Accreditation, Thapar University, Patiala, **Dr. Rupinder Singh**, Professor, Department of Production Engineering, Guru Nanak Dev Engineering College, Ludhiana, and **Dr. T.P. Singh**, Director, Symbiosis Institute of Technology, Pune for their unreserved guidance, constructive suggestions, thought provoking discussions and unabashed inspiration in nurturing this research work. The present work is a testimony to their alacrity, inspiration and ardent personal interest, taken by them during the course of this thesis work in its present form. I extend my heartfelt thanks to my supervisors forever.

Heartfelt thanks are due to Prof. Prakash Gopalan (Director, Thapar University, Patiala) and Dr. O.P. Pandey (Dean, Research and Sponsored Projects, Thapar University, Patiala), Dr. S.K. Mohapatra (Prof. & Head, Department of Mechanical Engineering, Thapar University, Patiala), Dr. Vinod Kumar (Associate Prof. Department of Mechanical Engineering, Thapar University, Patiala), Dr. Tarun Nanada (PhD coordinator) for their encouragement and support during this research work.

I wish to thank Sh. M.R. Sallan, Asstt. Director, Tool Room, Central Institute of Hand Tools, Jalandhar for providing valuable suggestions concerning this research work. I am particularly thankful to Mr. Sunil Saini and Mr. Aman Verma, Central Institute of Hand Tools, Jalandhar for providing technical assistance during the experimental work.

I would like to thank Dr. B. S. Sanga and Mr. Sanjeev Katoch, Institute for Auto Parts & Hand Tools Technology, Ludhiana for extending their utmost cooperation during the cryogenic treatment of materials.

My sincere thanks also goes to Dr. Harpreet Singh, Head, Department of Mechanical Engineering, Ms. Narinder Kaur and Mr. Amit Kaushal (Lab Superintendent), IIT, Ropar for providing me laboratory facilities in conducting the SEM, EDX and XRD for analyzing the machined specimens.

I wish to thank to my friends Dr. R.P. Singh, Mr. Sushil Mittal, Dr. Rajnish Kaushik, Dr. Anish Kaushik and Dr. Paras Chawla for their support, services and peaceful ambience during my research work.

I cannot close these prefatory remarks without expressing my deep sense of gratitude and reverence to my loving Mother, Late Smt. Satya Devi, Father, Sh. Rajeshwar Dass, Mother in-law, Smt. Satya Devi and Father in-law, Sh Brij Bhushan Sharma for their blessings and endeavor to keep my moral high throughout the period of my work.

No amount of thanks is enough, finally, for my beloved wife Anuradha Sharma, who held the key to my success. Her patience and encouragement kept my motivation up. Despite all odds, she single handedly and intelligently managed all family matters as well as my son Yashwin and daughter Sheena along with her job.

I want to express my sincere thanks to all those who directly or indirectly helped me at various stages of this research work.

Above all, I express my indebtedness to the "**ALMIGHTY**" for all His blessing and kindness.

(SANJEEV KUMAR)

CONTENTS

Description	Page No.
Preface	i
Certificate	iv
Acknowledgements	v
Contents	vii
List of Tables	xii
List of Figures	xvi
Abbreviations	xxiii
Abstract	xxiv
CHAPTER 1 INTRODUCTION	**1-15**
1.0 Introduction	1
1.1 Titanium and its alloys	1
1.1.1 Machining of titanium alloys	2
1.2 Electric discharge machining (EDM) process	3
1.3 Powder mixed electric discharge machining (PMEDM)	6
1.3.1 Experimental setup for PMEDM process	7
1.4 Cryogenic treatment	8
1.4.1 Cryogenic treatment of workpiece and tool materials	9
1.5 Objectives and scope of the work	11
1.6 Overall methodology of the study	12
1.7 Organization of the thesis	13
CHAPTER 2 LITERATURE REVIEW	**16-32**
2.1 Introduction	16
2.2 Categorization of literature	16
2.2.1 EDM of titanium and its alloys	16
2.2.2 EDM of other materials	22
2.2.3 Cryogenics in EDM	28
2.2.4 Modeling / optimization techniques used in EDM	30
2.3 Identification of research gaps	32
CHAPTER 3 DESIGN OF STUDY	**33-52**
3.1 Introduction	33

3.2 Experimental setup 34
3.2.1 Description of EDM machine 34
3.2.2 Setup details 35
3.3 Detailed description of experimental plan 38
3.4 Preliminary study 41
3.4.1 Pilot experimentation 42
- Material removal rate (MRR) 42
- Tool wear rate (TWR) 44
- Surface roughness (SR) 47
3.5 Methodology 49
3.5.1 Selection of input process parameters 49
- Selection of process parameters for Phase-A main experimentation 49
- Selection of process parameters for Phase-B experimentation 51
- Selection of process parameters for Phase-C experimentation 51
3.6 Instruments/equipments used for analysis 51
CHAPTER 4 MAIN EXPERIMENTATION (PHASE-A) 53-99
4.1 Introduction 53
4.2 Main experimentation (Phase-A) 55
4.2.1 Material Removal Rate (MRR) 58
- Analysis of results 60
- Analysis of variance (ANOVA) 60
- Identification of optimal conditions & theoretical prediction of MRR 64
4.2.2 Tool Wear Rate (TWR) 65
- Analysis of results 66
- Analysis of significant factor using ANOVA technique 67
- Determination and evaluation of main effects for optimal machining parametric combination 69
- Theoretical prediction of TWR by Taguchi methodology 70
4.2.3 Surface roughness (SR) of workpiece 70

- Analysis of results 72
- Analysis of variance (ANOVA) for SR 72
- Assessment of the main effects 74

4.2.4 Micro-hardness (MH) 77

- Analysis of results 78
- Analysis of variance (ANOVA) for Micro-hardness 79
- Assessment of the main effects 81
- Identification of optimal conditions, predictions of the mean and confirmation of experiments 85

4.3 Multi-response optimization of MRR, TWR, SR and MH using Analytic Hierarchy Process (AHP) 86

4.3.1 Implementation of AHP for optimization of responses 87

4.3.2 Results of Analytical Hierarchy Process (AHP) 95

4.4 Surface roughness of tool/electrode 96

4.4.1 Predictions of theoretical surface roughness value of tool/ electrode and confirmation test 99

CHAPTER 5 MODELING OF RESULTS 100-123

5.1 Introduction 100

5.2 Modeling for predicting MRR 100

5.3 Modeling for predicting TWR 105

5.4 Modeling to predict Surface Roughness by using ANN approach 111

5.5 Modeling to predict micro-hardness by using ANN approach 118

5.6 Summary 123

CHAPTER 6 EFFECT OF CRYOGENIC TREATMENT 124-169

(*Experimentation Phase-B & Phase-C*)

6.1 Introduction 124

6.2 Experimentation (Phase-B) 124

6.2.1 Material removal rate 125

6.2.2 Tool wear rate 129

6.2.3 Surface roughness 132

6.2.4 Micro-hardness 134

6.3 Experimentation (Phase-C) 137

6.3.1 Material removal rate 138
6.3.2 Tool wear rate 144
6.3.3 Surface roughness 150
6.3.4 Micro-hardness 156
6.4 Grey Relational Analysis (GRA) 162
6.4.1 Multi Response Optimization using GRA for WCT Ti 15 alloy 163
6.4.2 Multi Response Optimization using GRA for DCT Ti 15 alloy 165
CHAPTER 7 METALLOGRAPHIC ANALYSIS 170-217
7.1 Introduction 170
7.2 Metallographic process 170
7.3 Metallographic analysis of electric discharge machined titanium alloy workpiece for main experimentation (Phase-A) 171
7.3.1 Microstructure analysis using Scanning Electron Microscope 171
- Recast layer 178
- Formation of Cracks 179
7.3.2 Energy Dispersive X-Ray (EDX) Analysis 179
7.3.3 X-Ray Diffraction (XRD) Analysis 184
7.4 Metallographic analysis of tool/electrode surface after EDM of titanium alloys 194
7.4.1 Microstructure Analysis of Tool-Electrodes Using SEM 194
7.4.2 EDS Analysis of Tool/electrode surface 200
7.4.3 XRD Analysis of Tool-electrode 205
7.5 Metallographic analysis of titanium alloy work pieces for experimentation (Phase-C) 208
7.5.1 Microstructure Analysis 208
7.5.2 EDS Analysis 212
7.5.3 XRD Analysis 214
CHAPTER 8 CONCLUSIONS AND SCOPE FOR FUTURE WORK 218-227
8.1 Conclusions 218
8.1.1 Conclusions for main experimentation (Phase-A) 218
8.1.2 Conclusions for experimentation (Phase-B) 220
8.1.3 Conclusions for experimentation (Phase-C) 221

8.2 Scope for future work 226

REFERENCES **228-243**

APPENDICES **244-246**

A-1 Properties of titanium alloys 244

A-2 Dielectric fluid 244

A-3 Detailed technical specifications of EDM machine 245

LIST OF TABLES

Table No.	Description	Page No.
4.1	Chemical analysis (%) of work materials and electrode materials	54
4.2	Fixed input process parameters	54
4.3	Selected factors with their levels for machining	56
4.4	$L_{18}(2^1 \times 3^7)$ experimental design matrix with machining parameters	56
4.5	MRR after each trial and their calculated S/N Ratios	58
4.6	Average values by factor levels of S/N Data and Raw Data for MRR	59
4.7	Analysis of variance (ANOVA) for MRR (S/N Data)	60
4.8	Response table for S/N Ratios (Larger the better)	64
4.9	Tool Wear Rate with their calculated S/N Ratios	66
4.10	Average values by factor levels of S/N Data and Raw Data for TWR	67
4.11	ANOVA results for TWR (S/N Ratios)	68
4.12	Response table for S/N Ratios (Smaller the better)	68
4.13	Surface roughness values in Rz, Rq and Ra	71
4.14	Average values by factor levels of S/N Data and Raw Data for SR	72
4.15	Analysis of variance (ANOVA) of control parameters for SR	73
4.16	Micro-hardness with their calculated S/N Ratios	78
4.17	ANOVA results for micro-hardness (S/N Ratio)	79
4.18	ANOVA results for micro-hardness (Means)	80
4.19	Response table for S/N Ratios (Larger the better)	80
4.20	Response table for means	80
4.21	Satty's fundamental scale	87
4.22	Random consistency index	87
4.23	Average response for MRR, TWR, SR and Micro-hardness	88
4.24	Pair wise comparison matrix for different criteria	88
4.25	Pair wise comparison of MRR w.r.t. their alternatives (Sample-I)	90
4.26	Pair wise comparison of TWR w.r.t. their alternatives (Sample-I)	90
4.27	Pair wise comparison of SR w.r.t. their alternatives (Sample-I)	91

4.28	Pair wise comparison of MH w.r.t. their alternatives (Sample-I)	91
4.29	Pair wise comparison of MRR w.r.t. their alternatives (Sample-II)	92
4.30	Pair wise comparison of TWR w.r.t. their alternatives (Sample-II)	92
4.31	Pair wise comparison of SR w.r.t. their alternatives (Sample-II)	93
4.32	Pair wise comparison of MH w.r.t. their alternatives (Sample-II)	93
4.33	Overall weight matrix of sample-I priority	94
4.34	Overall weight matrix of sample-II priority	94
4.35	Optimal process parameter setting for sample I & II	95
4.36	Experimental results for SR of electrode with S/N Ratio	96
4.37	ANOVA results for S/N Data (S/N Ratio) SR of electrode	97
4.38	Average values of factor levels for S/N Data and Raw Data of surface roughness of tool-electrode	98
5.1	Dimensions of important parameters in EDM process used for modeling of MRR	101
5.2	Model parameter value in the form of their fundamental dimensions	101
5.3	Dimensions of important parameters in EDM process used for modeling of TWR	106
5.4	Model parameter value in the form of their fundamental dimensions	107
5.5	Experimental results and ANN predicted results for SR	111
5.6	Mean square error and regression error for results of training, validation and testing for surface roughness	116
5.7	Correlation between the experimental and ANN predicted value of surface roughness	117
5.8	Paired sample t- test for experimental value and ANN model's value of surface roughness	118
5.9	Experimental results and ANN predicted results for MH	119
5.10	Mean square error and regression error for results of training, validation and testing for micro-hardness	121
5.11	Correlation between the experimental and ANN predicted value of micro-hardness	121

5.12	Paired sample t- test for experimental value and ANN model's value of micro-hardness	122
6.1	L_9 design of experiment for Phase-B experimentation	125
6.2	Comparison of responses (MRR, TWR, SR and MH)	126
6.3	Percentage gain/loss in MRR	127
6.4	ANOVA results of MRR, TWR, SR and MH (WCT, SCT, DCT Alloy)	128
6.5	Percentage gain/loss in TWR	130
6.6	Percentage gain/loss in surface roughness	132
6.7	Percentage gain/loss in micro-hardness	135
6.8	Representation of control factor with their levels for Phase-C	137
6.9	L_9 experimental design for Phase- C experimentation	137
6.10	Observation table for MRR (WCT & DCT Ti 15 Alloy)	138
6.11	Observation table for MRR (WCT & DCT Ti 21 Alloy)	139
6.12	Observation table for MRR (WCT & DCT Ti 31 Alloy)	139
6.13	ANOVA results of S/N Data for MRR	141
6.14	Percentage change in MRR for WCT and DCT titanium alloys	142
6.15	Observation table for TWR (WCT & DCT Ti 15 Alloy)	145
6.16	Observation table for TWR (WCT & DCT Ti 21 Alloy)	145
6.17	Observation table for TWR (WCT & DCT Ti 31 Alloy)	146
6.18	ANOVA results of S/N Data for TWR	148
6.19	Percentage change in TWR for WCT and DCT titanium alloy	149
6.20	Observation table for SR (WCT & DCT Ti 15 Alloy)	150
6.21	Observation table for SR (WCT & DCT Ti 21 Alloy)	151
6.22	Observation table for SR (WCT & DCT Ti 31 Alloy)	151
6.23	ANOVA results of S/N Data for surface roughness	152
6.24	Percentage change in SR for WCT and DCT titanium alloys	155
6.25	Observation table for MH (WCT & DCT Ti 15 Alloy)	156
6.26	Observation table for MH (WCT & DCT Ti 21 Alloy)	156
6.27	Observation table for MH (WCT & DCT Ti 31 Alloy)	157
6.28	ANOVA results of S/N Data for micro-hardness	158
6.29	Micro-hardness of WCT and DCT titanium alloy specimens	161
6.30	Percentage change in MH for WCT and DCT titanium alloys	161

6.31	Signal-to-noise ratios of response values (WCT Ti 15 Alloy)	164
6.32	Normalization and deviation sequences of S/N Ratios (WCT Ti 15 Alloy)	164
6.33	Grey relational coefficient, grade and order (WCT Ti 15 Alloy)	165
6.34	Signal-to-noise ratios of response values (DCT Ti 15 Alloy)	165
6.35	Normalization and deviation sequences of S/N Ratios (DCT Ti15 Alloy)	166
6.36	Grey relational coefficient, grade and order (DCT Ti 15 Alloy)	166
6.37	Details of experiments with better performance	167
6.38	Response table for the grey relational grade (WCT TITAN 15 Alloy)	167
6.39	Response table for the grey relational grade (DCT TITAN 15 Alloy)	167
6.40	Performance results using the initial orthogonal array and optimal grey predicted process parameter	169
7.1	Observation of various elements after machining of workpiece samples	184
7.2	Summary of different elements observed on tool surfaces	204
A 1	Important properties of titanium alloys	244
A 2	Specifications of FERROLAC 3M EDM Oil	245
A 3	Detailed technical specifications EDM machine	245

LIST OF FIGURES

Figure No.	Description	Page No.
1.1	EDM set up	4
1.2	Schematic diagram of PMEDM set up	7
1.3 (a)	Set-up for PMEDM process	8
1.3 (b)	Large view of installed tank	8
1.4	The cycle for cryogenic treatment of titanium alloys	9
1.5	Schematic representation of cryogenic treatment cycle for tool material	10
1.6	SEM Micrographs of TITAN 15 (a) WCT, (b) SCT, (c) DCT	10
3.1	Pictorial view of EDM machine used for the experiments	35
3.2 (a)	Alignment of electrode	36
3.2 (b)	Tool and workpiece set-up	36
3.2 (c)	Tool and workpiece sink in dielectric liquid	36
3.2 (d)	Actual operation performed in dielectric	36
3.3	Detailed description of experimental design	37
3.4 (a)	Experimental layout	38
3.4 (b)	Experimental layout (main experimentation Phase-A)	39
3.4 (c)	Experimental layout (experimentation Phase-B)	40
3.4 (d)	Experimental layout (experimentation Phase-C)	40
3.5	Cause and effect diagram for responses	41
3.6	Effect of variation in peak current on MRR	43
3.7	Effect of variation in pulse-on-time on MRR	44
3.8	Effect of variation in pulse-off-time on MRR	44
3.9	Effect of variation in peak current on TWR	45
3.10	Effect of variation in pulse-on-time on TWR	46
3.11	Effect of variation in pulse-off-time on TWR	46
3.12	Effect of variation in peak current on surface roughness	47
3.13	Effect of variation in pulse-on-time on surface roughness	48
3.14	Effect of variation in pulse-off-time on surface roughness	48
3.15	Flow diagram for Taguchi experimental design	50
4.1(a)	Picture of three electrodes used	55

4.1 (b)	Cut titanium work pieces	55
4.1 (c)	Picture of two powders	55
4.2 (a)	Effect of pulse-off-time on MRR	61
4.2 (b)	Effect of peak current on MRR	61
4.2 (c)	Effect of pulse-on-time on MRR	61
4.2 (d)	Effect of dielectric fluid, with ‘Mn’ and ‘W’ powder on MRR	62
4.2 (e)	Effect of different electrode materials on MRR	62
4.2 (f)	Effect of cryogenic treatment of electrode materials on MRR	62
4.2 (g)	Effect of different titanium alloys work materials on MRR	63
4.2 (h)	Effect of cryogenic treatment of titanium alloys on MRR	63
4.3	Main effects plot for S/N ratios (Smaller-the-better) of TWR	69
4.4 (a)	Effect of pulse-off-time on SR	74
4.4 (b)	Effect of peak current on SR	75
4.4 (c)	Effect of pulse-on-time on SR	75
4.4 (d)	Effect of powder mixed dielectric fluid on SR	75
4.4 (e)	Effect of tool-electrode materials on SR	76
4.4 (f)	Effect of cryogenic treatment of electrode materials on SR	76
4.4 (g)	Effect of workpiece materials on SR	76
4.4 (h)	Effect of cryogenic treatment of workpiece materials on SR	77
4.5 (a)	Effect of pulse-off-time on MH	82
4.5 (b)	Effect of peak current on MH	82
4.5 (c)	Effect of pulse-on-time on MH	82
4.5 (d)	Effect of powder mixed dielectric fluid on MH	83
4.5 (e)	Effect of tool-electrode materials on MH	83
4.5 (f)	Effect of cryogenic treatment of electrode materials on MH	83
4.5 (g)	Effect of workpiece materials on MH	84
4.5 (h)	Effect of cryogenic treatment of workpiece materials on MH	84
4.6	AHP Hierarchy Structure	89
4.7	Graphical presentations of parameters for S/N ratio of surface roughness of tool-electrode	98
5.1	MRR versus peak current for titanium alloy (Ti-6Al-4V)	104
5.2	TWR vs peak current for machining of titanium alloys (Ti-6Al-4V) with copper electrode (T_{on} =120µs and T_{off} =45 µs)	110

5.3	A multi-layer tansig–purelin network with eight input neurons, one output neuron, and one hidden layer of twenty neuron	113
5.4	Configuration of the FFBP neural network model for the EDM process on response SR	114
5.5	Performance result of FFBP algorithm developed for model of SR	114
5.6	Comparison between the experimental results and the neural network predicted results of SR	115
5.7	Learning behavior of the FFBP neural network model for SR	116
5.8	Linear regression analysis between the experimental values and the FFBP-ANN predicted values of surface roughness (Ra) for training, validation, testing and overall	117
5.9	Comparison between the experimental results and the neural network predicted results of micro-hardness	120
5.10	Learning behavior of the FFBP neural network model for MH	121
5.11	Linear regression analysis between the experimental values and the FFBP-ANN predicted values of micro-hardness (HVN) for training, validation, testing and overall	122
6.1	Comparison of MRR in between WCT, SCT and DCT Ti 21 alloy	126
6.2	MRR v/s T_{on} and I_p (WCT, SCT,DCT) Ti 21 alloy	127
6.3	Comparison of TWR in between WCT, SCT and DCT Ti-5Al-2.5Sn alloy	130
6.4	TWR v/s T_{on} and I_p (WCT, SCT, DCT) Ti 21 alloy	130
6.5	Comparison of SR in between WCT, SCT and DCT Ti-5Al-2.5Sn alloy	132
6.6	SR v/s T_{on} and I_p (WCT, SCT, DCT) Ti 21 alloy	133
6.7	Comparison of micro-hardness in between WCT, SCT and DCT Ti-5Al-2.5Sn alloy	135
6.8	MH v/s T_{on} and I_p (WCT, SCT, DCT) Ti 21 alloy	135
6.9	Main effect plots for S/N ratios of MRR for TITAN 15 alloy	140
6.10	Main effect plots for S/N ratios of MRR for TITAN 21 alloy	140
6.11	Main effect plots for S/N ratios of MRR for TITAN 31 alloy	140

6.12	Percent contribution of control factors on MRR	143
6.13	% gain/loss in MRR	144
6.14	MRR comparative chart for WCT and DCT titanium alloys	144
6.15	TWR comparative chart for WCT and DCT titanium alloys	146
6.16	Main effect plots for S/N ratios of TWR for TITAN 15 alloy	147
6.17	Main effect plots for S/N ratios of TWR for TITAN 21 alloy	147
6.18	Main effect plots for S/N ratios of TWR for TITAN 31 alloy	147
6.19	% gain/loss in TWR	149
6.20	Percent contribution of control factors on TWR	150
6.21	SR comparative chart for WCT and DCT titanium alloys	152
6.22	Main effect plots for S/N ratios of SR for TITAN 15 alloy	153
6.23	Main effect plots for S/N ratios of SR for TITAN 21 alloy	153
6.24	Main effect plots for S/N ratios of SR for TITAN 31 alloy	154
6.25	Percent contribution of control factors on surface roughness	155
6.26	% gain/loss in SR	155
6.27	MH comparative chart for WCT and DCT titanium alloys	157
6.28	Main effect plots for S/N ratios of MH for TITAN 15 alloy	159
6.29	Main effect plots for S/N ratios of MH for TITAN 21 alloy	159
6.30	Main effect plots for S/N ratios of MH for TITAN 31 alloy	159
6.31	Percent contribution of control factors on micro-hardness	160
6.32	% gain/loss in micro-hardness	161
6.33	Grey relational grade graph for WCT & DCT TITAN 15 alloy	168
7.1	(a) Workpiece cut out samples, (b) workpiece sheet and (c) Electrode cut out samples	171
7.2	SEM micrograph of WCT Ti alloy for Exp. No. 1	172
7.3	SEM micrograph of SCT Ti-5Al-2.5Sn for Exp. No. 2	172
7.4	SEM micrograph of DCT Ti-6Al-4V alloy for Exp. No. 3	173
7.5	SEM micrograph of DCT Ti-6Al-4V alloy for Exp. No. 4	173
7.6	SEM micrograph of WCT Ti alloy for Exp. No. 5	174
7.7	SEM micrograph of SCT Ti-5Al-2.5Sn alloy for Exp. No. 6	174
7.8	SEM micrograph of DCT Ti-5Al-2.5Sn alloy for Exp. No 7	174
7.9	SEM micrograph of WCT Ti-6Al-4V alloy for Exp. No 8	174
7.10	SEM micrograph of SCT Ti alloy for Exp. No. 9	175

7.11	SEM micrograph of WCT Ti-5Al-2.5Sn alloy for Exp. No. 10	175
7.12	SEM micrograph of SCT Ti-6Al-4V alloy for Exp. No. 11	176
7.13	SEM micrograph of DCT Ti alloy for Exp. No. 12	177
7.14	SEM micrograph of SCT Ti-6Al-4V alloy for Exp. No. 13	177
7.15	SEM micrograph of DCT Ti alloy for Exp. No. 14	177
7.16	SEM micrograph of WCT Ti-5Al-2.5Sn alloy for Exp. No. 15	177
7.17	SEM micrograph of SCT Ti alloy for Exp. No. 16	177
7.18	SEM micrograph of DCT Ti-5Al-2.5Sn alloy for Exp. No. 17	178
7.19	SEM micrograph of WCT Ti-6Al-4V alloy for Exp. No. 18	178
7.20 (a to r)	EDX Spectrum of machined samples (Exp. No. 1-18)	180-183
7.21	Migration of different materials on workpiece samples	183
7.22	XRD pattern of SCT Ti-5Al-2.5Sn alloy for Exp. No. 6	185
7.23	XRD pattern of SCT Ti alloy for Exp. No. 9	186
7.24	XRD pattern of WCT Ti-5Al-2.5Sn alloy for Exp. No. 10	187
7.25	XRD pattern of DCT Ti alloy for Exp. No. 12	188
7.26	XRD pattern of SCT Ti alloy for Exp. No. 16	189
7.27	XRD pattern of SCT Ti-5Al-2.5Sn alloy for Exp. No. 2	190
7.28	XRD pattern of DCT Ti-5Al-2.5Sn alloy for Exp. No. 17	191
7.29	XRD pattern of DCT Ti-6Al-4V alloy for Exp. No. 3	191
7.30	XRD pattern of WCT Ti-6Al-4V alloy for Exp. No. 18	192
7.31	SEM micrograph of WCT Cu electrode (Exp. No. 1)	195
7.32	SEM micrograph of SCT Cu-Cr electrode (Exp. No. 2)	195
7.33	SEM micrograph of DCT Cu-W electrode (Exp. No. 3)	195
7.34	SEM micrograph of SCT Cu-Cr electrode (Exp. No. 4)	195
7.35	SEM micrograph of DCT Cu-W electrode (Exp. No. 5)	196
7.36	SEM micrograph of WCT Cu electrode (Exp. No. 6)	196
7.37	SEM micrograph of DCT Cu electrode (Exp. No. 7)	196
7.38	SEM micrograph of WCT Cu-Cr electrode (Exp. No. 8)	196
7.39	SEM micrograph of SCT Cu-W electrode (Exp. No. 9)	197
7.40	SEM micrograph of SCT Cu-W electrode (Exp. No. 10)	197
7.41	SEM micrograph of DCT Cu electrode (Exp. No. 11)	198
7.42	SEM micrograph of WCT Cu-Cr electrode (Exp. No. 12)	198
7.43	SEM micrograph of WCT Cu-W electrode (Exp. No. 13)	198

7.44	SEM micrograph of SCT Cu electrode (Exp. No. 14)	198
7.45	SEM micrograph of DCT Cu-Cr electrode (Exp. No. 15)	199
7.46	SEM micrograph of DCT Cu-Cr electrode (Exp. No. 16)	199
7.47	SEM micrograph of WCT Cu-W electrode (Exp. No. 17)	200
7.48	SEM micrograph of SCT Cu electrode (Exp. No. 18)	200
7.49 (a to r)	EDX spectrum of different tool-materials after machining of titanium alloys for Exp. No. 1-18	201-203
7.50	Migration of Different Materials on electrode surface	205
7.51	XRD pattern of WCT Cu-Cr electrode after machining of DCT Ti for Exp. No. 12	206
7.52	XRD pattern of WCT Cu-W electrode after machining of DCT Ti-5Al-2.5Sn alloy for Exp. No. 17	207
7.53	XRD pattern of SCT Cu electrode after machining of WCT Ti-6Al-4V alloy for Exp. No. 18	208
7.54	SEM images of TITAN 15 alloys for trial-1	209
7.55	SEM images of TITAN 15 alloys for trial-9	210
7.56	SEM images of TITAN 21 (Ti-5Al-2.5Sn) alloys for trial-9	210
7.57	SEM images of TITAN 31 (Ti-6Al-4V) alloys for trial-5	211
7.58	SEM images of TITAN 31 (Ti-6Al-4V) alloys for trial-9	212
7.59	EDX analysis of machined surface of DCT TITAN 15 sample	213
7.60	EDX analysis of WCT Ti-5Al-2.5Sn sample	213
7.61	EDX analysis of machined surface of WCT Ti-6Al-4V sample	213
7.62	EDX analysis of machined surface WCT Ti-6Al-4V sample	214
7.63	EDX analysis of machined surface of DCT Ti-6Al-4V sample	214
7.64	XRD analysis of machined surface of DCT TITAN 15 sample for trial-1	215
7.65	XRD analysis of machined surface of WCT TITAN 21 sample for trial-9	216
7.66	XRD analysis of machined surface of WCT Ti-6Al-4V sample for trial-5	217

ABBREVIATIONS

SYMBOL	DESCRIPTION
EDM	Electric discharge machining
PMEDM	Powder mixed electric discharge machining
I_p	Peak current
T_{on}	Pulse-on-time
T_{off}	Pulse-off-time
µs	Microsecond
A or Amp	Ampere
MRR	Material removal rate
TWR	Tool wear rate
SR	Surface roughness
MH	Micro-hardness
W/P	Workpiece
η or m	Overall average of S/N ratio
avg	Average
OA	Orthogonal array
Seq. SS	Sequential Sum of squares
DOF or dof	Degree of freedom
Adj. MS	Adjusted Mean of square (Variation)
F	Variance ratio
PC	Percent contribution
CT	Cryogenic treatment
WCT	Without cryogenic treatment
SCT	Shallow cryogenic treatment
DCT	Deep cryogenic treatment
w.r.t.	with respect to
i.e.	That is
ASTM	American Society for Testing and Materials

ABSTRACT

In the past, the development of titanium alloys came initially from the aerospace industry when there was a crucial need for new materials with high strength to weight ratios, which fall between those of iron and aluminum. Due to its excellent properties, titanium alloy are widely used in the aerospace, chemical, automotive, biomedical, power generation, nuclear plants and many other emerging fields of science and technology. Titanium is recognized as a material which is difficult-to-machine with conventional machining processes. Economical machining of titanium alloys becomes important for industrial products and research work. Although machining of titanium alloy becomes easier with non-traditional or non-conventional machining processes, but the selection of suitable machining process and their parameters is a challenging task for the researchers to increase its machinability.

Electric discharge machining (EDM) is a popular non-conventional machining process used for machining of any type of electrically conductive materials in a contact less mode especially when complex geometries are required. Due to its favorable characteristics and advantages, EDM process is extensively used for machining of titanium alloys. In EDM, the overall machining performance depends on the thermo-electrical properties of tool and workpiece materials. However, high electrical resistivity and poor thermal conductivity of titanium, makes the machining difficult by this process. Cryogenic treatment has a historical background of improving the properties of the materials, *i.e*. mechanical, electrical and thermal.

Cryogenic treatment process has been used for improving the mechanical, electrical and thermal properties of materials. Cryogenic treatment process consists of a slow cooling from room temperature to the liquid nitrogen temperature, soaked for a suitable time at this temperature, and after that the material is heated up to room temperature. The cooling rate, heating rate and soaking period are the most important parameters in cryogenic treatment that highly affected the properties of the materials. Two cooling temperatures were used for this study: (i) -110^0C for shallow cryogenic treatment (SCT) and (II) -184^0C for deep cryogenic treatment (DCT).

In the present study, the primary experimental work was completed during Phase-A (Main study). Subsequently, experimentation was carried out in two more phases (Phase-B and Phase-C). During Phase–A experimentation, three grades of titanium namely (i) Ti (ASTM grade 2), Ti-6Al-4V (ASTM grade 5) and (III) Ti-5Al-2.5Sn (ASTM grade 6) were machined

with three electrodes Copper (Cu), Copper-Chromium (Cu-Cr) and Copper-Tungsten (Cu-W). Peak current (I_p), pulse-on-time (T_{on}), pulse-off-time (T_{off}), dielectric medium, electrode material, workpiece material and cryogenic treatment of the electrode and workpiece materials were identified as the machining parameters. The parameters were varied to investigate their effect on Material Removal Rate (MRR), Tool Wear Rate (TWR), Surface Roughness (SR) and Micro-Hardness (MH) using Taguchi L_{18} orthogonal array (OA). Peak current (I_p) was observed to be the most significant factor, followed by tool or electrode material and pulse-on-time (T_{on}) that affected the MRR and TWR. Increase in MRR was observed in case of DCT titanium alloys due to improvement in electrical and thermal conductivity of the material. A mathematical model for predicting MRR and TWR was developed by using dimensional analysis (Buckingham's π theorem) based on the outcomes of Taguchi model and the thermal-physical properties of the workpiece and electrode material. The predicted results obtained from the developed mathematical model were validated by comparing with the experimental results and were found to be in good agreement with each other. The experimental results and the predicted results show good agreement. Experimental results also revealed that I_p, T_{on} and T_{off} significantly affected the surface roughness and micro-hardness of the surface. Artificial Neural Network (ANN) coupled with the Taguchi approach was applied for optimization and prediction of surface roughness and micro-hardness.

An optimum setting of machining parameters was identified for maximizing the micro-hardness and MRR and minimizes the TWR and SR by using the Taguchi approach. After optimization of the individual responses, the responses, namely MRR, TWR, SR and MH were collectively optimized by using the Analytical Hierarchy Process (AHP) technique. The surface properties of the tool-electrode materials were also investigated in terms of electrode surface roughness.

In the next Phase–B, experimentation, grade VI of titanium alloy (Ti-5Al-2.5Sn) without cryogenic treatment (WCT) and cryogenic treated (shallow and deep) were machined with untreated Cu-Cr tool. Simple FERROLAC 3M EDM Oil was used as the dielectric medium. Using the Phase-A results, two machine parameters (I_p and T_{on}) were identified as process variables and varied at three levels during the process, using Taguchi L_9 orthogonal array. Machining performances of WCT, SCT and DCT machined surface were analyzed and compared in terms of MRR, TWR, SR and MH. The result of the study show significant improvement with DCT alloy when compared with SCT and WCT workpieces. From the study, it was observed that there is a significant increase of 21.84% in MRR, a reduction of

27.40% in TWR, an improvement of 19.58% in surface finish and increase of 17.30% in micro-hardness.

During Phase–C experimentation, three materials; namely Ti, Ti-6Al-4V and Ti-5Al-2.5Sn were machined with three different types of cryogenically treated electrode material (WCT, SCT, DCT); namely Cu, Cu-Cr and Cu-W in Mn powder added dielectric. The machining performance of WCT titanium alloys was compared with DCT titanium alloys. Four different input parameters namely (i) peak current, (ii) pulse-on-time, (iii) electrode material and (iv) cryogenic treatment of electrode material were varied at three levels. Peak current was observed to be the most significant factor that affected the EDM performance followed by the pulse-on-time. The significant effect of cryogenic treatment of the tool was observed. The experimental results revealed that the higher MRR and MH, lower TWR and SR were observed in the case of DCT titanium alloy workpiece machined with DCT electrode as compared with WCT workpiece and tool material. In this stage, optimization of the input parameters for the EDM of TITAN 15 alloy was performed for multiple performance characteristics (MRR, TWR, SR and MH) by using Grey Relational Analysis (GRA) approach followed by confirmation experiments.

The present research work has also focused on study of surface integrity of the workpiece and tool surfaces after machining. For this purpose, each workpiece and tool/electrode surface after machining for main experimentation (Phase-A) and selected titanium workpiece samples for Phase-A and Phase-C were examined by Scanning Electron Microscope (SEM) coupled with Energy Dispersive X-Ray (EDX) analyzer followed by X-ray Diffraction (XRD) for surface integrity. The XRD patterns clearly show the formation of different chemical compounds and new phases on the machined surface. EDX spectrum represents the migration of various elements on the machined surface either of the workpiece base metal or transfer from the tool surface or migration from dielectric medium. SEM micrographs indicated surface defects such as surface cracks, larger and deeper size of craters, recast layer, micro pores, pin holes, debris, pock marks etc. on the machined surface. The amount of discharge energy significantly resulted in generation of such surface defects. Experimental results clearly showed that surface properties were significantly affected by current followed by pulse-on-time. A significant amount of carbon particles were migrated on both tool and workpiece surfaces due to decomposition of dielectric. Various carbides and oxides were formed either in free and/ or in compound form on both the workpiece and electrode surface. Different compounds, namely Titanium-Carbide (TiC), Aluminum-Titanium-Carbide ($Al_2Ti_4C_2$), Tin-Titanium-Carbide ($SnTi_2C$), Titanium-Zinc-Carbide (Zn_2Ti_4C), Titanium-

Oxide also known as hongquite (TiO), Titanium-Dioxide also known as rutile (TiO_2), Tin-Titanium-Tungsten-Oxide (Sn_2TiWO_7), Copper- Titanium-Oxide (Cu_2TiO_3), Manganese-Titanium-Oxide (Mn_2TiO_4) precipitated on the machined surface due to phase transformations and were analyzed by using the XRD analyzer.

In the last chapter, the results of the three phases of the study have been summarized. Some of the significant conclusions are:

I. During the EDM process spark energy increases as the value of I_p and T_{on} increases, which affect the machining performance significantly.

II. Arcing on workpiece or electrode surface was noticed at higher current (14A), longer duration of pulse-on-time (150µs) and smaller duration of pulse-off-time (30µs). Due to arcing the machining efficiency was reduced in terms of low MRR, poor surface finish, higher TWR and more deposition of carbon on the machined surface.

III. A mathematical model considering the significant machine parameters and the thermo-physical properties of the workpiece and electrode materials was developed for predicting MRR and TWR using dimensional analysis approach.

IV. The structural design of Artificial Neural Network (ANN) was selected, trained, validated, tested and then used for simulation to optimize the surface roughness and micro-hardness. Experimental results and ANN predicted results showed good agreement.

V. The SEM micrographs show that high discharge energy ($I_p \times T_{on}$) was responsible for producing the surface defects such as; surface or thermal cracks, craters, thick recast layer, micro pores, pin holes, residual stresses and debris.

Chapter 1

INTRODUCTION

1.0 INTRODUCTION

Modern manufacturing industries have been demanding hard and most strong materials with "high strength to weight" ratio such as titanium, stainless steel, nimonics, fiber-reinforced composites, ceramics, satellites and difficult to machine alloys. This needs development of improved cutting tool materials so that machining productivity is not hampered. Production of complex and intricate shapes with superior surface finish, close tolerances, higher production rates & economy using such materials is difficult using old traditional methods [1-3]. Making of holes (shallow entry angles, non-circular, micro holes, large aspect ratio, contoured holes and holes without burr) in difficult to machine materials is another area where extensive research is the need of the time [1- 2].

To meet such requirements, different kinds of machining processes, i.e. non-traditional machining (NTM) or non-conventional machining (NCM) processes have been employed. In non-conventional machining processes, the tool needs not to be harder than workpiece because there is always some gap between the tool and the job. [1-2, 4]. NTM processes can be classified on the basis of the type of energy used such as mechanical, thermo-electric, electro-chemical and chemical. Research to discover and develop non-traditional processes for different materials and different conditions must continue as no single process can provide optimal solutions for all materials and conditions. Selection of optimal parameters for machining different materials under different conditions is extremely important and the present work aims to accomplish this for titanium and its alloys.

1.1 TITANIUM AND ITS ALLOYS

Titanium and its alloys find their applications in different types of industries such as aerospace, chemical, power sectors, transportations, armament, sports and many more. In the periodic table, titanium is denoted by symbol '*Ti*' with atomic number 22 and atomic weight 47.9. Greek mythology granted it a new name, the titans, hence, named it *Titanium 'Ti'*.

Now a day, Ti and its alloys are made use of in many manufacturing industries due to their outstanding properties. The maximum consumption of titanium components/parts is found in the aerospace industry. The advantages of this material include: (i) low density, which fall between those of Al and Fe and give 'high strength to weight ratios' used for lighter and stronger structures; (ii) better corrosion and erosion resistance, in particular to pitting and corrosion cracking and (iii) high temperature capability. However, one of the most significant disadvantages of this material is its cost [5-7].

Titanium materials are available commercially in pure and different alloy grades. Based on the microstructure or phase, titanium can be classified into three major groups, namely alpha (α), alpha-beta (α-β) and beta (β). At room temperature, titanium has a Hexagonal Close-Packed (HCP) crystal structure, which is referred to as "α" phase. This structure transforms to a Body-Centered Cubic (BCC) crystal structure, designated as "β" phase, at 882 °C and remains stable up to the melting point of 1680°C [8]. Low density Al is the most effective alloying element which contributes to strengthening the α-phase at room temperature or elevated temperature up to 550^0C. However, α-phase can be strengthened by the addition of Tin (Sn) or Zirconium (Zr) [5-8]. These alloys have HCP crystal structure at low temperature and classified as α alloys. Ti-5Al-2.5Sn belongs to α-phase group used for corrosion resistance and cryogenic application and is commercially available and has a microstructure of α-phase [5-8]. The majority of the commercial alloys belongs to the α+ β phase alloys. Ti-6Al-4V titanium alloy is the most widely used alloy of α-β group having mixtures of alpha-beta phase microstructure. Ti-6Al-4V alloy can be used for high strength applications [5-8, 12, 157].

1.1.1 MACHINING OF TITANIUM ALLOYS

Due to poor different inherent properties, the machining of Ti and its alloys is usually considered to be difficult with conventional cutting processes. Ti has a tendency that its chips produced during machining weld to the tool due to its *chemical reactive property*, which leads to chipping and premature tool-failure. Further, as reported, cutting of Ti is difficult due to its *poor thermal conductivity*. The generated heat energy at cutting zone cannot dissipate quickly. This issue badly affects the tool life [8-12, 165]. In addition to that, machining of Ti becomes difficult due to its *high strength at elevated temperature and low modulus of elasticity* [8, 10, 13]. Siekmann pointed out that there is no machining process available which can convert titanium material into chips efficiently and economically [14]. The above

factors point out that traditional machining processes are not efficient in giving desired shape and close tolerances to this material. Khanna and Sangwan stated that pre heat treatment of titanium alloys increase the machining performance [167].

There is thus a crucial need for a machining process which can machine Ti and its alloys efficiently, economically and precisely. Over the last few decades, due to advancement in cutting tool materials, machining of Ti and its alloys become possible up to some extent. Still, none of these newer cutting tool materials have been successfully used in improving the machinability [8]. Some researchers reported that by using generous cutting fluids, machining of titanium alloys can be improved with traditional machining processes. But, toxicity of cutting fluids may degrade the quality of the machining atmosphere [15]. Efforts have been made to provide cryogenic cooling or cryo-treatment of the titanium alloy work material as well as cutting tool material [16-18].

Considering the above said problems faced during machining of Ti and its alloys with ordinary machining processes, there is a crucial need of NCM process which can machine titanium easily, efficiently and economically. As reported by several researchers, Electrical Discharge Machining (EDM) is one of the most suitable non-conventional machining processes that can machine Ti and its alloys into complex and intricate shapes in close dimensions [19].

In the present research work, an attempt has been made to investigate the machining characteristics of titanium alloys by using an EDM process. However, EDM process has its own limitation; low metal removal rate, higher tool wear rate, dimensional accuracy, surface finish and change in micro structural properties which would also be studied in this work.

1.2 ELECTRIC DISCHARGE MACHINING (EDM) PROCESS

In 1770, Joseph Priestly, first discovered the erosive effect of electric sparks on metals [20]. However, in 1943, two Soviet Scientists took advantage of the electric sparks for constructive use *i.e.* machining. EDM is one of the most popular machining processes used in manufacturing industries to produce complex and intricate shapes of parts in small batches or even on the job - shop basis, especially dies and molds. EDM removes material from the surface of job material by a rapid succession of short duration electric sparks between the two electrodes *i.e.* the tool and the job. The final shape of the profile / cavity generated on the job

is the mirror image of the tool shape. This process uses thermo-electric energy to machine electrically conductive materials by melting and evaporation. Metal is removed from the job surface in powder form, known as debris. The most important aspects of EDM process are that it is a contact-less machining process, no mechanical stresses, no burrs on machined surface, no constraint of workpiece hardness, free from problems like chatter and vibration as observed during conventional machining. On the other hand, EDM process suffers only from two major drawbacks (i) significant tool wear and (ii) large machining time [1-2, 21-23].

In EDM process, metal is removed from the surface of a job with frequent sparks. These sparks are generated when the two electrodes, workpiece and tool, submerged in the dielectric are maintained at a specified distance (gap) [24-25]. A spark is generated when a suitable voltage is applied across the anode and cathode. The spark occurs at the closest point between the two electrodes. The temperature of the small area under the spark is extremely high [26, 27]. The EDM setup is shown in Figure 1.1.

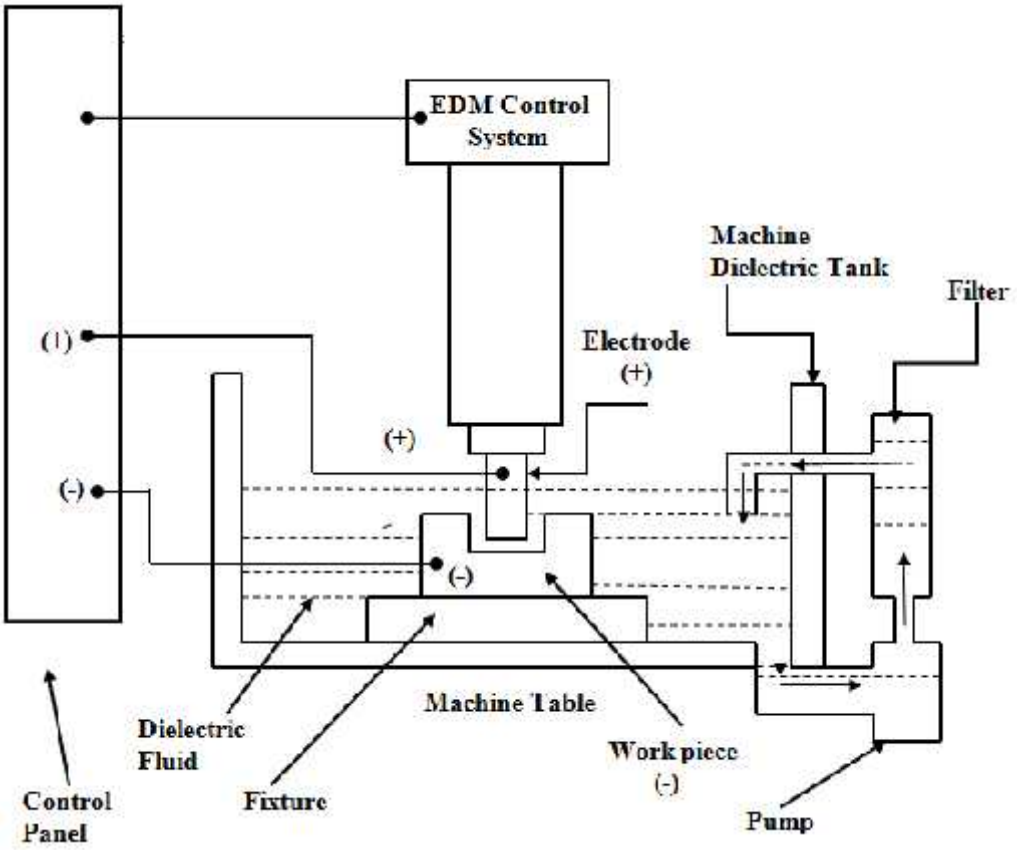

Figure 1.1: EDM Set up

During the EDM process, workpiece, or job is fixed in the fixture or directly on table of the EDM machine and tool, generally known as electrode is fixed to the ram of the machine. A servo-control mechanism operated by the control panel of the machine is used to control the movement of the tool in a downward direction towards the workpiece, to maintain a constant gap (10-100µm) between the two electrodes. When pulsed DC voltage of 80-100 volt at approximately 5Hz- 5 kHz frequency is passed through the two electrodes, intense electric field at the narrowest gap is produced. Negatively charged particles (electrons) break loose from the cathode pole and move in the direction of anode surface under the influence of electric field forces. During this movement, there is a collision of electrons with the neutral molecules of the dielectric. Further, electrons also get separated from these neutral molecules of the dielectric resulting in still more ionization. Thus, a very narrow ionization channel forms of continuous conductive. This narrow ionization channel is also known as plasma channel. In this plasma channel, there is a considerable amount of continuous flow of electrons to the anode (positive terminal) and that of ions towards the cathode (negative terminal). Due to this phenomenon, kinetic energy is produced which is converted into thermal energy. Thus, heating of anode due to bombardment of electrons and heating of cathode due to bombardment of ions takes place. It ends up in momentary current impulse resulting in a discharge which may be an arc or spark. The spark energy raises the temperature of a localized area in the range of 8000 ^{0}C to 12,000^{0}C or sometimes as high as 20,000^{0}C causing melting, or melting as well as vaporization of material at both ends [1, 2, 22, 28]. At the end of 'on-time' plasma channel collapses due to 'turn off' pulsating current, causing a sudden fall in temperature. Thus, the surface of both poles gets cooled due to the continuous flow of dielectric. Vaporized material is removed from poles by flushing in the form of microscopic debris. However, some amounts of un-flushed materials remains attached to the surface of a workpiece and the tool depending on the machining conditions [22].

The amounts of material eroded from both terminals are in the form of small craters which depend upon the machining conditions. Generally, MRR varies in the range of 2 -400 mm^3/min, while the cubic material removed per spark varies in the range of 10^{-6}-10^{-4} mm^3 depending on the setting of input parameters of the process.

1.3 POWDER MIXED ELECTRIC DISCHARGE MACHINING (PMEDM)

The major drawback of the conventional EDM process is low MRR, higher TWR and poor surface finish which restrict its use in manufacturing industries. Efforts have been made by the researchers to develop solutions to overcome these problems and enhance machining efficiency. To improve the machining efficiency of a process, suitable metal particles in powder form are mixed with the dielectric. This hybrid technique is known as PMEDM or additive *EDM* [21, 31]. PMEDM process has a more complex mechanism than simple EDM process. Different metallic powders such as Aluminum (Al), Silicon (Si), Nickel (Ni), Titanium (Ti), Manganese (Mn), Tungsten (W), Chromium (Cr), Graphite (Gr), Copper (Cu) and many more can be suspended in a dielectric fluid. These mixed powders in a dielectric medium significantly affect the machining efficiency [21, 31-33]. The powder concentration is the most critical factor that highly affects the machining performance.

Throughout the PMEDM process, the spark gap is filled with the powder suspended into dielectric by the flushing. An electric field in the range of 10^5 to 10^7 V/m is generated due to voltage, applied between the two electrodes submerged in dielectric and metal particles moving in a zigzag fashion [31, 34]. These metal particles act as a conductor and are responsible for the significant reduction in the breakdown strength of the insulating liquid between the spark gap. Due to contamination, gap size is increased as well as ignition process improved, thus, stability of the machining process is also improved. However, too much contamination leads to arching and inefficient machining [35].

The individual powder particles come closer and then form a chain like structures between the spark gap due to interlocking of powder particles. This is known as bridging effect, which reduces the insulating strength of the dielectric fluid. Due to this mechanism, rate of generation of sparks becomes faster, hence, the erosion process becomes faster, causing an increase in MRR. At the same time, plasma channel is modified due to mixed powder particles, thereby increasing the size of the plasma channel [31, 34]. This modified plasma channel uniformly distributes the sparks, which decreases the density of spark. Due to this issue, shallow craters are produced, which improve the surface finish of the machined parts.

1.3.1 EXPERIMENTAL SETUP FOR PMEDM PROCESS

In the PMEDM process, experiments were conducted in the powder mixed dielectric medium. For performing the machining operation in the powder added dielectric medium, some major precautions must be considered:

- Ensure that powder particles should not reach the main tank of the machine.
- The machining in the powder mixed dielectric fluid should be limited to a small volume so as to minimize the consumption of powder particles.
- The powder particles should not be settled down at the bottom of the tank.
- Proper conductivity at the tool-electrode and workpiece interface must be maintained.

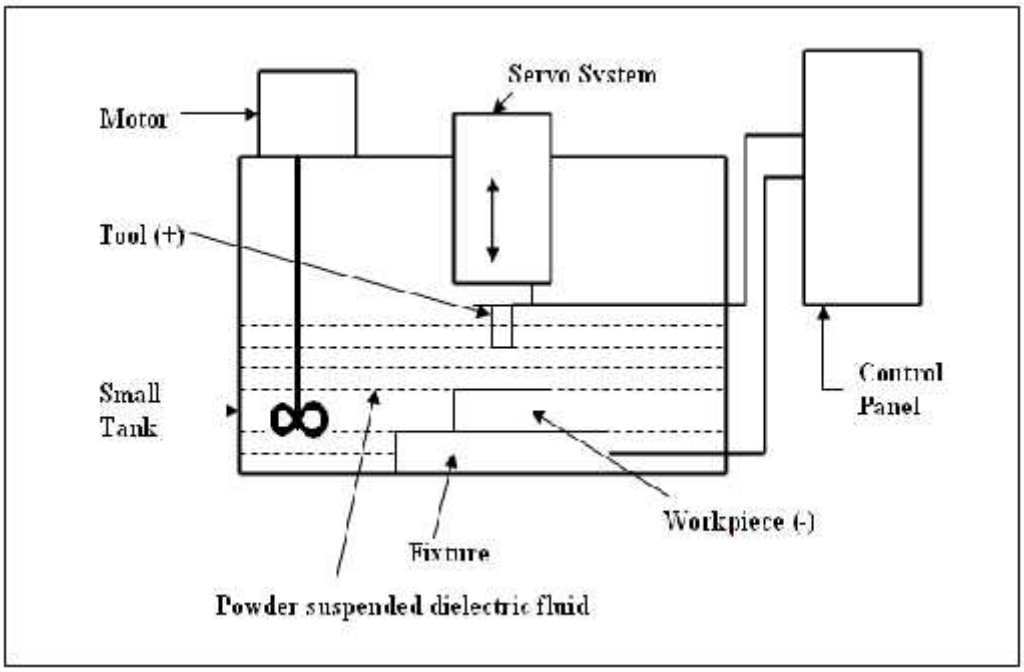

Figure 1.2: Schematic Diagram of PMEDM set up

Keeping in view all these points, a specially designed tank was fabricated using 3mm mild steel sheet of size 330 mm length x 180 mm breadth x 187 mm height. The capacity of this small container is approximately 9 liter after deducting the volume of fixture and other accessories. A motorized stirrer rotating at 1400 RPM was provided in the left corner of the tank for blending of powder particles. The schematic line diagram of the PMEDM process setup is shown in Figure 1.2. The small tank was installed properly on machine table as shown in Figure 1.3 (a) and Figure 1.3 (b) shows the large pictorial view of the tank.

(a) **(b)**

Figure 1.3: (a) Set-up for PMEDM Process, (b) Large View of Installed Tank

1-Motorized Stirrer, 2- Small tank, 3- Powder mixed dielectric, 4- Electrode holder, 5- Magnetic block, 6- Lower part of ram, 7- Electrode adjusting screws, 8- Machine table (Machine dielectric tank)

1.4 CRYOGENIC TREATMENT (CT)

Cryogenics is a cooling process performed at ultra low temperature, *i.e.* below -310°F. The metallurgical and structural properties of the materials can be significantly improved by using this cooling process. CT is widely used for treating ferrous and non-ferrous metals and their alloys [36]. In cryogenic process, generally conversion of austenite to martensite in the microstructure of materials is observed. During the heat treatment process, 85% of the retained austenite can transfer to martensite, while CT can transform only an addition of 8 to 15%. After cryogenic processing, more uniform microstructure of the material is formed with greater density.

Deep Cryogenic Treatment (DCT) and Shallow Cryogenic Treatment (SCT) are the two treatments of cryogenic process. DCT is performed around -320^0F (-196^0C), near the temperature of liquid Nitrogen (LN2) where as SCT takes place around -120^0F near the temperature of dry ice. DCT enhances the desired metallurgical and structural properties of materials at ultra low temperature about -320^0F, -196^0C, or 77^0K. Under this treatment,

parts/components are placed inside a well-insulated chamber in which LN2 is flowing. The cooling rate, heating rate and soaking time are the three important factors which must be carefully controlled. Cooling and heating rates are accurately controlled by a computer program. Tempering is performed on parts to avoid them from thermal stresses [37].

1.4.1. CRYOGENIC TREATMENT OF WORKPIECE AND TOOL MATERIALS

Before going to final experimentation, cryogenic treatment (CT) of both the workpiece and electrode material has been conducted in cryogenic processor (make; Primero EnServe, CP 220LH) with temperature range -184°C to 150°C having a size of 450mm x 1200mm x 450mm. Cryogenic treatment, namely SCT and DCT were applied to the workpiece as well as on electrode materials to investigate their effect on machining characteristics. The cryogenic treatment cycle for titanium alloy workpiece and electrode are represented in Figure 1.4 and 1.5 respectively.

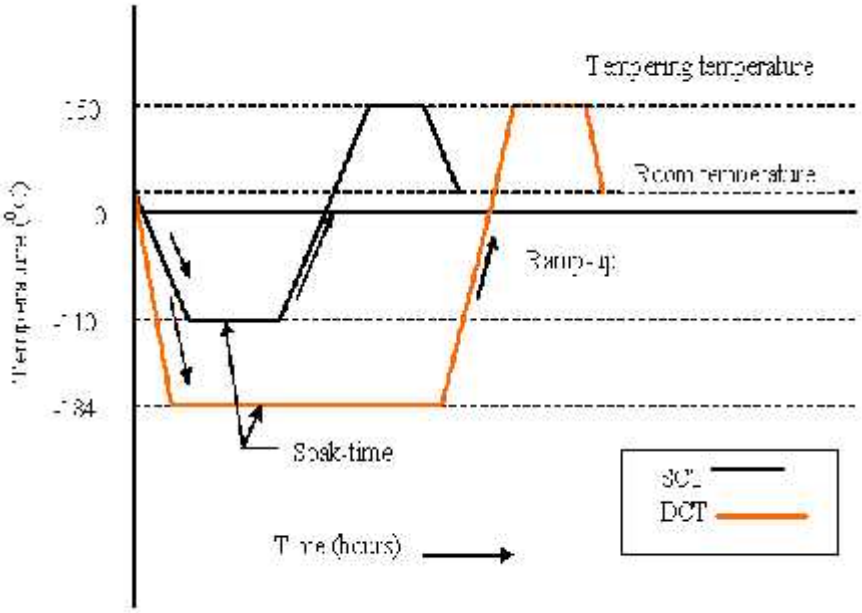

Figure 1.4: The Cycle for Cryogenic Treatment of Titanium Alloys

During the CT, the components were cooled down from ambient temperature to ultra sub low temperature i.e. temperature of liquid nitrogen. At this low temperature, parts were held for a long time depends upon the types of CT process. During the cool-down cycle, cooling

temperature must be controlled precisely to avoid the components from thermal shocks. During SCT cycle, both the workpiece (TITAN 15, TITAN 21, and TITAN 31) and electrode (Cu, Cu-Cr, Cu-W) materials were cooled to -110 ^{0}C by using a slow cooling rate of 1^{0}C/min from room temperature, and then it is soaked at this temperature for 6 hours. After that, the titanium alloys (workpiece) were tempered at 150^{0}C with a heating rate of 1^{0}C/min for two hours so as to relieve the stresses.

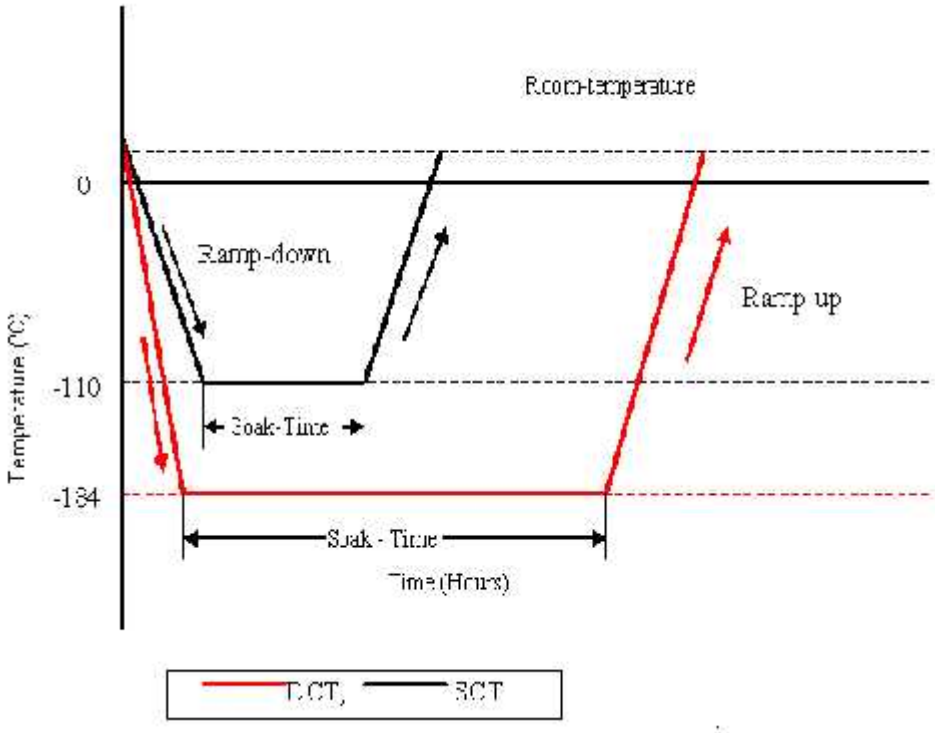

Figure 1.5: Schematic Representation of Cryogenic Treatment Cycle for Tool Material

During the DCT process, the temperature of the parts was brought to -184 ^{0}C with a cooling rate of 1^{0}C/min. Here, the parts were kept in the insulated chamber for 24 hours and then the temperature was kept constant for this period. The temperature was raised to room temperature slowly again with a heating rate of 1^{0}C/min. Thereafter, the samples of titanium alloy workpiece were subjected to tempering cycle to relieve stresses induced by cryogenic treatment. During tempering, the temperature of the parts was raised up to 150^{0}C with a heating rate of 1^{0}C/min, soaked for two hours and were then brought back to room temperature. The tempering was done for titanium materials only.

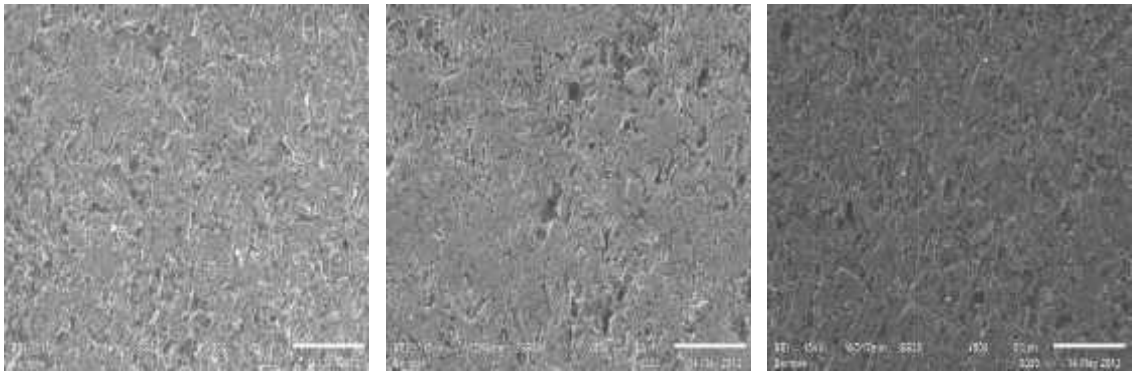

(Fig. a) **(Fig. b)** **(Fig. c)**

Figure 1.6: SEM Micrographs of TITAN 15 (a) WCT, (b) SCT, (c) DCT

Figure 1.6 shows the three micrographs of TITAN 15 workpiece material, *i.e* without cryogenic treatment (Fig. a), shallow cryogenic treatment (Fig. b) and deep cryogenic treatment (Fig. c). The microstructure of the DCT Ti 15 material shows the fine structure than SCT or WCT alloy. It means population or density of grains were improved in DCT alloy.

1.5 OBJECTIVES AND SCOPE OF THE WORK

For the present study, three grades of titanium alloy, namely Ti (TITAN 15, ASTM Grade 2), Ti-6Al-4V (TITAN 31, ASTM Grade 5) and Ti-5Al-2.5Sn (TITAN 21, ASTM Grade 6) were selected as workpiece materials. Copper (Cu), Copper-chromium (Cu-Cr) and Copper-tungsten (Cu-W) were selected as electrode materials. SCT and DCT have been applied on both tool and work materials to investigate their effect on output characteristics. Two different powders, namely Manganese (Mn) and Tungsten (W) were used with dielectric fluid to study their influence or improvement on the responses. In the field of die-sinking EDM technology, the use of commercially available kerosene oil as dielectric fluid is common. However, air pollution is the biggest problem with kerosene. Hence, FERROLAC 3 M EDM Oil was used in this study as dielectric medium. Machining characteristics of machined surface have been investigated in terms of MRR, TWR, SR and micro-hardness. Metallographic analysis of components was done by using SEM, EDS, and XRD techniques. I_p, T_{on} and T_{off} were identified as machine input parameters for conducting experimentations which can be varied by control panel of the machine.

The objectives of the present study are to:

1. investigate the effect of cryo-treatment of titanium alloys on machining characteristics in an electric discharge machining process on various output characteristics such as MRR, TWR, Surface Roughness and Hardness

2. investigate the effect of cryo-treatment of electrodes on machining characteristics of titanium alloys in an electric discharge machining process on various output characteristics such as MRR, TWR, Surface Roughness and Hardness

3. study and validate the improvement in material properties of titanium alloys with regard to transfer of suspended powder particles in the dielectric fluid

4. validate the effect of these parameters using advanced statistical methods by developing a generalized mathematical model for the results.

1.6 OVERALL METHODOLOGY OF THE STUDY

On the whole research work in the present study has been categorized is as follows:

I. In depth study of literature
II. Design of experiment
III. Experimentation
IV. Analysis of the results
V. Metallographic analysis
VI. Conclusions

Different machining parameters can be varied to explore their effect on EDM performance. Each parameter has its own importance on machining performance in different terms. Due to this reason, detailed literature survey has been carried out to differentiate the impact of the various input parameters on different aspects of machining such as MRR, TWR, SR, micro-hardness and surface integrity. Thereafter, pilot experimentation was conducted for preliminary study on Ti-6Al-4V workpiece with copper electrode. The different machining conditions, their ranges and levels were finalized based upon the results of a pilot study. Taguchi methodology was used for the design of experiments. Shallow and deep cryogenic

treatments were performed in the cryogenic processor under controlled cooling environment for the workpiece and tool materials to explore their effect on EDM performance.

To achieve the objectives of the study, the research work has been performed in three phases of experiments. Main experimentation is termed as Phase-A. After that experimentation has been further carried out in two phases, *i.e.* Phase-B and Phase-C. L_{18} OA was used for designating the control log table for the main experimentation (Phase-A) and L_9 OA was used for Phase-B and Phase-C experimentation.

All experiments were carried out on an EDM machine (Model OSCAR MAX S 645). After the completion of experimental work, analysis of the results was done by using MINITAB version16 statistical software. Modeling and optimization of the results were carried out by using advanced statistical techniques. To study the surface integrity of the machined samples, metallographic analyses were performed by using SEM, EDX and XRD.

1.7 ORGANIZATION OF THE THESIS

The research work presented in this thesis has been divided into eleven chapters. Brief description of each chapter is given below:

Chapter – I Introduction

This chapter highlights the brief description of the non-traditional machining processes. Introduction to EDM process, working principle, historical background of EDM process and aspects of surface integrity has been discussed under this chapter. An overview of PMEDM process has been discussed in brief. A brief introduction to titanium alloys and cryogenic processing is also presented here. The chapter concludes with scope, overall methodology adopted for the study and organization of the thesis.

Chapter – II Literature review

This chapter presents an extensive review of research work carried out in the field of EDM, which leads to an understanding of various aspects of machining characteristics (MRR, TWR, SR, MH) and Surface Morphology. The impact of different machining input parameters on the machining characteristics has been discussed in detail. Importance of cryogenic treatment related to conventional machining and un-conventional machining is also presented here. A review of research work on EDM/PMEDM of titanium alloys and other materials are also discussed in this chapter. Application of experimental methodologies for planning and

analyzing the experiments has been given in detail. Various techniques for optimization of input parameters have also been discussed.

Chapter – III Design of study

This chapter presents the complete details of experiment conducted for this research work. Experimental setup and various measuring instruments were discussed in this chapter. The experimental plan is presented to achieve the objectives of the study based on the available literature. In the initial stage, pilot experimentation was performed to identify the control factors and their levels. Peak current, pulse-on-time and pulse-off-time were selected as the process variables for the pilot study. Taguchi methodology was applied for design of experiment by using a suitable orthogonal array for executing the experiments. Data was collected and analysis has been performed for MRR, TWR, SR and MH. Thereafter, the input parameters and their levels were selected for further experimentation.

Chapter – IV Main Experimentation (Phase-A)

This chapter explains the detail description of observations and their statistical analysis for main experimentation (Phase-A) to achieve the objectives of the study. During the main experimentation total of eight machining parameters with their levels were identified for Phase-A experimentation. MRR, TWR, SR and micro-hardness were identified as the response characteristics. ANOVA and S/N ratio were determined. The significance and the percent contribution of the associated input process parameters were found out. Optimal design conditions, main effects plots and theoretical prediction of response values are outlined for machining characteristics.

Analytical Hierarchy Process (AHP) approach was used for global optimization of response parameters such as MRR, TWR, surface roughness and micro-hardness.

Chapter – V Modeling of results

This chapter presents the mathematical modeling of MRR and TWR. Micro-modeling approach (*Buckingham π theory*) based on the macro modeling and thermo-physical properties of the workpiece and electrode material was applied to obtain the regression equation in terms of identifying input parameters. Artificial neural network (ANN) coupled with the Taguchi approach was applied for optimization and prediction of surface roughness and micro-hardness of workpiece.

Chapter – VI Effect of cryogenic treatment (Phase B & C)

This chapter discusses the effect of cryogenic treatment of workpiece and electrode materials on machining characteristics. Under this section, experimentation was carried out in two phases. The observed experimental results of shallow cryogenic treated and deep cryogenic treated were compared with the results of without cryogenic treated materials.

Chapter – XII Metallographic Analysis

In this chapter, discussions of surface properties of the machined samples at different settings of the input process parameters are presented. Metallographic analyses were carried out using SEM, XRD and EDS analyzer for both the workpieces and the electrodes. Analyses of different migrated elements were performed by using EDS analyzer. Formations of various phase/compounds were analyzed using XRD equipment. All these aspects are studied in detail under this chapter.

Chapter – XIII Conclusions and scope for future work

This chapter presents the summary of the research work in the form of conclusions and also suggested the recommendations for future work in this area.

This chapter is followed by references and appendices.

Chapter 2

LITERATURE REVIEW

2.1 INTRODUCTION

The EDM process has a very long historical background since 1770, but in the last two decades, a lot of research work has been carried out in its different areas resulting in enormous literature resource. More than enough research work has been carried out by the researchers on different machining aspects during EDM of various grades of steels, composites, ceramics, high strength, temperature resistant alloys, titanium and its alloys and many more needed to be explained critically. Moreover, machining characteristics and surface properties of workpiece were improved by using metallic powders with dielectric during the EDM process by the researchers. Effect of cryogenic treatment in the field of machining also has been studied by the researchers to improve the machining efficiency.
This chapter gives an overview of available literature on various aspects of the EDM process, active research areas and future trends of its applications.

2.2 CATEGORIZATION OF LITERATURE

The review of literature here in this section is divided into four major sections.

- EDM of titanium and its alloys
- EDM of other materials
- Cryogenics in EDM
- Modeling / optimization techniques used in EDM

2.2.1 EDM OF TITANIUM AND ITS ALLOYS

In this section, literature is focused on the EDM of Ti and its alloys to improve the machining performance. Here, in this section, the related literature is discussed in detail.

Soni and Chakraverti (1994) investigated the machining characteristics of Ti with a Copper-Tungsten (Cu-W) tool in terms of MRR, tool wear, and SR by varying current and

rotational speed of the tool. Experimental results showed that MRR improves in the case of rotating tool, because flushing and spark efficiency during the process was improved. But on the other hand, due to the rotation of the tool SR increased and tool wear also increased as the rotational speed of the tool is increased [38].

In another study, Soni (1994) performed the microanalysis of debris by using SEM, EDS and Electron Probe Microanalysis produced during machining of Ti-6Al-4V and die steel high carbon high chromium (T215Cr12). The results confirmed that the chemical composition of debris considerably differs from its original composition due to transfer of different elements from Cu-W tool and dielectric medium [39].

Lin et al. (2000) used two processes simultaneously, *i.e.* EDM with ultrasonic machining during machining of Ti-6Al-4V. Dielectric type, abrasive size, abrasive concentration, current and on-time were considered as the input parameters, while MRR, TWR, relative electrode wear ratio, SR and recast layer thickness as the response parameters. However, the combined process showed the remarkable improvement in MRR due to the larger size of craters, but slightly increases the SR and decreases the thickness of a recast layer than simple EDM. Further, better SR was observed with kerosene dielectric than distilled water in case of combined process [40].

Wansheng et al. (2002) utilized the ultrasonic vibration with EDM during machining of small and deep holes in Ti-6Al-4V workpiece and reported that the behavior of circulating dielectric flow significantly improved. Due to this issue machining stability was improved, resulting in better machining efficiency with improved surface finish [41].

Hascalık and Caydas (2007a) applied the post-treatment Abrasive Electrochemical Grinding (AECG) process on the machined surface to improve the surface integrity of Ti-6Al-4V. During the conventional EDM process, machined surface with a recast layer or with surface cracks were produced. SEM, EDS, XRD and SR analysis were performed during the study. The observed results explained that AECG process significantly improved the SR as well as eliminate the surface damages completely by selecting the suitable grinding parameters. But AECG process at low voltage produced the film of Titanium-Oxide (TiO), which was strongly attached to the machined surface, hindered the flow of current between the wheel and workpiece [42].

Hascalık and Caydas (2007b) in another study investigated the effect of different electrode materials such as Graphite (Gr), Copper (Cu) and Aluminum (Al) on various characteristics of surface integrity and other machining performance measures during EDM of Ti64 alloy. The results highlighted that MRR, SR, electrode wear and average thickness of white layer

had a tendency of increased by increasing the current density and pulse duration. SEM, EDS, XRD and micro-hardness analysis were performed during the study. Due to the formation of Titanium-Carbide ($Ti_{24}C_{15}$), the surface hardness of machined specimen was increased. Highest MRR was found with Gr electrode, followed by Cu and Al. Because of higher melting temperature of Gr, low tool wear was observed. Al electrode offered better surface finish than Gore and Cu electrode [19].

Ho et al. (2007) used solid and powder compacted (PM) electrodes for surface alloying or modification of Ti-6Al-4V in the presence of water based dielectric. The experimental result purposed that PM electrode produced greater alloying as compared to solid electrode. Thicker recast layer was observed with positive polarity PM electrode than solid. A significant increase in MH (up to 1100 HV) with negative polarity solid Cu electrode was observed, most likely due to formation of Titanium-Oxide ($TiO_{2)}$ [43].

Fonda et al. (2008) investigated the effect of thermo-electric properties of Ti-6Al-4V on the machinability. Owing to the poor thermal conductivity and electrical resistivity, the input energy must be controlled during the EDM process to avoid rapid heat generation in the workpiece. For this purpose, temperature measurement of machined specimens with various duty factors have been made to find out the optimal duty factor, so that productivity and quality of EDM process can be improved [44].

Caydas and Hascalik (2008) attempted to model the output characteristics such as Electrode Wear (EW) and White Layer Thickness (WLT) during machining of Ti-6Al-4V. Three control factors, namely T_{on}, T_{off} and I_p were varied at five levels during the experimentation. After making the comparison between experiment and model predicted results, strong relationship between two results were observed. Pulse current was observed as the highly influential input parameter that affected the both EW and WLT, while T_{off} had no significant effect on EW and WLT [45].

Pardhan and Bhattacharyya (2008) reported the polarity effect in micro machining of Ti64 alloy [46]. In another study, **Pardhan et al. (2009)** optimized the input parameters during micro-EDM of Ti-6Al-4V. ANOVA results indicated that I_p and T_{on} significantly affected the machining performance. A mathematical model was developed to show the percentage error within the acceptable limit [47].

Kao et al. (2010) optimized the machining characteristics (MRR, SR and Electrode Wear Ratio) collectively in EDM of Ti-6Al-4V by using GRA approach. L_9 (3^4) OA was used to assign the four identified factors such as open voltage, discharge current, pulse duration and duty factor. For lower EWR, higher MRR and better SR the combinations of optimal input

parameters setting were identified and after that for verification of the results confirmation experiment were performed. An improvement in EWR of 15%, MRR of 12% and SR of 19% were observed at optimal setting given by GRA [48].

Rahman et al. (2010) attempted to construct a mathematical model for MRR, TWR and SR and find out the optimal settings of input parameters (I_p, T_{on} and T_{off}) during machining of Ti-6Al-4V. It was concluded that the mathematical model results based on RSM are within the acceptable limits, *i.e.* approximately 4% [49].

Cheng et al. (2011) developed an axisymmetric 3-D thermo-physical model using finite element method in EDM of Ti-6Al-4V. Simulation of single spark discharge was performed by using ANSYS software. The observed results confirmed that, the model can efficiently predict the MRR [50].

Harcuba et al. (2012) modified the characteristics of a Ti64 specimen through surface treatment by using an EDM process. The EDMed specimen can be effectively used for manufacturing the bone, implants for medical applications [51].

Rahman et al. (2012) explored the effects of T_{on}, T_{off}, I_p and servo voltage on MRR, TWR and SR in EDM of TI-6Al-4V alloy. RSM technique was implemented for design of experiment. Artificial Neural Network (ANN) was adopted to construct the model for output characteristics. Sensitivity analysis highlighted that peak current had the highest influence on three output characteristics and observed that TWR initially decreases with T_{on}, increased with the increase in T_{on}. Moreover, MRR increases at higher values of I_p and long duration of on time [52].

Jabbaripour et al. (2012) explored the effects of pulse current, pulse-on- time and open circuit voltage on MRR, TWR and surface integrity aspects during EDM of Ti–6Al–4V. From the graphs, it can be clearly seen that MRR increased with increase in T_{on}, but its effect was smaller in comparison with current and voltage. Though, TWR was increased as T_{on} increases, but increasing T_{on} in the higher range, less effect on TWR was observed. Further, it was also observed that as pulse current increases, micro holes, pits, crack dimensions, larger and deeper cracks increases the surface inequalities. Moreover, due to the formation of TiC, micro-hardness of recast layer was observed in the range 1100 and 1310 HV, which was appreciably higher than the hardness of HAZ and bulk material [53].

Meena and Azad (2012) applied Taguchi method and GRA approach for multi-objective optimization of input parameters (current, voltage, frequency, and pulse width) in µEDM of Ti-6Al-4V work material by using Tungsten Carbide tool. MRR, TWR and OC were taken as

the machining characteristics. Significant improvements in output results were obtained, when experiments were conducted at parameter setting given by GRA [54].

Tang and Du (2014) used tap water as the dielectric medium due to health and environmental point of view in EDM of Ti-6Al-4V. A standard L_9 OA was selected to assign machine parameters like gap voltage, discharge current, pulse duty factor and lifting height. MRR, EWR and SR were selected as objective parameters. For multi optimization of parameters, GRA with Taguchi method was applied. The obtained results indicated that EDM with tap water increased the machining rate, decreased the machining cost, avoid the operators and the environment from harmful effects [55].

Porwal et al. (2014) developed an integrated model for hybrid optimization of responses (MRR, TWR and hole taper) in μEDM of Ti-6Al-4V alloy. Gap voltage, the capacitance of capacitor was considered as the machining variables. Further, it was concluded that the predicted and optimized results were within reasonable accuracy under different machining conditions [56].

Shen et al. (2014) reported that energy distribution highly affected the objectives of the study in EDM of Ti-6Al-4V. The energy distribution has been investigated by a novel method at different parameters setting, including inter-electrode distance, pulse duration, polarity, and electrode shape. The obtained experimental results explored that energy distribution characteristics were highly affected by the power density and more energy was distributed into the anode than into the cathode [57].

Palanisamy et al. (2014) attempted to optimize the EDM input parameters (T_{on}, T_{off}, I_p) after machining of Ti64 alloy by using OA and GRA techniques. MRR, TWR and SR were identified as the response characteristics for optimization simultaneously and observed the significant improvement [153].

Khan et al. (2015) investigated the surface finish characteristic of titanium alloy (Ti-5Al-2.5Sn) through an EDM process. During the study, various electrical parameters (T_{on}, T_{off}, I_p and servo voltage) and different electrodes (Cu, Cu-W and Gr) were selected to explore their effect on SR. The experimental results revealed that SR decreases with decrease in I_p and T_{on} and increases with servo voltage. Study further suggested that better surface texture could be obtained by using Cu-W electrode at low discharge energy [58].

The several researchers during EDM of titanium and its alloys used the different metal powders with dielectric liquid to enhance the machining characteristics. The results of some of the studies are discussed below:

Chow et al. (2000) studied the effect of three dielectric fluids; (i) kerosene mixed with Al powder, (ii) kerosene mixed with SiC powder and (iii) simple kerosene oil in micro-slit machining of Ti-6Al-4V with thin Cu diskette electrodes on different machining performances. The observed results indicated that material removal depth and SR were increased with suspended Al or SiC powder kerosene dielectric as compared to simple kerosene oil. Low TWR and material removal depth were observed, when plain kerosene was used as the dielectric medium (without powder) [59].

Yan et al. (2005) explored the effect of urea solution (10g/l) mixed distilled water dielectric on the pure titanium by using the Cu electrode. Peak current, dielectric type and pulse duration were selected as the input parameters, whereas MRR, EWR and SR identified as the objective functions. Nitrogen was decomposed from urea mixed dielectric and transferred to the machined surface, resulted in the formation of the hard layer of Titanium Nitride (TiN), causing in good wear resistance surface. This TiN compound increased the micro-hardness of the machined surface. It was also concluded that the urea mixed dielectric increased the MRR, EWR as well as deteriorated the surface finish when the amperes of peak current were increased [60].

Chow et al. (2008) observed that the electrical conductivity of dielectric (pure water) increased due to suspended SiC powder, resulted in increased the spark gap which helps in easily removal of debris, as a result MRR increased in micro slit EDM of Ti64 alloy. Moreover, SiC powder mixed dielectric bridge the gap between the two electrodes; disperse the discharge energy that improves the surface finish effectively than pure water [61].

Kibria et al. (2010) addressed the issues of various dielectrics during micro-EDM of Ti-6Al-4V. As reported by the experimental results, higher MRR and TWR were observed with deionized water than kerosene oil. In addition to that, MRR was increased when Boron-Carbide (B_4C) powder was used with deionized water, but TWR decreased with B_4C powder mixed kerosene. MRR and TWR were observed higher in deionized water than kerosene, because of the formation of Titanium-oxide (TiO_2) on the machined surface. Due to low melting point of (TiO_2), it melts with low discharge energy than high melting point Titanium-Carbide (TiC) which was produced due to cracked carbon from kerosene [62].

Kuriachen and Mathew (2015) experimentally investigated the effect of SiC powder added dielectric on Ti-6Al-4V work material machined with tungsten carbide tool. During the study powder concentration, voltage and capacitance were considered as the input variables, whereas MRR and TWR response characteristics. From the results significant improvement in MRR and TWR were observed with powder concentration of 0.5g/l [155].

2.2.2 EDM OF OTHER MATERIALS

In this section, literature review on the EDM of several other materials (non titanium) like different types of die steels, tool steels, composites, aluminum alloys and many more are reported. Brief description of few selected research papers is given below:

Pandey and Jilani (1987) studied the machining characteristics of three grades of cemented carbide materials using commercial available Cu electrode when EDM was performed in presence kerosene Oil. [63].

Yarlagadda et al. (1993) used the EDM process to make electrodes using stereo lithography technique of rapid prototyping [159].

Mohri et al. (1993) attempted to improve the surface properties of Carbon Steel and Al workpiece with Cu, Al, WC and Ti electrodes submerged in hydrocarbon dielectric oil. From the study, it was observed that surface layer and its characteristics significantly changed by the migrated materials from the electrode. Significant improvement on machined surface was observed [64].

Muller and Monaghan (2000) performed the machining of SiC particle reinforced aluminum metal matrix composites by applying different non-conventional machining process namely EDM, laser cutting and abrasive water jet to investigate its machining characteristics [160].

Tsai and Wang (2001) developed a mathematical model by using dimensional analysis of surface finish quality characteristic based upon the significant input parameters. Best fitted curve showed that the developed model is reasonably accurate [65].

Lee (2003) evaluated micro-structure and phase transformation phenomenon of a recast layer of Fe-Mn-Al alloy, and reported that as pulse duration increases thickness of recast layer increases. Traces of copper can be seen on the recast layer due to melting of Cu electrode, and amounts of migrated Cu elements were affected by the pulse duration and discharge current [66].

Singh et al. (2004) reported the effects of pulsed current on MRR, SR, overcut and tool wear when hardened and tempered EN-31 tool steel was machined with Cu, Cu-W, Al and brass electrodes. The experimental results highlighted that pulsed current significantly affected the performance of EDM, and further concluded that the best machining were obtained when Cu and Al electrode were used than Cu-W and brass [67].

Ramasawmy et al. (2005) correlated WLT with 3D surface texture parameters in EDM of M300 stainless martensitic chromium tool steel. Pulse duration and current two major factors were selected to investigate their effect on the white layer thickness. Current has slightly higher effect than pulse-on-time, on the dimension of the crater *i.e.* surface roughness [68].

Lin et al. (2006) determined the influence of process variables during machining of SKH 57 high-speed steel on various output parameters namely MRR, EWR and SR. A well known L_{18} OA was used to design the experimentation matrix. The significant control factors were identified from the ANOVA that affected the machining performance [69].

Marafona (2007, 2009) claimed that Electrode Wear Ratio (EWR) was affected by the change in elemental composition of black layer with an interaction of input parameters during EDM of high carbon steel with Cu-W electrode, when both tool and workpiece submerged in hydrocarbon dielectric oil. Migrated carbon from dielectric was deposited on the bottom surface of the tool in layer form, called black layer. Further, it was observed that black layer mixture of different materials (C, Fe, Cr, V, Mo) changes the thermal conductivity of Cu-W electrode, resulted in improved EWR [70-71].

Chiang and Tsai (2008) reported the effect of silicon (Si) variation (4 to 29%) in Al-Si alloy workpiece on re-solidified layer. Layer thickness, surface roughness and ridge density of the re-solidified layer was considered as the performance criteria. Experimental results explored that increase in Si particles has tendency to increase the thickness of layer and SR [72].

Dvivedi et al. (2008, 2010) experimentally observed that MRR increases with an increase in current and on-time up to a certain optimal range and after that it starts to decrease during EDM of cast Al 6063 SiCp composite. The SR of machined surface was highly affected by the pulse current followed by the flushing pressure. Pulse current was observed as a more significant factor than other process parameters affecting the performance measures [73-74].

Rao et al. (2009) used ANN and GA techniques to construct a hybrid model for optimization of SR. Different work materials were machined at various settings of peak current and voltage. As reported by the study, a better relationship between the experimental and network model results were obtained. Experimental results showed that better results can be obtained

in EDM of titanium when current up to 15A was used, while better surface finish was observed with voltage 40V and current 16A [75].

Garg et al. (2010) studied the eighty six research papers of various authors to review the issues on metal matrix composite materials in sinking EDM and wire EDM. The main aim of this review paper is how the productivity, efficiency, accuracy and capability of the machining performance can be improved, so that product of better quality can be produced [76].

Patel et al. (2010) developed the ceramic (Al_2O_3-SiC_w-TiC) materials and machining was performed by varying the values of pulse-on time, discharge current, gap voltage and duty cycle to investigate their effect on machinability *i.e.* MRR and SR. The multiple performances MRR and SR were optimized by using GRA approach. Out of four parameters, duty cycle and discharge current were identified as the most influential process variables [77].

Rahman et al. (2011) presented the experimental results in terms of MRR, TWR and SR during EDM of austenitic stainless steel (grade 304) with positive polarity Cu electrode to assess the effectiveness of machining process. The experimental results revealed that all the three response parameters highly affected by the T_{on} and I_p. Further, the results showed that MRR and SR were increased almost linearly with increase in I_p for all values of T_{on}. Moreover, TWR also increased with increase in I_p and the effect of T_{on} on TWR is opposite of current [78].

Patel et al. (2011) applied the RSM technique to develop the models for MRR, EWR and SR in EDM of Al_2O_3–SiC_w–TiC. The ANOVA results explored that parameters, namely current, pulse-on-time, and duty cycle highly affected the MRR and EWR, while SR was significantly affected by the current and on-time. The surface characteristics have also been analyzed by using SEM analyzer [79].

Zhang et al. (2013) proposed that EDM in water-in-oil emulsion dielectric with longer T_{on} and high I_p could lead to achieve higher MRR compared to kerosene dielectric. Due to use of water-in-oil emulsion as dielectric, low carbon was adhered to the electrode surface when compared with kerosene, thus higher REWR was obtained [80].

Singh et al. (2013) modified the machine set up so that electrodes can rotate during EDM of Al6063/10% SiC, and noticed the effect of tool geometry on MRR. Practically, it has been found that different tool geometries highly affected the MRR [81].

Mohanty et al. (2014) experimentally investigated the machining characteristics of Inconel 825 material used in the highly corrosive environment. I_p, duty factor, and T_{on} were

considered as the variable factors against MRR, SR, radial over-cut and surface crack density. GRA with Taguchi method was used for multi-objective optimization. Peak current was observed as the most influencing factor for performance measures [82].

Kiyak et al. (2015) investigated the effect of the density of discharge energy on the machining performance evaluated in terms of MRR, EWR, SR of a workpiece as well as tool during machining of AISI 1040 steel with Cu electrode. During the EDM, T_{on} and T_{off} were varied at two levels, whereas other two parameters current and voltage were fixed. It was concluded from the observed results that the density of spark energy plays a significant role in selecting the suitable machining parameters for better results [129].

The many researchers during EDM of tool & die steel materials, composites, aluminum alloys and many mores used the various powders with dielectric liquid to study the effects powder mixed dielectric on different machining characteristics. The related results of some studies are discussed below:

Jeswani (1981) explored that graphite (Gr) powder mixed kerosene dielectric increased the spark gap for discharge initiation and lower down the breakdown voltage of the dielectric. Thus, stable the machining process, which further improves the MRR [83].

Mohri et al. (1988, 1991) and Narumiya et al. (1989) studied the concentration effect of Si, Al and Gr powders on the machining performance. The analyzed results highlighted that the gap distance increases during PMEDM process due to powder concentration and it was larger in the case of Al powder mixed dielectric. Further, it was also concluded that the better surface finish was obtained when Si and Gr powders with low concentration were used for machining [84-86]

Ming and Hi (1995) purposed that the productivity of EDM process could be raised when additive suspended kerosene was used as dielectric. Moreover, by using the additive mixed dielectric, alloy elements can be increased. Due to this phenomenon, micro-hardness of machined surface was increased, reduced the molten metal layer thickness and decreased the cracks on the machined surface [87].

Furutani et al. (2001) modified the surface properties of carbon steel (AISI-1049) with green compact electrode by adding Ti powder in the dielectric medium. A thick layer of Titanium-Carbide (TiC) was formed on the machined workpiece surface with a hardness of 1600HV [88].

Uno et al. (2001) purposed a new surface modification technology by mixing Nickel (Ni) powder with kerosene to obtain high wear resistance surface in EDM of alloy tool steel (SKD 61) by using Ti electrode. Hard and high wear resistance surface with better surface finish was obtained in the case of Ni powder suspended dielectric than plain dielectric *i.e.* without Ni powder. Hard layer of TiC was formed during a process, which further produced the high wear resistance surface due to transfer of carbon [89].

Pecas and Henriques (2003) attempted to improve the quality of AISI H13 die steel, machined surface by using Cu electrode of different dimensions in Si powder mixed dielectric. In this study, improvements in performance of typical EDM were compared with Si powder mixed dielectric in terms of surface quality and process time measurements. The positive influence of Si powder was observed in the form of less process time with improved surface quality [90].

Wu et al. (2005) added surfactant and Al powders in kerosene to investigate their effect on SR in EDM of SKD 61 workpiece machined with Cu electrode of Φ 25mm. During the experiments polarity of the electrode (+ve and –ve), T_{on}, open voltage, I_p, gap voltage and concentration of surfactant were varied. Due to mixed level of input parameters, L_{18} OA was used to assign the control factors and run the experiments. An improvement in SR up to 60% was observed than pure dielectric [91].

Kansal et al. (2005, 2006) employed the RSM for design of experiments in Si powder mixed EDM. I_p, T_{on}, duty cycle and powder concentration were identified as the input parameters. MRR and SR were chosen as the performance measures. Added Si powder enhanced the MRR and surface finish as observed by the experimental results. Higher MRR may be obtained with more concentration of added Si powder. Current and amount of powder mixed with dielectric were observed as the most important variables those highly affected the performance criteria [92-93].

Pecas and Henriques (2008, a&b) reported the effect of Si powder and dielectric flow on the morphology of machined surface during PMEDM process. The experiments were performed at different concentration level (kerosene-Castrol SE Fluid 180) and flushing flow rate with Cu electrode. After analyzing the results, it came to know that Si powder suspended dielectric highly affected the surface morphology in a positive manner by reducing of crater's dimensions, WLT and SR. [94-95].

Furutani et al. (2009) performed the machining of AISI 1049 workpiece with a 1mm diameter copper electrode in the presence of the powder mixed dielectric. Thereafter, they studied that how pulse duration and discharge current affected the TiC deposition process.

Due to formation of TiC compound a maximum surface hardness of 2000Hv was obtained. Analytical results showed that the discharge energy was the key factor that affected the thickness of TiC layer [96].

Kumar and Singh (2010) examined the surface properties of OHNS die steel parts machined with a Cu electrode in Mn powder mixed kerosene liquid. The experimental result showed the incredible improvement in machined surface hardness by 73% with no micro-cracks. Significant increase in Mn and C elements was confirmed through the quantitative analysis of chemical composition [97].

Kumar et al. (2010) identified the significant factors and investigated their effect during EDM of EN-24 tool steel by using Cu tool and Si powder (2 g/l) mixed kerosene oil. GRA and OA have been used for optimization of input parameters, namely powder concentration, I_p, T_{on}, and duty factor. The significant improvement in gray relation grade was observed by 10% at optimal setting of input process parameters [98].

Kumar and Davim (2011) reported the role of Si powder during machining of metal matrix composites. Experimental results indicated the significant improvement in performance Characteristics in term of higher machining rate with lower surface finish [99].

Ojha et al. (2011) conducted the experiments on EN-8 steel to analyze the influence of Cr powder mixed dielectric on MRR and TWR output parameters. The RSM was used for experimentation and analysis of the obtained experimental data. Diameter of electrode, powder concentration, I_p and T_{on} were identified as the process variables to explore their effect on MRR and TWR. Key factors and their levels affected the machining performance were determined after analyzing the results [100].

Batish et al. (2012) investigated that surface modification of parts can be achieved through the material deposition process in powder suspended dielectric. Due to transfer of different materials, characteristics of machined surface were modified, which was measured in terms of micro-hardness. Results showed that 80% increase in micro-hardness was observed. Also, the analysis of the experimental results pointed out that the best results were obtained with Cu tool material on EN31 and H11 die steel, while Cu-W tool was better for HCHCr die steel. In addition to the electrode material, graphite powder highly increased the micro-hardness as compared to the aluminum powder on all three types of die steel [101].

Bhattacharya et al. (2012) identified the optimal input parameter settings of seven control factors on die steel materials (EN31, H11and HCHCr) during the PMEDM machining. The MRR was influenced by the T_{off}, T_{on} and I_p. From the experimental observed results, it can be seen that SR was significantly affected by T_{on}, I_p, powder type and the combined effect of

workpiece, powder, and tool material. The study also purposed that modification of machined parts can be done by using powder mixed dielectric. Copper electrode with Al powder increased the MRR, where as graphite powder reduced the MRR but improved the surface finish [102].

Kumar (2014) improved the surface finish and micro-hardness of hot die steel material H13 by using Gr powder suspended dielectric and copper electrode. By observing the results significant improvement of 42% in micro-hardness and 68% in surface finish was observed [152].

Singh et al. (2015) studied the influence of W powder mixed dielectric on 6061/10%SiC composite workpiece material by changing the values of T_{on}, T_{off}, I_p and gap voltage. After analyzing the results an increase of 48.43% in MRR was noticed in the case of W powder mixed kerosene dielectric than simple. Moreover, depositions of W and C elements were observed in recast layer [156].

2.2.3 CRYOGENIC IN EDM

Performance of EDM process very much depends upon the electrical and thermal properties electrode materials *i.e.* tool/job. CT has a background of improving the properties of materials, namely mechanical, electrical, and thermal. Presently, very few studies have been carried out by the researchers to apply a cryogenic cooling effect on materials in conventional EDM process and obtained the significant improvements in machining performance. The related literature has been discussed below:

Zhisheng et al. (2003) applied the DCT on the electrode in spot welding and found significant increases in electrode life from 550 to 2234 welds due to significant improvement in thermal and electrical conductivity electrode [103].

Yildiz and Nalbant (2008) reviewed 96 research papers of various researchers on cryogenic cooling related to machining processes. In cryogenic cooling, liquid nitrogen is utilized as a cryogenic coolant. Effects of cryogenic cooling on cutting tool and workpiece properties in different characteristics were highlighted in this paper. In view of that, it has been considered as one of the most favorable technique for improving the machinability [104].

Abdulkareem et al. (2009) reported the cooling effect of Cu electrode during EDM of Ti-6Al-4V alloy in kerosene dielectric with different input parameters (current intensity, T_{on}, T_{off} and gap voltage). Investigations have been made on electrode wear and SR of by injecting the

liquid Nitrogen (LN_2) inside the special designed Cu electrode. Use of LN_2 as coolant media improves the thermal and electrical conductivities of the electrode, in this manner reducing heat from the electrode. Therefore, wear of electrode is reduced due to reduction in melting of electrode material. Highest reduction in TWR of 27% and 8% improvement in SR was achieved by this cooling process [105].

Gill and Singh (2010) investigated the effect of DCT Ti6246 titanium alloy conducted at a temperature of LN_2 (-196^0C) on the machinability during Electric Discharge Drilling (EDD). Accuracy of holes drilled in DCT Ti6246 titanium alloy and non-treated Ti 6246 alloy using a 10mm diameter of the Cu electrode has been compared to SR and over cut. Machinability of DCT alloy appreciably improves up to 8.5% for MRR, 34.78% for TWR, and 30.16% for WR of different machining times, due to increase in thermal and electrical conductivities of the workpiece materials [17]. In addition to that, **Gill et al. (2010)** also suggested that cooling temperature, soaking time, heating rate and cooling rate were recognized as the most important factors in cryogenic treatment that highly affected the material properties [16].

Yildiz et al. (2011) claimed 20-30% increase in MRR of cold and cryogenically treated beryllium copper alloy workpiece in EDM process. Small variations in TWR, SR and average white layer thickness were observed, when a workpiece subjected to cold and cryogenic temperature [106].

Srivastava and Pandey (2011) experimentally investigated the effect of liquid nitrogen cooled Cu electrode on the performance of EDM process. The observed results reported the reduction in SR, EWR, and better shape retention of electrode [107].

Singh and Singh (2011) reported the role of CT in EDM of titanium and compared the performance of cryogenic treated with un-treated tool and workpiece materials. The experimental study showed significant improvement in machining characteristics. The improvement in MRR by 60.39%, TWR by 58.77%, SR by 7.99% and dimensional accuracy by 80% were observed with CT [108].

Srivastava and Pandey (2012) compared the results of machining (MRR, EWR and SR) by using normal, cryogenically cooled and ultrasonic assisted cryogenically cooled electrodes (UACEDM). The results indicated that EWR and SR in UACEDM process were observed significantly lower than simple EDM, where as MRR was at par in case of simple EDM. Better surface integrity was obtained by the UACEDM process than the simple EDM process [109].

Kumar et al. (2012) experimentally investigated that DCT Cu electrode significantly improved the SR of the workpiece (Inconel 718 super alloy) when graphite powder (6g/liter) was used during the EDM process than none treated electrode [110].

Jafferson and Hariharan (2013) compared the experimental results of both cryogenically treated and without cryogenically treated micro electrode in micro EDM of AISI 304 stainless steel by using different electrode materials (brass tube, copper tube and tungsten rod). All the electrodes were cooled at -185^0C by passing liquid nitrogen. From the experimental results, significant reduction of 58%, 51% and 35% in TWR for tungsten electrode, brass and copper electrode respectively were observed. Electrical conductivity, micro-hardness and average crystallite size of all the three electrodes were exceptionally improved with CT [18].

Jatti and Singh (2014) investigated the effect of DCT NiTi memory on machininability in terms of MRR and TWR during the EDM process. Significant improvement in electrical conductivity of workpiece was observed after DCT, which showed the increase in MRR of 19% and marginal variations in TWR.

2.2.4 MODELING / OPTIMIZATION TECHNIQUES USED IN EDM

The analytical and statistical methods have been used to find out the optimal settings of input parameters so that better results can be obtained. In general regression analysis, S/N ratio and ANOVA are used to analyze the experimental results. Several researchers have applied the Taguchi technique for design of experiment (DOE) as well as for the optimization of input parameters. Taguchi method can be applied for analysis of each response characteristic and therefore, process parameter settings can be optimized for each individual characteristic at a time [30, 69, 71, 97, 101, 102 and 111].

Wang et al. and Bharti et al. (2003, 2012) developed and applied a hybrid ANN with Genetic Algorithm (GA) for modeling and optimization of input parameters in EDM for MRR and SR [112-113].

Kao and Tarng (1997) applied the Feed-Forward Neural Network in EDM to establish the relationship for inter electrode gap signal and pulse [114]. Tzeng and Chen (2007) used Fuzzy Logic technique coupled with a Taguchi methodology for optimization of different process parameters [115].

Assarzadeh and Ghoreishi (2008) developed a Back Propagation Neural Network (BPNN) model to assess the MRR and SR during EDM [116]. Markopoulos et al. (2008) used ANN model for predicting SR in EDM of different grade of steels [117]. Fonda et al. (2008) used RSM to find the best optimal solution for MRR, EWR, SR and gap size. The effect of thermo-electrical properties of Ti-6Al-4V was investigated during EDM [44].

Rao et al. (2009) used two techniques ANN and GA simultaneously to develop a hybrid model for optimizing the SR of different work materials [75]. Rahman et al. (2010) developed a mathematical model to determine the effect of process variables (I_p, T_{on}, T_{off}) by using Cu-W electrode during EDM of Ti-6Al-4V [49].

Tzeng and Chen (2013) applied a hybrid method (BPNN, GA, and RSM) to determine optimal input parameter settings for EDM on MRR, Relative Electrode Wear Ratio (REWR), SR and purposed that GA methodology predict the results in better ways [118]. Sidhu et al. (2013) implemented ANN model to predict the residual stresses during EDM of an Aluminum metal matrix composite [119].

Muthukrishnan and Davim (2009) tested the experimental results by applying ANOVA and ANN techniques during machining of MMC [120]. Olabi et al. (2006) applied Back Propagation ANN and Taguchi approach for design of experiments during laser welding of steel plates to find out the optimal combination of parameters [121]. Dobrzański at el. (2012) applied ANN technique for modeling of properties of PVD and CVD coatings [161].

Sidhu et al. (2013) optimized the results in EDM of metal matrix composite (MMC) by applying the lexicographic goal programming technique to predict the best combination of input parameters for machining of MMCs [122].

Jeswani (1979) applied Dimensional Analysis technique to develop a mathematical model for tool wear response in the EDM process [123]. Yahya and Manning (2004) formulated the mathematical equation using dimensional analysis on MRR [124].Patil and Brahmankar (2010) used Buckingham π theory on metal matrix composites in wire-EDM to construct a mathematical model for output [125]. Singh and Khamba (2009) developed a mathematical model for TWR and SR in USM process using dimensional analysis approach [126-127]. Kumar and Khamba (2010) constructed a micro- mathematical model based on outcomes of Taguchi methodology to predict MRR in USM process by applying the dimensional analysis [128]. Franco et al. (2004) presented a numerical model for predicting surface roughness as a function of input parameters in face milling [168].

2.3 IDENTIFICATION OF RESEARCH GAPS

From the literature related to EDM process, it was concluded that the effect of electrical and non-electrical input parameters were discussed on machining performance. The effects of different powders on surface characteristics were also discussed. In addition to that, effect of cryogenic cooling in machining explored in the available literature. Different techniques for optimization of input parameters, prediction of theoretical results were also discussed in detail.

After a detailed study of the research work published in various journals related to EDM process, it was observed that few studies have been reported on machining characteristics of different grades of titanium alloy; (i) Ti alloy, ASTM grade II, TITAN 15, (ii) Ti-5Al-2.5Sn alloy, ASTM grade VI, TITAN 21 and (iii) Ti-6Al-4V alloy, ASTM grade V, TITAN 31. Moreover, it is also came to know that although several studies have been reported on machining of titanium with EDM, but the effect of shallow and deep cryogenic treatment of titanium alloys as well as electrodes has not been explored. Also, the effect of Manganese (Mn) and Tungsten (W) powder mixed with EDM oil has not been reported in the literature. Though, very little work has been reported on evaluation of surface integrity of the TITAN 31 (Ti-6Al-4V), but there is almost no study reported on surface integrity of TITAN 15 (Ti), and TITAN 21 (Ti-5Al-2.5Sn) using EDM process. Material transfer mechanism and metallurgical aspects of the machined surface of titanium alloys is also missing in the available literature. Moreover, no work has been stated on the surface characteristics of the electrodes after EDM.

All these aspects have been addressed in this research work.

Chapter 3

DESIGN OF STUDY

3.1 INTRODUCTION

In any type of manufacturing process, selection of machine and tool is the first and important step. It is well known that the dimensional accuracy of the parts largely depends upon these two entities. The selection of appropriate process parameters or control factors is the next important aspect of machining. These control factors may be varied over different values during experimentation with an aim to evolve a set of parameters and their values which will result in optimizing the objectives. The individual value of a control factor is termed as its. The selection of different control factors and their levels depends upon the desired results *i.e.* output characteristics. Therefore, the selection of the parameters and their levels is a challenging task for the researchers to obtain optimal machining results and output characteristics. Experimentation to determine an optimal value of input parameters is generally done in two steps; pilot experimentation and main experimentation. Pilot experiments are performed with some identified input parameters to determine their effect on the responses before going to main experimentation. In this work material removal rate (MRR), tool wear rate (TWR), surface roughness (SR) and micro-hardness (MH) were the response parameters. The input parameters and their classification were as under:

(i) ***Electrical parameters :*** Current, pulse-on-time, pulse-off-time, electrode polarity, supply voltage, duty cycle.

(ii) ***Nonelectrical parameters:*** Flushing method, flushing pressure, lift time, workpiece and tool materials.

(iii) ***Dielectric fluid:*** Type and properties of dielectric medium, size and concentration of suspended powders

The effect of all these parameters on machining performances in EDM has been discussed in detail in Chapter-2 (*literature review*). The review of literature brought out that the following factors directly influence the performance of an EDM process:

(i) Current

(ii) Pulse-on-time

(iii) Pulse-off-time

(iv) Dielectric fluid

(v) Workpiece materials

(vi) Electrode materials

(vii) Cryogenic treatment of workpiece and or tool materials

The effects of all these parameters on machining performance have been investigated under this research work. The levels and range of the identified input parameters were finalized on the basis of pilot experimentation.

3.2 EXPERIMENTAL SETUP

3.2.1 DESCRIPTION OF THE EDM MACHINE

The entire experimental work was carried out on commercial type CNC Electric Discharge Machine (Model OSCARMAX S 645 CMAX manufactured by OSCAR EDM Co. Ltd., Taichung, Taiwan) available at Central Institute of Hand Tools, Jalandhar, Punjab, India (A Govt. of India society). A pictorial view of the machine is shown in Figure 3.1. During the machining process a pre-set level (minimum 40 mm above sparking point) of dielectric is maintained with the dielectric level indicator. If the level falls below this setting due to any reason, the machine is switched off immediately. All the process parameters can be set from the computerized control panel of the machine located on the right hand side as shown in Figure 3.1. The important technical specifications of the machine are summarized in Table A3 (*Appendix A3*).

3.2.2 SETUP DETAILS

FERROLAC 3M EDM oil was used as a dielectric, which is supplied and produced by the OSCARMAX, EDM Company. It's very high breakdown voltage (BDV) makes it ideally suited as a dielectric fluid. It has good dielectric strength, is safe to use due to high flash point, is non-corrosive and has less topping up requirement. The important technical specifications of the dielectric fluid and properties are summarized in *Appendix Table A2.* It is well known that titanium has poor magnetic properties, so it cannot be directly fixed or held on the machine table for machining. Thus, to hold the titanium workpiece properly, a fixture as shown in Figure 3.2 was developed in the workshop. Before conducting the experiments, both workpiece and tool were polished with different grades of emery papers to ensure flatness. The step by step procedure of EDM operation is shown in Figure 3.2. First of all alignment of electrode was done with a dial indicator with the workpiece surface as shown in Figure 3.2 (a & b). Both workpiece and tool were submerged in dielectric medium and flushing nozzles were placed properly inside the dielectric tank as shown in Figure 3.2 I. Figure 3.2 (d) shows the actual operation performed on the machine.

Figure 3.1: Pictorial View of EDM Machine used for the Experimentation

Figure (a)

Figure (b)

Figure (c)

Figure (d)

Figure 3.2: (a) Alignment of Electrode, (b) Tool and Workpiece set-up, (c) Tool and Workpiece Sink in Dielectric Liquid and (d) Actual Operation Performed in Dielectric

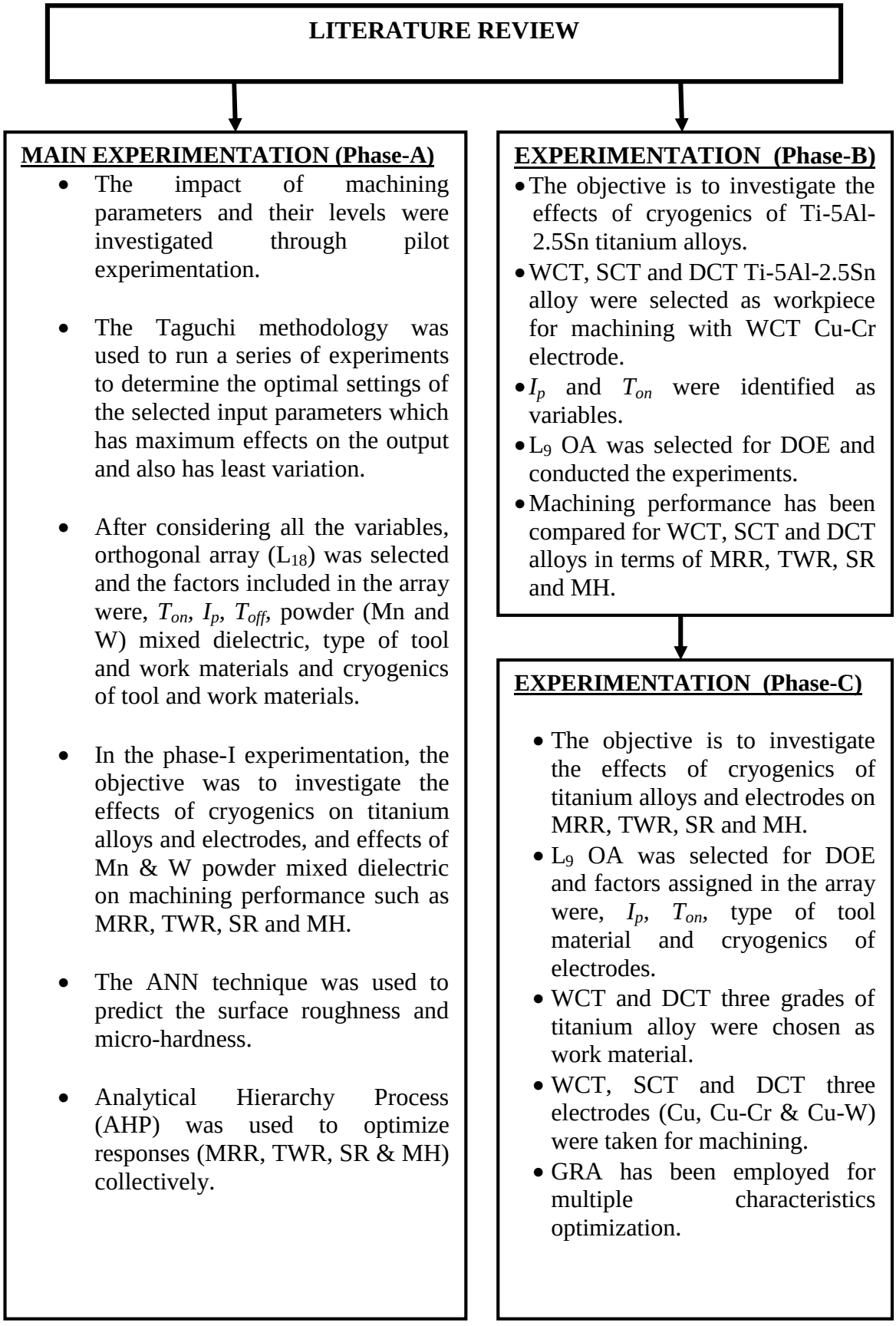

Figure 3.3: Detailed Description of Experimental Design

3.3 DETAILED DESCRIPTION OF EXPERIMENTAL PLAN

To achieve the objectives of the present study, the entire experimental work was planned to conduct experiments and drawn in the form of layout as shown in Figure 3.4 (a). First of all pilot experimentation has been conducted on Ti-6Al-4V workpiece with Cu electrode to study the effect of input parameters (I_p, T_{on}, T_{off}) on responses such as MRR, TWR and SR. Based on the results of the pilot study and the literature review main experimentation (Phase-A) was planned and performed by taking the eight process parameters with mixed type L_{18} OA. Thereafter, more experimentation was carried out in two phases, *i.e.* Phase-B and Phase-C with standard L_9 OA. The detailed description of experimental work is presented in Figure 3.4. In addition to that, Figure 3.3 presents the detailed description of experimental design which was drawn on the basis of the available literature survey.

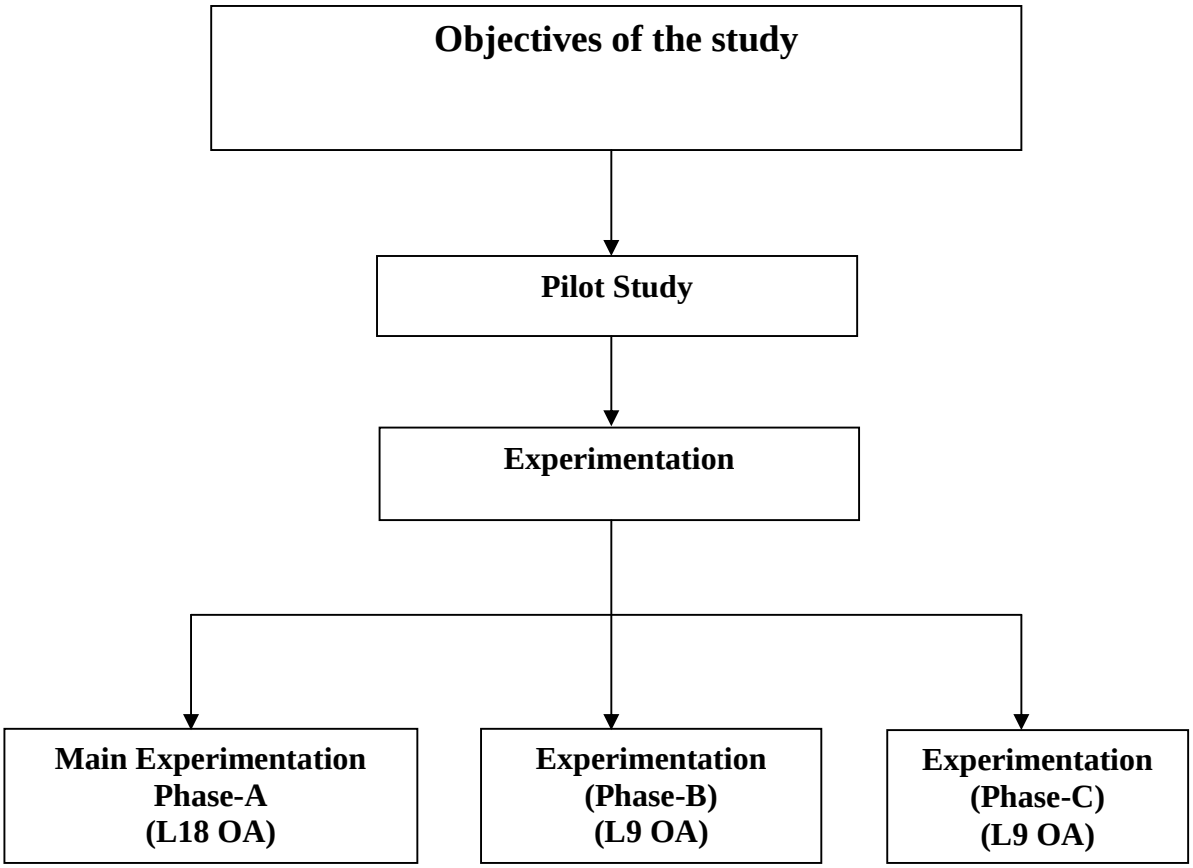

FIGURE 3.4 (a): Experimental Layout

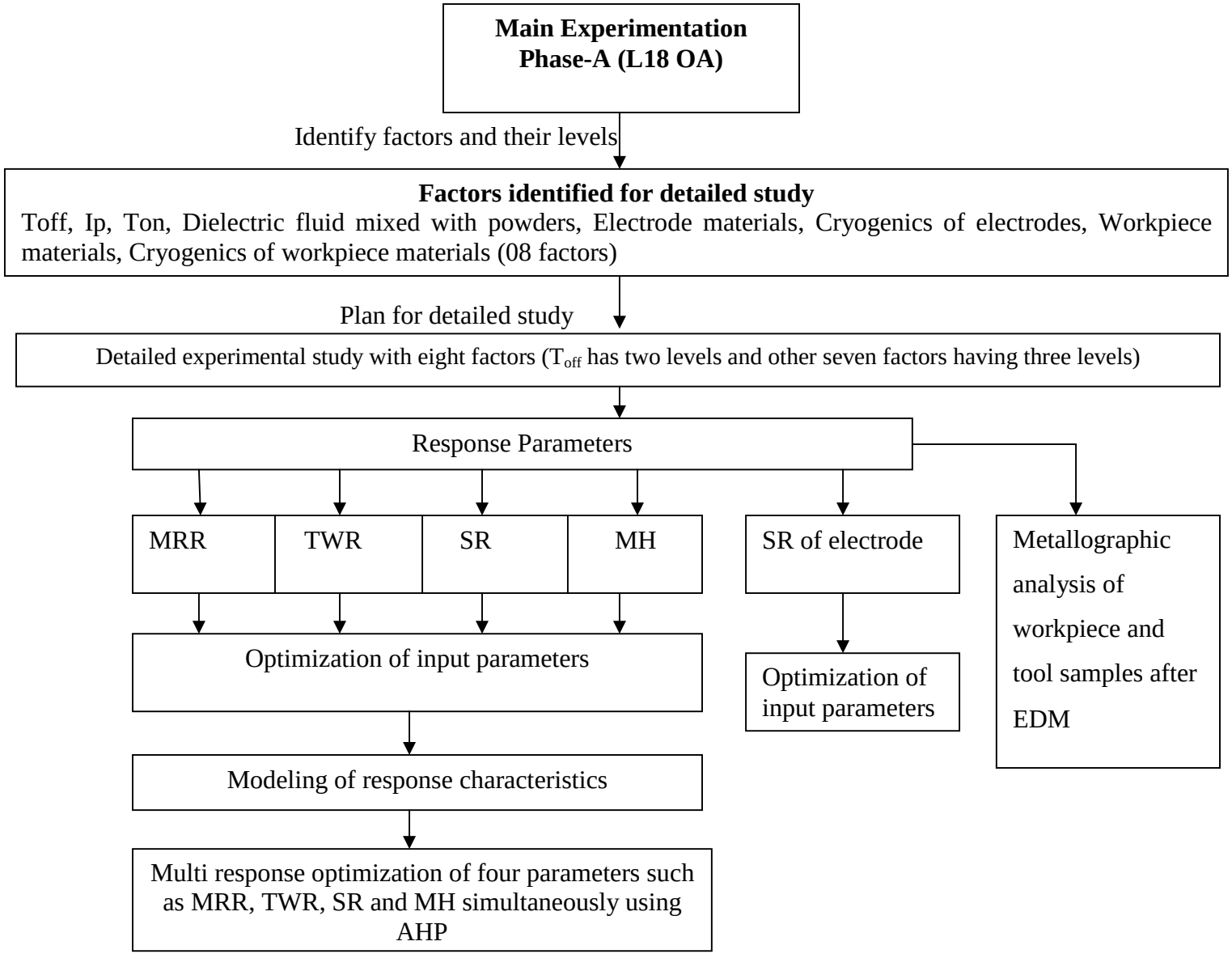

FIGURE 3.4: (b) Experimental Layout (Main Experimentation Phase-A)

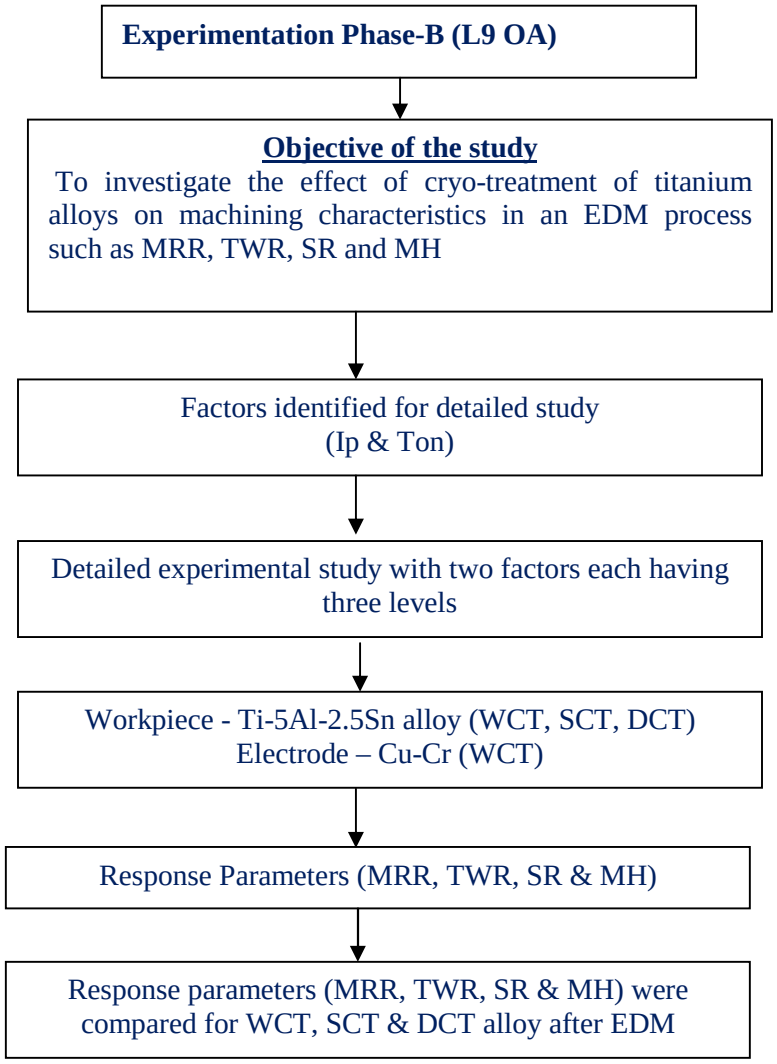

Figure 3.4: (c) Experimental Layout (Phase-B)

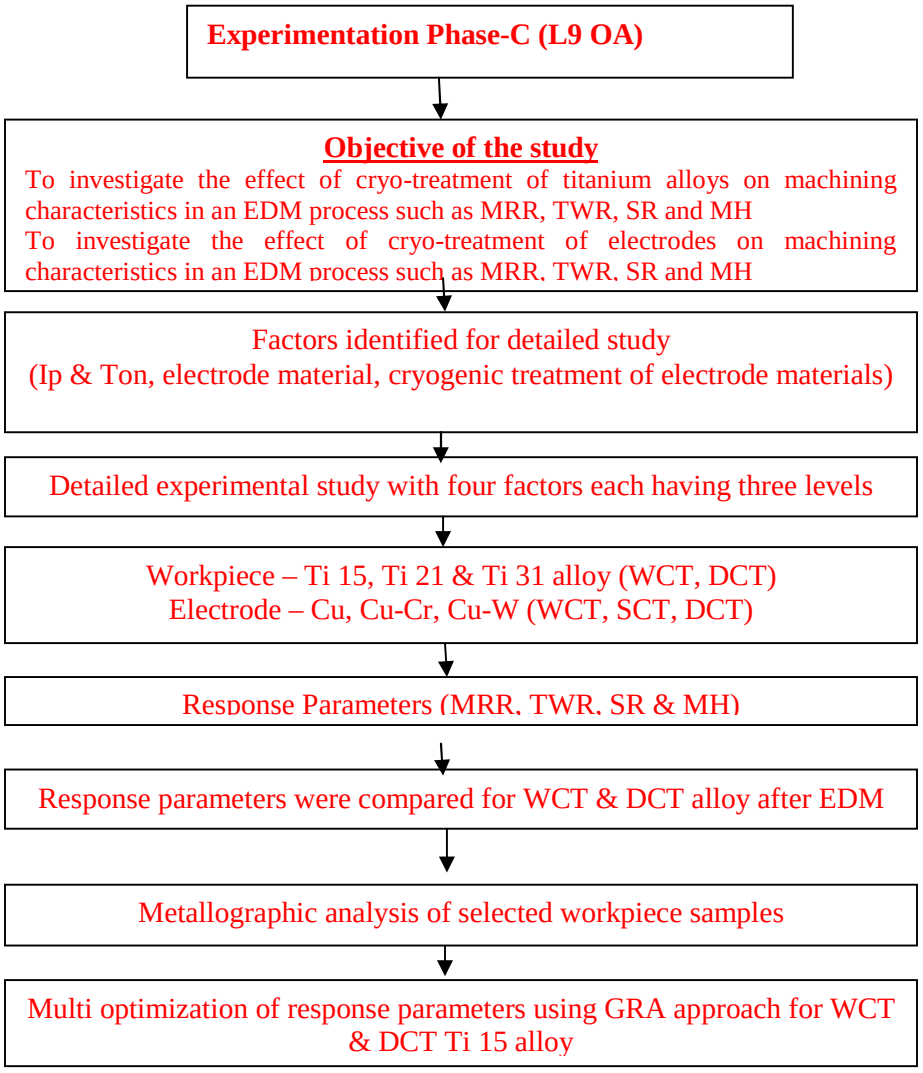

Figure 3.4: (d) Experimental Layout (Phase-C)

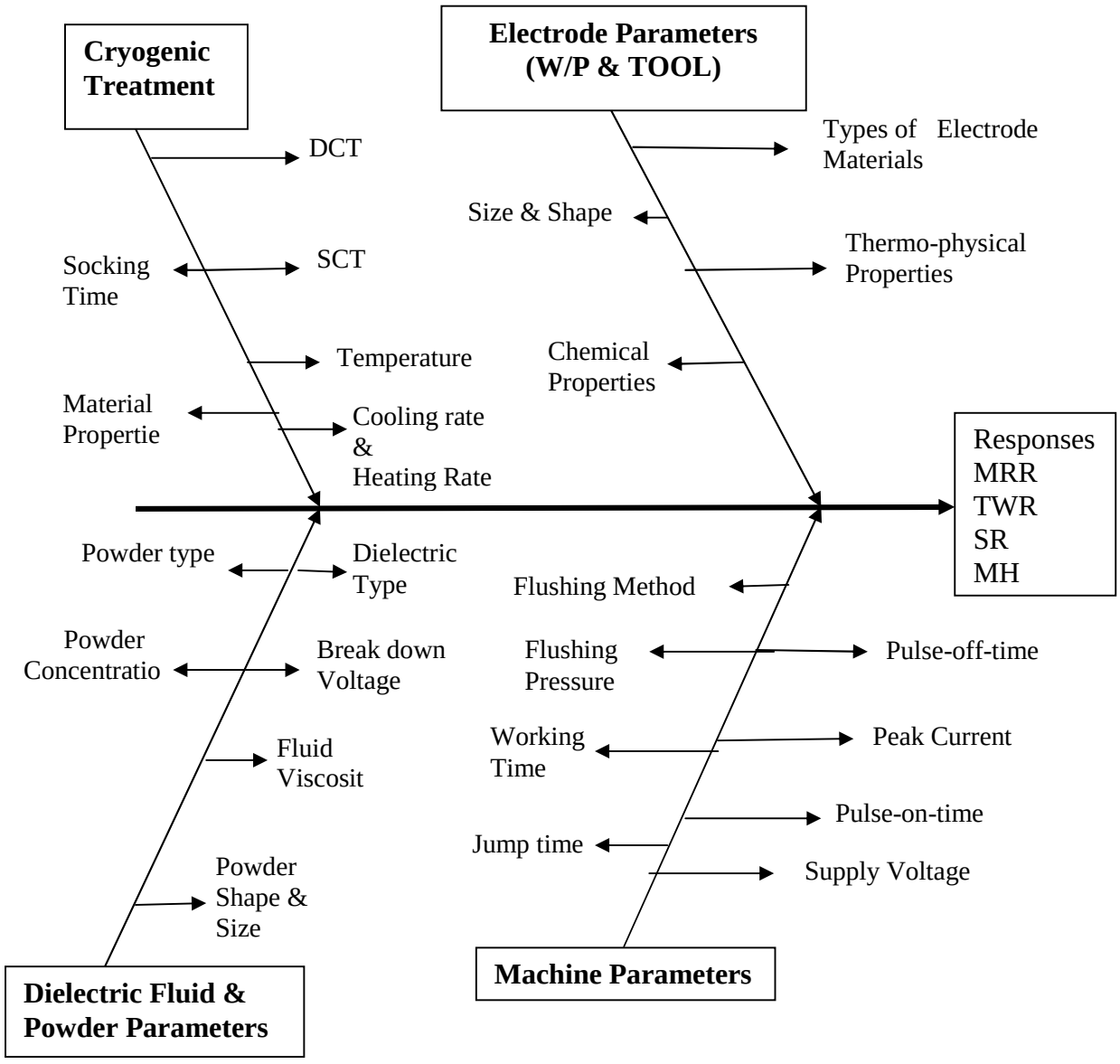

Figure 3.5: Cause and Effect Diagram for Responses (MRR, TWR, SR and MH)

3.4 PRELIMINARY STUDY

A cause and effect diagram as shown in Figure 3.5 was drawn to identify the input process parameters that may affect the response characteristics such as MRR, TWR, SR, MH and surface integrity. The EDM parameters can be classified as follows:

1. Machine based parameters
2. Dielectric based parameters
3. Electrodes based parameters
4. Cryogenic treatment based parameters

3.4.1 PILOT EXPERIMENTATION

Ti-6Al-4V titanium alloy (TITAN 31, ASTM Grade VI) was used as a workpiece material for the preliminary study, and Cu rod of 18 mm diameter as an electrode material. For the initial stage of pilot study, three factors such as I_p, T_{on} and T_{off} were selected and varied to determine their effect on the responses. The actual values of these three electrical parameters were finalized after examining the results of a pilot study. The literature survey showed that a lot of work was carried out by researchers by varying the values of I_p and T_{on}, where as T_{off} was kept constant. The researchers also varied the duty cycle, because T_{off} used is part of the duty cycle along with the T_{on}. The effect of variation in T_{off} as an independent parameter was missing in the available literature, thus T_{off} considered as the independent parameter to explore its influence on the responses.

The values of I_p, T_{on} and T_{off} used for the pilot experimentation based on machine manual and control panel are as under:

- Current (I_p) : 4, 6, 8, 10, 12, 14, 16 and 20 ampere.
- Pulse-on-time (T_{on}) : 30, 45, 90, 120, 150 , 200 and 300 µs
- Pulse-off-time (T_{off}) : 10,15, 30, 45, 60, 90 and 120 µs

During the pilot experimentation, One-Factor-at-a-Time approach (OFAT) has been used for conducting the experiments. In OFAT approach, only one factor is varied at a time for different levels instead of all simultaneously *i.e.* other factors are kept constant. Material removal rate (MRR), Tool wear rate (TWR) and surface roughness (SR) has been selected as the responses for a pilot study.

- ***Material Removal Rate (MRR)***

The volumetric loss in weight of workpiece per unit machining time is known as MRR. The weight of part/job before and after machining operation was taken by using a precision electronic digital weighing machine and the difference in weight for each sample is calculated. A stopwatch was used to measure the machining time accurately during the experiments. The weight difference was then converted into volumetric loss in mm^3/min as shown by equation (3.1):

$$MRR(mm^3/\min) = \frac{(wi - wf)\times 1000}{^\circ \times t} \qquad (3.1)$$

Where wi = weight of the workpiece before machining *i.e.* initial weight (gms)

wf = weight of the workpiece after machining *i.e.* final weight (gms)

ρ = density of workpiece (gm/cm^3)

t = machining time (minutes)

The following three graphs presenting the effect of I_p, T_{on} and T_{off} on MRR are shown in Figure 3.6 to 3.8 respectively. In Figure 3.6, the values of I_p were varied from 4A to 20A to investigate their effects on MRR, where as T_{on} (150 µs) and T_{off} (60 µs) both were kept constant during the experiments. From the plot, it was observed that as current increases the rate of metal removal also increases. Up to 14A the MRR increased uniformly, but beyond 14A, MRR increased sharply. During the process, it was also observed that machining with lower value of T_{off} and higher value of I_p resulted in unstable machining conditions due to arcing. Due to smaller off-time, short deionization time was available to the dielectric fluid, thus, inadequate flushing of the spark gap, caused arcing on the machined surface. Therefore, lower values of off-time (10 µs and 15µs) and higher values of current (16A and 20A) were eliminated from the identified range. Moreover, low value of I_p and T_{on} resulted in low metal removal from the workpiece due to low discharge energy available in the machining zone. Thus, current 4A and on-time (30 µs, 45 µs) were not considered for the final experimentation. The higher values of on-time such as 200 µs and 300 µs were also not selected for final experimentation, because by expanding $T_{on,}$ the width of plasma channel was also expanded, as a result the energy level was reduced after a moment of discharging time, which provides a negative effect on MRR.

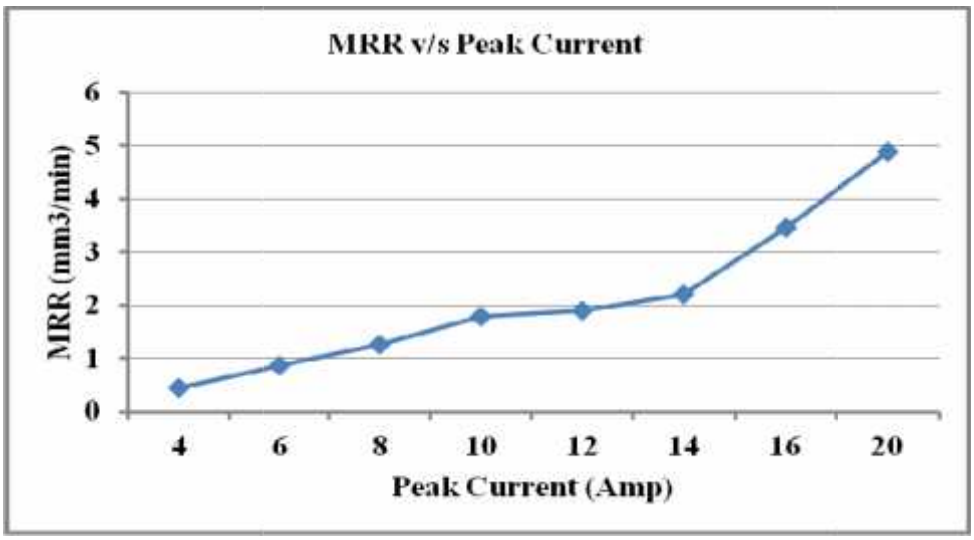

Figure 3.6: Effect of Variation in I_p on MRR (T_{on} = 150 µs and T_{off} = 60 µs)

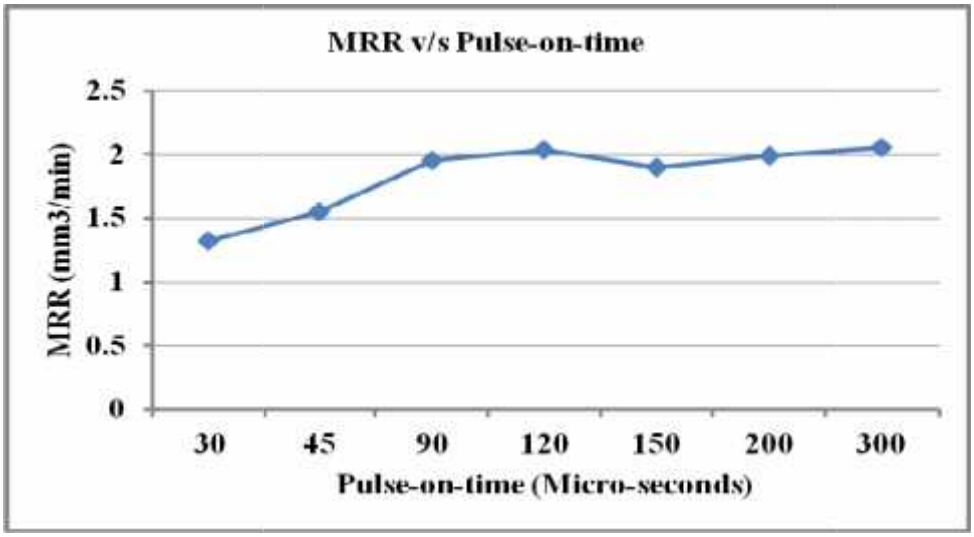

Figure 3.7: Effect of Variation in T_{on} on MRR ($Toff$ = 45 µs and I_p = 12A)

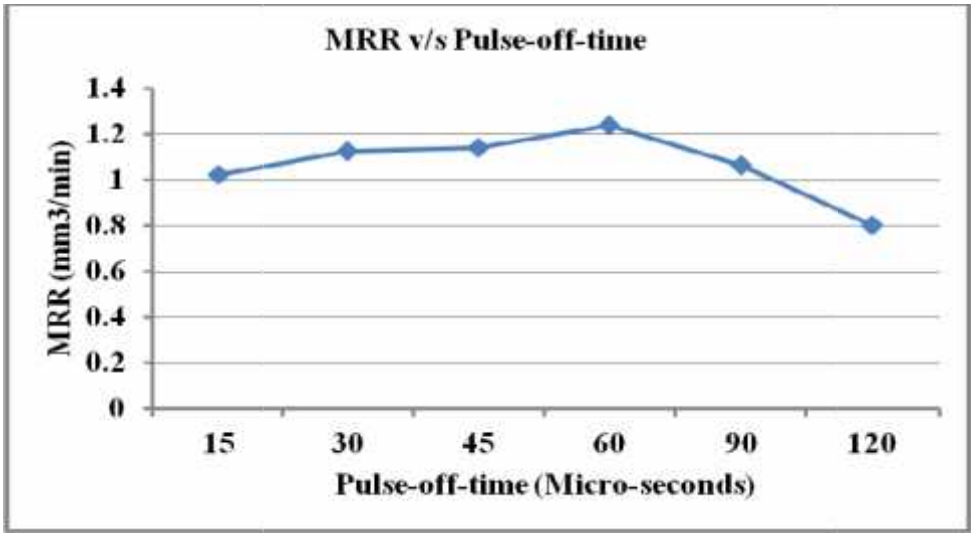

Figure 3.8: Effect of Variation in T_{off} on MRR (T_{on} = 90 µs and I_p = 8A)

The effect of T_{on} on MRR can be seen in Figure 3.7 in which T_{on} was varied from 30 µs to 300 µs and current 12A and T_{off} 45µs was kept constant during the experiments. Theoretically, it is well known that the machining rate could be increased at short duration of T_{off} and vice-versa. The effect of T_{off} is shown in Figure 3.8, which shows the MRR decreases as T_{off} increases beyond a certain limit. Hence, the higher values of off-time are not considered for further experimentation.

- ***Tool Wear Rate (TWR)***

Less wear rate is one of the most important requirements of any type of tool or electrode material. The thermal and electrical conductivity of electrode material is another important

requirement. To accomplish these requirements, Cu material was used as the tool material for the preliminary stage of experimentation. TWR is generally described as the reduction in weight of tool material per unit machining time. The weight of electrode material must be noted before and after the process, so that loss in weight can be easily obtained by taking the difference of both weights. The density of Cu electrode material 8.95 gm/cm^3 was used to calculate the volumetric tool wear rate in mm^3/min.

Mathematically TWR can be calculated using Equation (3.2), as under:

$$\text{Tool wear rate}\left(\text{mm}^3/\text{min}\right) = \frac{\text{Reduction in weight of tool (gm)} \times 1000}{\text{Density of tool material (gm/cm}^3) \times \text{ Machining time (min)}}$$

$$TWR(mm^3/\text{min}) = \frac{(wi - wf) \times 1000}{\rho \times t} \qquad (3.2)$$

Where wi = initial weight of the tool (gm)

wf = final weight of the tool (gm)

ρ = density of tool material (gm/cm^3)

t = machining time (minutes)

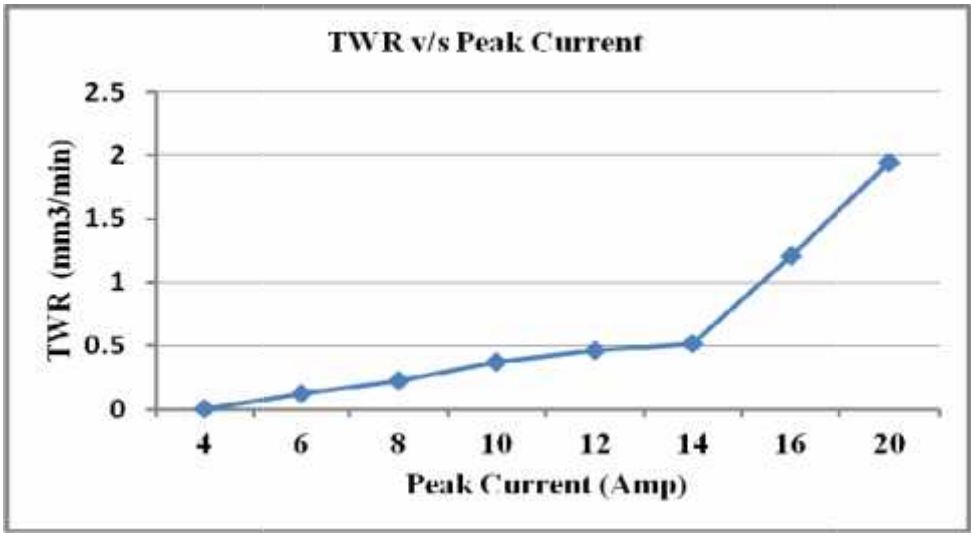

Figure 3.9: Effect of Variation in I_p on TWR (T_{on} = 150 µs and T_{off} = 60 µs)

By using Equation (3.5), the TWR was calculated for each experiment. During the machining tests, I_p, T_{on} and T_{off} were varied to measure their effects on TWR. The effect of I_p variation on TWR can be seen in Figure 3.9. TWR values were calculated at different levels of I_p (4, 6,8,10,12,14,16 and 20 ampere), other two parameters (T_{on} 150 µs, T_{off} 60 µs) were fixed during the experiments. As the value of current increases, the discharge energy also increases, thus, thermal energy also increases. This issue leads to removal of more metal from the base

of the tool materials due to more melting and vaporization of tool material, hence, TWR is increased. Beyond 14A current, TWR increases sharply as shown in Figure 3.9. Due to this issue, 16A and 20A current levels could not be considered for final experimentation. From Figure 3.10, it is found that in the higher range of T_{on}, it has less effect on TWR, the slope of the line starts to decrease. Thus, higher on-time value would not be considered for further experimentation. Machining at lower values of I_p and T_{on}, reduced TWR and SR, but at the same time MRR decreased considerably, because low discharge energy is available in spark zone. The effect of variation of T_{off} is shown in Figure 3.11, where the machining was conducted at a fixed value of current 8A and T_{on} 90 µs. At low values of T_{off} , *i.e.*15µs, higher TWR was observed. Further increases in off-time to 30 µs and 45 µs reduced the TWR. Again in the higher range, TWR decreases due to sufficient time for cooling of the electrode and flushing. But this issue leads to low MRR.

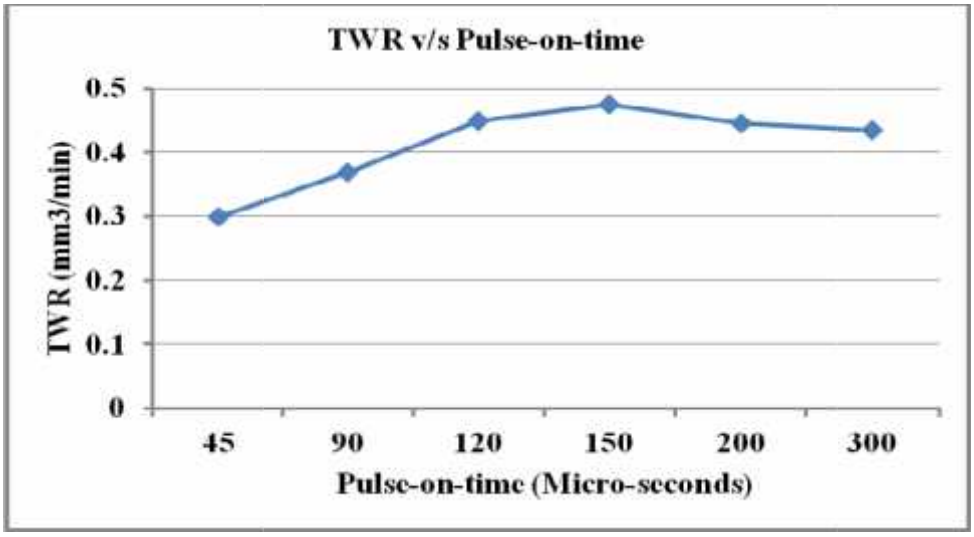

Figure 3.10: Effect of Variation in T_{on} on TWR (T_{off} = 45 µs and I_p = 12A)

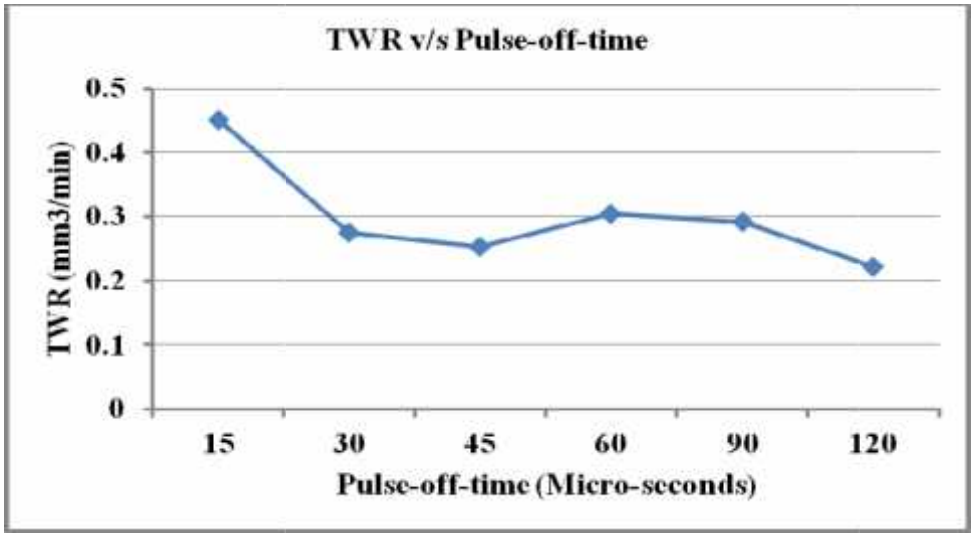

Figure 3.11: Effect of Variation in T_{off} on TWR (T_{on} = 90 µs and I_p = 8A)

I_p and T_{on} are the two most important factors used in EDM process that highly affects the TWR as well as MRR. By increasing I_p and T_{on}, density of electrical sparks increases for the longer time. Due to this, more metal is eroded from the surface of the tool and the workpiece, thus, leading to higher TWR and MRR.

During the experiment, negative polarity was applied to the work material and positive to the Cu tool. During the machining process, at the initial stage of discharge current electrons have less inertia and mass and thus, move towards the positive electrode due to the generation of electric field between the two electrodes. These electrons continuously hit the lower surface of the electrode. Due to this bombardment of electrons, small amount of material is removed from the tool surface, resulting in tool wear. This statement is also supported by Jabbaripour et al. [53].

- ***Surface Roughness (SR)***

Surface roughness is one of the most significant surface characteristics and importance in industrial applications. Basically, SR represents the surface texture. SR of the machined components can be expressed by arithmetic average and denoted by 'Ra'. The plots 3.12, 3.13 and 3.14 highlight the effect of variation of I_p, T_{on} and T_{off} respectively on SR measured in Ra values in microns. Initially, the values of I_p were varied from 4A to 20A, values of T_{on} 150 µs and T_{off} 45 µs were kept constant. Variation of Ra values graph is plotted between Ra and I_p is shown in Figure 3.12.

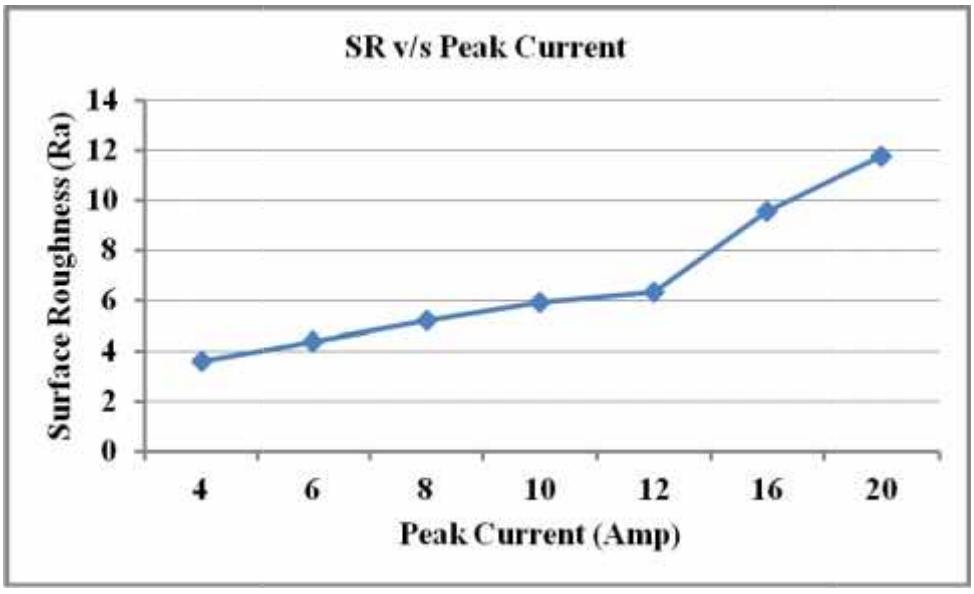

Figure 3.12: Effect of Variation in I_p on SR (T_{on} = 150 µs and T_{off} = 60 µs)

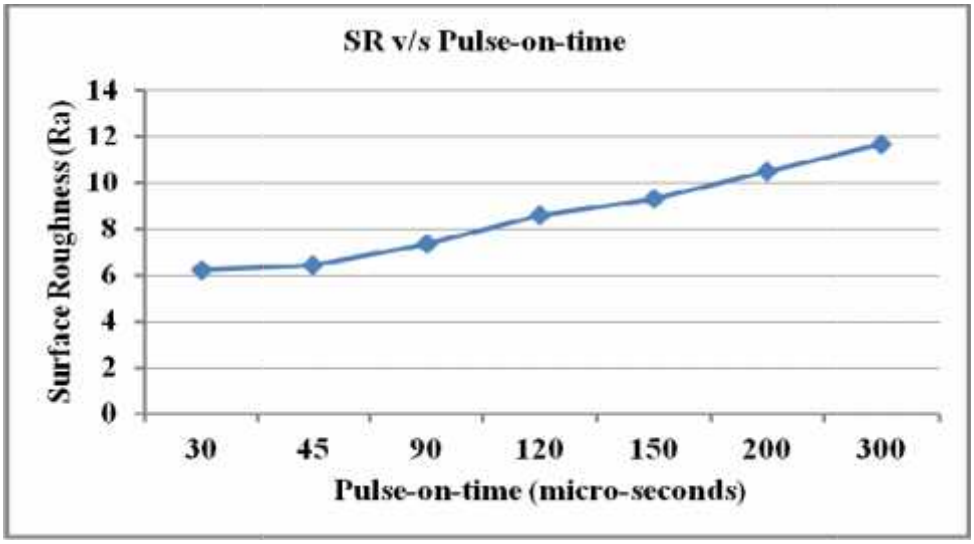

Figure 3.13: Effect of Variation in T_{on} on SR (T_{off} = 45 µs and I_p = 12A)

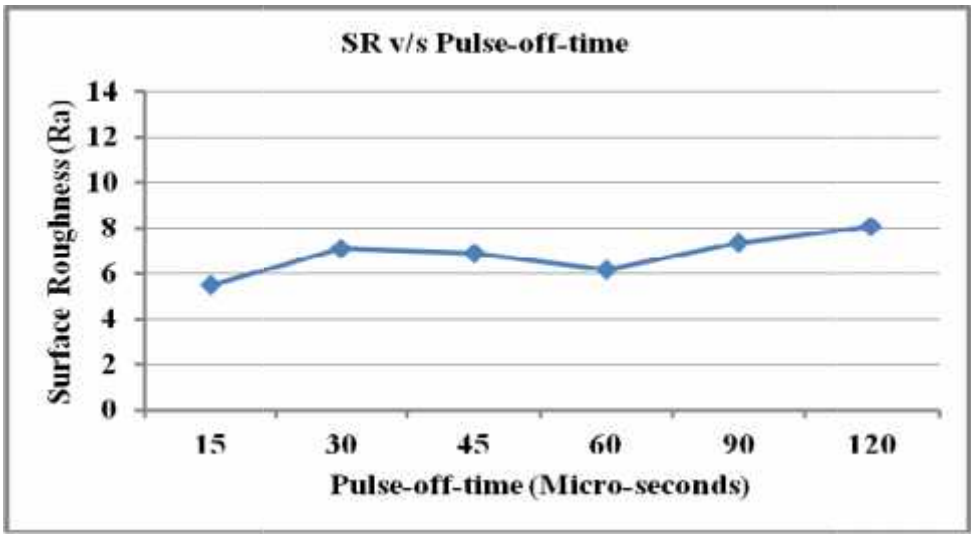

Figure 3.14: Effect of Variation in T_{off} on SR (T_{on} = 90 µs and I_p = 8A)

From Figure 3.12 and 3.13, it is experimentally observed that SR steadily increases as the value of I_p and T_{on} is increased. It is expected that more discharge energy available at higher current for longer duration will result in, more melting and vaporization of material. Due to this phenomenon, craters of bigger dimensions were produced on the surface, which is responsible for poorer surface texture.

At 16A and 20A the SR drastically increased. At low I_p and T_{on} setting, better surface finish was observed as shown in Figures 3.12 & 3.13. Low value of T_{off} with high I_p and T_{on} , surface finish was highly affected because of arcing on the machined surface. Due to poor flushing at low T_{off}, generation and sticking of more carbon on the machined surface as well as bottom surface of electrode were observed resulting in unstable machining which causes rough surface finish. Variation of SR against T_{off} is presented in Figure 3.14.

3.5 METHODOLOGY

A very useful approach known as Design of Experiment (DOE) is always preferred over OFAT approach due to a number of advantages that are as follows [130-131]:

- Reduce the number of experiments.
- Estimation of the error incurred during the experiments.
- DOE allows evaluation and statistical significance of process parameters and is able to find out the interaction effects between the two factors.
- Modeling of the performances can be done in terms of input parameters.
- Identified the combination of optimal process parameters gives larger or smaller response value.

DOE techniques, particularly, OA, are used to appropriately change and test the various levels of input parameters [131]. A number of innovations such as Full Factorial Design, Fractional Factorial Design and Taguchi method, etc. have been introduced to extract maximum possible usage of the concept [130,136].
The detailed flow diagram for the Taguchi experimental design is shown in Figure 3.15.

3.5.1 SELECTION OF INPUT PROCESS PARAMETERS

From the experimental results observed during pilot experimentation and also from literature review the different input process parameters (control variables) and their levels were finalized, which are used during the main experimentation to investigate their effect on machining characteristics such as MRR, TWR, SR, Micro-hardness and surface topography.

- ***Selection of Process Parameters for Phase-A Main Experimentation***

During the Phase-A main experimentation, keeping in view the objectives of the study, the factors and their levels were decided. The identified process parameters used during this phase are given below:

(A) Pulse-off-time (T_{off}): 30µs, 45µs
(B) Peak Current (I_p): 6A, 10A and 14 A
(C) Pulse-on-time (T_{on}): 90µs , 120µs, 150µs
(D) Dielectric fluid: No powder, Mn powder, W powder
(E) Electrode material : Cu, Cu-Cr, Cu-W

(F) Cryogenic treatment of electrode material: WCT, SCT, DCT

(G) Workpiece materials: Ti 15, Ti 21, Ti 31

(H) Cryogenic treatment of workpiece material: WCT, SCT, DCT

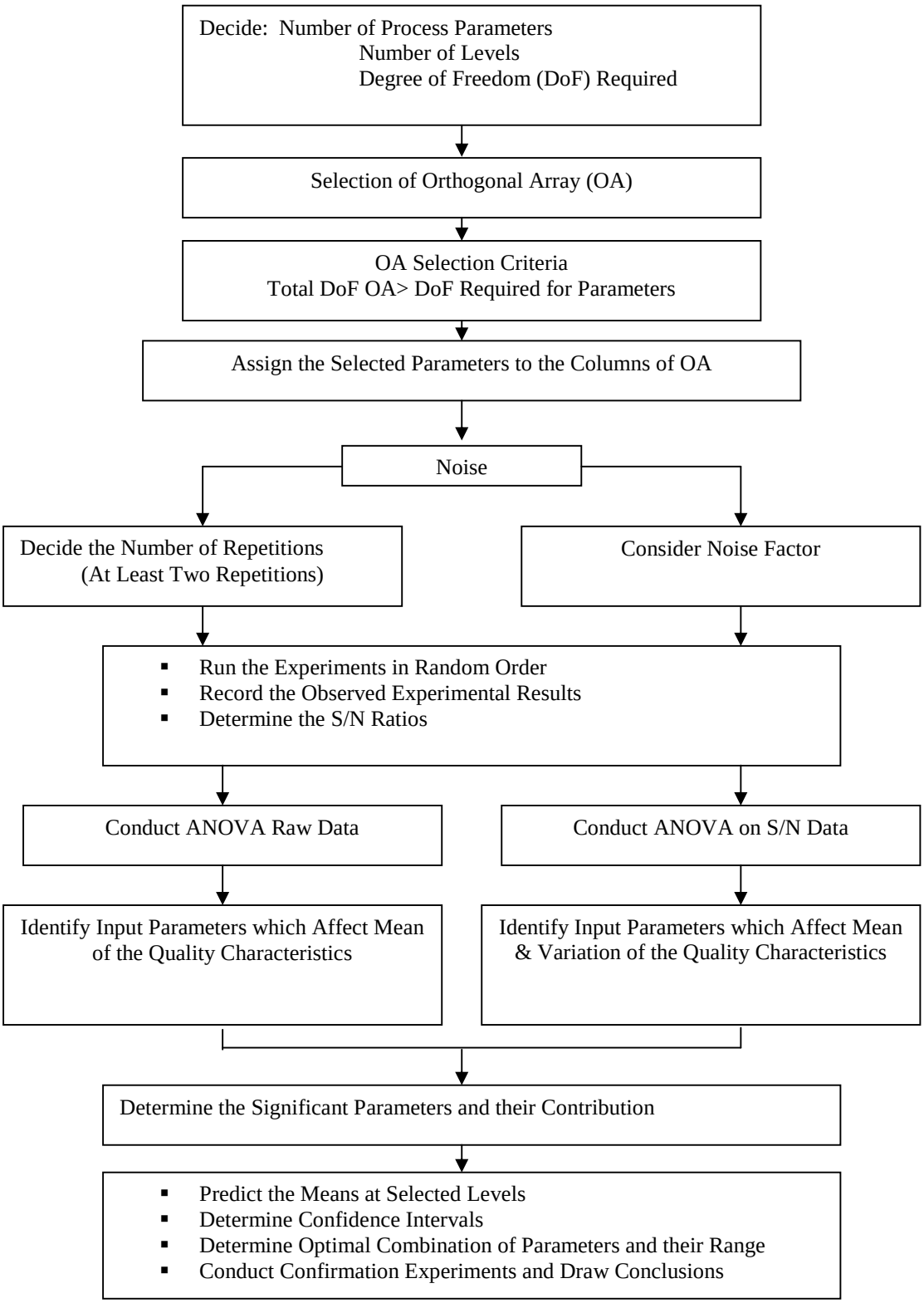

Figure 3.15: Flow Diagram for Taguchi Experimental Design

- ***Selection of Process Parameters for Phase-B Experimentation***

For Phase-B experimentation, based on the literature and results observed during Phase-A experimentation, the most significant factors affecting the performance measures were I_p and T_{on} , selected for conducting the experiments under this phase. Value of T_{off} was fixed during this phase of experimentation. The three levels of both process parameters for the EDM of Ti-5Al-2.5Sn titanium alloy are given as below:

(A) Pulse-off-time (T_{off}): 45 µs (fixed)

(B) Peak Current (I_p): 6A, 10A and 14 A.

(C) Pulse-on-time (T_{on}): 90µs, 120µs, 150µs

- ***Selection of Process Parameters for Phase-C Experimentation***

During the Phase-C experimentation, keeping in view the objectives of the study, without cryo-treated and deep cryo-treated three grades of titanium alloys (Ti, Ti-5Al-2.5Sn and Ti-6Al-4V) were selected as workpiece materials. Four input parameters, namely I_p, T_{on}, electrode material and cryogenic treatment of electrodes were selected to investigate their effect on MRR, TWR, SR and micro-hardness. The three level values of all the four parameters are given as below:

(A) Pulse-off-time (µs): 45 (fixed)

(B) Peak Current (I_p): 6A, 10A and 14 A.

(C) Pulse-on-time (T_{on}): 90µs , 120µs, 150µs

(E) Electrode material : Cu, Cu-Cr, Cu-W

(F) Cryogenic treatment of electrode material: WCT, SCT, DCT

3.6 INSTRUMENTS/EQUIPMENT USED FOR ANALYSIS

In this experimental study, the instruments used for analysis are discussed here in this section. The brief description of each instrument is given below:

I. Surface roughness tests were performed on SR tester; model SJ-400 of MITYTOYO, available at Thapar University, Patiala.

II. Micro-hardness tests were carried out on MH Tester; model HVS-1000B, Chiana, available at GNDEC, Ludhiana, Punjab. The value of micro-hardness is available in Vickers hardness as well as in Rockwell Scale. Here, the Vickers hardness number was used to measure the hardness value.

III. Study of microstructure of all the machined workpiece and electrode, sample were performed on SEM analyzer, model JSM-6610 LV, make JEOL of Japan, which has a magnification range from 5x to 3,00,000x. This machine is available at IIT, Ropar, Punjab, and it is attached with an EDX unit.

IV. XRD analyses of the selected samples were performed on X-Ray Diffractometer, PANalytical's X'Pert Pro MPD, Netherlands available at IIT, Ropar, Punjab. This equipment is a horizontal fixed, laboratory based system. The maximum 2θ angle, accessible to the instrument was limited to 145^0. The 2θ range was used from 20^0 to $120^{0.}$

V. Chemical composition analysis of the tool was performed on Optical Emission Spectrometer (OES), model Foundry Master, make-WAS Worldwide Analytical System AG, Germany, available at Central Institute of Hand Tools, Jalandhar, Punjab. The argon gas was used in the equipment and is capable of measuring the percentage of elements in iron-base, copper-base and aluminum-base materials with an accuracy of 0.0001%.

Chapter 4

MAIN EXPERIMENTATION

(*EXPERIMENTATION PHASE-A*)

4.1 INTRODUCTION

In this section, the entire experiential work was conducted according to the experimental plan (*Chapter 3, Figure 3.4*) to achieve the objectives of the study. Three grades of titanium alloys TITAN 15, TITAN 21 and TITAN 31 were identified as workpiece materials, arranged from Mishra Dhatu Nigam Limited (A Govt. of India Enterprise, Ministry of Defense), Hyderabad, India. The titanium alloy sheets were cut using ELECTRONICA SPRINTCUT 734 CNC Wire EDM in desired sizes at the Central Tool Room. Three materials namely (i) copper, (ii) copper-chromium and (iii) copper-tungsten were used as electrode materials. The dimensions of three electrode rod were diameter of 18mm and length of 300mm. The rod was subsequently parted at length of 40mm and the face of all the cut lengths was ground using emery paper for flatness. The chemical compositions of three grades of work materials and electrode materials are listed in Table 4.1.

The need for the main experimentation is to investigate the effects of different machine input process parameters on the machining performance characteristics in different dielectric mediums. To improve the properties of titanium alloy cryogenic treatment on three grades of titanium alloys were applied, so that efficiency of EDM process can be improved.

Overall need of this experimentation is to improve the machinability by using all the above said parameters because titanium and its alloys are widely used in various industries to manufacture numerous parts/components.

Manganese (Mn) with mesh size of 325or 44 microns and tungsten powder of size 3-5 micron blended with EDM oil in a concentration of 10 g/l and purity 99.5% were used during experimentation. Moreover, cryo-treatment on both workpiece and electrode materials were applied to investigate their effect on machining characteristics. All the experiments were performed on die sinking CNC EDM (Model OSCARMAX S 645 CMAX). To complete the experimental work, there are some parameters which were kept constant, are given below in Table 4.2. A pictorial view of different electrode (Cu, Cu-Cr, Cu-W), workpiece materials (Ti 15, Ti 21, Ti 31) and powders (Mn and W) used for the experimentation are shown in Figure 4.1.

Table 4.1: Chemical Analysis (%) of Work Materials and Electrode Materials

Work Materials				Electrode Materials			
Elements	**TITAN 15**	**TITAN 21**	**TITAN 31**	**Elements**	**Cu**	**Cu-Cr**	**Cu-W**
C	0.015	0.013	0.012	**Cu**	99.5	99.2	29.27
O	0.106	0.0689	0.01744	**Zn**	0.175	<0.0050	0.68
N	0.0052	0.0033	0.0032	**W**	---	----	68.10
H	0.0005	0.00145	0.0035	**Cr**	<0.001	0.605	----
Fe	0.04	0.025	0.07	**Pb**	0.0395	0.0128	0.023
Al	---	5.32	6.19	**Sn**	0.0423	<0.0050	0.012
V	---	---	4.04	**Fe**	0.0837	0.0294	0.46
Sn	---	2.76	---	**Ni**	<0.0050	<0.0050	0.56
Ti	Balance	Balance	Balance	**Mn**	<0.002	0.003	-----

Table 4.2: Fixed Input Process Parameters

S.No.	Machining Parameters	Fixed Value
1.	Polarity	Electrode: +ve, Workpiece: -ve
2.	Flushing Method	Side jet flushing
3.	Flushing Pressure	0.5 Kg/cm^2
4.	Depth of Cut	1.0 mm
5.	Dielectric Type	FERROLAC 3M EDM Oil
6.	Powder Concentration in Dielectric	10g/liter
7.	Input Voltage	40V
8.	Electrode Size	Dia 18 mm, length 40mm
9.	Open Gap Output Voltage	135±5% V
10.	Jump time	1.4mm
11.	Working time	0.7s
12.	Gap	6/7

(Figure a)

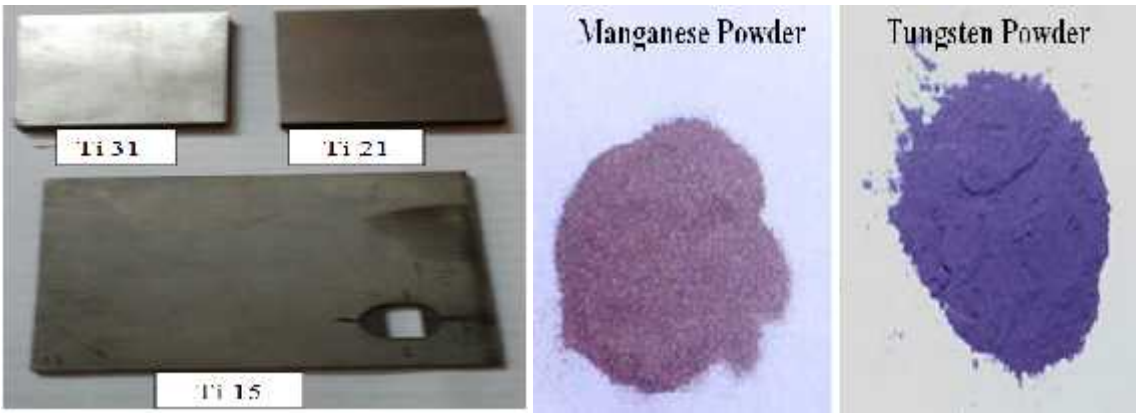

(Figure b) (Figure c)

Figure 4.1: (a) Picture of three Electrodes Used, (b) Cut Titanium Alloys Work pieces and (c) Manganese and Tungsten Powders

4.2 MAIN EXPERIMENTATION (PHASE-A)

Keeping in view the objectives of the study, a total of eight machining parameters with their levels were identified for the main experimentation. One factor, pulse-off-time varied at two levels and the remaining factors (i) peak current, (ii) pulse-on-time, (iii) dielectric fluid (iv) electrode material, (v) cryo-treatment of electrode materials, (vi) workpiece material and (vii) cryo-treatment of workpiece materials, were varied at three levels each to understand their impact on the machining characteristics such as MRR, TWR, SR, MH and surface integrity. The selected factors, their symbols and their levels are listed in Table 4.3.

Since, the selected input parameters were combinations of two and three levels and the degree of freedom of selected factors are 15; hence, a mixed type of experimental design ($2^1 \times 3^7$) *i.e.* L_{18} OA was identified as the most appropriate array for main experimentation [130]. MINITAB statistical software, version 16 was used for assigning the factors to the

array. L_{18} OA contains a total eight columns and 18 rows. Therefore, a total eighteen experiments were performed during this phase. Another important thing is that to reduce the influence of noise factors, all the 18 experiments were repeated with the same set of input parameters three times in random order. It means a total 54 (18×3) numbers of experiments were carried out for Phase-A main experimentation.

Table 4.3: Selected Factors with their Levels for Machining

Symbol	Factors	Levels	Levels		
			Level-1	Level-2	Level-3
A	Pulse-off-time (µs)	2	A1 = 30	A2 = 45	----
B	Current (Amp)	3	B1 = 06	B2 = 10	B3 = 14
C	Pulse-on-time (µs)	3	C1 = 90	C2 = 120	C3 = 150
D	Dielectric fluid (EDM Oil)	3	D1 = No powder	D2 = Mn powder	D3 = W powder
E	Electrode material	3	E1 = Cu	E2 = Cu-Cr	E3 = Cu-W
F	Cryo-treatment of electrode material	3	F1 = WCT	F2 = SCT	F3 = DCT
G	Workpiece material	3	G1 = Ti 15	G2 = Ti 21	G3 = Ti31
H	Cryo-treatment of workpiece material	3	H1 = WCT	H2 = SCT	H3 = DCT

Table 4.4: L_{18} ($2^1 \times 3^7$) Experimental Design Matrix with Machining Parameters

Experiment	Actual Values of Machining Parameters							
Number	A	B	C	D	E	F	G	H
1.	30	6	90	Oil	Cu	WCT	Ti15	WCT
2.	30	6	120	Oil+Mn	CuCr	SCT	Ti 21	SCT
3.	30	6	150	Oil+W	CuW	DCT	Ti 31	DCT
4.	30	10	90	Oil	CuCr	SCT	Ti 31	DCT
5.	30	10	120	Oil+Mn	CuW	DCT	Ti15	WCT
6.	30	10	150	Oil+W	Cu	WCT	Ti 21	SCT
7.	30	14	90	Oil	Cu	DCT	Ti 21	DCT
8.	30	14	120	Oil+Mn	CuCr	WCT	Ti 31	WCT
9.	30	14	150	Oil	CuW	SCT	Ti15	SCT
10.	45	6	90	Oil+W	CuW	SCT	Ti 21	WCT

11.	45	6	120	Oil	Cu	DCT	Ti 31	SCT
12.	45	6	150	Oil+Mn	CuCr	WCT	Ti15	DCT
13.	45	10	90	Oil+Mn	CuW	WCT	Ti 31	SCT
14.	45	10	120	Oil+W	Cu	SCT	Ti15	DCT
15.	45	10	150	Oil	CuCr	DCT	Ti 21	WCT
16.	45	14	90	Oil+W	CuCr	DCT	Ti15	SCT
17.	45	14	120	Oil	CuW	WCT	Ti 21	DCT
18.	45	14	150	Oil+Mn	Cu	SCT	Ti 31	WCT

In this selected array, the two-level factor was assigned to the first column and the other seven were assigned to remaining columns. Two levels factor, *pulse-off-time (T_{off})* (A) was assigned in the first column of an array and the other three levels factors *peak current (I_p)* (B) in the second column, *pulse-on-time (T_{on})* (C) in the third column, *dielectric fluid* (D) in the fourth column, *electrode materials* (E) in the fifth column, *cryogenics of electrode materials* (F) in the sixth column, *workpiece material* (G) in the seventh column and *cryogenics of workpiece materials* (G) in the eighth column. The assignment of actual parameter values with trial run conditions is shown in Table 4.4.

Total three sets based on L_{18} OA were carried out for Phase-A main experimentation. The value of I_p, T_{on} and T_{off} were varied using the machine control panel. The observations of all the 18 experiment results were recorded in tabular form for further analysis. For this study, quality characteristic *"higher-the-better"* was used for MRR, MH and *"lower-the-better"* for TWR, SR was used for calculating the S/N ratios. The obtained results were analyzed to find out:

- Optimal combination of input parameters for each response.
- The percent contribution of each factor from ANOVA.
- Significance of each factor.
- The theoretically predicted values of output characteristics at the optimum parameters setting.

Then, the obtained experimental results have been compared with the theoretical predicted results for verification.

The following issues related to Phase-A main experimentation have been addressed here:

- The effects of cryogenically treated titanium alloys on MRR, TWR, SR and MH were explored.

- The effects of cryogenically treated tool materials on machining performance MRR, TWR, SR of workpiece and electrode surface and MH were investigated during EDM.
- The effect of dielectric medium was explored. A standard FERROLAC 3 M EDM oil dielectric fluid was used for the experiments.
- Two powders manganese (325 Mesh, 44 microns) and tungsten (3- 5 micron) of concentration 10 g/l and purity 99.5% were used with FERROLAC 3M EDM oil to investigate their influence on the machining characteristic**s**.
- Metallographic analysis of the machined surfaces was explored in terms of microstructure analysis using SEM, quantitative analysis of transferring elements with EDS analysis and formation of different compounds and phases on the machined surface using XRD analysis.
- Mathematical Modeling of MRR and TWR was developed using dimensional analysis.
- ANN was applied to model and predict the SR and MH of work samples
- Multi optimization of machining characteristics such as MRR, TWR, SR and MH was performed by using Analytic Hierarchy Process (AHP) approach.

4.2.1 MATERIAL REMOVAL RATE (MRR)

MRR is the removal of metal from the workpiece surface per unit machining time. The observed values of MRR after machining of three different grades of titanium alloys with different electrode materials and their calculated values of S/N ratios (*as per L_{18} OA*) are listed in Table 4.5. Since MRR is a higher the better output, equation (4.1) was used to calculate the S/N Ratio.

$$HB: S/N\ ratio = -10\log_{10}\left[\frac{1}{n}\sum_{i=1}^{n} yi^{-2}\right] \qquad (4.1)$$

Where yi represent the experimentally observed value of the ith experiment, n is the repeated number of each experiment. The unit of calculated S/N ratio from the observed values is the decibel (dB) and is denoted by η.

Table 4.5: MRR after Each Trial and their Calculated S/N Ratios

Experiment Number	Material Removal Rate (mm^3/min)			Mean MRR	S/N Ratios (dB)
	R1	R2	R3		

1.	0.956	0.9642	0.98524	0.969	-0.279
2.	1.169	1.1921	1.1869	1.183	1.455
3.	1.045	1.01088	1.0236	1.026	0.225
4.	1.592	1.7005	1.6627	1.652	4.349
5.	1.543	1.5085	1.5459	1.532	3.706
6.	1.693	1.7279	1.7047	1.708	4.652
7.	2.066	2.1371	2.1435	2.115	6.505
8.	2.015	2.0619	2.1007	2.059	6.269
9.	1.486	1.5337	1.5132	1.511	3.583
10.	0.796	0.8706	0.8498	0.838	-1.545
11.	0.948	0.9979	0.9721	0.973	-0.246
12.	1.092	1.143	1.12606	1.120	0.981
13.	1.322	1.3059	1.3237	1.317	2.392
14.	1.52	1.428	1.4625	1.470	3.339
15.	2.102	2.0845	2.0159	2.067	6.305
16.	1.629	1.6778	1.6983	1.668	4.443
17.	2.206	2.2191	2.1741	2.199	6.847
18.	2.089	2.1186	2.11108	2.106	6.470

$\overline{T_{MRR}}$ = Overall mean of MRR = 1.584 mm^3/min, Mean of S/N ratio η = 3.303

Table 4.6: Average Values by Factor Levels of S/N Data and Raw Data for MRR

Control Factors	Raw Data (mm^3/min)			S/N Ratio (dB)		
	Level 1	Level 2	Level 3	Level 1	Level 2	Level 3
A	1.528	1.529	-------	3.385	3.221	---------
B	1.018	1.625	1.943	0.098	4.124	5.686
C	1.427	1.569	1.590	2.644	3.562	3.703
D	1.562	1.562	1.462	3.426	3.585	2.897
E	1.557	1.625	1.404	3.407	3.967	2.534
F	1.562	1.460	1.564	3.477	2.942	3.489
G	1.379	1.685	1.522	2.629	4.036	3.243
H	1.595	1.393	1.597	3.488	2.713	3.708

- ***Analysis of Results***

From the experimental data, the average values of MRR (raw data) and corresponding values of S/N ratios for all the eight factors at each level was calculated and listed in Table 4.6. The raw data values for MRR are listed in first half of the table and S/N ratios in the second half of the table for each level of the factors varied during experimentation.

- ***Analysis of Variance (ANOVA)***

The data were analyzed using ANOVA and are summarized in Table 4.7. The F-value and percent contribution (PC) represent the factor effects of input parameters. Larger the F-value and PC shows the significance of the factor. The results were plotted to analyze the variation trend of MRR with change in each factor level. Since MRR is a ‘‘*larger the better*’’ response, the peak for each plot represents the optimal condition at which that parameter should be set. The plots for each factor are depicted in Figure 4.2 (a)–(h). The I_p was observed to be the most significant factor with a PC of 81% as shown in Table 4.7.

Table 4.7: Analysis of Variance (ANOVA) for MRR (S/N Data)

Control Factors	DOF	Seq. SS	Adj. MS	F	%PC	Remarks
A	1	0.121	0.121	0.22	0.098	
B	2	99.741	49.87	90.93	80.98	Most Significant
C	2	3.965	1.98	3.61	3.22	
D	2	1.556	0.778	1.42	1.26	
E	2	6.253	3.126	5.70	5.08	Less Significant
F	2	1.174	0.587	1.07	0.95	
G	2	5.975	2.987	5.45	4.85	Less Significant
H	2	3.273	1.6365	2.98	2.65	
Error	2	1.097	0.548			
Total	17	123.156			100.00	
Error polled	11				9.09	

DOF: degree of freedom; SS: sum of square; MS: mean of square;

Rsq = 99.1% and Rsq (adj) = 92.4%. F_{tab} = F (2,11) = 3.9823; F (1,11) = 4.8443

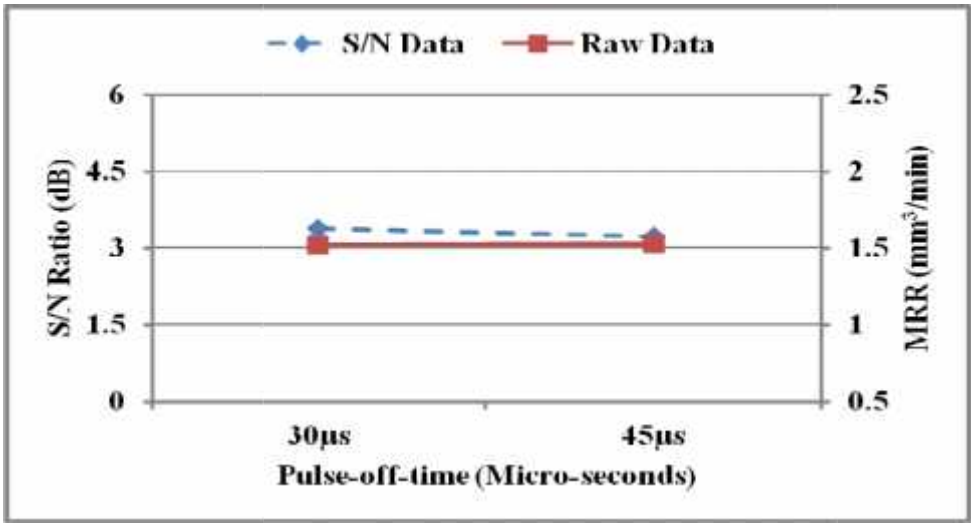

Figure 4.2: (a) Effect of Pulse-off-time on MRR

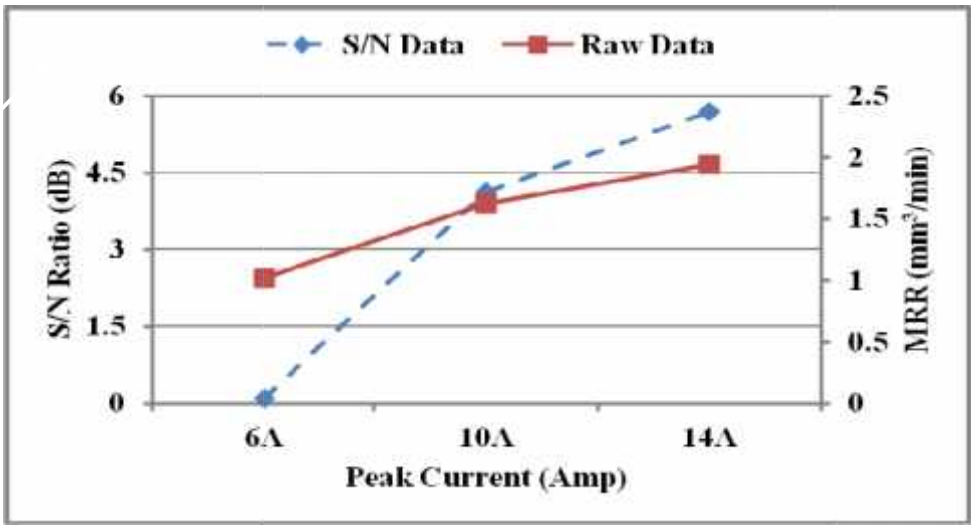

Figure 4.2: (b) Effect of Peak Current on MRR

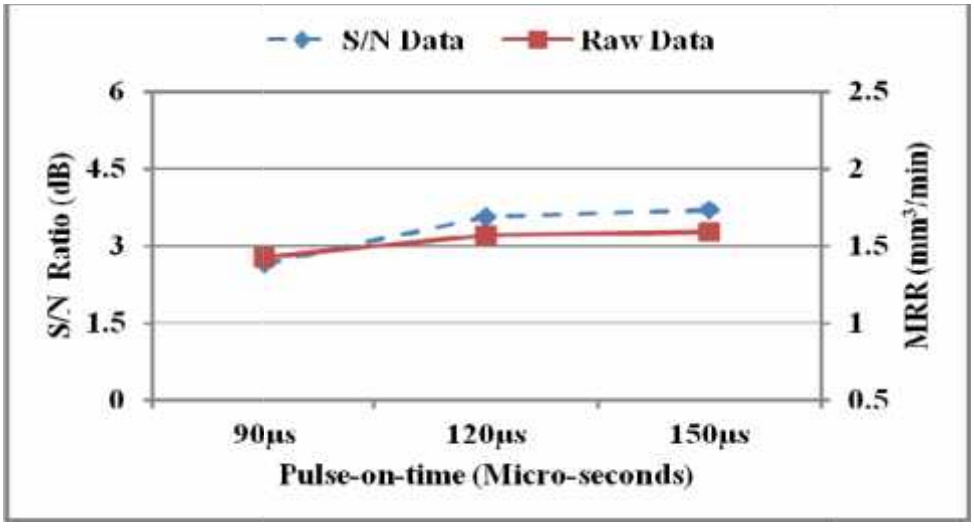

Figure 4.2: (c) Effect of Pulse-on-time on MRR

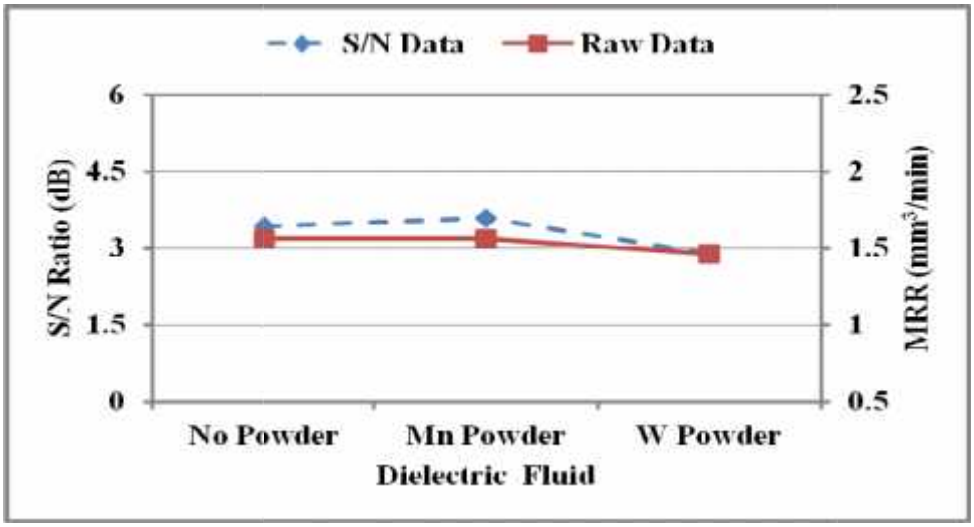

Figure 4.2: (d) Effect of Dielectric Fluid, with 'Mn' and 'W' Powder on MRR

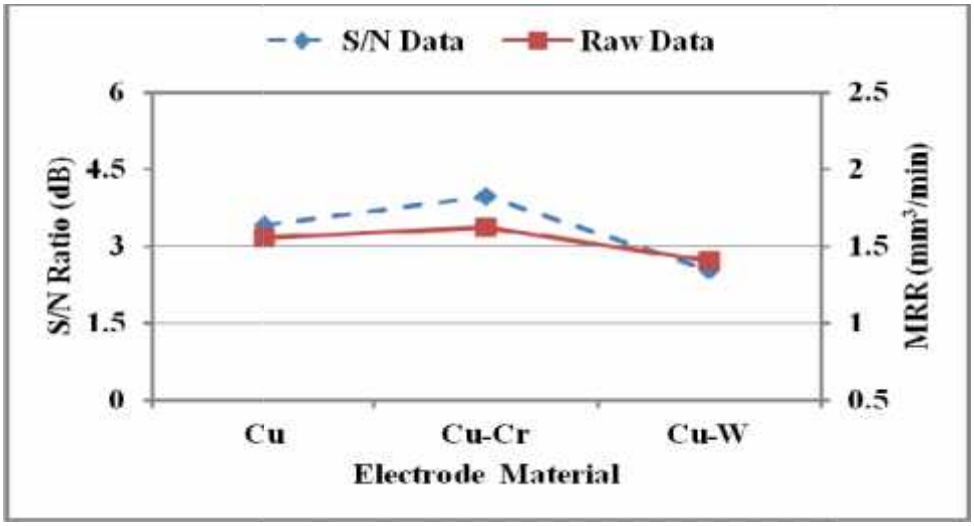

Figure 4.2: (e) Effect of Different Electrode Materials on MRR

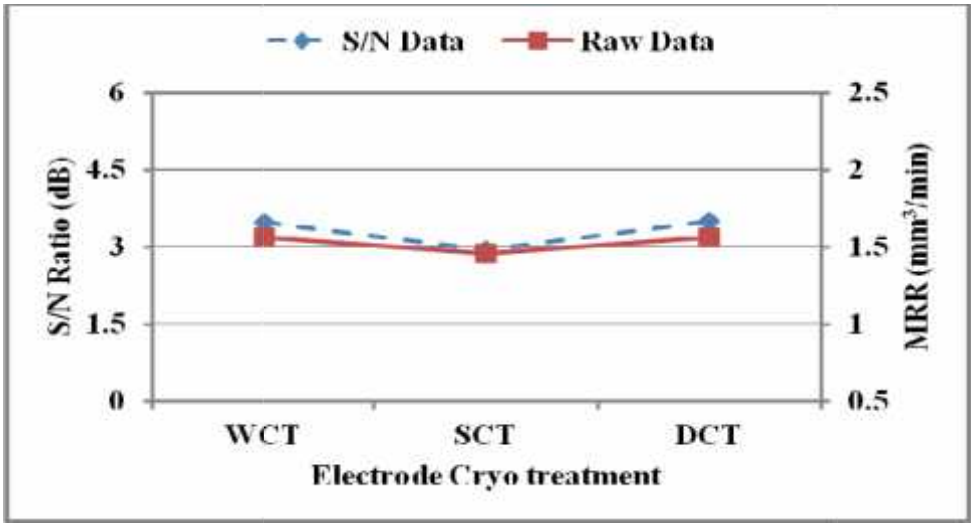

Figure 4.2: (f) Effect of Cryogenic Treatment of Electrode Materials on MRR

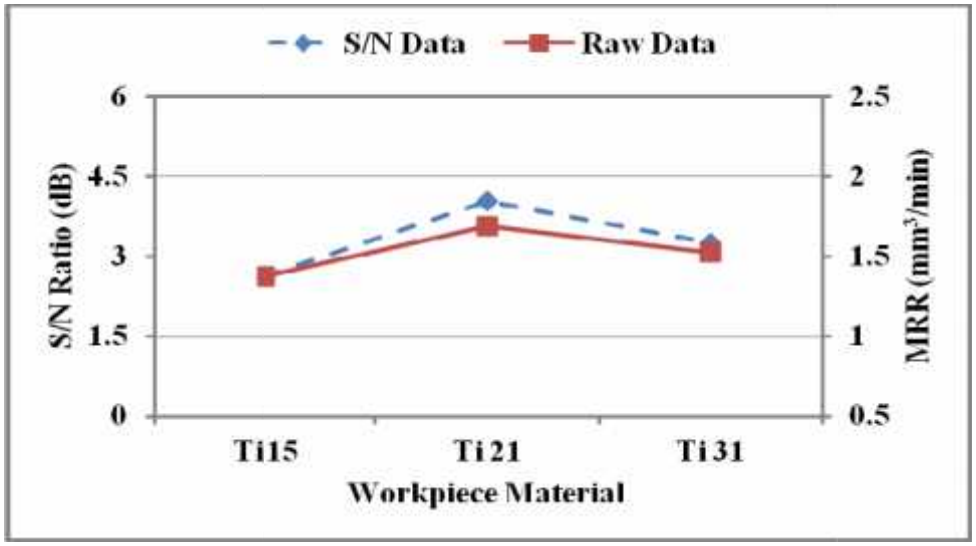

Figure 4.2: (g) Effect of Different Titanium Alloys Work Materials on MRR

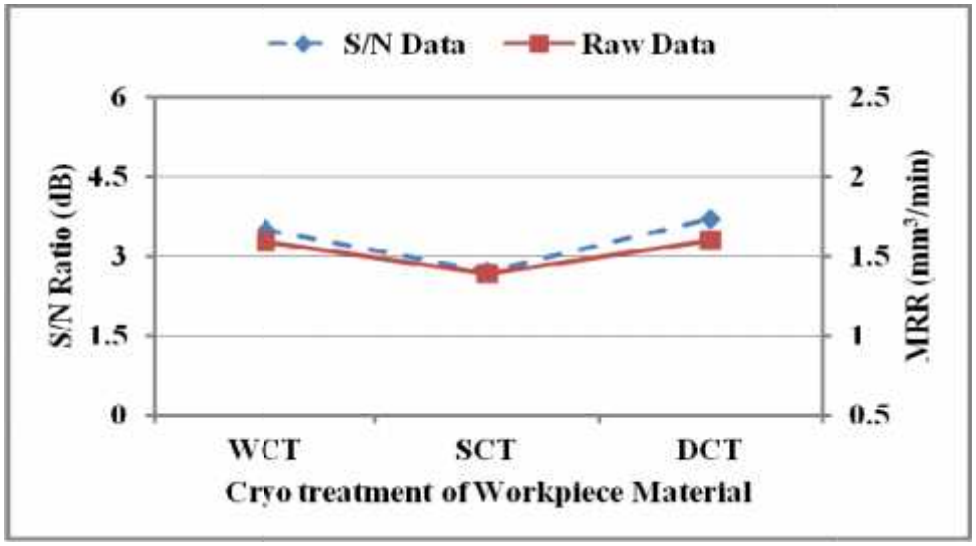

Figure 4.2: (h) Effect of Cryogenic Treatment of Titanium Alloys on MRR

As the value of current increases, the available electric discharge energy in EDM also increases, which results in a deeper crater to be formed during each spark, this issue leads to an increase in MRR. Two other factors, namely, electrode material and pulse-on-time, in that order also affect the MRR, although their impact is lower on MRR than that of the peak current. The effect of other parameters had a smaller effect on MRR as can be seen in Figure 4.2. Although the effect of cryogenic treatment is smaller, a lower MRR is realized using cryogenic treatment because of higher wear resistance of the material.

Table 4.8: Response Table for S/N Ratios (Larger the better)

Level	A	B	C	D	E	F	G	H
1	3.385	0.098	2.644	3.426	3.406	3.477	2.628	3.487
2	3.220	4.124	3.562	3.585	3.967	2.942	4.036	2.713
3	-------	5.686	3.703	2.897	2.534	3.489	3.243	3.707
Delta	0.165	5.587	1.059	0.688	1.433	0.547	1.407	0.994
Rank	8	1	4	6	2	7	3	5

The plot in Figure 4.2 (d) shows the effect of addition of powder to the dielectric on the MRR. The plot shows that the addition of either 'W' or 'Mn' powder to the dielectric fluid did not significantly alter the MRR in comparison to results obtained without mixing of powder to the dielectric. Response values, delta values and ranking of all the factors for S/N ratio for MRR as a '*larger-the-better'* characteristic are tabulated in Table 4.8.

Based on these results, it can be concluded that MRR can be maximized using lower values of T_{off} (30µs), highest level of I_p (14 A) and T_{on} (150 µs), with manganese powder mixed with oil and machined with Cu-Cr electrode. It can be observed from the ANOVA results that cryogenic treatment of electrode material has less than 1% contribution in affecting MRR because of the wear resistance imparted to the workpiece due to transfer of material from powder, electrode or the dielectric. A DCT made the largest impact of increasing the MRR as it increases the electrical conductivity, thereby improving the thermal conductivity of the material. This improves the heat dissipation capacity of the material, thus lowering the work material temperature leading to higher MRR [17]. The computed values of R_{sq} and R_{sq} (adj) were 99.1% and 92.4%, respectively.

- ***Identification of Optimal Conditions & Theoretical Prediction of MRR***

As MRR is '*higher-the-better*' type of response characteristic. For that reason, higher values of MRR are considered for optimal conditions. The peak of the plots for each factor represented the optimum condition for those factors. From the plots 4.2 (a-h), it was observed that the first level of T_{off} (A_1), third level of I_p (B_3) and T_{on} (C_3) would give the largest MRR. Further, second level of dielectric fluid (D_2), second level of electrode material (E_2), third level of electrode material cryo-treatment (F_3), second level of workpiece material (G_2), and third level of workpiece material cryo-treatment (H_3) represents the highest values for MRR. Hence, the optimum condition of process parameters is $A_1B_3C_3D_2E_2F_3G_2H_3$. Taguchi's

additive model was used to predict the theoretical MRR, if the factors are set at their optimal levels. The theoretical value of η_{opt} (MRR) under the optimum condition for the factors is given by the following model equation (4.2) [71]:

$$\eta_{opt} = \eta + (\eta_A - \eta) + (\eta_B - \eta) \text{----------} + (\eta_H - \eta) \quad (4.2)$$

$$\eta_{opt} = \eta + (\eta_{B3} - \eta) + (\eta_{E2} - \eta) + (\eta_{G2} - \eta) = 7.083$$

Where η is the overall mean of S/N ratios for MRR for the entire OA and η_A, η_B, η_C, η_D, η_E, η_F, η_G and η_H are the mean values of the S/N ratio for each factor at their respective levels. $Y_{Predicted}$ is the expected theoretical value for the characteristic MRR and was calculated to be The corresponding values of material removal rate are given by the following equation:

$$y^2_{\text{Pr}edicted} = \frac{1}{10^{-\eta_{opt}/10}} \quad (4.3)$$

Or, $y_{predicted} = 2.26$ mm^3/min

The predicted value for response has been calculated using Taguchi's additive model on the significant parameters. As it can be clearly seen in L_{18} OA, that it didn't contain this optimal setting, *i.e.* ($A_1B_3C_3D_2E_2F_3G_2H_3$), thus, to validate the results three numbers of experiments were performed at this setting. The mean value of MRR observed at this setting was 2.325 mm^3/min, which is very close to the theoretical value predicted by the Taguchi's additive model.

The detailed mathematical modeling to predict MRR using these results is presented in Chapter 5, Section 5.2 [163].

4.2.2 TOOL WEAR RATE (TWR)

To calculate the TWR, the weight of electrode was measured before and after machining, so that loss in weight can be calculated by taking their difference. The TWR with two repetitions was calculated and is presented in Table 4.9. The TWR is generally expressed in units of mm^3/min. A range of variation, *i.e.* an average TWR of 0.3277 mm^3/min, the lowest of 0.025 mm^3/min and highest TWR of 1.054 mm^3/min were observed.

Since copper is 99.5% pure and Cu-Cr 99.2% as compared to copper- tungsten in which copper percentage is just 29.27%, the rate of heat dissipation is more in case of copper and copper-chromium electrode, which results in more cooling effects on the electrode surface. Hence, it contributes in reduction of TWR. From observed results, it is clear that the maximum TWR was obtained 1.054 mm^3/min when copper- tungsten electrode was used and minimum value 0.025 mm^3/min, while using copper-chromium electrode.

- ***Analysis of Results***

The three repetitions of TWR were converted to a single value by calculating S/N ratio. Since TWR is a '*lower the better*' characteristic, equation 4.4 was used to measure the S/N ratio.

$$LB: S/N\ ratio = -10\log_{10}\left[\frac{1}{n}\sum_{i=1}^{n} yi^2\right] \qquad (4.4)$$

The observed values of TWR and calculated values of S/N ratios are presented in Table 4.9. The overall mean of S/N ratios (η) *i.e* 13.367 was calculated by taking the average of all the values. The corresponding S/N ratios at each level of eight input parameters and raw data are tabulated in Table 4.10.

Table 4.9: Tool Wear Rate with their Calculated S/N Ratios

Exp. No.	Levels of parameters								Tool wear rate (mm^3/min)			Mean value	S/N ratio (dB)
	A	B	C	D	E	F	G	H	R-1	R-2	R-3		
1	1	1	1	1	1	1	1	1	0.098	0.090	0.095	0.094	20.493
2	1	1	2	2	2	2	2	2	0.029	0.027	0.027	0.028	31.219
3	1	1	3	3	3	3	3	3	0.134	0.138	0.134	0.135	17.373
4	1	2	1	1	2	2	3	3	0.197	0.194	0.185	0.192	14.331
5	1	2	2	2	3	3	1	1	0.389	0.444	0.418	0.417	7.585
6	1	2	3	3	1	1	2	2	0.204	0.146	0.169	0.173	15.145
7	1	3	1	2	1	3	2	3	0.631	0.619	0.629	0.626	4.063
8	1	3	2	3	2	1	3	1	0.402	0.391	0.378	0.391	8.165
9	1	3	3	1	3	2	1	2	0.712	0.735	0.726	0.724	2.798
10	2	1	1	3	3	2	2	1	0.177	0.136	0.189	0.167	15.442

11	2	1	2	1	1	3	3	2	0.056	0.069	0.071	0.065	23.651
12	2	1	3	2	2	1	1	3	0.021	0.028	0.023	0.025	32.161
13	2	2	1	2	3	1	3	2	0.459	0.445	0.457	0.454	6.857
14	2	2	2	3	1	2	1	3	0.259	0.218	0.233	0.236	12.502
15	2	2	3	1	2	3	2	1	0.169	0.122	0.153	0.148	16.498
16	2	3	1	3	2	3	1	2	0.594	0.509	0.582	0.5618	4.989
17	2	3	2	1	3	1	2	3	1.027	1.045	1.089	1.054	-0.457
18	2	3	3	2	1	2	3	1	0.393	0.424	0.405	0.407	7.794

$\overline{T_{TWR}}$ = Overall mean of TWR = 0.3277 mm^3/min Mean of S/N ratio η = 13.367

- ***Analysis of Significant Factor using ANOVA Technique***

In this section, the significant parameters which influence the TWR were determined by using ANOVA approach by comparing the statistically calculated F-value with standard tabulated F_{tab}-values at 95% confidence level. For significance of different parameters, F-values should be greater than F_{tab}- values (refer Table 4.11). The percentage contribution of each input process parameter is presented in Table 4.11. By observing Table 4.11, it can be concluded that peak current (factor-B) is the most significant factor with a percentage contribution of 73.93 %. Type of tool material and their properties (factor-E) also affect the TWR, and had a contribution of 19.30%. The pulse-on-time (factor-C) and powder mixed dielectric (factor-D) have less significance with a contribution of 3.85% and 1.62 %, respectively, whereas, pulse-off-time shows insignificant effect on TWR. The effect of CT of tool and workpiece on TWR was observed to be insignificant. Moreover, delta value and ranking of individual factors can be seen in Table 4.12, which shows the peak current has the first rank, electrode material second rank and pulse-on-time third rank.

Table 4.10: Average Values by Factor Levels of S/N Data and Raw Data for TWR

Control Factors	Raw data (mm^3/min)			S/N ratio (dB)		
	Level 1	Level 2	Level 3	Level 1	Level 2	Level 3
A	0.309	0.346	----	13.464	13.271	----
B	0.086	0.270	0.627	23.390	12.153	4.559
C	0.349	0.365	0.269	11.029	13.777	15.295
D	0.380	0.326	0.277	12.886	14.946	12.269
E	0.267	0.224	0.492	13.941	17.894	8.266

F	0.365	0.292	0.326	13.727	14.014	12.360
G	0.343	0.366	0.274	13.422	13.652	13.028
H	0.271	0.334	0.378	12.663	14.110	13.329

Table 4.11: ANOVA Results for TWR (S/N Ratios)

Control Factors	DOF	Seq. SS	Adj. SS	Adj. MS	F-value	%PC	Remarks
A	1	0.17	0.17	0.17	0.16		
B	2	1077.08	1077.08	538.542	519.57	73.93	***
C	2	56.10	56.10	28.050	27.06	3.85	*
D	2	23.59	23.59	11.793	11.38	1.62	*
E	2	281.05	281.05	140.524	135.57	19.30	**
F	2	9.38	9.38	4.689	4.52		
G	2	1.19	1.19	0.596	0.57		
H	2	6.30	6.30	3.148	3.04		
Error	2	2.07	2.07	1.037			
Total	17	1456.92					

*** Most Significant, ** Significant, * Less Significant, $F_{tab} = F(2,9) = 4.2565$

While comparing TWR for three cases conducted at 6A current: (i) Cu WCT and Cu DCT for experiment number 1 and 11, (ii) Cu-W SCT and Cu-W DCT for experiment 3 and 10 and (iii) Cu-Cr WCT and Cu-Cr SCT, significant improvement of 30.7%, 19.20%, 12% respectively was observed. Current was observed to be the most significant factor as compared to other input parameters. Gill et al. in another study reported that cryogenic treatment performs more consistently under interrupted machining mode than continuous machining mode [132]. As EDM is a continuous machining process, so due to this reason less effect of cryogenic treatment was observed on TWR during the process.

Table 4.12: Response Table for S/N Ratios (Smaller the better)

Level	A	B	C	D	E	F	G	H
1	13.464	23.390	11.029	12.886	13.941	13.727	13.422	12.663
2	13.271	12.153	13.777	14.946	17.894	14.014	13.652	14.110

3	-----	4.559	15.295	12.269	8.266	12.360	13.028	13.329
Delta	0.193	18.831	4.266	2.677	9.628	1.654	0.623	1.447
Rank	8	1	3	4	2	5	7	6

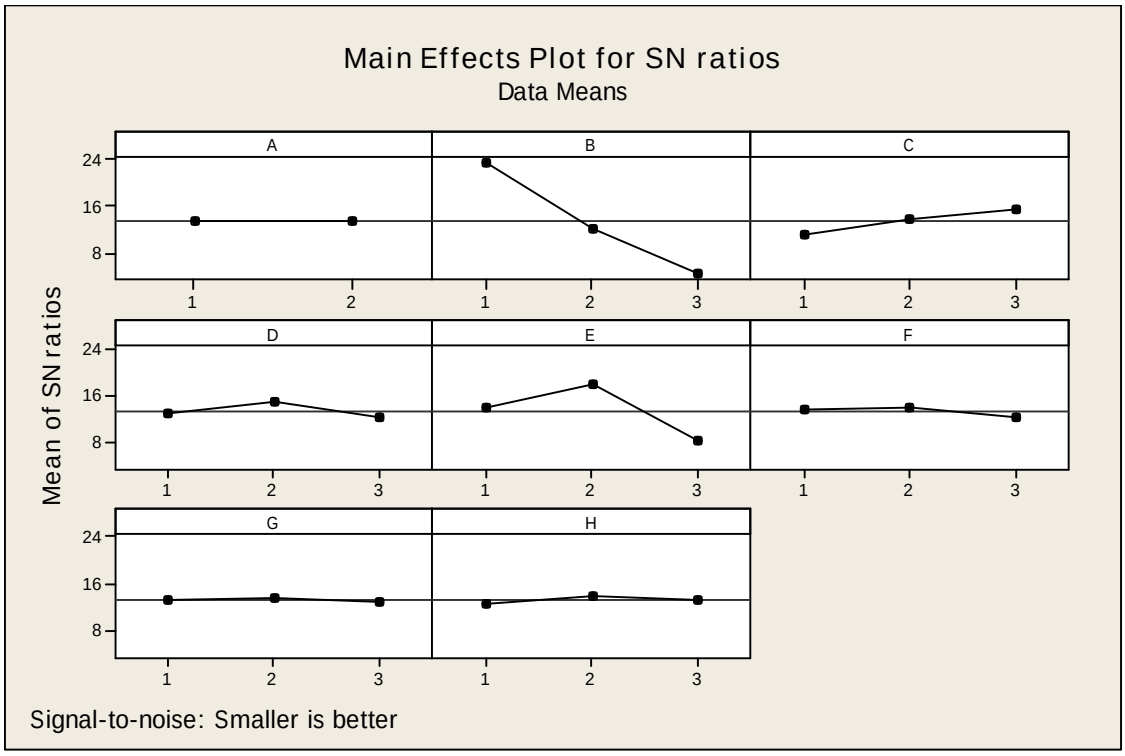

Figure 4.3: Main Effects Plot for S/N Ratios (Smaller-the-better) of TWR

- ***Determination and Evaluation of Main Effects for Optimal Machining Parametric Combination***

The level wise average values and corresponding S/N ratios of TWR of all the eight parameters are listed in Table 4.12. These average values represent the factor effect of all the input parameters. In addition to this, the effect of all the control factors is plotted in Figure 4.3, from where it can be concluded that a low TWR is measured at first level of T_{off} 30 µs (A_1), first level of I_p 6A (B_1), third level of T_{on} 150 µs (C_3), second level of dielectric fluid i.e Mn powder mixed with EDM oil (D_2), second level of electrode material (E_2) *i.e.* copper-chromium electrode, second level of electrode cryo-treatment (F_2) *i.e.* SCT, second level of workpiece material (G_2) *i.e.* TITAN 21 (Ti-5Al-2.5Sn) and second level of cryo-treatment of workpiece material (H_2) *i.e.* SCT. Therefore, the optimum condition of input process parameters can be written as $A_1B_1C_3D_2E_2F_2G_2H_2$.

Where A, B, C….. represent the control factors and 1, 2 or 3 depict the level at which factors were varied.

- ***Theoretical Prediction of TWR By Taguchi Methodology***

From Figures 4.3, the optimum combination of input parameters for low TWR during EDM of different titanium alloy was observed $A_1B_1C_3D_2E_2F_2G_2H_2$.

The estimated value of η_{opt} under the optimum condition for factors is then given by equation (4.5) [97]:-

$$\eta_{opt} = \eta + (\eta_{A1}-\eta) + (\eta_{B1} - \eta) + (\eta_{C3} - \eta) + (\eta_{D2} - \eta) + (\eta_{E2} - \eta) + (\eta_{F2} - \eta) + (\eta_{G2} - \eta) + (\eta_{H2} - \eta) \quad (4.5)$$

Where η is the overall mean of S/N data, η_{A1} is the mean of S/N data for factor A at level 1, ηB1 is the mean of S/N data for factor B at level 1 and so on.

Thus, value of η_{opt} = 33.196

The corresponding best value for tool wear rate is given by equation (4.6):

$$Y_{opt}^{\ 2} = 10^{-\eta_{opt}/10} \quad (4.6)$$

Or Y_{opt} = 0.02188 mm^3/min

A set of three confirmation experiments at optimal setting was performed to check the validity of the results. The mean value of TWR at this setting ($A_1B_1C_3D_2E_2F_2G_2H_2$) was found to be 0.02127 mm^3/min which is close to the predicted theoretical value 0.02188 mm^3/min.

The detailed mathematical modeling to predict TWR using these results is presented in Chapter 5, Section 5.3.

4.2.3 SURFACE ROUGHNESS (SR) OF WORKPIECE

Superior surface finish is a major requirement for all machined components. Simply, SR is the evaluation of the surface texture in terms of surface irregularities, waviness and flaws. Different methods are available for measuring the SR values of the machined work pieces. After, the experimentation, all the machined samples were cleaned with acetone solution. The surface roughness of all the samples was measured using MITUTOYO Surface Roughness

Tester (Model: Surf test SJ-400) at a cut of length of 0.8 mm. During the present study, surface roughness values in terms of arithmetic average deviation of the assessed profile (R_a), root mean square deviation of the assessed profile (R_q) and average maximum height of the profile (R_z) was measured for machined samples after each trial. However, the analysis has been done using only the arithmetic average roughness expressed in terms of R_a expressed in microns. The three values of surface roughness R_1, R_2 and R_3 for R_a are shown in Table 4.13. Standard deviation of the three roughness readings after each of the 18 experiments was calculated with the help of MINITAB 16 and is given in Table 4.13. The variance and reliability coefficient (Cronbach Alpha = 0.891) was calculated using SPSS. Since, surface roughness is a "*smaller the better*" response, the S/N ratio was also calculated using MINITAB 16 and the results are given in Table 4.13.

Table 4.13: Surface Roughness values in Rz, Rq and Ra

Trial No	Surface Roughness (Rz)			Surface Roughness (Rq)			Surface Roughness (Ra)				Std. Dev.	S/N ratios (dB)
	R1	R2	R3	R1	R2	R3	R1	R2	R3	Avg.		
1	22.4	23.6	25.5	4.52	4.72	5.66	3.60	3.70	4.53	3.94	0.51	-11.96
2	32.3	29.8	27.1	7.27	7.03	5.64	5.53	5.71	4.46	5.23	0.68	-14.42
3	25.4	27.5	24.8	5.93	6.35	5.85	4.82	5.07	4.79	4.89	0.15	-13.79
4	24.4	26.0	31.7	5.59	4.86	6.35	4.60	3.67	4.86	4.38	0.63	-12.88
5	40.9	40.8	43.4	10.55	9.92	9.73	8.52	7.96	7.44	7.97	0.54	-18.05
6	31.4	28.2	43.1	7.93	6.16	11.46	6.33	4.79	9.42	6.85	2.36	-17.04
7	35.9	38.5	40.7	8.72	9.83	9.13	7.02	8.19	7.28	7.49	0.61	-17.52
8	29.9	38.3	30.4	6.58	8.40	7.08	5.19	6.62	5.66	5.82	0.73	-15.35
9	46.27	43.0	44.0	11.52	10.7	11.07	9.52	8.84	9.12	9.16	0.34	-19.24
10	26.6	27.3	19.8	4.95	5.66	3.80	3.66	4.37	3.01	3.68	0.68	-11.41
11	22.0	23.8	24.4	4.90	4.78	5.66	3.97	3.76	4.61	4.11	0.44	-12.32
12	27.2	26.9	28.7	5.21	5.69	5.96	4.13	4.36	4.43	4.31	0.16	-12.69
13	26.0	24.1	30.9	6.78	4.37	7.08	4.90	3.30	5.60	4.60	1.18	-13.44
14	37.4	31.3	34.4	7.93	7.31	7.27	6.14	5.93	5.54	5.87	0.30	-15.38
15	40.4	27.7	26.5	9.17	6.61	6.66	7.21	5.36	5.50	6.02	1.03	-15.68
16	31.2	28.1	30.7	6.91	6.62	6.94	5.42	5.48	5.54	5.48	0.06	-14.77
17	34.8	40.6	31.3	8.17	9.18	6.99	6.38	7.20	5.68	6.42	0.76	-16.19
18	37.0	41.0	33.1	9.13	9.20	7.27	7.59	7.18	5.66	6.81	1.02	-16.73

- ***Analysis of Results***

Table 4.13 shows the results of SR values and S/N ratios of all the data. The calculated S/N ratios based on '*Lower-the-better*' quality characteristic are listed in Table 4.13. The overall mean value of S/N ratio -14.94 and overall mean value for SR 5.73 (Ra) was observed. The corresponding average values of raw data and S/N ratios for all the selected control factors at each level was calculated and listed in Table 4.14.

Table 4.14: Average Values by Factor Levels of S/N Data and Raw Data for SR

Process Parameters	Levels	Average value (Ra)	S/N Ratio (dB)
Pulse-off-time (A)	1	6.19	-15.58
	2	5.25	-14.29
Peak current (B)	1	4.36	-12.77
	2	5.95	-15.41
	3	6.86	-16.63
Pulse-on-time I	1	4.93	-13.67
	2	5.91	-15.28
	3	6.34	-15.86
Dielectric fluid (D)	1	5.67	-14.71
	2	6.07	-15.47
	3	5.43	-14.63
Electrode materials (E)	1	5.85	-15.16
	2	5.21	-14.30
	3	6.12	-15.36
Cryogenics of	1	5.32	-14.45
electrode materials (F)	2	5.85	-15.01
	3	5.99	-15.36
Workpiece materials (G)	1	6.12	-15.35
	2	5.95	-15.38
	3	5.10	-14.09
Cryogenics of work	1	5.71	-14.86
materials (H)	2	5.91	-15.21
	3	5.56	-14.74

- ***Analysis of Variance (ANOVA)***

Information can be obtained from ANOVA about the controlled parameters that how much individual parameter is significant which affects the response characteristics. The analysis of variance for S/N data and raw data was carried out to determine the significance of input process parameters (see Table 4.15).

Table 4.15: Analysis of Variance (ANOVA) of Control Parameters for SR

Factors	DOF	ANOVA for S/N Data					ANOVA for Raw Data				
		Seq. SS	Adj. SS	F	%PC	Remarks	Seq. SS	Adj. SS	F	%PC	Remarks
A	1	7.53	7.53	193.13	8.74	√√	3.96	3.96	29.01	10.14	√√
B	2	46.87	23.44	600.92	54.38	√√√	19.25	9.62	70.49	49.27	√√√
C	2	15.55	7.77	199.36	18.04	√√	6.26	3.13	22.93	16.03	√√
D	2	2.61	1.31	33.46	3.03	√	1.25	0.62	4.56	3.19	X
E	2	3.78	1.89	48.44	4.38	√	2.64	1.32	9.66	6.75	X
F	2	2.53	1.27	32.46	2.94	√	1.51	0.76	5.54	3.87	X
G	2	6.54	3.27	83.84	7.59	√	3.57	1.79	13.09	9.15	X
H	2	0.69	0.35	8.92	0.81	x	0.36	0.18	1.32	0.92	X
Error	2	0.08	0.04	1.00	0.09		0.27	0.14		0.70	
Total	17	86.19			100.0		39.07			100.00	

x- not significant, √ - less significant, √√- significant, √√√-most significant

F_{tab} = F (2,2) = 19.000; F (1,2) = 18.513

The current was observed to be the most significant parameter with contribution 54.38 %, followed by a pulse-on-time with 18% affecting surface roughness. Pulse-on-time is the time which indicates the time period in which energy is supplied to the machining zone [58]. The pulse-off-time shows their impact on surface roughness with percent contribution of 8.74%. During this period, machining cycle is completed. On the other hand, too much short duration of this time creates a problem during flushing, because eroded material from the gap will not be flushed completely by the continuously circulating liquid medium, thus, it will affect the surface finish in a negative way. The types of workpiece material and electrode material also influence the surface texture. Here, work material affects the surface roughness with 7.59% and electrode material with 4.38%. The other parameters, such as powder mixed dielectric fluid, cryogenic treatment of electrode material contributes approximately 3% each. The

individual influence of all the parameters with their significance is summarized in Table 4.15 for both data.

- ***Assessment of the Main Effects***

The analysis was carried out by considering the average of SR (raw data) and S/N ratios for each parameter at levels 1, 2 and 3 as shown in Table 4.14. The obtained values were plotted in graphical form. The main effects of each parameter are shown in Figures 4.4 (a –h). The average of response levels helps in studying the trend of the performance with respect to the variation of the selected factors.

Figure 4.4 (a) shows that SR improves as T_{off} increased from 30 µs to 45 µs because debris particles flushed away from the gap with pressurized dielectric. Figure 4.4 (b) shows the trend of peak current. The curve shows that as current increases, surface roughness also increases. The minimum SR is observed at I_p 6A and maximum at I_p 14A. At higher current 14A more energy is applied to the machining zone resulted in larger and deeper craters on the surface, which deteriorates the surface finish. Similarly, T_{on} affects the SR. Longer T_{on} reduces the surface finish because energy is applied for a longer time. At short T_{on}, better surface finish is produced as shown in Figure 4.4 (c). Figure 4.4 (d) explores the effect of powders on the surface finish. Tungsten powder mixed dielectric improves the surface texture as compared to manganese powder. The electrode material copper-tungsten produced the poorer surface finish than copper, where copper-chromium improves the surface finish as shown in Figure 4.4 (e). The alloy Ti-6Al-4V gives a better surface finish than other two grades of titanium alloy as shown in Figure 4.4 (g). The effect of cryogenic treatment of a workpiece and electrode is less on the surface finish as presented in Figures 4.4 (f &h).

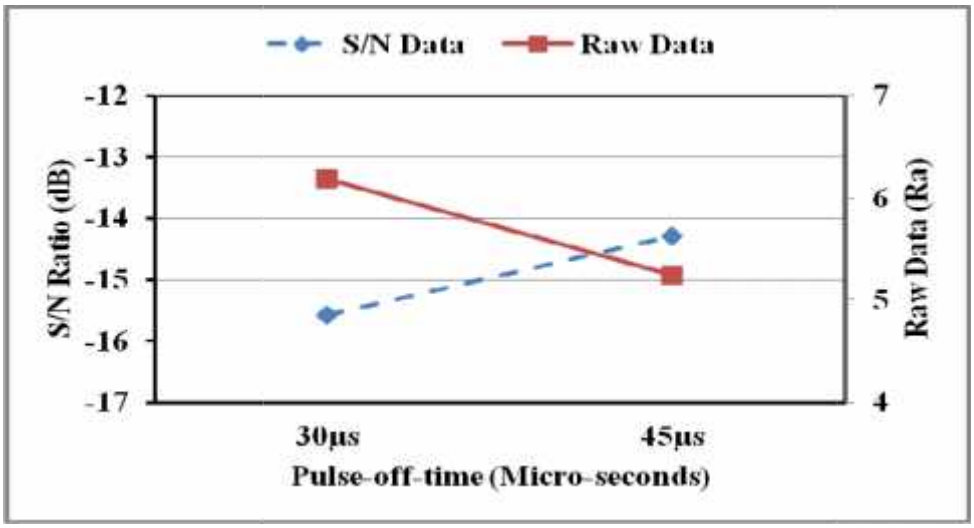

Figure 4.4: (a) Effect of Pulse-off-time on SR

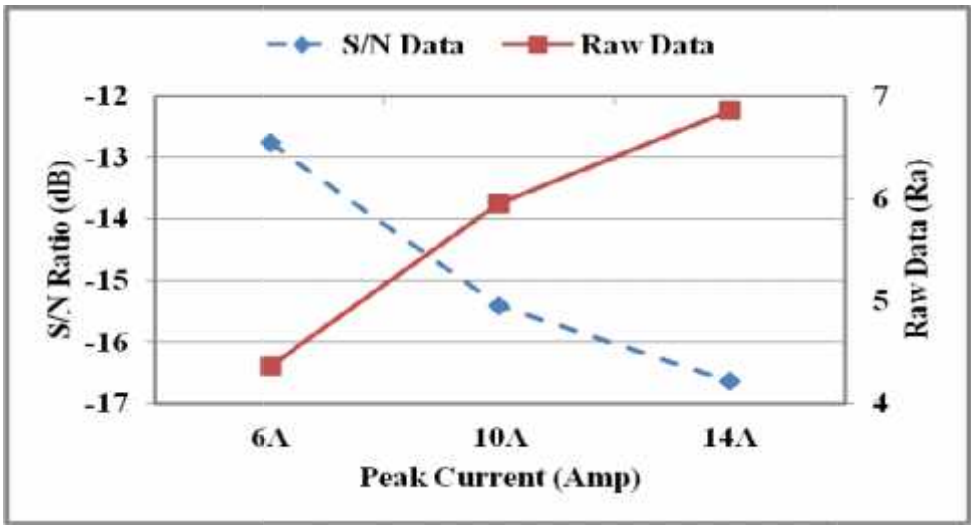

Figure 4.4: (b) Effect of Peak current on SR

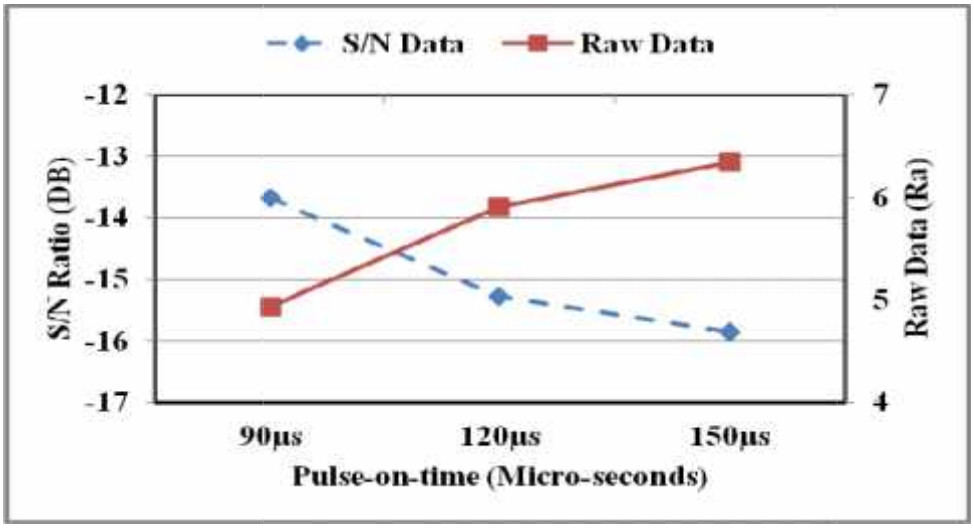

Figure 4.4: I Effect of Pulse-on-time on SR

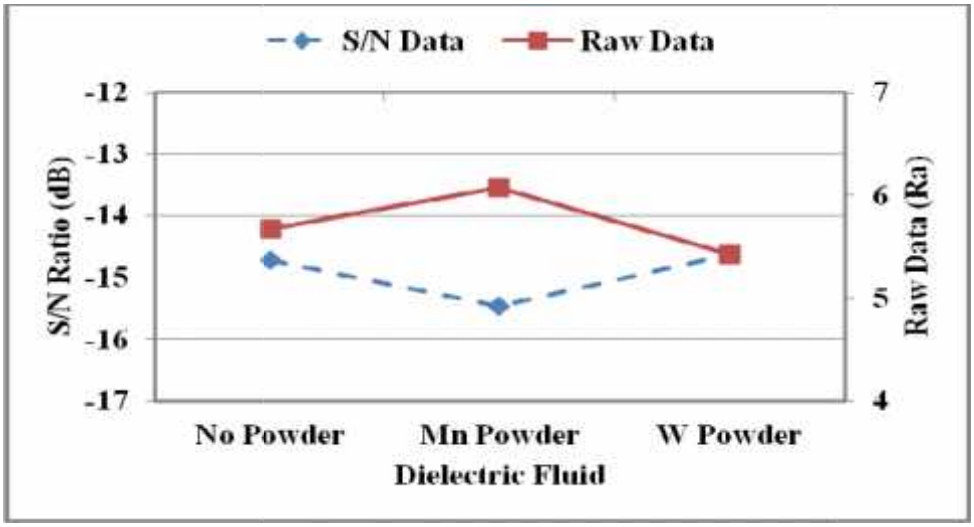

Figure 4.4: (d) Effect of Powder Mixed Dielectric Fluid on SR

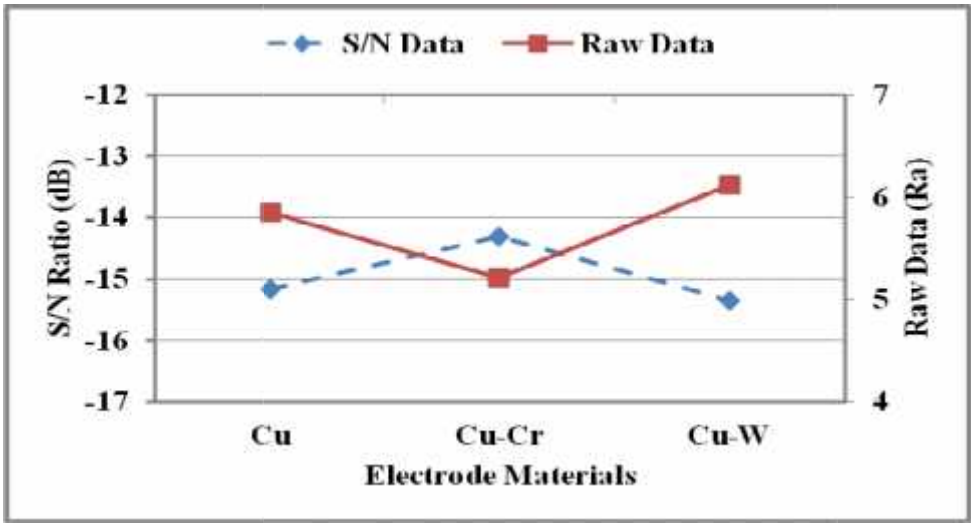

Figure 4.4: (e) Effect of Tool-electrode Materials on SR

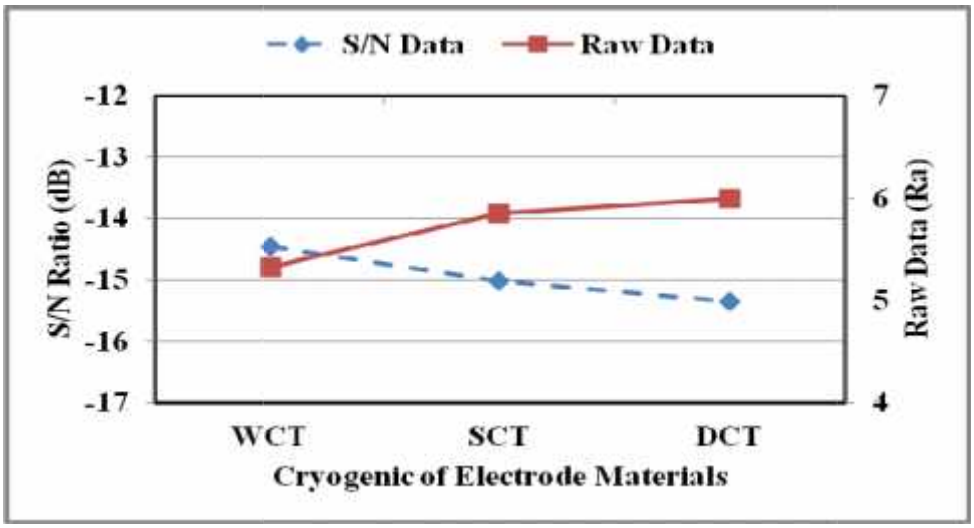

Figure 4.4: (f) Effect of Cryogenic Treatment of Electrode Materials on SR

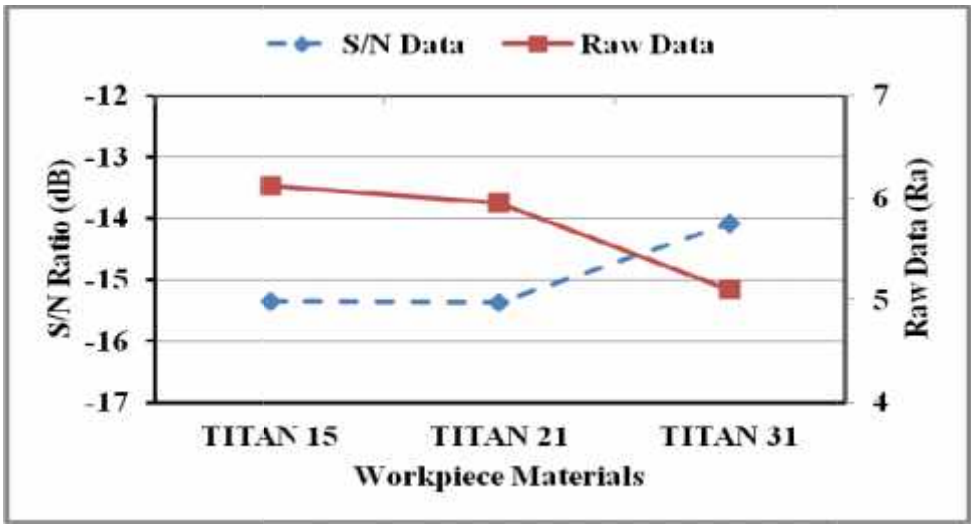

Figure 4.4: (g) Effect of Workpiece Materials on SR

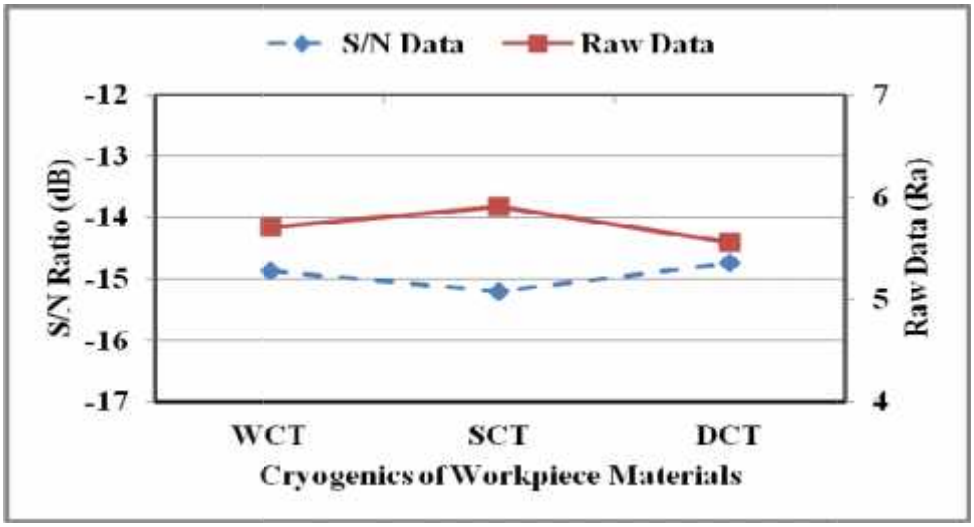

Figure 4.4: (h) Effect of Cryogenic Treatment of Workpiece Materials on SR

From Figures 4.4 (a-h) and Table 4.14, it was observed that the second level of T_{off} (45µs), first level of I_p (6A), first level of T_{on} (90µs), third level of dielectric fluid (mixed with tungsten powder), second level of electrode material (Cu-Cr), first level of cryogenic treatment of electrode material, *i.e.* without cryo-treatment (WCT), third level of work material (Ti-6Al-4V) and third level of work material's cryogenic treatment i.e. deep cryo-treatment (DCT) gives the best value of surface roughness. Hence, the optimum condition of input process parameters is ($A_2B_1C_1D_3E_2F_1G_3H_3$).

The detailed modeling to predict surface roughness of workpiece using these results with ANN approach is presented in Chapter 5, Section 5.4 [162].

4.2.4 MICRO-HARDNESS (MH)

Due to the migration of materials from electrode and dielectric medium, the surface properties of machined specimen is modified and measured in terms of micro-hardness. The wear resistance of the machined surface also increases, which is desirable for various industrial applications. Micro-hardness of the surface has been measured on a digital display micro-hardness tester (model: HVS-1000B). Before measuring the micro-hardness, all the specimens were properly cleaned with acetone solution to remove any dust particles by using soft brush. During the micro-hardness test, the indentation was made using a diamond indenter of pyramid shape under a test force of 9.807 N and dwell time of 10 Sec. The values

of surface micro-hardness for all the machining tests are presented in Table 4.16 in terms of R1, R2 and R3.

Table 4.16: Micro-hardness with their Calculated S/N Ratios

Exp. No.	Micro-hardness of machined samples				Before Machining	Improvement (%)	S/N of Ratios
	R1	R2	R3	Average			
1.	393	412	352	385.667	270	42.85	51.667
2.	432	397	425	418.000	310	34.85	52.406
3.	438	435	472	448.333	366	22.48	53.014
4.	465	445	425	445.000	366	21.58	52.949
5.	443	510	465	472.667	270	75.07	53.447
6.	482	465	502	483.000	310	55.80	53.666
7.	517	508	522	515.667	320	61.15	54.246
8.	562	610	548	573.333	315	82.00	55.141
9.	495	557	527	526.333	272	93.50	54.395
10.	457	437	445	446.333	305	46.33	52.989
11.	465	481	427	457.667	340	34.62	53.178
12.	442	415	435	430.667	287	50.07	52.674
13.	527	490	538	518.333	340	52.44	54.271
14.	475	517	510	500.667	287	74.45	53.973
15.	526	510	465	500.333	305	64.03	53.949
16.	540	515	535	530.000	272	94.85	54.480
17.	582	615	602	599.667	320	87.40	55.552
18.	592	602	620	604.667	315	91.96	55.626

$\overline{T_{MH}}$ = The overall mean of MH = 492 HVN, Mean of S/N ratio η = 53.757

- ***Analysis of Results***

'*Higher-the-better*' type of quality characteristic was applied for transforming the raw data to S/N ratio. The calculated S/N ratios for all the 18 number of trials are listed in Table 4.16. A range of variation, *i.e.* 352 HVN to 620HVN of micro-hardness, overall mean 492 (HVN), the minimum value 352 HVN and the maximum value 620HVN was observed. The micro-hardness of all the work samples before machining was also measured, and the observed

values are presented in the same Table 4.16. It is clear from Table 4.16 that the improvement in surface hardness after EDM was observed in the range of 21.58% to 94.85%.

- ***ANOVA for Micro-Hardness***

The results for response which have been listed in Table 4.16 were analyzed by using ANOVA technique. Table 4.17 and 4.18 shows the ANOVA results calculated by using MINITAB 16 software for S/N ratio and means respectively.

Table 4.17: ANOVA Results for Micro-hardness (S/N Ratio)

Control Factors	DOF	Seq. SS	Adj. MS	F-value	P	%PC	Significance of Factors
A	1	1.842	1.842	298.07	0.003	9.33	Significant
B	2	15.233	7.616	1232.35	0.001	77.15	Most Significant
C	2	0.951	0.476	76.94	0.013	4.82	Significant
D	2	0.210	0.105	17.01	0.056	1.06	Not Significant
E	2	0.365	0.183	29.54	0.033	1.85	Less Significant
F	2	0.046	0.024	3.74	0.211	0.23	Not Significant
G	2	1.065	0.533	86.14	0.011	5.40	Significant
H	2	0.019	0.009	1.56	0.390	0.10	Not Significant
Error	2	0.012	0.006			0.06	
Total	17	19.744					

F_{tab} = F (2,2) = 19.000; F (1,2) = 18.513

Only one factor current was identified as the most significant parameter with highest percent contribution of 77.15% and has the first rank in the response table with a higher delta value 2.25, which highly affected the micro-hardness value of machined surface. Thereafter, pulse-off-time with 9.33% identified as the second significant parameter, also contributing in increases the surface hardness value. The contribution of pulse-on-time (4.82%) and workpiece (5.40%) and electrode material (1.85%) on MH was minimal. The other

parameters, namely powder mixed dielectric fluid, cryogenic treatment of electrode and workpiece materials had no effect on MH.

Table 4.18: ANOVA Results for Micro-hardness (Means)

Control Factors	DOF	Seq. SS	Adj. MS	F-value	P	%PC	Significance of Factors
A	1	5700.7	5700.7	78.44	0.013	9.00	Significant
B	2	48771.9	24385.9	335.56	0.003	77.05	Most Significant
C	2	3154.9	1577.5	21.71	0.044	4.98	Significant
D	2	389.6	194.8	2.68	0.272	0.62	Not Significant
E	2	1095.0	547.5	7.53	0.117	1.73	Not Significant
F	2	393.9	196.9	2.71	0.270	0.62	Not Significant
G	2	3407.6	1703.8	23.44	0.041	5.38	Significant
H	2	242.2	121.1	1.67	0.375	0.38	Not Significant
Error	2	145.3	72.7			0.24	
Total	17	63301.2					

Table 4.19: Response Table for S/N Ratios (Larger the better)

Level	A	B	C	D	E	F	G	H
1	53.44	52.65	53.43	53.62	53.73	53.83	53.44	53.80
2	54.08	53.71	53.95	53.78	53.60	53.72	53.80	53.73
3	---	54.91	53.89	53.88	53.94	53.72	54.03	53.73
Delta	0.64	2.25	0.52	0.26	0.34	0.11	0.59	0.07
Rank	2	1	4	6	5	7	3	8

Table 4.20: Response Table for Means

Level	A	B	C	D	E	F	G	H
1	474.2	431.1	473.5	485.8	491.2	498.4	474.3	497.2
2	509.8	486.7	503.7	493.3	482.9	490.2	493.8	488.9
3	---	558.3	498.9	496.9	501.9	487.4	507.9	490.0
Delta	35.6	127.2	30.2	11.2	19.1	11.0	33.6	8.3
Rank	2	1	4	6	5	7	3	8

Tables 4.19 and 4.20 presents the response of quality characteristic for S/N ratio and means respectively. Both the tables show the ranks of the various control factors in order of their significance. Besides ranking of the control factors, these tables are also presented S/N ratios and means values of each factor according to their levels.

- ***Assessment of the Main Effects***

The main effects plots represent the variation of micro-hardness with each input process parameters are plotted in Figure 4.5 (a-h). From Figure 4.5 (a), it can be clearly seen that the value of MH increases as T_{off} increases from 30 µs to 45 µs. Machining at the setting of the low value of T_{off} and higher value of I_p and T_{on} resulted in arcing, resulting in unstable machining. It may be due to less deionization time, available to the dielectric medium. Hence, maximum surface hardness was obtained at higher values of T_{off} setting.

The peak current was observed to be the most significant machining parameter in the EDM process as is evident from the ANOVA results (See Table 4.17 & 4.18). The trend of peak current shows that MH increases linearly as the value of current increases from 6A to 10A and further from 10A to 14A. Peak current facilitates in generating the sparks, which help to obtain a higher temperature depending upon the current density. Due to this phenomenon, deposition of the materials on the machined surface takes place. Hence, in a simple way, it means higher the value of peak current, higher is the deposition rate of the various materials on the workpiece surface. The most important reason behind the increase in micro-hardness of workpiece surface in EDM of titanium alloy is the formation of TiC compound due to the interaction of Ti element and cracked carbon transfer from the dielectric medium. Figure 4.5 (b) highlights that maximum hardness was observed at 14A current also shown in Table 4.16 for trial number 18. Some researchers also reported that the MH increases for higher current setting [97, 101].

The effect of T_{on} on MH is shown in Figure 4.5 I. It can be seen that, initially, the MH increases sharply as T_{on} increases from 90 µs to 120 µs, and steady decrease in hardness was observed in the range of 120 µs to 150 µs. The same results are also reported by Kumar et al. [135].

Figure 4.5 (d) explored the effect of powder mixed dielectric on MH. It was concluded that tungsten powder mixed dielectric gives higher MH followed by manganese powder mixed dielectric. The trend shows that the powder mixed dielectric had less effect on MH as compared to other parameters. Here, the effect of powder mixed dielectric is less on micro-hardness (< 1%), which has sixth rank in the response table. It may be possible that change in powder concentration may affect the surface hardness significantly.

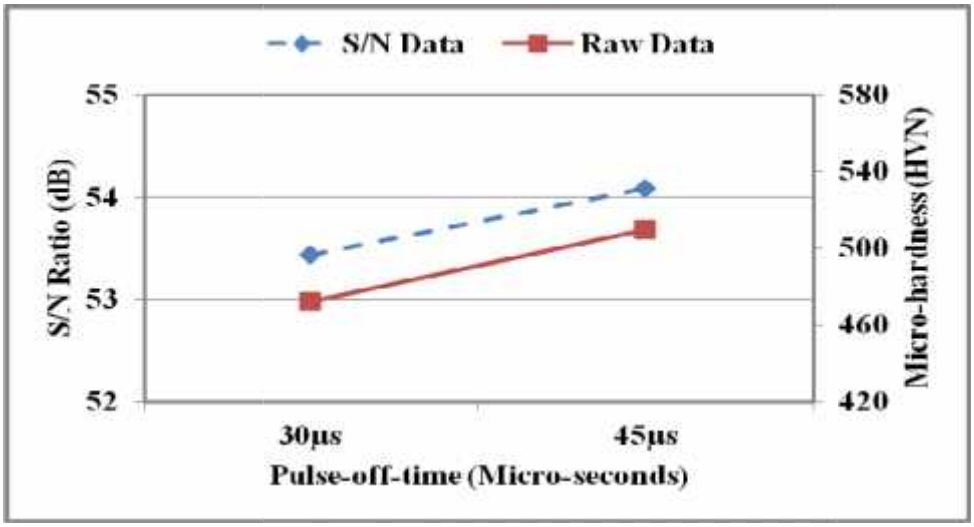

Figure 4.5: (a) Effect of Pulse-off-time on Micro-hardness

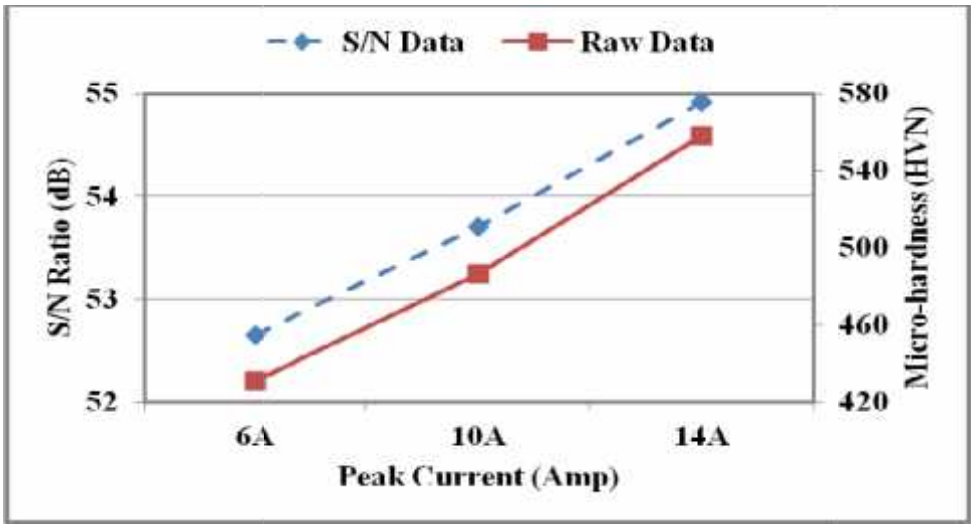

Figure 4.5: (b) Effect of Peak Current on Micro-hardness

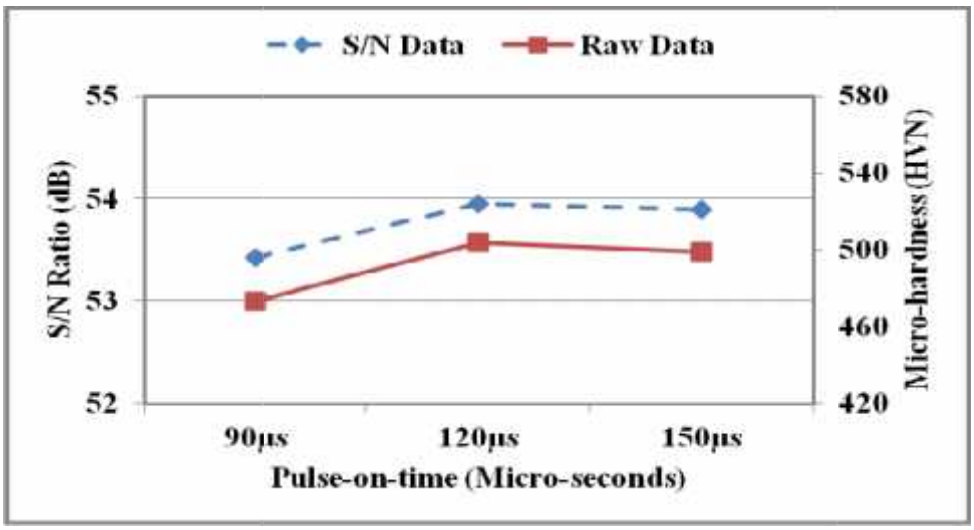

Figure 4.5: (c) Effect of Pulse-on-time on Micro-hardness

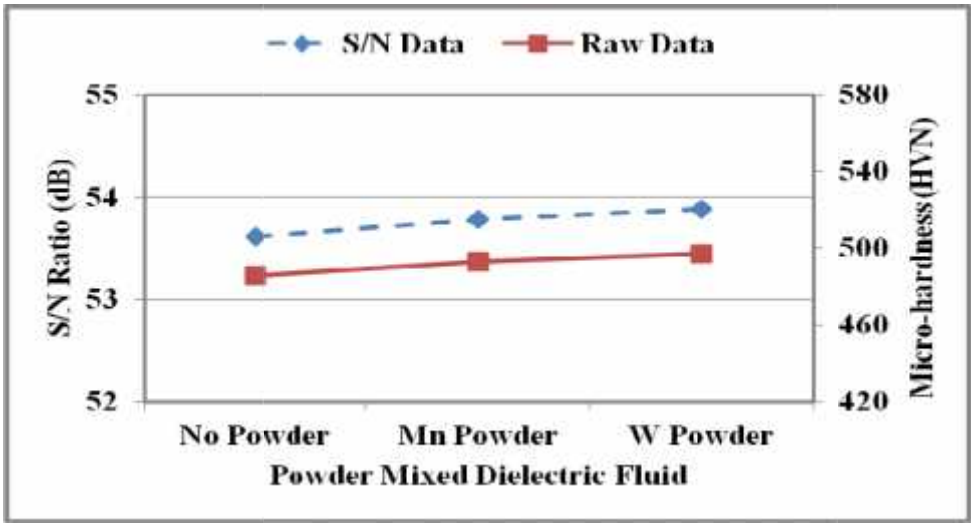

Figure 4.5: (d) Effect of Powder Mixed Dielectric Fluid on Micro-hardness

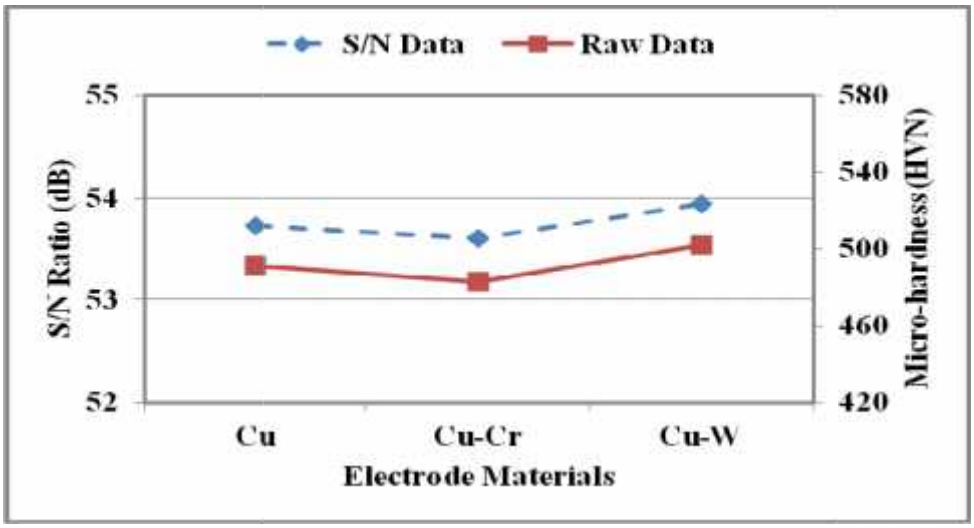

Figure 4.5: (e) Effect of Electrode Materials on Micro-hardness

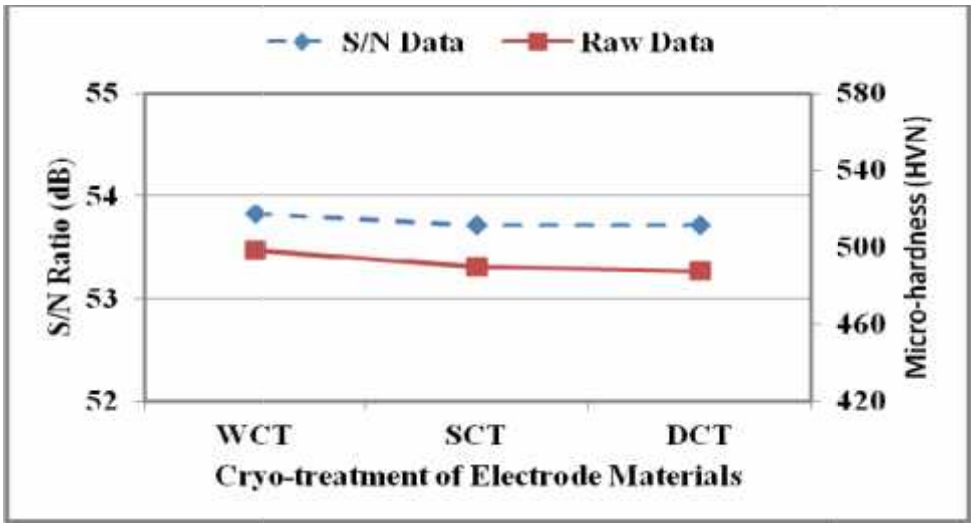

Figure 4.5: (f) Effect of Cryogenic Treatment of Electrode on Micro-hardness

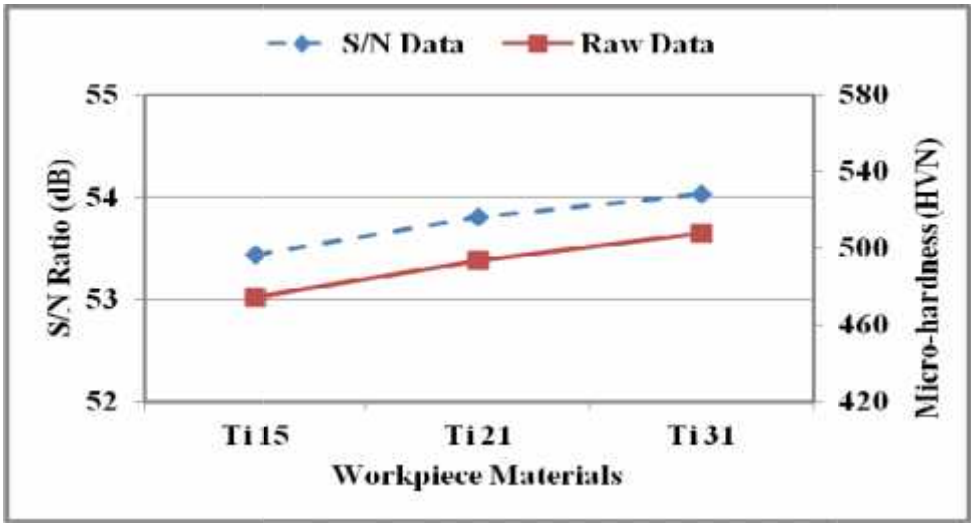

Figure 4.5: (g) Effect of Workpiece Materials on Micro-hardness

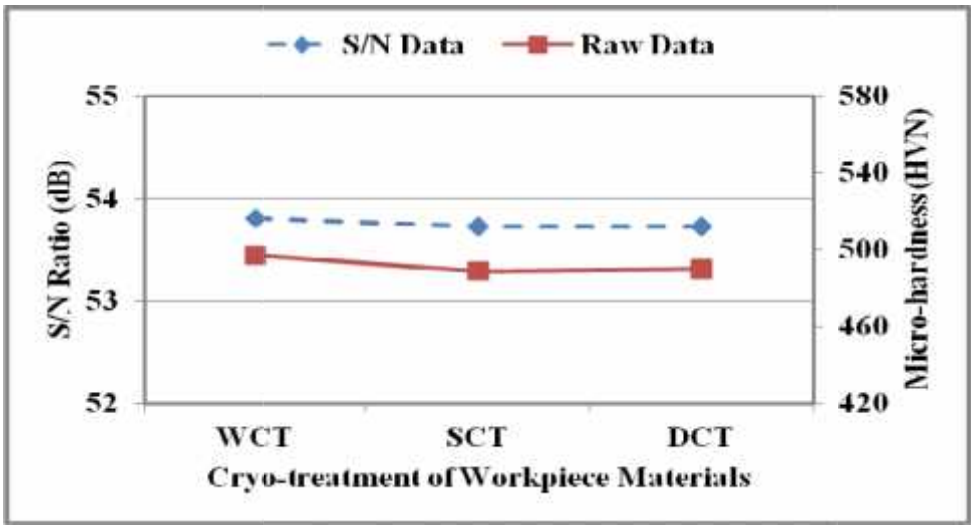

Figure 4.5: (h) Effect of Cryogenic Treatment of Workpiece on Micro-hardness

It was noticed from Figure 4.5 (e) that Cu-W electrode gives higher micro-hardness followed by Cu electrode, while Cu-Cr electrode shows a decrease in micro-hardness. A steady increase in micro-hardness has been observed with increasing the value of peak current with copper-tungsten electrode. The maximum hardness of 604.667 HVN was achieved at 14A current because of the migration of various elements from the electrode material to the specimen. The work material type and their properties significantly affected surface hardness as shown in Figure 4.5 (g). The micro-hardness is increased from grade Ti15 (Ti alloy) to grade Ti21 (Ti-5Al-2.5Sn alloy) and thereafter, from Ti21 to grade Ti31 as clearly seen in Figure 4.5 (g). Higher value 604.667 HVN of MH was observed for workpiece material Ti31 (Ti-6Al-4V) alloy due to the presence of alloying elements for trial number 18 as shown in

Table 4.5. Effects of cryogenically treated workpiece material and tool-electrode material on the micro-hardness are plotted in Figures 4.5 (f &h).

- ***Identification of Optimal Conditions, Predictions of the Mean and Confirmation of Experiments***

For maximizing the micro-hardness the peak of the plots for each control factor corresponds to the optimum condition. From the trend as shown in Figures 4.5 (a-h) maximum micro-hardness was observed at setting of input parameters such as T_{off} = 45µs; I_p =14A; T_{on} =120µs; dielectric fluid = tungsten powder mixed dielectric; electrode material =Cu-W; CT of electrode material =WCT; work material =Ti-6Al-4V and CT of work material = WCT. Hence, the optimum setting for maximum micro-hardness can be written in this form $A_2B_3C_2D_3E_3F_1G_3H_1$.

As L_{18} OA did not consist of this optimal setting of input parameters $A_2B_3C_2D_3E_3F_1G_3H_1$, therefore, a set of three confirmation experiments was conducted by using this combination. The results obtained after conducting the confirmation experiments must fall within the 95% confidence interval (CI) (α = 0.05).

The estimated mean of the response micro-hardness can be determined as follows:

The overall mean value of the observed results is; $\overline{T}$ = 492HVN

The predicted optimum value at significant factor of MH is calculated as (Table 4.18)

$MH_{opt} = \left(\overline{T}A_2 + \overline{T}B_3 + \overline{T}C_2 + \overline{T}E_3 + \overline{T}G_3\right) - \left(4\overline{T}\right)$ =613. 6 HVN

The limits were calculated at 95% confidence interval by using the following equation (4.7) [130,136]

$$ConfidenceInterval = \pm\sqrt{\frac{F_{\sim,}\left(f_1, f_2\right)\times V_e}{n_{eff}}} \qquad (4.7)$$

Where,

F_α (f_1, f_2) = Variance ratio for DOF f1 and f_2 at the level of significance α. The confidence level is (1- α)

α = 0.05, risk

f_1 = degree of freedom for mean, which is always = 1

f_2 = degree of freedom for error term = 8

n_{eff} = number of tests under that condition participating factors

From F table at 95% confidence level F_α = 5.3177

Ve = pooled error variance for MH = 146.375 (Table 4.18)

N = the total number of trials =18

$$N_{eff} = \frac{N}{1+DOF} = 18/(1+9)$$

The effective number of replications is Ne_{ff} = 1.8.

Thus, the calculated confidence interval for MH = ± 20.80

Therefore, at 95% confidence interval, the estimated mean of MH is 613.6 ± 20.80 HVN

The average value of MH obtained at this setting of ($A_2B_3C_2D_3E_3F_1G_3H_1$) was 635.667 HVN, which is very close to the theoretical value predicted value.

The detailed modeling to predict micro-hardness of using these results with ANN approach is presented in Chapter 5, Section 5.5.

4.3 MULTI-RESPONSE OPTIMIZATION OF MRR, TWR, SR AND MH USING ANALYTIC HIERARCHY PROCESS (AHP)

In this section, four responses, namely MRR, TWR, SR and MH of machined workpiece samples were globally optimized using Analytical Hierarchy Process (AHP) approach. AHP is a multi-criteria decision-making approach used to solve the complex decision problems. The optimization of various output responses with different combination of input parameters is a difficult process [137-138]. For example, if TWR is optimized individually it would have, some input parameters may be identified as which decrease the TWR (*as TWR is lower the better characteristic*). It is not necessary that these parameters may decrease the SR. The same concept applies for MRR and MH that was identified *as higher the better characteristics*. Therefore, it becomes important that all the responses must be optimized together to get useful and accurate results. Due to this reason, AHP technique is applied for multiple optimizations. AHP is a multi-level hierarchical structure of objectives, criteria, sub criteria, and alternatives.

The steps involved in AHP can be summarized as [138, 158]:

- Develop a hierarchical structure of a decision problem in terms of decision goal, alternatives and criteria for evaluating the alternatives.

- Based on the judgments, set up the priorities between the elements of hierarchical structure by using 9-point “Fundamental Scale of Saaty” presented in Table 4.21.

- Compute relative weight for the pair wise comparison matrices using eigenvector method.
- Judge the scope of inconsistency using the largest eigenvector (λ_{max}). The judgment of accepted degree of consistency can be checked by means of a consistent ratio (CR) of consistency index (CI) with the appropriate value of random index (RI) from Table 4.22.
- Repeat the above steps for all levels in the hierarchy.
- Evaluate the overall relative value of the linear addition function.
- Conclude the final decision of this process.

Table 4.21: Satty's Fundamental Scale [139]

Scale Value	Explanation
1	Equally preferred
3	Slightly more preferred
5	Strongly more preferred
7	Very strongly more preferred
9	Extremely preferred
2,4,6,8	Used to reflect comprise between scale value

Table 4.22: Random Consistency Index

k	**1**	**2**	**3**	**4**	**5**	**6**	**7**	**8**	**9**	**10**	**11**	**12**	**13**
RI	0.00	0.00	0.58	0.90	1.12	1.24	1.32	1.41	1.45	1.49	1.51	1.48	1.48

4.3.1 IMPLEMENTATION OF AHP FOR MULTI OPTIMIZATION OF MACHINING RESPONSES

AHP was implemented step by step for optimizing the machining input parameters to determine the best combination of input parameters. Here, the criteria are to maximize the MRR and MH and minimize the TWR and SR. The design of experiments as presented in Table 4.23 represents 18 trials with 09 trials each for different T_{off}, sample-I of 30µs for trial number 1-9 and sample-II of 45µs for trial number 10-18, which leads to two optimum solutions, one for each assigned T_{off} i.e. 30µs and 45µs. In the present case, hierarchy formed for AHP solution is shown in Figure 4.6. The average results for four output parameters are listed in Table 4.23.

Machining of titanium is an important issue. Due to this reason, largest weight is given to MRR followed by TWR, SR and MH. Also, in place of using a subjective criteria illustrated in Table 4.21, the decision to give the relative importance to the alternatives was made using the observed experimental results for MRR, TWR, SR and MH as presented in Table 4.23. A pair wise comparison matrix of criteria such as MRR, TWR, SR and MH (4×4) matrix was constructed as shown in Table 4.24. The criteria weight (Priority Vector) as obtained from the normalized eigen vector (also called a **priority vector)** corresponding to maximum eigen value i.e. $\lambda_{max} = 4.1138$. Since it is normalized, the sum of all elements in priority vector is 1.

Table 4.23: Average Response for MRR, TWR, SR and Micro-hardness

Exp.	Control Parameters								Average of Responses			
No.	A	B	C	D	E	F	G	H	MRR	TWR	SR	MH
1.	30	6	90	Oil	Cu	WCT	Ti15	WCT	0.969	0.094	3.94	385.667
2.	30	6	120	Oil+Mn	CuCr	SCT	Ti21	SCT	1.183	0.028	5.23	418.000
3.	30	6	150	Oil+W	CuW	DCT	Ti31	DCT	1.026	0.135	4.89	448.333
4.	30	10	90	Oil	CuCr	SCT	Ti31	DCT	1.652	0.192	4.38	445.000
5.	30	10	120	Oil+Mn	CuW	DCT	Ti15	WCT	1.532	0.417	7.97	472.667
6.	30	10	150	Oil+W	Cu	WCT	Ti21	SCT	1.708	0.173	6.85	483.000
7.	30	14	90	Oil	Cu	DCT	Ti21	DCT	2.115	0.626	7.49	515.667
8.	30	14	120	Oil+Mn	CuCr	WCT	Ti31	WCT	2.059	0.391	5.82	573.333
9.	30	14	150	Oil	CuW	SCT	Ti15	SCT	1.511	0.724	9.16	526.333
10.	45	6	90	Oil+W	CuW	SCT	Ti21	WCT	0.838	0.167	3.68	446.333
11.	45	6	120	Oil	Cu	DCT	Ti31	SCT	0.973	0.065	4.11	457.667
12.	45	6	150	Oil+Mn	CuCr	WCT	Ti15	DCT	1.120	0.025	4.31	430.667
13.	45	10	90	Oil+Mn	CuW	WCT	Ti31	SCT	1.317	0.454	4.60	518.333
14.	45	10	120	Oil+W	Cu	SCT	Ti15	DCT	1.470	0.236	5.87	500.667
15.	45	10	150	Oil	CuCr	DCT	Ti21	WCT	2.067	0.148	6.02	500.333
16.	45	14	90	Oil+W	CuCr	DCT	Ti15	SCT	1.668	0.5618	5.48	530.000
17.	45	14	120	Oil	CuW	WCT	Ti21	DCT	2.199	1.054	6.42	599.667
18.	45	14	150	Oil+Mn	Cu	SCT	Ti31	WCT	2.106	0.407	6.81	604.667

Table 4.24: Pair wise Comparison Matrix for Different Criteria

Criteria	MRR	TWR	SR	MH	Criteria Weight
MRR	1	3	5	7	0.5646
TWR	1/3	1	3	5	0.2629
SR	1/5	1/3	1	3	0.1176
MH	1/7	1/5	1/3	1	0.0549
$\lambda_{max} = 4.1138$ CI = 0.03793 RI = 0.90 CR = 0.04214 (4.214%)					

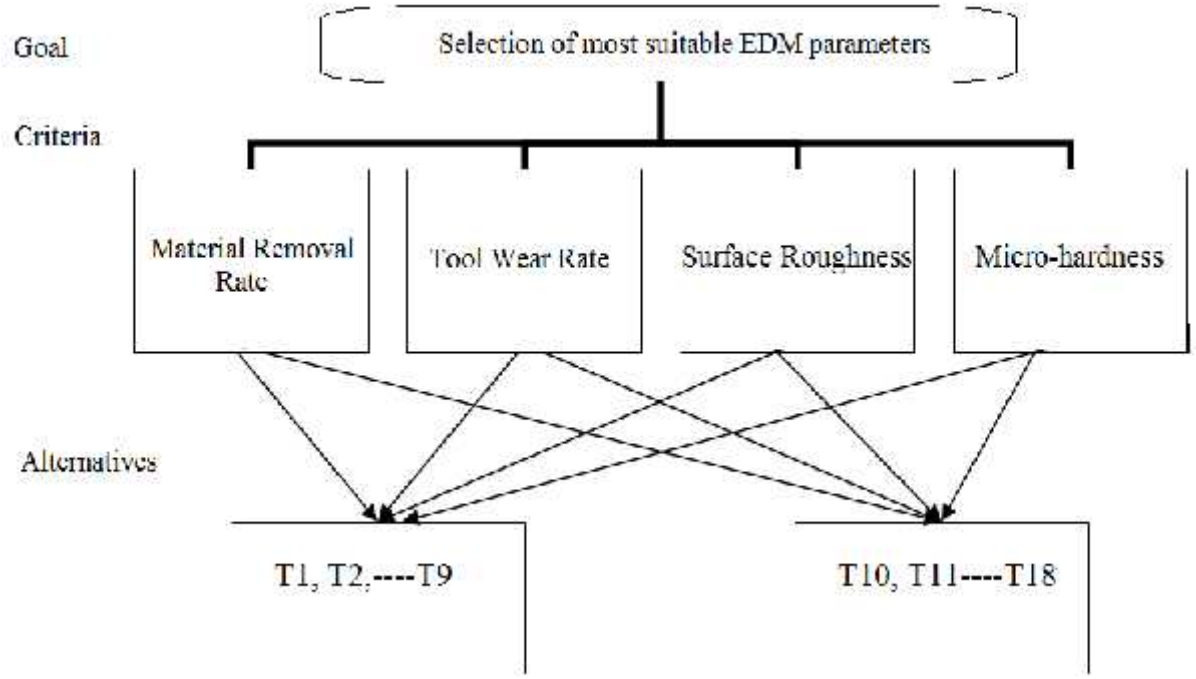

Figure 4.6: AHP Hierarchy Structure

The largest Eigen value is equal to the number of comparisons, or λ_{max}-n for consistent reciprocal matrix. Consistency index (CI) also known as deviation or degree of consistency, for a pair wise comparison matrix can be calculated using equation (4.8), which very much depends upon λ_{max}

$$CI = \frac{\lambda_{max} - n}{n-1} \tag{4.8}$$

Where n is the order of the pair wise comparison matrix.

Consistency Ratio (CR), which is a comparison between Consistency Index (CI) and Random Consistency Index (RI), can be calculated by using equation (4.9).

$$CR = \frac{CI}{RI} \tag{4.9}$$

If the value of Consistency Ratio is smaller or equal to 10%, the inconsistency is acceptable. If the Consistency Ratio is greater than 10%, it needs to be revising the subjective judgment [139-141]. Table 4.25 to 4.28 and Table 4.29 to 4.32 shows the pair wise comparison with respect to their alternatives of sample-I and sample-II for response characteristics such as MRR, TWR, SR and MH respectively.

Table 4.25: Pair wise Comparison of MRR w.r.t. their Alternatives (Sample-I)

Trial	T1	T2	T3	T4	T5	T6	T7	T8	T9	Priority Vector
T1	1	1/2	1/2	1/4	1/4	1/5	1/9	1/9	1/4	0.02233
T2	2	1	3	1/3	1/3	1/5	1/7	1/7	1/3	0.03537
T3	2	1/2	1	1/3	1/2	1/3	1/5	1/5	1/2	0.03786
T4	4	3	3	1	1	1/2	1/5	1/5	1	0.07771
T5	4	3	2	1	1	1/2	1/5	1/5	1	0.07428
T6	5	5	3	1	2	1	1/3	1/3	2	0.12852
T7	9	7	5	5	5	3	1	1	2	0.26644
T8	9	7	5	5	5	3	1	1	2	0.26644
T9	4	3	2	1	1	1/2	1/2	1/2	1	0.09105
λ_{max} = 9.332127, CI = 0.0441516, RI = 1.45, CR = 0.0286 (2.86%)										1.000

Table 4.26: Pair wise Comparison of TWR w.r.t. their Alternatives (Sample-I)

Trial	T1	T2	T3	T4	T5	T6	T7	T8	T9	Priority Vector
T1	1	3	1/2	1/4	1/5	1/4	1/7	1/5	1/9	0.02488
T2	1/3	1	1/4	1/5	1/5	1/5	1/7	1/6	1/9	0.01683
T3	2	4	1	1/2	1/4	1	1/7	1/5	1/9	0.03871
T4	4	5	2	1	1/4	1	1/5	1/3	1/7	0.05648
T5	5	5	4	4	1	3	1/2	1	1/3	0.13215
T6	4	5	1	1	3	1	1/4	1/3	1/5	0.07335
T7	7	7	7	5	2	4	1	2	1/2	0.21129
T8	5	6	5	3	1	3	1/2	1	1/3	0.13389
T9	9	9	9	7	3	5	2	3	1	0.31242
λ_{max} = 9.89281, CI = 0.1116018, RI = 1.45, CR = 0.0769 (7.697%)										1.000

Table 4.27: Pair wise Comparison of SR w.r.t. their Alternatives (Sample-I)

Trial	T1	T2	T3	T4	T5	T6	T7	T8	T9	Priority Vector
T1	1	1/3	1/3	1/2	1/5	1/5	1/5	1/3	1/7	0.0252
T2	3	1	1	2	1/3	1/3	1/3	1	1/5	0.0591
T3	3	1	1	2	1/3	1/3	1/3	1	1/5	0.0591
T4	2	1/2	1/2	1	1/4	1/4	1/4	1/3	1/6	0.0354
T5	5	3	3	4	1	1	1	3	1/3	0.1489
T6	5	3	3	4	1	1	1	3	1/3	0.1489
T7	5	3	3	4	1	1	1	3	1/3	0.1489
T8	3	1	1	3	1/3	1/3	1/3	1	1/5	0.0618
T9	7	5	5	6	3	3	3	5	1	0.3127
λ_{max} = 9.22268, CI = 0.0278349, RI = 1.45, CR = 0.0192 (1.92%)										1.000

Table 4.28: Pair wise Comparison of MH w.r.t. their Alternatives (Sample-I)

Trial	T1	T2	T3	T4	T5	T6	T7	T8	T9	Priority Vector
T1	1	1/2	1/3	1/3	1/4	1/4	1/5	1/7	1/5	0.02737
T2	2	1	1/2	1	1/3	1/3	1/4	1/5	1/4	0.04389
T3	3	2	1	1	1/2	1/2	1/3	1/5	1/3	0.06247
T4	3	1	1	1	1/2	1	1/2	1/4	1/2	0.07007
T5	4	3	2	2	1	1	1/2	1/3	1/2	0.10633
T6	4	3	2	1	1	1	1/2	1/3	1/2	0.09845
T7	5	4	3	2	2	2	1	1/2	2	0.15516
T8	7	5	5	4	3	3	2	1	2	0.28108
T9	5	4	3	2	2	2	1/2	1/2	1	0.15517
λ_{max} = 9.39259, CI = 0.0490745, RI = 1.45, CR = 0.0338 (3.38%)										1.000

Table 4.29: Pair wise Comparison of MRR w.r.t. their Alternatives (Sample-II)

Trial	T10	T11	T12	T13	T14	T15	T16	T17	T18	Priority Vector
T10	1	1/2	1/2	1/3	1/4	1/5	1/6	1/7	1/5	0.02373
T11	2	1	1	1/2	1/3	1/5	1/5	1/7	1/5	0.03297
T12	2	1	1	1/2	1/3	1/5	1/4	1/7	1/5	0.03297
T13	3	2	2	1	1	1/4	1/5	1/7	1/4	0.05159
T14	4	3	3	1	1	1/4	1/3	1/5	1/4	0.06405
T15	5	5	5	4	4	1	2	1	1	0.19872
T16	6	5	4	5	3	1/2	1	1/3	1/2	0.13799
T17	7	7	7	7	5	1	3	1	2	0.27402
T18	5	5	5	4	4	1	2	1/2	1	0.18401
λ_{max} = 9.32915, CI = 0.041144, RI = 1.45, CR = 0.0284 (2.84%)										1.000

Table 4.30: Pair wise Comparison of TWR w.r.t. their Alternatives (Sample-II)

Trial	T10	T11	T12	T13	T14	T15	T16	T17	T18	Priority Vector
T10	1	1/2	1/3	5	3	2	7	9	5	0.17729
T11	2	1	1/2	5	3	2	7	9	5	0.21627
T12	3	2	1	5	3	2	7	9	5	0.26391
T13	1/5	1/5	1/5	1	1/3	1/2	2	5	1	0.04842
T14	1/3	1/3	1/3	3	1	1/2	3	5	2	0.08279
T15	1/2	1/2	1/2	2	2	1	5	7	3	0.12146
T16	1/7	1/7	1/7	1/2	1/3	1/5	1	2	1/2	0.02802
T17	1/9	1/9	1/9	1/5	1/5	1/7	1/2	1	1/2	0.01816
T18	1/5	1/5	1/5	1	1/2	1/3	2	2	1	0.04373
λ_{max} = 9.40335, CI = 0.05042, RI = 1.45, CR = 0.03477 (3.477%)										1.000

Table 4.31: Pair wise Comparison of SR w.r.t. their Alternatives (Sample-II)

Trial	T10	T11	T12	T13	T14	T15	T16	T17	T18	Priority Vector
T10	1	1/3	1/3	1/3	1/5	1/5	1/4	1/7	1/9	0.02012
T11	3	1	1	1	1/3	1/3	1/2	1/5	1/7	0.04235
T12	3	1	1	1	1/3	1/3	1/2	1/5	1/7	0.04235
T13	3	1	1	1	1/3	1/3	1/2	1/5	1/7	0.04235
T14	5	3	3	3	1	1	2	1/3	1/5	0.10576
T15	5	3	3	3	1	1	2	1/3	1/5	0.10576
T16	4	2	2	2	1/2	1/2	1	1/3	1/5	0.07153
T17	7	5	5	5	3	3	3	1	1/3	0.20786
T18	9	7	7	7	5	5	5	3	1	0.36191
λ_{max} = 9.38789, CI = 0.0484657, RI = 1.45, CR = 0.0334 (3.343%)										1.000

Table 4.32: Pair wise Comparison of MH w.r.t. their Alternatives (Sample-II)

Trial	T10	T11	T12	T13	T14	T15	T16	T17	T18	Priority Vector
T10	1	1/2	1	1/3	1/3	1/3	1/3	1/5	1/5	0.03455
T11	2	1	2	1/2	1/2	1/2	1/3	1/5	1/5	0.04983
T12	1	1/2	1	1/2	1/2	1/2	1/3	1/5	1/5	0.03955
T13	3	2	2	1	1	1	1/2	1/4	1/4	0.07797
T14	3	2	2	1	1	1	1/2	1/3	1/3	0.09095
T15	3	2	2	1	1	1	1/2	1/4	1/4	0.07797
T16	3	3	3	2	2	2	1	1/2	1/2	0.13544
T17	5	5	5	4	3	4	2	1	1	0.24686
T18	5	5	5	4	3	4	2	1	1	0.24686
λ_{max} = 9.26174, CI = 0.032717, RI = 1.45, CR = 0.02256 (2.256%)										1.000

Table 4.33: Overall Weight Matrix of Sample-I Priority

Trial	MRRR (0.5646)	TWR (0.2629)	SR (0.1176)	MH (0.0549)	Overall Priority Vector	Ideal Weight Vector
T1	0.02233	0.02488	0.0252	0.02737	0.023615	0.101783
T2	0.03537	0.01683	0.0591	0.04389	0.033754	0.145487
T3	0.03786	0.03871	0.0591	0.06247	0.041932	0.180736
T4	0.07771	0.05648	0.0354	0.07007	0.066734	0.287633
T5	0.07428	0.13215	0.1489	0.10633	0.100029	0.431142
T6	0.12852	0.07335	0.1489	0.09845	0.114762	0.494643
T7	**0.26644**	**0.21129**	**0.1489**	**0.15516**	**0.232009**	**1.00000***
T8	0.26644	0.13389	0.0618	0.28108	0.208331	0.897942**
T9	0.09105	0.31242	0.3127	0.15517	0.178834	0.770808

Table 4.34: Overall Weight Matrix of Sample-II Priority

Trial	MRRR (0.5646)	TWR (0.2629)	SR (0.1176)	MH (0.0549)	Overall Priority Vector	Ideal Weight Vector
T10	0.02373	0.17729	0.02012	0.03455	0.081342	0.254625
T11	0.03297	0.21627	0.04235	0.04983	0.107809	0.337478
T12	0.03297	0.26391	0.04235	0.03955	0.11469	0.359017
T13	0.05159	0.04842	0.04235	0.07797	0.089643	0.280612
T14	0.06405	0.08279	0.10576	0.09095	0.120297	0.376568
T15	0.19872	0.12146	0.10576	0.07797	0.199372	0.624099
T16	0.13799	0.02802	0.07153	0.13544	0.168044	0.526032
T17	**0.27402**	**0.01816**	**0.20786**	**0.24686**	**0.319456**	**1.000000***
T18	0.18401	0.04373	0.36191	0.24686	0.293475	0.918672**

4.3.2 RESULTS OF AHP

In this section, AHP technique was applied for optimization of multiple quality characteristics globally. Performance characteristics, including the MRR, TWR, SR and micro-hardness were chosen for optimization. From the results, it was concluded that the maximum overall weight for a sample-I was observed for trial T7 as given and highlighted in Table 4.33. The trial run conditions for trial number 7 (T7) was given in Table 4.23 in the standard L_{18} control log sheet. The experiment (T7) was performed on DCT TITAN 21 (Ti-5Al-2.5Sn) with the DCT copper tool using EDM oil at a setting of I_p 14A, T_{on} 90µs and T_{off} 30µs. By following the same steps, trial T17 for sample-II was observed the optimal level of experiment which has highest weight vector as indicated in Table 4.34. The ideal machining condition for experiment number 17 at which EDM was performed is T_{off} 45µs, I_p14A, T_{on} 120µs, dielectric without any powder, WCT Cu-W electrode material and DCT workpiece material (Ti-5Al-2.5Sn). Therefore, the optimal solution that globally optimized the entire four performance characteristics for two samples I & II given below in Table 4.35:

Table 4.35: Optimal Process Parameter Setting for Sample I & II

Process Parameter	**Sample-I (T1---T9)**	**Sample-II (T10- -T18)**
Optimum Setting	*Trial No. 7*	*Trial No. 17*
Pulse-off-time	30µs	45µs
Peak current	14A	14A
Pulse-on-time	90µs	120µs
Dielectric medium	EDM Oil (NO Powder)	EDM Oil (NO Powder)
Electrode material	Cu	Cu-W
Cryogenics of electrode	DCT	WCT
Workpiece material	TITAN 21 (Ti-5Al-2.5Sn)	TITAN 21 (Ti-5Al-2.5Sn)
Cryogenics of workpiece	DCT	DCT

4.4 SURFACE ROUGHNESS OF TOOL/ELECTRODE

In EDM process, electrode has the opposite shape of the cavity required in the workpiece. Due to advancement in the product technology, demands of complex and precise parts are increasing day by day. For that reason quality of the EDMed products depend on the shape and surface quality of the electrode. Therefore, in this section surface quality of electrode in terms of surface roughness has been studied. Three values of electrode surface roughness measured in Ra of all the 18 trials are summarized in Table 4.36. Since, smaller values of roughness are desired, thus, 'smaller-the-better' quality characteristics has been used to calculate S/N ratios (dB) by using MINITAB 16 software and the results are given in Table 4.36.

Table 4.36: Experimental Results for SR of Electrode with S/N Ratio

Trial No.	Surface roughness (Ra)			Average	S/N ratio
	R-1	R-2	R-3	(Ra)	(dB)
1.	2.89	3.27	3.12	3.09	-9.82
2.	1.7	2.13	1.95	1.93	-5.73
3.	2.92	2.97	3.01	2.97	-9.45
4.	1.82	1.94	1.87	1.88	-5.47
5.	4.36	3.85	4.12	4.11	-12.3
6.	4.66	4.43	4.54	4.54	-13.15
7.	3.82	4.1	3.95	3.96	-11.95
8.	2.89	2.95	2.91	2.92	-9.29
9.	4.36	4.62	4.54	4.51	-13.08
10.	2.84	2.93	3.13	2.97	-9.45
11.	3.22	4.52	3.86	3.87	-11.83
12.	1.6	1.54	1.5	1.55	-3.79
13.	3.12	3.24	3.46	3.27	-10.31
14.	3.66	5.79	4.68	4.71	-13.61
15.	2.65	2.45	2.33	2.48	-7.89
16.	2.34	2.55	2.42	2.44	-7.74
17.	3.53	5.19	4.87	4.53	-13.23
18.	4.58	5.75	4.95	5.09	-14.17
Overall mean of Surface roughness = 3.38 (Ra), Mean of S/N ratio = -10.125dB					

A range of variation 1.5 to 5.79 of SR of electrode, an average SR of 3.38 Ra, minimum of 1.5 Ra and maximum of 5.79Ra was observed (see Table 4.36). ANOVA for S/N ratio was conducted and significance of the parameters was checked at 95% confidence level (refer Table 4.37). The main effects of each control factor for a S/N ratio of SR of electrode are shown in Figure 4.7.

The electrode material (factor-E) was observed as the most significant parameter with a contribution of 69.95%, followed by current (factor-B) with 20.16% on SR of electrode as listed in Table 4.37. Smaller effect of cryo-treatment of work material was observed with a contribution of 1.72%. Pulse duration, *i.e.* T_{on} shows their effect with percent contribution of 6.56 on SR of the tool. During this period energy is supplied to the machining zone.

Table 4.37: ANOVA Results for S/N Data (S/N Ratio) SR of Electrode

Control Factors	DOF	Seq. SS	Adj. SS	Adj. MS	F-value	%PC	Remarks	Best Level
A	1	0.18	0.18	0.18	5.18		x	A1
B	2	32.35	32.35	16.18	468.89	20.16	√√√	B1
C	2	10.68	10.68	5.34	154.78	6.656	√√	C1
D	2	1.73	1.73	0.86	25.01	1.08	√	D2
E	2	112.25	112.25	56.12	1626.78	69.95	√√√	E2
F	2	0.35	0.35	0.17	5.014		x	F1
G	2	0.11	0.11	0.05	1.58		x	G1
H	2	2.75	2.75	1.38	39.94	1.72	√	H3
Error	2	0.07	0.07	0.035	5.18			
Total	17	160.47						
Error Pooled	7	0.71				0.44		

x- not significant, √ - less significant, √√- significant, √√√-most significant

F_{tab} = F (2,2) = 19.000; F (1,2) = 18.513

The effect of all the input parameters is plotted in Figure 4.7, from here it can be concluded that a low SR of electrode surface is measured at pulse-off-time 30µs (A_1), 6 Amp current (B_1), pulse-on-time 90 µs (C_1), manganese powder mixed with EDM Oil (D_2), Cu-Cr electrode (E_2), without cryo-treatment of electrode (F_1), TITAN 15 workpiece material (G_1) and deep cryogenic treatment of workpiece (H_3). Hence, the optimum condition of input process parameters can be written as $A_1B_1C_1D_2E_2F_1G_1H_3$.

The calculated mean value of SR of electrode (raw data) and S/N ratios for each control factor at levels 1, 2 and 3 are summarized in Table 4.38.

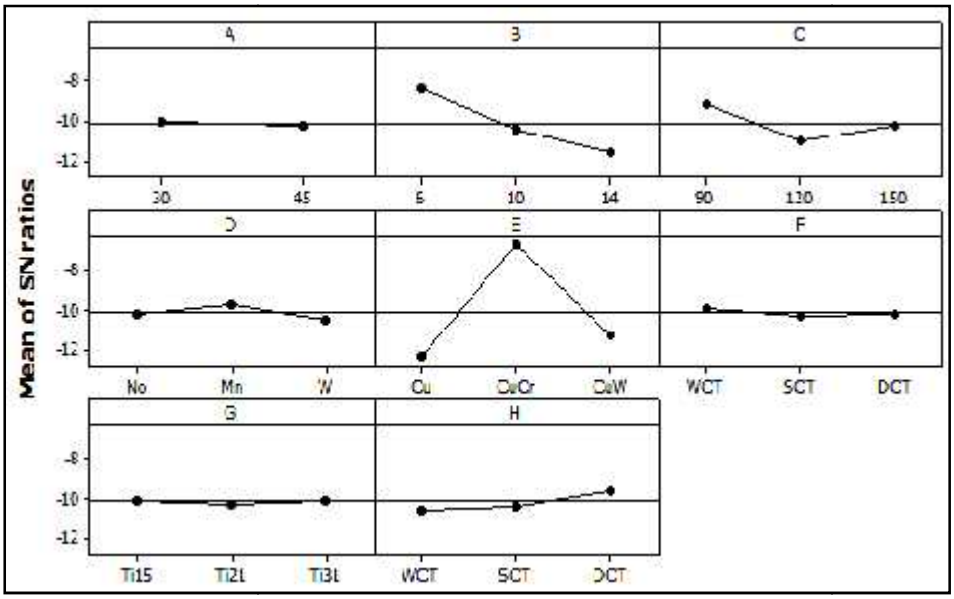

Figure 4.7: Graphical Presentations of Parameters for S/N Ratio of Surface Roughness of Electrode

Table 4.38: Average Values of Factor Levels for S/N Data and Raw Data of Surface Roughness of Tool-electrode

Control Factors	S/N ratio (dB)				Raw data			
	Level 1	Level 2	Level 3	Best Level	Level 1	Level 2	Level 3	Best Level
A	-10.03	-10.22	-----	A1	3.32	3.43	-----	A1
B	-8.34	-10.45	-11.58	B1	2.73	3.49	3.91	B1
C	-9.12	-10.99	-10.25	C1	2.93	3.68	3.52	C1
D	-10.22	-9.70	-10.45	D2	3.39	3.32	3.42	D2
E	-12.42	-6.65	-11.30	E2	4.21	2.19	3.73	E2
F	-9.93	-10.25	-10.19	F1	3.32	3.51	3.30	F3
G	-10.05	-10.23	-10.08	G1	3.40	3.40	3.33	G3
H	-10.48	-10.31	-9.58	H3	3.44	3.43	3.26	H3

The trend of I_p in Figure 4.7 shows that as current increases, SR of the electrode also increases. It increases sharply in the range of 6A to 10A and thereafter at 14A slightly decreases, similarly, a trend was observed in case of T_{on} from 90 µs to 120 µs and then decrease up to 150 µs. Higher SR is obtained at higher values of current, *i.e.* 14A and lower

at low value *i.e* 6A. Further, from Figure 4.7, it can be seen that electrode material Cu produced higher SR than Cu-W, where SR of electrode improves with Cu-Cr tool material. Mn powder mixed dielectric reduced the SR of electrode as compared to W powder mixed dielectric as shown in Figure 4.7. Further, surface finish of electrode can be improved during machining of DCT titanium alloy workpiece as indicated in Figure 4.7. The ANOVA for S/N data and raw data for SR (Ra) of electrodes were performed to classify the significant parameters and to measure their effect on response characteristic. From the observed results, it was observed that low values of I_p and T_{on} give the best surface finish to the electrode surface. It means low discharge energy was available for a smaller period, generated less amount of heat at the closest point, resulted in the removal of material from the electrode surface in smaller size of craters with less number of surface cracks. Thus, uniform surface was observed at low discharge energy as compared to surface obtained at higher values of I_p and T_{on}. The Cu electrode material more damaged as compared to Cu-Cr and Cu-W electrode, because of purity of copper electrode is 99.5%.

4.4.1 PREDICTIONS OF THEORETICAL SURFACE ROUGHNESS VALUE OF TOOL/ELECTRODE AND CONFIRMATION TEST

The theoretical value of SR of the electrode under optimum conditions was calculated by using the following equation given below:

$$\eta_{opt} = \eta + (\eta_{A1}-\eta) + (\eta_{B1} - \eta) + (\eta_{C1} - \eta) + (\eta_{D2} - \eta) + (\eta_{E2} - \eta) + (\eta_{F1} - \eta) + (\eta_{G1} - \eta) + (\eta_{H3} - \eta)$$

After substituting the respective values,

Thus, value of η_{opt} = -2.551

$$y^2_{predicted} = 10^{-y_{opt}/10}$$ Or, $y_{predicted}$ = 1.35 μm

According to the 95% confidence interval of population confidence interval of confirmation experiments was calculated.

Thus, the calculated confidence interval, CI_{CE} for SR = ± 0.397

Therefore, the estimated value of electrode SR is given by 1.35 ± 0.397

At the optimum setting of parameters $A_1B_1C_1D_2E_2F_1G_1H_3$, experiments have been conducted to verify the results and the average value of three sets of experiments was obtained 1.42 Ra for SR of electrode, which is within the limit of the estimated results.

Chapter 5

MODELING OF RESULTS

5.1 INTRODUCTION

In EDM process, the machining efficiency very much depends upon the thermo-electric properties of the two electrodes, *i.e.* tool and workpiece. These properties include thermal conductivity, electrical conductivity, melting/boiling point of materials, specific heat, latent heat etc. [123,125]. Two approaches were used for optimizing the machining characteristics of titanium alloys, namely (i) macro modeling and (ii) micro modeling [126,130].

In macro modeling, there is no need to establish a mathematical model for the performance characteristic. Macro model has been developed for all the four responses namely MRR, TWR, SR of workpiece and micro-hardness using the information provided by the Taguchi methodology.

The micro-modeling approach is based on the in-depth study of the system. It provides the sufficient information enough for developing the mathematical model for the performances. Some assumptions are made to simplify the modeling process so that the complexity of the system can be handled easily. First of all, macro-model has been developed for all response characteristics, thereafter; the output of this model has been used to develop a micro-model using dimensional analysis based upon the Buckingham's π theorem approach [125,126,130].

Initially, the Buckingham's π theorem approach was applied to construct a micro-mathematical model for all the four response characteristics such as MRR, TWR, SR and MH. During the validation of these models, the results did not observe within the agreeable limit for surface roughness and micro-hardness response characteristics due to large number of variables or dimensionless groups. Hence, ANN approach was used to establish the relationship between process parameters and output characteristic surface roughness and micro-hardness of titanium alloy workpiece.

Dimensional analysis approach was used for MRR and TWR response characteristics for developing a micro model.

5.2 MODELING TO PREDICT MRR

The results obtained after the experimental analysis were utilized to develop a mathematical micro-model using different parametric combinations by applying Buckingham's π theorem,

which is a dimensional analysis. Subsequently, the predicted MRR using the mathematical model was compared with the experiment results to validate the model.

Based on the experiment results and reported work in literature, thermal-physical properties of titanium alloy work material and most significant factor peak current obtained from the results of ANOVA test were used for modeling the MRR. The basic fundamental dimensions for development of the model are Mass (M), Length (L), Time (T), Temperature (θ) and Current (I) [125]. Table 5.1 illustrates the dimensions of the selected parameters for constructing the model.

Table 5.1: Dimensions of Important Parameters in EDM Process used for MRR

S.No.	Characteristics	Properties	Symbol	Unit	Dimensions
1.	Quantity characteristics	Material removal rate	Z	mm^3/min	L^3T^{-1}
2.	Machine parameter	Peak current	Ip	A	I
3.	Thermo-physical Properties of material	Density	ρ	g/cm^3	ML^{-3}
		Thermal conductivity	k	W/m-k	$MLT^{-3}\theta^{-1}$
		Electrical conductivity	σ	Siemens/m	$M^{-1}L^{-3}T^3I^2$
		Specific heat	Cp	J/kg-k	$L^2T^{-2}\theta^{-1}$
		Melting point	T_m	^oC	–
		Boiling point	T_v	^oC	–
		Latent heat of fusion per unit mass	L_f	J/kg	L^2T^{-2}
		Latent heat of vapor per unit mass	L_v	J/kg	L^2T^{-2}

Table 5.2: Model Parameter Value in the Form of their Fundamental Dimensions

Dimensions	Dimensions of parameters on MRR							
	Z	**Ip**	**k**	**σ**	**ρ**	**Cp**	**Tv**	**Lv**
Mass (M)	0	0	1	-1	1	0	0	0
Length (L)	3	0	1	-3	-3	2	0	2
Time (T)	-1	0	-3	3	0	-2	0	-2
Temperature (θ)	0	0	-1	0	0	-1	1	0
Current (I)	0	1	0	2	0	0	0	0

Table 5.2 provides the model parameter value in the form of their fundamental dimensions. Applying dimensional analysis, the MRR, *Z* can be given by the following equation:

$Z = f(Ip, \kappa, \sigma, \rho, Cp, Tv, Lv)$

The total number of variables, n = 8 and the fundamental dimensions are m =5.
Hence, the dimensionless groups that can be formed are n-m = 3 and are given by π_1, π_2 and π_3. This can be written as given by equation (5.1).

$f(\pi_1, \pi_2, \pi_3) = 0$ (5.1)

Taking *Z, Ip, Lv* as the quantities which directly go in three dimensionless groups π_1, π_2 and π_3 respectively, the three dimensionless groups are then given by equation (5.2), (5.3) and (5.4).

$$®_1 = Z(©)^{a_1}(°)^{b_1}(Cp)^{c_1}(Tv)^{d_1}(±)^{e_1} \quad (5.2)$$

$$®_2 = Ip(©)^{a_2}(°)^{b_2}(Cp)^{c_2}(Tv)^{d_2}(±)^{e_2} \quad (5.3)$$

$$®_3 = L_v(©)^{a_3}(°)^{b_3}(Cp)^{c_3}(Tv)^{d_3}(±)^{e_3} \quad (5.4)$$

Putting the dimensions for each quantity and equating to zero and solving for π_1

$$®_1 = (L^3T^{-1})(MLT^{-3\text{—}-1})^{a_1}(ML^{-3})^{b_1}(L^2T^{-2\text{—}-1})^{c_1}(\text{—}^1)^{d_1}(M^{-1}L^{-3}T^3I^2)^{e_1} \quad (5.5)$$

$$M: a_1 + b_1 - e_1 = 0$$
$$L: 3 + a_1 - 3b_1 + 2c_1 - 3e_1 = 0$$
$$T: -1 - 3a_1 - 2c_1 + 3e_1 = 0$$
$$\text{—}: -a_1 - c_1 + d_1 = 0$$
$$I: 2e_1 = 0$$

Solving the above, $a_1 = -2, b_1 = 2, c_1 = 2.5, d_1 = 1/2, e_1 = 0$

$$®_1 = Z(©)^{-2}(°)^2(Cp)^{2.5}(Tv)^{1/2}(±)^0 \quad (5.6)$$

$$®_1 = Z\frac{°^2 Cp^{2.5}Tv^{1/2}}{k^2} \quad (5.7)$$

Similarly, $®_2 = (Ip)(MLT^{-3\text{—}-1})^{a_2}(ML^{-3})^{b_2}(L^2T^{-2\text{—}-1})^{c_2}(\text{—}^1)^{d_2}(M^{-1}L^{-3}T^3I^2)^{e_2}$ (5.8)

Here,

$M: a_2 + b_2 - e_2 = 0$

$L: a_2 - 3b_2 + 2c_2 - 3e_2 = 0$

$T: -3a_2 - 2c_2 + 3e_2 = 0$

$^{-}: -a_2 - c_2 + d_2 = 0$

$I: 1 + 2e_2 = 0$

Solving the above, $a_2 = -3/2, b_2 = 1, c_2 = 3/2, d_2 = 0, e_2 = -1/2$

$$®_2 = Ip(©)^{-3/2}(°)^1(Cp)^{3/2}(Tv)^0(±)^{-1/2} \quad (5.9)$$

$$®_2 = Ip\frac{°Cp^{3/2}}{©^{3/2}±^{1/2}} \quad (5.10)$$

Similarly, solving for π_3

$$®_3 = (L^2T^{-2})(MLT^{-3-^{-1}})^{a_3}(ML^{-3})^{b_3}(L^2T^{-2-^{-1}})^{c_3}(^{-1})^{d_3}(M^{-1}L^{-3}T^3I^2)^{e_3} \quad (5.11)$$

Here,

$M: a_3 + b_3 - e_3 = 0$

$L: 2 + a_3 - 3b_3 + 2c_3 - 3e_3 = 0$

$T: -2 - 3a_3 - 2c_3 + 3e_3 = 0$

$^{-}: -a_3 - c_3 + d_3 = 0$

$I: 2e_3 = 0$

After solving, $a_3 = 0, b_3 = 0, c_3 = -1, d_3 = -1, e_3 = 0$

$$®_3 = Lv(©)^0(°)^0(Cp)^{-1}(Tv)^{-1}(±)^0 \quad (5.12)$$

$$®_3 = \frac{Lv}{CpTv} \quad (5.13)$$

The final relationship can be assumed to be of the form

$$®_i = f(®_j, ®_k) \quad (5.14)$$

Assuming i = 1, j =2, k =3.

Then the final functional relationship of dimensionless parameters is written as

$$®_1 = f(®_2, ®_3) \quad (5.15)$$

Or

$$Z\frac{°^2Cp^{2.5}Tv^{1/2}}{©^2} = f(Ip\frac{°Cp^{3/2}}{©^{3/2}±^{1/2}}, L_v\frac{1}{CpTv}) \quad (5.16)$$

The experimental results show that MRR (Z) is largely influenced by the current. The MRR can be calculated by keeping all parameters constant and varying peak current. Therefore, peak current has been taken as the representative for the development of mathematical equation for MRR. Hence, the equation for MRR can be written as under:

$$Z \frac{\circ^{2} Cp^{2.5} Tv^{1/2}}{\copyright^{2}} = Ipf\left(\frac{\circ Cp^{3/2}}{\copyright^{3/2} \pm^{1/2}}, L_{v} \frac{1}{CpTv}\right) \tag{5.17}$$

$$Z = C\left\{IpL_{v} \frac{k^{1/2}}{\circ Cp^{2} \pm^{1/2} Tv^{3/2}}\right\} \tag{5.18}$$

Here, C represents the constant of proportionality

For validating the results, experiments were performed on titanium alloys (Ti-6Al-4V); TITAN 31, ASTM Grade 5 by varying peak current and keeping all other parameters constant. The MRR was plotted against peak current and is shown in Figure 5.1. A third-degree polynomial equation was observed to be the best- fit curve, with coefficient of correlation equal to 0.9837. Thus, the polynomial equation for MRR for this case is given by equation (5.19).

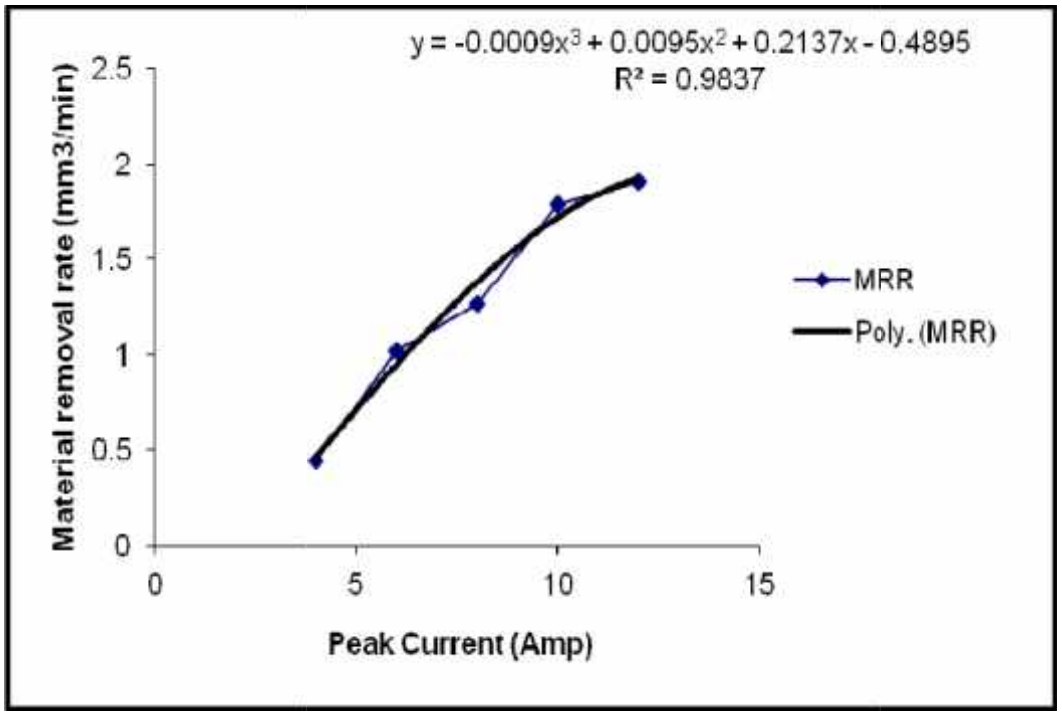

Figure 5.1: MRR versus Peak Current for Titanium Alloy (Ti-6Al-4V)

$$Z = \left(-0.0009Ip^3 + 0.0095Ip^2 + 0.2137Ip - 0.4895\right) L_v \frac{©^{1/2}}{\circ Cp^2 \pm^{1/2} T_v^{3/2}} \quad (5.19)$$

Subsequently, a comparison between the experimental results and the predicted results for MRR was made. The percentage variation in the predicted value can be calculated by equation (5.20).

$$\text{Variation (\%)} = \left(\frac{\text{Experimental Results - Predicted Results}}{\text{Experimental Results}}\right) \times 100 \quad (5.20)$$

Here, for validating the mathematical model, three confirmation experiments were performed on Ti-6Al-4V titanium alloy workpiece with copper electrode machined with peak current set at 6, 10, 12A respectively. The other parameters, such as T_{off} (60µs), T_{on} (150µs), EDM oil without powder and no cryogenic treatment of workpiece or tool material were kept constant. From the results obtained, the percentage variation between experiment and the predicted results at peak current of 6, 10, 12A was observed as 2.92%, 0.37% and 4.21% respectively. Hence, there is a good relationship between the two results for MRR *i.e.* experimental and the predicted.

5.3 MODELING TO PREDICT TWR

The significant machining parameters which obtained from Taguchi's ANOVA analysis like I_p, T_{on}, dielectric medium and electrode material were considered to develop the micro model. From ANOVA results, peak current was observed as the most significant parameter affecting the TWR. Further, thermal-physical properties such as thermal conductivity, electrical conductivity, specific heat, melting point, boiling point, latent heat of evaporation, latent heat of fusion were considered to develop the mathematical model.

Further, all the individual variables were determined in the form of algebraic expressions, which is related to with each dimensionless group (πi). A dimensional matrix of the dependent as well as independent process variables was generated according to their fundamental dimensions written in equation (5.21). According to The Buckingham' pi (π) theorem, it is important to select carefully the repeating and non-repeating variables to develop a mathematical model [65]. The five basic fundamental dimensions for constructing model are Mass (M), Length (L), Time (T), Temperature (θ) and Current (I) [65].

The following assumptions have been made in developing the model for the TWR:

1. The insignificant factors which come out from ANOVA for S/N ratios have been omitted from the mathematical modeling.
2. Effect of environment that is temperature or humidity has to be turned down.
3. Machining constant parameters cannot be used to construct the micro-mathematical model.
4. The effect of mechanical properties has to be neglected.
5. Tool wear rate (TWR) as a dependent variable should not be repeated.
6. The properties of the entire repeated variable should be different.
7. The dimensions of two repeating variables should not be same.
8. Both sides of the equation dimensions of the quantity must be same.
9. Wherever a sum of quantities appears in the function (f), all the terms in the sum must have the same dimensions.

Table 5.3 illustrates the dimensions of the selected parameters for constructing the model. Table 5.4 provides the model parameter value in the form of their fundamental dimensions.

Table 5.3: Dimensions of Important Parameters in EDM process for TWR

S.No.	Characteristics	Properties	Symbol	Unit	Dimensions
1.	Quantity characteristics	Tool wear rate	V	mm^3/min	L^3T^{-1}
2.	Machine parameter	Peak current	Ip	A	I
		Pulse on-time	T_{on}	µs	T
3.	Dielectric fluid	Break down voltage	V_b	Kv	$ML^2T^{-3}I^{-1}$
4.	Thermo-physical Properties of material	Density	ρ	g/cm^3	ML^{-3}
		Thermal conductivity	k	W/m-k	MLT^{-3-1}
		Electrical conductivity	σ	Siemens /m	$M^{-1}L^{-3}T^3I^2$
		Specific heat	Cp	J/kg-k	L^2T^{-2-1}
		Melting point	T_m	ºC	–
		Latent heat of fusion per unit mass	L_f	J/kg	L^2T^{-2}

Table 5.4: Model Parameters Value in the Form of their Fundamental Dimensions

Dimensions	Dimensions of parameters for TWR									
	V	**Ip**	**T_{on}**	**V_b**	**k**	**σ**	**ρ**	**Cp**	**T_m**	**L_f**
Mass (M)	0	0	0	1	1	-1	1	0	0	0
Length (L)	3	0	0	2	1	-3	-3	2	0	2
Time (T)	-1	0	1	-3	-3	3	0	-2	0	-2
Temperature (θ)	0	0	0	0	-1	0	0	-1	1	0
Current (I)	0	1	0	-1	0	2	0	0	0	0

Applying dimensional analysis, the TWR, (V) can be given by the equation (5.21).

$$V = f(Ip,\ T_{on,} V_b, k,\ \pm,\ °,\ Cp,\ T_{m,}\ L_f) \quad (5.21)$$

The total number of variables were 10 (n = 10) & the fundamental dimensions are 5 (m = 5), hence, dimensionless groups in the present study are n-m = 5. These five dimensionless groups represented by π_1, $\pi_{2,}$ $\pi_{3,}$ $\pi_{4,}$ and π_5 can then be written as:

On the other hand, it can be written as:

$$f(\pi_1, \pi_{2,} \pi_{3,} \pi_4, \pi_5) = 0 \quad (5.22)$$

$$®_1 = V(\pm)^{a_1}(©)^{b_1}(°)^{c_1}(Cp)^{d_1}(T_m)^{e_1} \quad (5.23)$$

$$®_2 = Ip(\pm)^{a_2}(©)^{b_2}(°)^{c_2}(Cp)^{d_2}(T_m)^{e_2} \quad (5.24)$$

$$®_3 = T_{on}(\pm)^{a_3}(©)^{b_3}(°)^{c_3}(Cp)^{d_3}(T_m)^{e_3} \quad (5.25)$$

$$®_4 = V_b(\pm)^{a_4}(©)^{b_4}(°)^{c_4}(Cp)^{d_4}(T_m)^{e_4} \quad (5.26)$$

$$®_5 = L_f(\pm)^{a_5}(©)^{b_5}(°)^{c_5}(Cp)^{d_5}(T_m)^{e_5} \quad (5.27)$$

By putting the dimensions of each quantity in equation 5.23 to 5.27 and equating to zero, we can solve the five dimensional groups

Solving for $\pi_{1,}$ we get

$$®_1 = (L^3T^{-1})(M^{-1}L^{-3}T^3I^2)^{a_1}(MLT^{-3-1})^{b_1}(ML^{-3})^{c_1}(L^2T^{-2-1})^{d_1}(¯)^{e_1} \quad (5.28)$$

Here,

M : $-a_1+b_1 + c_1 = 0$

L : $3 -3a_1 +b_1- 3c_1 + 2d_1 = 0$

T : $-1+3a_1 -3b_1 -2d_1 = 0$

θ : $-b_1 – d_1 + e_1 = 0$

I : $2a_1 = 0$

$a_1= 0$, $b_1= -2$, $c_1= 2$, $d_1= 2.5$, $e_1= 1/2$

$$®_1 = V(±)^0(©)^{-2}(°)^2(Cp)^{2.5}(T_m)^{1/2}$$

$$®_1 = V\frac{°^2 Cp^{2.5} T_m^{1/2}}{©^2} \tag{5.29}$$

In the same manner, the values for π_2, π_3, π_4, and π_5 can be calculated and are given by equations (5.30) to (5.33)

$$®_2 = Ip(±)^{a_2}(©)^{b_2}(°)^{c_2}(Cp)^{d_2}(T_m)^{e_2}$$

$$®_2 = Ip(M^{-1}L^{-3}T^3I^2)^{a_2}(MLT^{-3}—^{-1})^{b_2}(ML^{-3})^{c_2}(L^2T^{-2}—^{-1})^{d_2}(¯)^{e_2}$$

$$a_2 = -1/2, b_2 = -3/2, c_2 = 1, d_2 = 3/2, e_2 = 0$$

$$®_2 = Ip(±)^{-1/2}(©)^{-3/2}(°)^1(Cp)^{3/2}(T_m)^0$$

$$®_2 = Ip\frac{°Cp^{3/2}}{±^{1/2}©^{3/2}} \tag{5.30}$$

$$®_3 = T_{on}(±)^{a_3}(©)^{b_3}(°)^{c_3}(Cp)^{d_3}(T_m)^{e_3}$$

$$®_3 = T(M^{-1}L^{-3}T^3I^2)^{a_3}(MLT^{-3}—^{-1})^{b_3}(ML^{-3})^{c_3}(L^2T^{-2}—^{-1})^{d_3}(¯)^{e_3}$$

$$a_3 = 0, b_3 = -1, c_3 = 1, d_3 = 2, e_3 = 1$$

$$®_3 = T_{on}\frac{°Cp^2T_m}{k} \tag{5.31}$$

$$®_4 = ML^2T^{-3}I^{-1}(M^{-1}L^{-3}T^3I^2)^{a_4}(MLT^{-3}—^{-1})^{b_4}(ML^{-3})^{c_4}(L^2T^{-2}—^{-1})^{d_4}(¯)^{e_4}$$

$$a_4 = 1/2, b_4 = -1/2, c_4 = 0, d_4 = 0, e_4 = -1/2$$

$$®_4 = V_b\frac{±^{1/2}}{©^{1/2}T_m^{1/2}} \tag{5.32}$$

$$®_5 = L_f(±)^{a_5}(©)^{b_5}(°)^{c_5}(Cp)^{d_5}(T_m)^{e_5}$$

$$®_5 = L^2T^{-2}(M^{-1}L^{-3}T^3I^2)^{a_5}(MLT^{-3}—^{-1})^{b_5}(ML^{-3})^{c_5}(L^2T^{-2}—^{-1})^{d_5}(¯)^{e_5}$$

$$a_5 = 0, b_5 = 0, c_5 = 0, d_5 = -1, e_5 = -1$$

$$®_5 = L_f \frac{1}{CpT_m} \tag{5.33}$$

The final functional relationship of dimensionless parameters is given by

$$®_i = f(®_{j,}®_k, ®_l, ®_m) \tag{5.34}$$

Let us assume i = 1, j =2, k =3 and so on

Then the final functional relationship of dimensionless parameters is here

$$\pi_1 = f(\pi_{2,}\, \pi_{3,}\, \pi_4, \pi_5) \tag{5.35}$$

Substituting the values of π_1, $\pi_{2,}$ $\pi_{3,}$ $\pi_{4,}$ π_5 in equation (5.36)

$$V°^2 \frac{Cp^{2.5} T_m^{1/2}}{©^2} = f\left(Ip \frac{°Cp^{3/2}}{±^{1/2}©^{3/2}}, T_{on} \frac{°Cp^2 T_m}{©}, V_b \frac{±^{1/2}}{©^{1/2} T_m^{1/2}}, L_f \frac{1}{CpT_m} \right) \tag{5.36}$$

$$V°^2 \frac{Cp^{2.5} T_m^{1/2}}{©^2} = Ipf\left(\frac{°Cp^{3/2}}{±^{1/2}©^{3/2}}, T_{on} \frac{°Cp^2 T_m}{©}, V_b \frac{±^{1/2}}{©^{1/2} T_m^{1/2}}, L_f \frac{1}{CpT_m} \right)$$

Or

$$V = C\left\{ \frac{IpT_{on} V_b L_f}{©T_m} \right\} \tag{5.37}$$

Where, C represents the constant of proportionality.

The coefficient ‘C’ was calculated by conducting the experiments, keeping $T_{on} V_b L_f / ©T_m$ constant, varying only the value of peak current to get TWR ‘V’. Thus, peak current was taken as the representative for the development of mathematical equation for TWR as it was the most dominant factor with a 74% contribution (*Table 4.11)*. The most important aspect of this developed mathematical model is the thermal conductivity of copper tool material (k) which has appeared in the four dimensionless products, thereby signifying that thermal conductivity plays a significant role. The developed model, as shown in equation 5.37, has both machining parameters as well as thermo-physical properties of the electrode material.

Case- Titanium alloys (Ti-6Al-4V) machined with WCT copper electrode

The actual experiments were conducted at different values of current, as shown in Figure 5.2 to study the effect of current on TWR. The data obtained from the experiments was used for finding the best-fit curve, as shown in Figure 5.2. The third- degree polynomial equation was observed as the best- fit curve. Thus, the polynomial equation for TWR becomes in this case is given by equation (5.38):

$$V = \left(0.0091Ip^3 - 0.0385Ip^2 + 0.1241Ip - 0.069\right)\frac{T_{on}V_bL_f}{©T_m} \qquad (5.38)$$

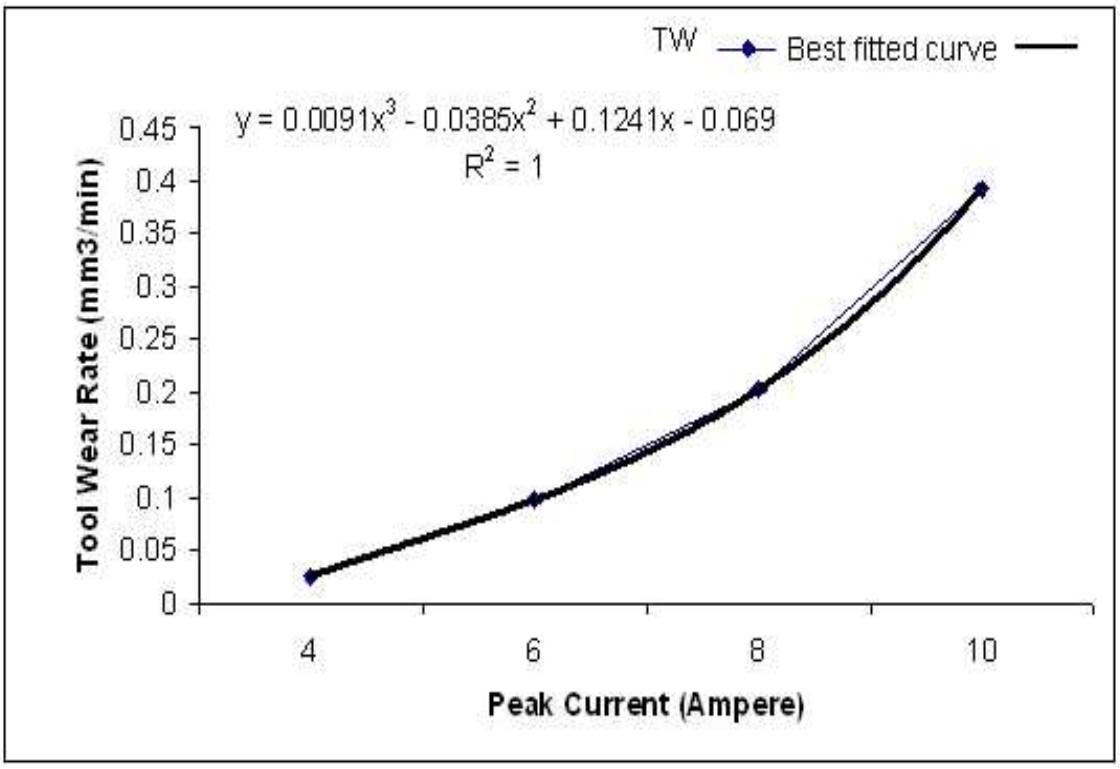

Figure 5.2: TWR vs Peak Current for Machining of Titanium Alloys (Ti-6Al-4V) with Copper Electrode (T_{on} = 120µs and T_{off} = 45 µs)

A verification experiment was conducted at 6A I_p, 120 µs T_{on}, 45µs T_{off}, dielectric Oil without powder, workpiece Ti-6Al-4V and copper electrode. TWR for this experiment was obtained as 0.06537 mm^3/min and where as the model predicted TWR was 0.068 mm^3/min, which indicates a 4.02 % variation in the results.

5.4 MODELING TO PREDICT SURFACE ROUGHNESS BY USING ARTIFICIAL NEURAL NETWORK (ANN) TECHNIQUE

ANN is a flexible modeling tool which has the capabilities of learning the mapping between the input parameters and the output characteristics to solve non- linear problems using a software computing technique [133]. The ANN validation has been developed using the neural network toolbox of MATLAB 7.12.0 software. A multilayer feed-forward network was used, whereas the back propagation algorithm was used to train the network [52, 75, 134]. A total of 54 (18x3) readings were taken to measure change in surface roughness due to variable level setting of the eight input process parameters.

Table 5.5: Experimental Results and ANN Predicted Results for SR

Exp. N0.	Pulse-off-time	Peak current	Pulse-on-time	Dielectric fluid	Electrode material	Cryogenic treatment of electrode	Work Piece material	Cryogenic treatment of workpiece	Exp. Value (Ra)	ANN Predicted Value (Ra)	% Relative Error
1	30	6	90	Oil	Cu	WCT	Ti15	WCT	3.60	3.6028	-0.825
2	30	6	120	Oil+Mn	CuCr	SCT	Ti 21	SCT	5.53	5.5618	-0.116
3	30	6	150	Oil+W	CuW	DCT	Ti 31	DCT	4.82	4.8092	-0.753
4	30	10	90	Oil	CuCr	SCT	Ti 31	DCT	4.60	4.6020	-0.182
5	30	10	120	Oil+Mn	CuW	DCT	Ti15	WCT	8.52	8.5383	0.328
6	30	10	150	Oil+W	Cu	WCT	Ti 21	SCT	6.33	6.2950	0.202
7	30	14	90	Oil	Cu	DCT	Ti 21	DCT	7.02	6.9695	2.217
8	30	14	120	Oil+Mn	CuCr	WCT	Ti 31	WCT	5.19	5.1623	-0.401
9	30	14	150	Oil	CuW	SCT	Ti15	SCT	9.52	9.5327	-0.552
10	45	6	90	Oil+W	CuW	SCT	Ti 21	WCT	3.66	3.6734	0.615
11	45	6	120	Oil	Cu	DCT	Ti 31	SCT	3.97	3.9712	-0.591
12	45	6	150	Oil+Mn	CuCr	WCT	Ti15	DCT	4.13	4.1250	0.033
13	45	10	90	Oil+Mn	CuW	WCT	Ti 31	SCT	4.90	4.9093	0.041
14	45	10	120	Oil+W	Cu	SCT	Ti15	DCT	6.14	6.1619	0.726
15	45	10	150	Oil	CuCr	DCT	Ti 21	WCT	7.21	7.2917	-0.259
16	45	14	90	Oil+W	CuCr	DCT	Ti15	SCT	5.42	5.4099	0.447
17	45	14	120	Oil	CuW	WCT	Ti 21	DCT	6.38	6.3729	-0.267
18	45	14	150	Oil+Mn	Cu	SCT	Ti 31	WCT	7.59	7.6526	-0.716
19	30	6	90	Oil	Cu	WCT	Ti15	WCT	3.70	3.7043	-0.286
20	30	6	120	Oil+Mn	CuCr	SCT	Ti 21	SCT	5.71	5.7530	-0.421
21	30	6	150	Oil+W	CuW	DCT	Ti 31	DCT	5.07	5.0792	0.915

22	30	10	90	Oil	CuCr	SCT	Ti 31	DCT	3.67	3.6579	0.264
23	30	10	120	Oil+Mn	CuW	DCT	Ti15	WCT	7.96	7.9439	-0.395
24	30	10	150	Oil+W	Cu	WCT	Ti 21	SCT	4.79	4.6838	0.456
25	30	14	90	Oil	Cu	DCT	Ti 21	DCT	8.19	8.2228	-2.346
26	30	14	120	Oil+Mn	CuCr	WCT	Ti 31	WCT	6.62	6.6565	0.208
27	30	14	150	Oil	CuW	SCT	Ti15	SCT	8.84	8.7856	-0.120
28	45	6	90	Oil+W	CuW	SCT	Ti 21	WCT	4.37	4.3958	0.292
29	45	6	120	Oil	Cu	DCT	Ti 31	SCT	3.76	3.7588	-0.018
30	45	6	150	Oil+Mn	CuCr	WCT	Ti15	DCT	4.36	4.3582	-0.316
31	45	10	90	Oil+Mn	CuW	WCT	Ti 31	SCT	3.30	3.2760	0.006
32	45	10	120	Oil+W	Cu	SCT	Ti15	DCT	5.93	5.9454	-1.286
33	45	10	150	Oil	CuCr	DCT	Ti 21	WCT	5.36	5.3360	0.049
34	45	14	90	Oil+W	CuCr	DCT	Ti15	SCT	5.48	5.4946	0.251
35	45	14	120	Oil	CuW	WCT	Ti 21	DCT	7.20	7.2516	-0.340
36	45	14	150	Oil+Mn	Cu	SCT	Ti 31	WCT	7.18	7.2005	0.458
37	30	6	90	Oil	Cu	WCT	Ti15	WCT	4.53	4.5491	0.866
38	30	6	120	Oil+Mn	CuCr	SCT	Ti 21	SCT	4.46	4.4192	-0.825
39	30	6	150	Oil+W	CuW	DCT	Ti 31	DCT	4.79	4.7773	-0.116
40	30	10	90	Oil	CuCr	SCT	Ti 31	DCT	4.86	4.8792	-0.753
41	30	10	120	Oil+Mn	CuW	DCT	Ti15	WCT	7.44	7.4061	-0.182
42	30	10	150	Oil+W	Cu	WCT	Ti 21	SCT	9.42	9.6409	0.328
43	30	14	90	Oil	Cu	DCT	Ti 21	DCT	7.28	7.2649	0.202
44	30	14	120	Oil+Mn	CuCr	WCT	Ti 31	WCT	5.66	5.6668	2.217
45	30	14	150	Oil	CuW	SCT	Ti15	SCT	9.12	9.1196	-0.401
46	45	6	90	Oil+W	CuW	SCT	Ti 21	WCT	3.01	3.0105	-0.552
47	45	6	120	Oil	Cu	DCT	Ti 31	SCT	4.61	4.6246	0.615
48	45	6	150	Oil+Mn	CuCr	WCT	Ti15	DCT	4.43	4.4297	-0.591
49	45	10	90	Oil+Mn	CuW	WCT	Ti 31	SCT	5.60	5.6720	0.033
50	45	10	120	Oil+W	Cu	SCT	Ti15	DCT	5.54	5.5373	0.041
51	45	10	150	Oil	CuCr	DCT	Ti 21	WCT	5.50	5.4862	0.726
52	45	14	90	Oil+W	CuCr	DCT	Ti15	SCT	5.54	5.5588	-0.259
53	45	14	120	Oil	CuW	WCT	Ti 21	DCT	5.68	5.6540	0.447
54	45	14	150	Oil+Mn	Cu	SCT	Ti 31	WCT	5.66	5.6109	-0.267

Table 5.5 shows the experimental conditions, actual experimental result, ANN predicted results and % relative error between experimental and ANN predicted results for all the 54 observations. Out of these 54 observations, 38 (which are roughly 70% of the total number of data sets) were taken for training purpose, another 08 (about 15%) were taken for validation and the remaining 08 (15%) were taken for testing. The generated data was preferred for

testing as well training of neural network for feed-forward back propagation (FFBP) algorithm. The FFBP algorithm consists of eight input layer, twenty hidden layer and one output layer (SR). A two layer *transig – purelin* neural network with eight input neurons, one output neuron, and a single hidden layer of twenty neurons was used as shown in Figure 5.4 for prediction of surface roughness.

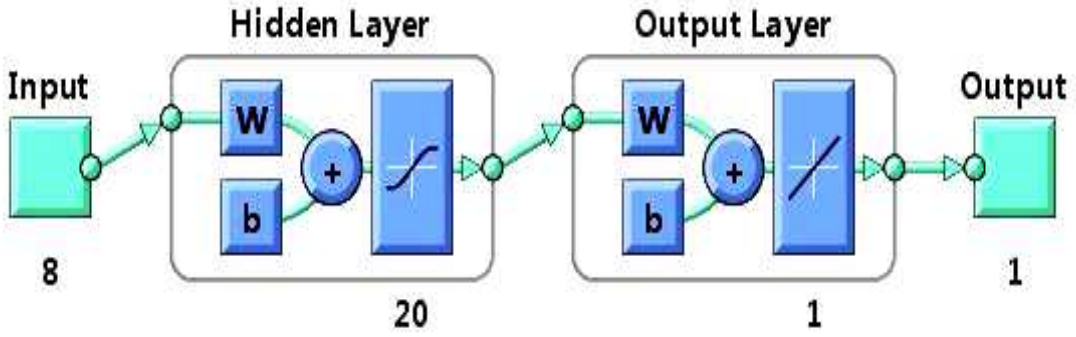

Figure 5.3: A Multi-layer Tansig–purelin Network with Eight Input Neurons, One Output Neuron, and One Hidden Layer of Twenty Neuron

The FFBP neural network architecture used in this study been shown in Figure 5.3. The FFBP algorithm considers the gradient decent method for learning and to train the ANN process. The ANN method automatically adjusts its threshold and weight values during training such that the difference between the sample outputs and target is kept low. The adjustments are computed by the propagation algorithm. The network has been trained using Lavenberg–Marquardt algorithm, i.e. *trainlm* algorithm of aneural network tool box of MATLAB 7.12.0 software. The error goal and learning rate were set to be 0.001 and 0.1, respectively. The transfer functions which were preferred are *tansig and purelin* in hidden and output layer respectively [134].

The *tansig* and *purelin* transfer functions shown by equation (5.39) and (5.40) calculate their output as follows [134, MATLAB, 7.12.0 software, 166]:

$$transig(\mathrm{n}) = \frac{2}{1+\exp^{-2n}} - 1 \qquad (5.39)$$

$$purelin\ (\mathrm{n}) = \mathrm{n} \qquad (5.40)$$

Where n is input to the function.

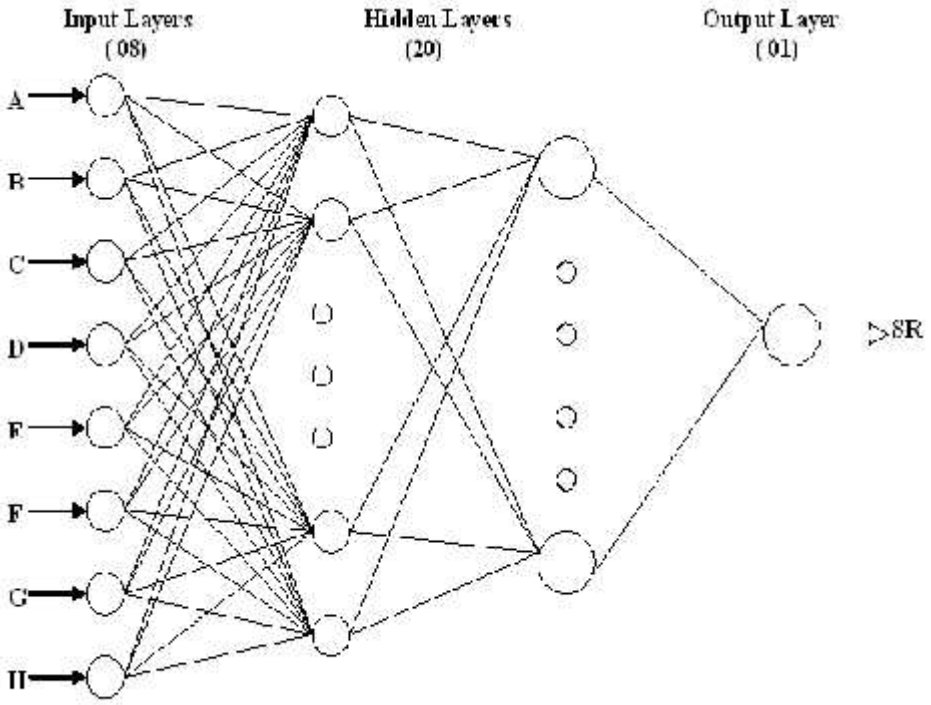

Figure 5.4: Configuration of the FFBP Neural Network Model for the EDM Process on Response Surface Roughness

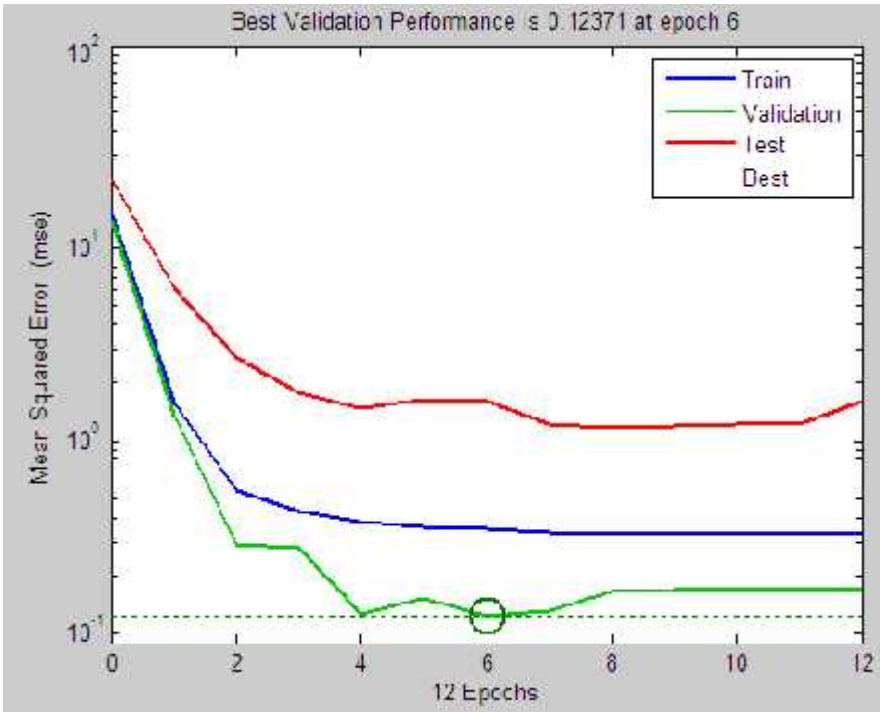

Figure 5.5: Performance Result of FFBP Algorithm Developed for Model of SR

The performance graph of the result after training showed the best results. The best validation performance of the network was 0.1237 at epoch 06 and the model is completed in 12 epochs as shown in Figure 5.5. Table 5.5 shows the percentage relative errors of experimental and ANN predicted results for surface roughness. The ANN model shows a good agreement between the actual and the predicted results of the FFBP neural network.

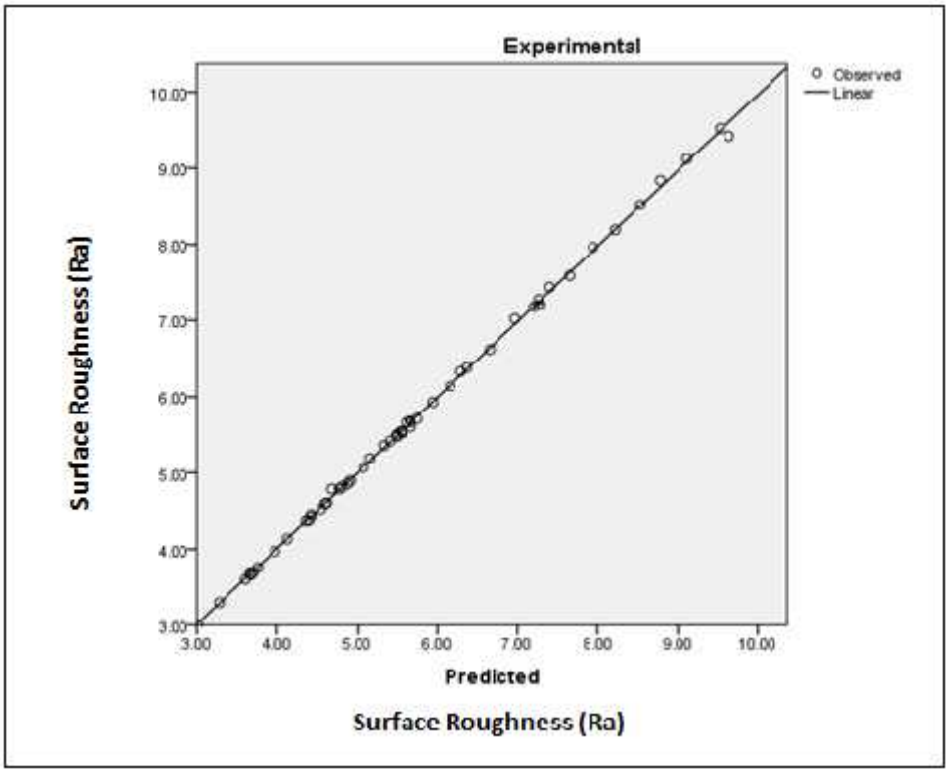

Figure 5.6: Comparison between the Experimental Results and the Neural Network Predicted Results

The percentage relative error percentage was calculated by using following equation (5.41):

$$\% \text{ Relative Error} = \left(\frac{\text{Experimental Results -ANN Predicted Results}}{\text{Experimental Results}} \right) \times 100 \qquad (5.41)$$

The comparison of the experimental results and the predicted results from the FFBP neural network for surface roughness is illustrated in Figure 5.6 which shows a close relationship between the two results for SR. From the Table 5.5, it is clear that the maximum error is -2.346% for trial number 25, minimum is 0.006 % for trial number 31 and overall mean of % relative error is 0.502. Figure 5.7 shows the convergence or gradient of mean square error (MSE) for surface roughness with the number of epochs during training of the selected network. In addition, for analyzing the capabilities of the network, a linear regression

between the network response and the experimental target value was performed. In the present case, the entire data of SR were put through for training, validation and testing to perform the regression analysis. The obtained regression results have been presented separately for the output, which are shown in Figure 5.8. The correlation coefficients (R) are 0.89 for training, 0.95 for validation, 0.94 for testing and 0.89 for overall in simulating the Ra. The network can be considered more accurate and powerful from a statistical point of view if the value of correlation coefficient approaches near to one. Table 5.6 shows the values for the mean square error and regression error of 38 samples for training, 08 samples for validation and 08 samples for testing.

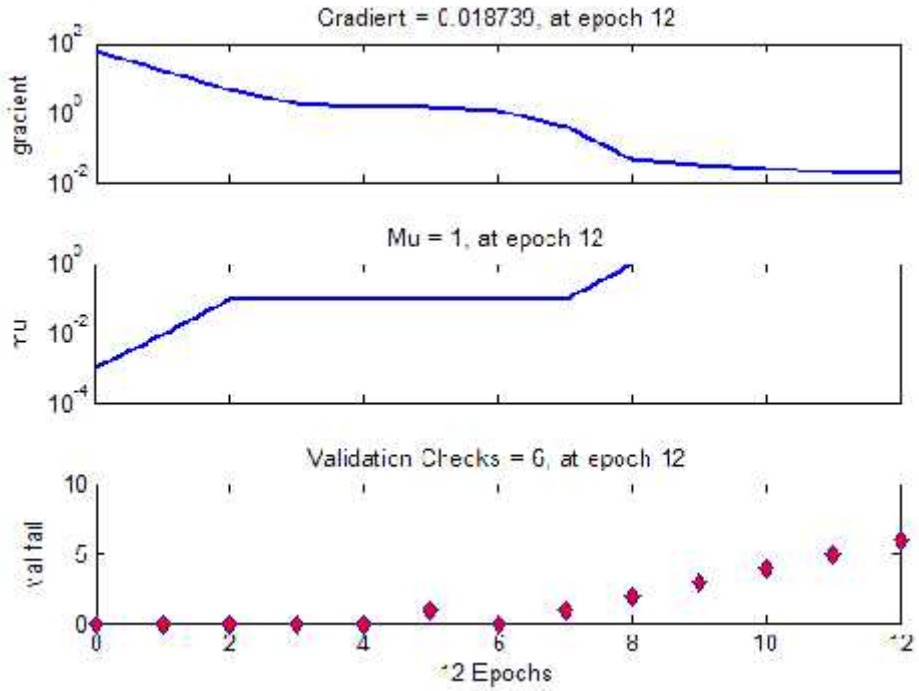

Figure 5.7: Learning Behavior of the FFBP Neural Network Model

Table 5.6: Mean Square Error and Regression Error for Results of Training, Validation and Testing for Surface Roughness

Results	Samples	Mean square error (MSE)	Regression error
Training	38	1.41729e-1	9.68488e-1
Validation	8	5.50307e-1	9.16105e-1
Testing	8	1.55300e-1	6.22211e-1

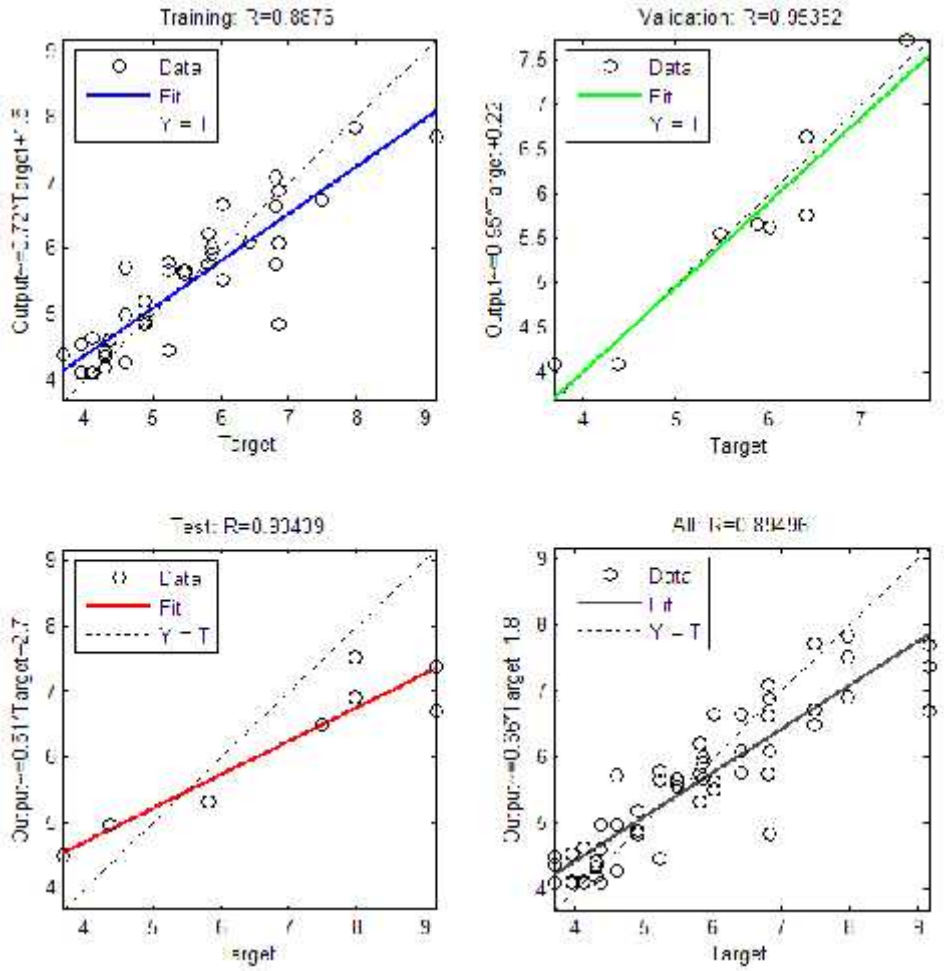

Figure 5.8: Linear Regression Analysis between the Experimental and the FFBP-ANN Predicted Values of SR (Ra) for Training, Validation, Testing and Overall

Table 5.7: Correlation between the Experimental Value and ANN Predicted Value

Variables	No. of exp. (N)	Mean	Standard deviation	Standard error mean	Correlation	Significance
Experimental value	54	5.7250	1.6422	0.2235	1.00	0.000
ANN predicted value	54	5.7306	1.6557	0.2253		

Other statistical analysis, namely correlation test and paired-sample t-test were performed to measure the variation between the experimental and ANN predicted value obtained from the network. The observed results are listed in Table 5.7 and 5.8. Table 5.7 shows that experimental value and ANN predicted value are positively correlated, r (N=54) = 1.00. Further, from Table 5.8, it can be concluded that the mean surface roughness value decreased from the experimental value to the ANN predicted value by -0.0056, t (53) = 0.938, p = 0.353>0.05. Therefore, it is concluded that there are no significant difference between the observed experimental value and ANN predicted value at 95% confidence level.

Table 5.8: Paired Sample t- test for Experimental Value and ANN Model Value

Pair (N=54)	**Paired Differences**					**t-test**	**Signifi-cance**
	Mean	**Standard Deviation**	**Standard Error Mean**	**95% confidence Interval of the Difference**			
				Lower	**Upper**		
Experimental and ANN Predicted Value	-0.0056	0.0439	0.00598	-0.01759	0.00638	-0.938	0.353

5.5 MODELING TO PREDICT MICRO-HARDNESS USING ANN APPROACH

By following the same procedure described in section 5.4, ANN was applied between the input parameters and output characteristic for modeling to predict micro-hardness. A total of 54 (18×3) readings were taken to measure change in micro-hardness values due to different level setting of input parameters. Table 5.9 shows the actual experimental results; ANN predicted results and % relative error. The ANN model shows a good agreement between the actual and the predicted results of the FFBP neural network.

The comparison of the experimental results and the predicted results from the FFBP neural network for micro-hardness is illustrated in Figure 5.9 which shows a close relationship between the two results for micro-hardness. From the Table 5.9, it is clear that the maximum error is 6.06% for trial number 44; minimum is 0.20 % for trial number 20.

Table 5.9: Experimental Results and ANN Predicted Results for Micro-hardness

Exp. No.	Actual Value	ANN Value	% Relative Error	Exp. No.	Actual Value	ANN Value	% Relative Error
1.	393	402.88	2.51	**28.**	437	429.13	1.80
2.	432	437.97	1.38	**29.**	481	501.66	4.29
3.	438	427.64	2.37	**30.**	415	424.92	2.39
4.	465	457.88	1.53	**31.**	490	485.35	0.94
5.	443	452.62	2.17	**32.**	517	528.3	2.18
6.	482	488.15	1.27	**33.**	510	514.1	0.80
7.	517	499.78	3.33	**34.**	515	492.95	4.28
8.	562	557.67	0.77	**35.**	615	587.06	4.54
9.	495	503.22	1.66	**36.**	602	595.88	1.01
10.	457	472.44	3.37	**37.**	352	353.12	0.32
11.	465	463	0.43	**38.**	425	431.74	1.58
12.	442	451.84	2.23	**39.**	472	492.27	4.29
13.	527	537.52	2.00	**40.**	425	421.96	0.72
14.	475	469.27	1.20	**41.**	465	458.27	1.45
15.	526	532.64	1.26	**42.**	502	512.38	7.65
16.	540	542.79	0.52	**43.**	522	534.55	2.40
17.	582	597.33	2.63	**44.**	548	514.76	6.06
18.	592	582.25	1.64	**45.**	527	518.35	1.64
19.	412	414.1	0.51	**46.**	445	437.77	1.62
20.	397	396.06	0.24	**47.**	427	419.21	1.82
21.	435	427.11	1.82	**48.**	435	452.71	4.07
22.	445	438.74	1.41	**49.**	538	547.94	1.85
23.	510	506.2	0.75	**50.**	510	512.4	0.47
24.	465	456.72	1.78	**51.**	465	449.13	3.41
25.	508	499.92	1.60	**52.**	535	544.11	1.70
26.	610	620.82	1.77	**53.**	602	585.88	2.68
27.	557	573.12	2.90	**54.**	620	612.28	1.25

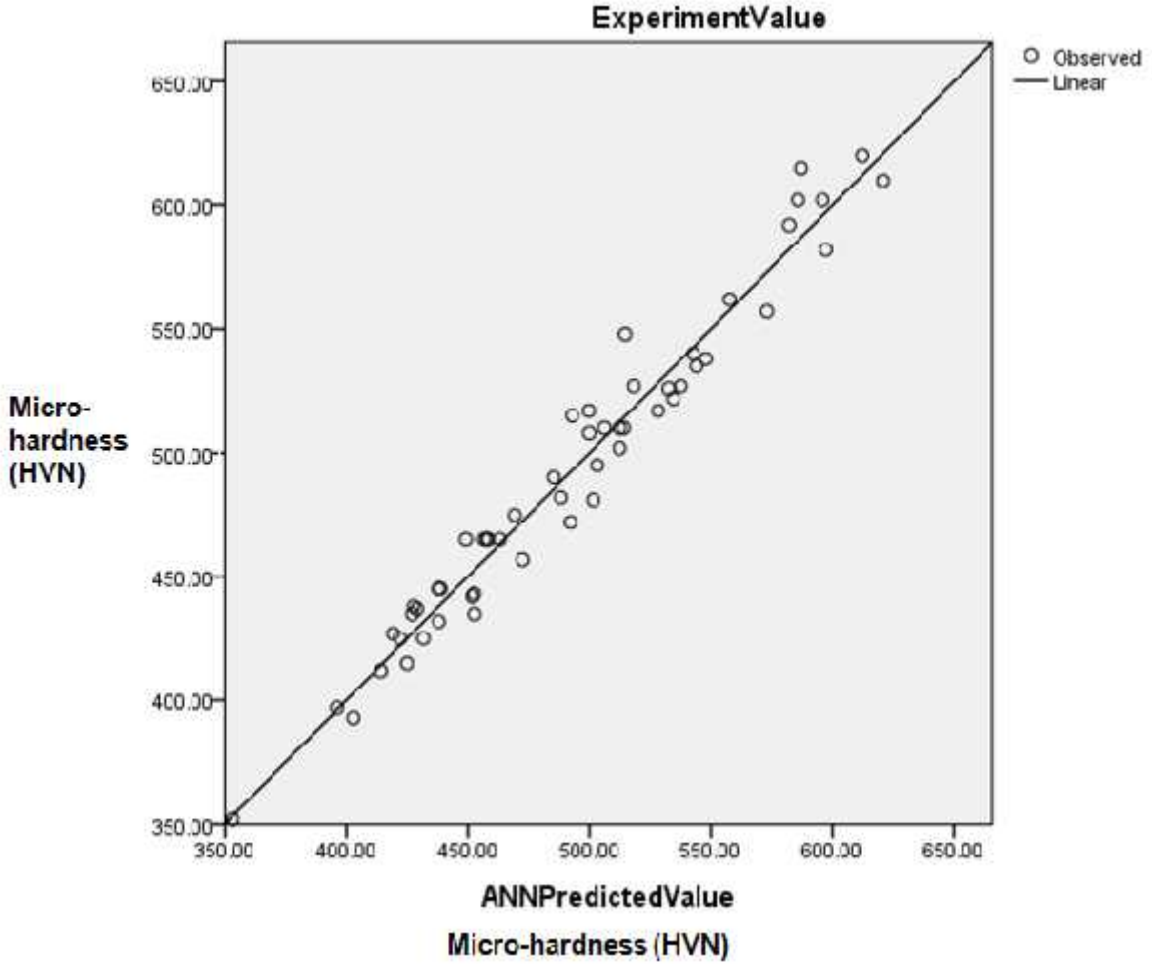

Figure 5.9: Comparison between the Experimental Results and the ANN Predicted Results of Micro-hardness

Figure 5.10 shows the convergence or gradient of mean square error (MSE) for micro-hardness with the number of epochs during training of the selected network. In addition, for analyzing the capabilities of the network, a linear regression between the network response and the experimental target value was performed. In the present case, the entire data of micro-hardness were put through for training, validation and testing to perform the regression analysis. The obtained regression results have been presented separately for the output, which are shown in Figure 5.11. The correlation coefficients are 0.87185 for training, 0.94024 for validation, 0.94776 for testing and 0.88099 for overall in simulating the micro-hardness. The network can be considered more accurate and powerful from a statistical point of view if the value of correlation coefficients (R) approaches near to one. Table 5.10 shows the values for the mean square error and regression error of 38 samples for training, 08 samples for validation and 08 samples for testing.

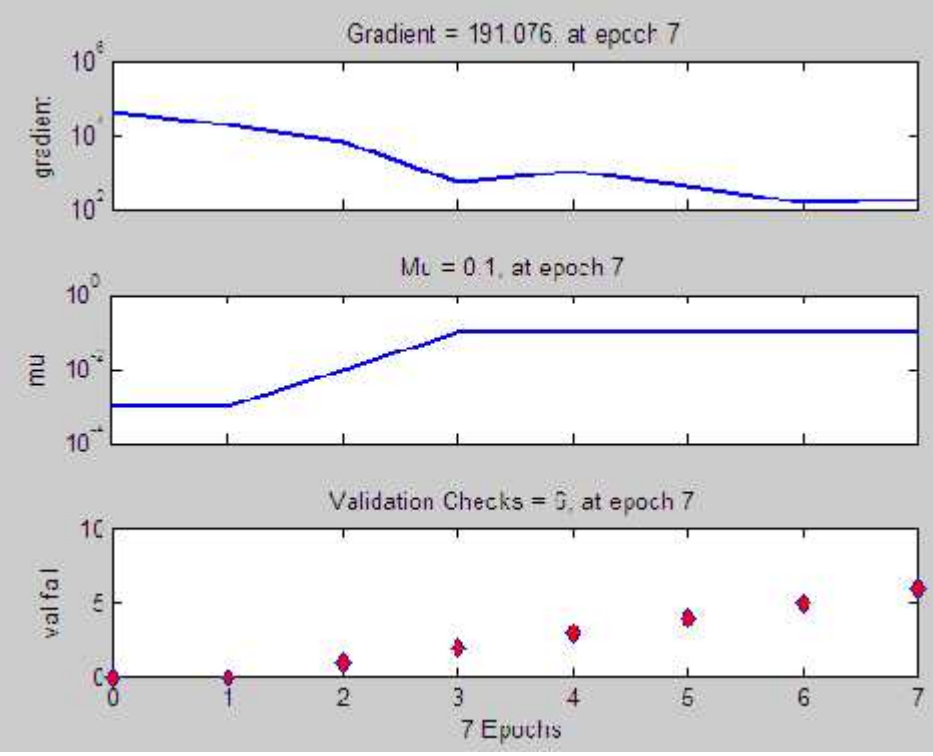

Figure 5.10: Learning Behavior of the FFBP Neural Network Model

Table 5.10: Mean Square Error and Regression Error for Results of Training, Validation and Testing for Micro-hardness

Results	Samples	Mean square error (MSE)	Regression error
Training	38	1558.09316e-0	8.71852e-1
Validation	8	1898.48334e-0	9.40242e-1
Testing	8	836.53418e-0	9.47761e-1

Table 5.11: Correlation between the Experimental Value and ANN Predicted Value for Micro-hardness

Variables	No. of exp. (N)	Mean	Standard deviation	Standard error mean	Correlation	Significance
Experimental value	54	492.0185	62.79481	8.54529	0.904	0.000
ANN predicted value	54	491.9974	61.72368	8.39953		

Table 5.12: Paired Sample t- test for Experimental Value and ANN Model Value for Micro-hardness

Pair (N=54)	Paired Differences					t-test	Signifi-cance
	Mean	Standard Deviation	Standard Error Mean	95% confidence Interval of the Difference			
				Lower	Upper		
Experimental and ANN Predicted Value	0.02111	11.89673	1.61894	-3.22607	3.26829	0.013	0.937

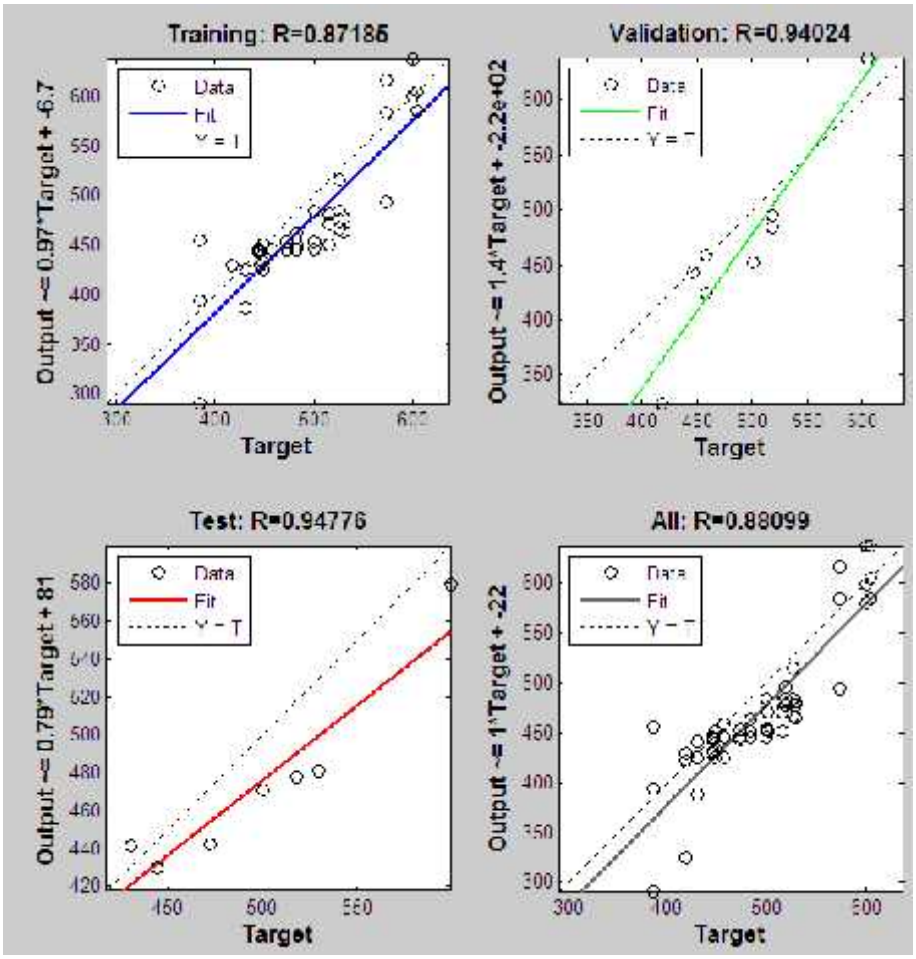

Figure 5.11: Linear Regression Analysis between the Experimental and the FFBP-ANN Predicted Values of Micro-hardness (HVN) for Training, Validation, Testing and Overall

Other statistical analysis, namely correlation test and paired-sample t-test were performed to measure the variation between the experimental and ANN predicted value obtained from the network for micro-hardness. The observed results are listed in Table 5.11 and 5.12. Table 5.11 shows that experimental value and ANN predicted value are positively correlated, r (N=54) = 0.904. Further, from Table 5.12, it can be concluded that the mean micro-hardness value increased from the experimental value to the ANN predicted value by 0.02111, t (53) = 0.013, p = 0.937>0.05. Therefore, it is concluded that there are no significant difference between the observed experimental value and ANN predicted value at 95% confidence level.

5.6 SUMMARY

Through dimensional analysis, micro-mathematical model for MRR and TWR were developed which represent experimental results in the form of empirical equations.

$$Z = \left(-0.0009Ip^3 + 0.0095Ip^2 + 0.2137Ip - 0.4895\right) L_v \frac{©^{1/2}}{\circ Cp^{2}\pm^{1/2} T_v^{3/2}} \quad \text{(For MRR)}$$

$$V = \left(0.0091Ip^3 - 0.0385Ip^2 + 0.1241Ip - 0.069\right) \frac{T_{on} V_b L_f}{©T_m} \quad \text{(For TWR)}$$

After the validation of the models, results shows that the there is a good relationship between the model results and experimental results with very small error. ANN approach was applied to establish the relationship between the input parameters and the output response characteristics namely surface roughness and micro-hardness. Small percentage of errors between the experimental response and ANN response were observed. A good agreement between the experimental and model predicted results were obtained for all the four responses.

Chapter 6

EFFECT OF CRYOGENIC TREATMENT

(*EXPERIMENTATION PHASE-B & PHASE-C*)

6.1 INTRODUCTION

During the main experimentation (Phase-A), total eight factors were considered for machining of three grades of titanium alloy such as pulse-off-time, peak current, pulse-on-time, dielectric fluid, electrode material, workpiece material and cryogenic treatment of both workpiece and electrode material. To investigate the effect of cryogenic treatment of workpiece or electrode separately in details, the experimentation was further carried out in two phases, *i.e.* Phase-B & Phase-C.

The need for the Phase-B experimentation is to study the effect of shallow and deep cryogenic treatment on Ti-5Al-2.5Sn titanium alloy and compared the machining performance of SCT and DCT treated workpiece with untreated workpiece.

Under Phase-C experimentation, machining performance of deep cryogenically treated titanium alloys were compared with untreated titanium alloys when machined with WCT, SCT and DCT electrodes.

6.2 EXPERIMENTATION PHASE-B

Since, very little work has been conducted on Ti-5Al-2.5Sn titanium alloy using an EDM process. Due to this reason, this alloy has been considered as a workpiece material for Phase-B experimental work.

In Phase-B experimentation, three types of Ti-5Al-2.5Sn alloy material: (i) without cryogenic treated (WCT), (ii) shallow cryogenic treatment (SCT) and (iii) deep cryogenic treatment (DCT) were machined with WCT Cu-Cr electrode. Based on the literature review and results of preliminary experimentation or main experimentation (Phase-A), it was observed that two parameters, *i.e.* I_p and T_{on} significantly affected the performance measures. Hence, these two factors were taken for this study and each factor was varied at three levels. The value of T_{off} 45µs was kept constant throughout the experimentation. Process conditions used for conducting the experiments are listed in Table 6.1 in the form of Taguchi L_9 array. During this Phase-B experimentation, a total of 9 sets of experiments were performed, *i.e.* three sets for each WCT, SCT and DCT material.

The following issues related to Phase-B experimentation have been addressed here:

- The effect of cryogenic treatment of Ti-5Al-2.5Sn titanium alloys on EDM performance (MRR, TWR, SR and MH) was investigated by using un-treated copper-chromium electrode.
- The observed experimental results of WCT, SCT and DCT Ti-5Al-2.5Sn alloy have been compared.
- The effects of two significant parameters (I_p and T_{on}) on machining characteristics have been investigated.

Table 6.1: L_9 Design of Experiment for Phase-B Experimentation

Experiment Number	Control Factors	
	Pulse-on-time (μs)	Peak Current (A)
1.	90	06
2.	90	10
3.	90	14
4.	120	06
5.	120	10
6.	120	14
7.	150	06
8.	150	10
9.	150	14

6.2.1 MATERIAL REMOVAL RATE

The average values of the MRR for Ti-5Al-2.5Sn titanium alloy for WCT, SCT and DCT conditions are shown in Table 6.2, whereas graphical representation of the experimental observation of the MRR for WCT, SCT and DCT alloy are also shown in Figure 6.1. From Figure 6.1 and Table 6.2 it can be seen that the DCT alloy gives higher MRR as compared to SCT and WCT alloy except for experiment number 8.

The percentage changes in MRR were calculated after comparing the MRR of SCT and DCT with WCT as shown in Table 6.3. The maximum gain in MRR as 13.92% for SCT and 21.84% for DCT alloy were observed for trial number 4 and 5 respectively. This may be due to fact that the thermal conductivity of titanium alloy is improved because of cryogenic

treatment. Reduction in MRR of SCT workpiece for experiment number 3 & 6 in comparison of WCT alloy was also observed. From Figure 6.1, it can be clearly seen that there is a significant effect of DCT of Ti-5Al-2.5Sn alloy on MRR as compared to SCT alloy.

Table 6.2: Comparison of Responses (MRR, TWR, SR and MH)

Exp. No.	MRR (mm^3/min)			TWR (mm^3/min)			SR (Ra)			MH (HVN)		
	WCT	SCT	DCT	WCT	SCT	DCT	WCT	SCT	DCT	WCT	SCT	DCT
1.	0.99	1.06	1.16	0.037	0.035	0.030	3.28	3.12	2.95	365.3	345.2	390.5
2.	1.68	1.81	1.90	0.173	0.182	0.145	4.68	4.75	4.22	396.7	415.2	435.2
3.	2.62	2.57	2.86	0.423	0.410	0.402	5.89	5.65	6.05	430.0	452.2	475.2
4.	1.14	1.30	1.33	0.056	0.048	0.041	4.29	3.92	3.45	408.3	417.5	382.5
5.	2.29	2.59	2.79	0.230	0.215	0.208	5.57	5.12	4.85	440.0	452.6	482.5
6.	2.85	2.75	3.43	0.482	0.465	0.425	7.16	7.52	6.55	454.7	478.4	512.5
7.	1.38	1.39	1.48	0.073	0.069	0.053	4.59	3.92	4.20	396.7	422.4	440.4
8.	2.39	2.53	2.42	0.257	0.245	0.225	6.00	5.74	5.32	433.3	464.5	498.6
9.	2.89	3.13	3.38	0.501	0.465	0.442	8.25	7.52	7.12	469.3	485.3	550.5

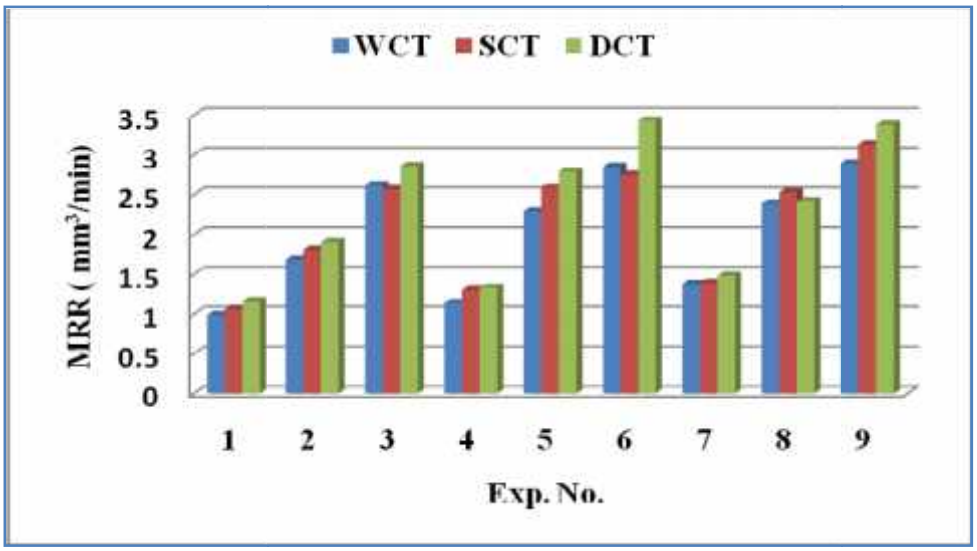

Figure 6.1: Comparison of MRR in between WCT, SCT and DCT Ti 21Alloy

Table 6.3: Percentage Gain/Loss in MRR

Cryogenic Treatment	Experiment Number								
	1	**2**	**3**	**4**	**5**	**6**	**7**	**8**	**9**
SCT	6.61	7.56	-2.06	13.92	13.07	-3.52	11.63	5.68	8.13
DCT	16.22	13.28	9.23	16.10	21.84	20.39	8.00	1.21	16.88

The variation in MRR of three types of workpiece, *i.e.* WCT, SCT and DCT against input parameters (I_p and T_{on}) is shown in Figures 6.2 a, b and c respectively. In Figure 6.2 (a, b and c), three curves were plotted at 6A, 10A and 14A current for 90µs, 120µs and 150µs on-time, which indicates that as a value of current increases MRR also increases. This may be due to high current intensifying the thermal energy due to high spark energy. Higher MRR was observed at the 14A current, because an increase in current value strengthens the pulsation energy; hence, more metal is easily removed from the workpiece [48]. Further, it was also observed that MRR increases sharply as current increases from 6A to 10A during on-time 90µs to 120µs, after that in the higher range of on-time (120µs to 150µs) at higher values of current, a reduction in MRR was observed. It may be happening due to deposition of carbon in free or compound form on the surface, which increases the machining time and reduces the MRR. This statement agrees with the results of Hascalik and Caydas [19]. As the value of I_p and T_{on} increases, discharge energy also increases, this results in higher impulsive force. Due to this mechanism, removal of debris particles from the machining zone is increased, which is responsible for the increase of crater size produced by the each single discharge on the machined surface, resulted in higher removal of material from workpiece [60, 53, 109].

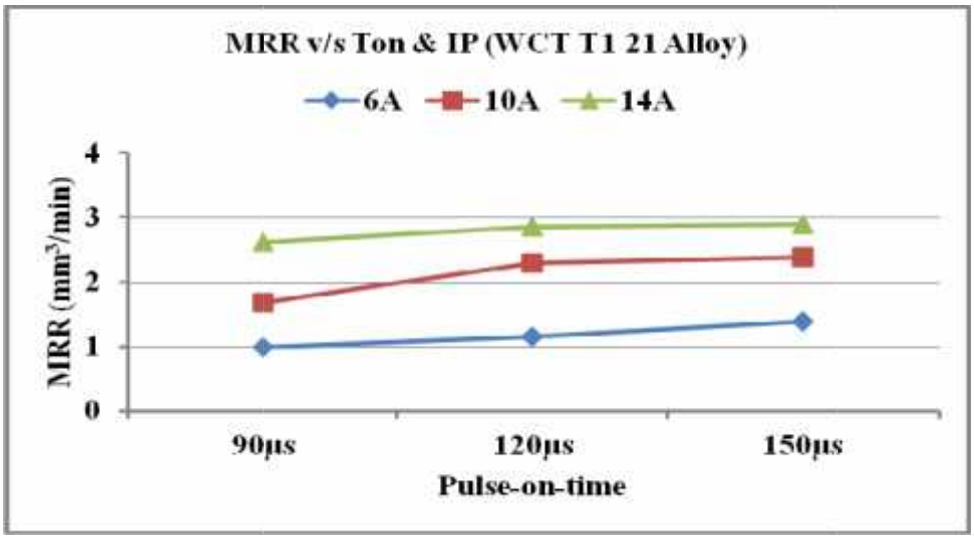

(Figure 6.2 a, WCT Ti 21 Alloy)

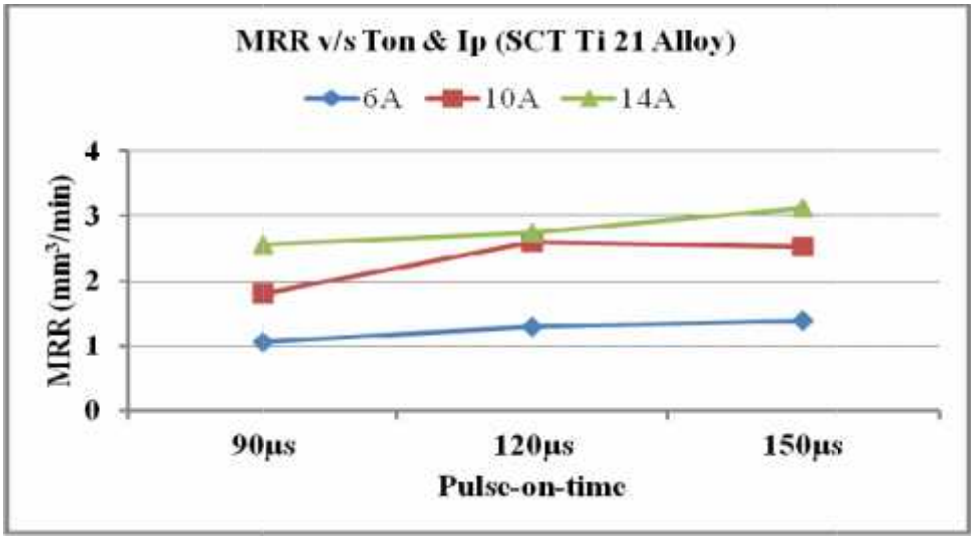

(Figure 6.2 b, SCT Ti 21Alloy)

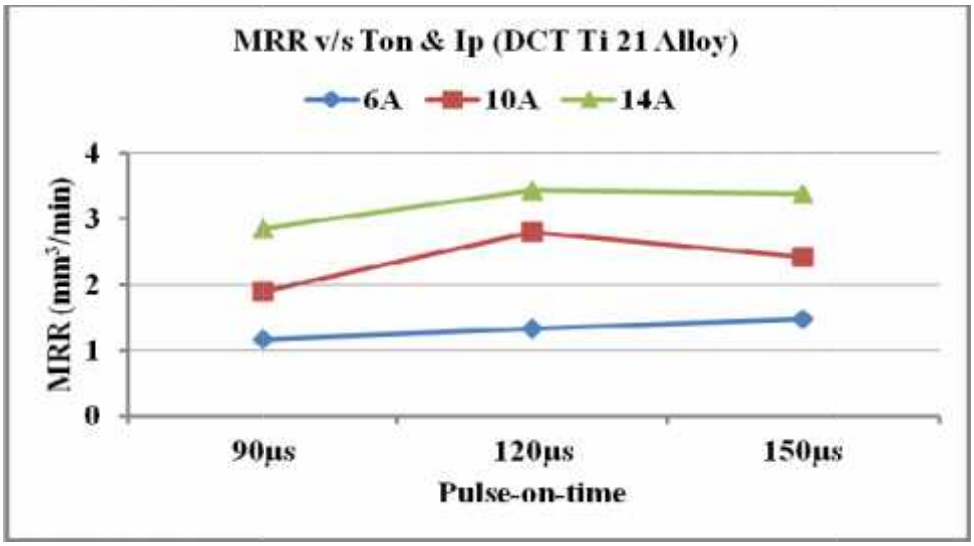

(Figure 6.2 c, DCT Ti 21 Alloy)

Figure 6.2: MRR v/s T_{on} and I_p (WCT, SCT, DCT) Ti 21 Alloy

Table 6.4: ANOVA Results of MRR, TWR, SR and MH (WCT, SCT, DCT Alloy)

Source	DOF	WCT			SCT			DCT		
		SS	V	PC	SS	V	PC	SS	V	PC
Material Removal Rate (mm^3/min)										
T_{on}	2	7.13	3.57	7.00	8.98	4.493	9.78	7.73	3.86	7.58
I_p	2	93.02	46.51	91.26	81.30	40.65	88.48	92.54	46.27	90.70
Error	4	1.77	0.44	1.74	1.60	0.40		1.75	0.44	
Total	8	101.92			91.89			102.02		

Tool Wear Rate (mm^3/min)										
T_{on}	2	20.19	10.09	3.52	15.32	7.66	2.60	15.83	7.92	2.37
I_p	2	549.25	274.63	95.63	574.44	287.22	96.40	647.77	323.38	97.0
Error	4	4.93	1.23	0.85	6.23	1.558		5.05	1.26	
Total	8	574.37			595.99			667.65		
Surface Roughness (Ra)										
T_{on}	2	11.19	5.59	23.80	7.17	3.58	13.38	7.03	3.52	13.40
I_p	2	35.52	17.76	75.50	45.48	22.74	84.87	44.78	22.39	85.25
Error	4	0.33	0.08	0.70	0.94	0.23		0.75	0.19	
Total	8	47.05			53.58			52.56		
Micro-hardness (HVN)										
T_{on}	2	1.528	0.764	36.14	2.191	1.09	33.54	2.08	1.04	23.0
I_p	2	2.649	1.325	62.65	3.864	1.93	59.15	6.57	3.29	72.85
Error	4	0.050	0.125	1.21	0.477	0.12		0.37	0.09	
Total	8	4.228			6.532			9.02		

ANOVA was completed using MINITAB 16 for WCT, SCT and DCT alloys which shows the percent contribution of I_p and T_{on} on different responses as shown in Table 6.4. Peak current was observed as the most significant factor highly affected the response characteristics.

6.2.2 TOOL WEAR RATE (TWR)

The calculated average values of TWR observed after machining of WCT, SCT and DCT Ti-5Al-2.5Sn with un-treated Cu-Cr is presented in Table 6.2. A column graph as shown in Figure 6.3 indicates the comparison of TWR of WCT, SCT and DCT in graphical form. From the variation of TWR as shown in Figure 6.3, it was concluded that low TWR was observed for DCT work specimen followed by SCT specimen.

The significant improvement in TWR was noticed in case of DCT workpiece compared to SCT workpiece. The maximum improvement in TWR (27.40%), and minimum (4.96%) was observed in case of DCT alloys than non-treated titanium alloys respectively (see Table 6.5). On the other side, maximum improvement in TWR (14.28%), and a minimum (3.07%) was observed with SCT alloys as can be seen in Table 6.5. In addition to improvement in TWR, an increase in TWR was also noticed for experiment number 2 for SCT alloy.

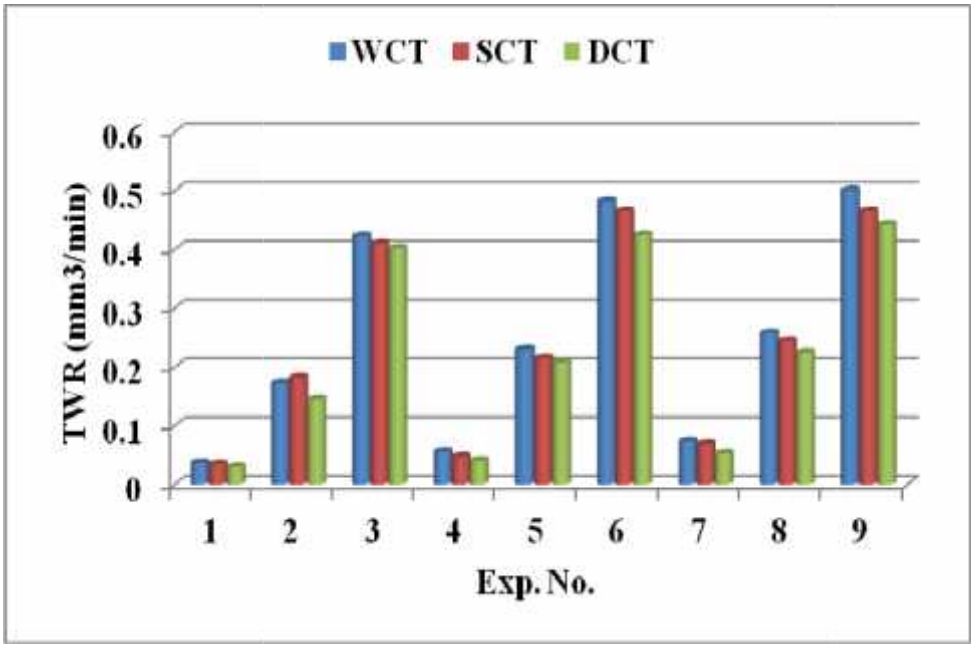

Figure 6.3: Comparison of TWR in between WCT, SCT and DCT Ti 21Alloy

Table 6.5: Percentage Gain/Loss in TWR

Cryogenic Treatment	Experiment Number								
	1	2	3	4	5	6	7	8	9
SCT	-5.41	5.20	-3.07	-14.28	-6.52	-3.53	-5.48	-4.67	-7.18
DCT	-18.92	-16.18	-4.96	-26.78	-9.56	-11.82	-27.40	-12.45	-11.78

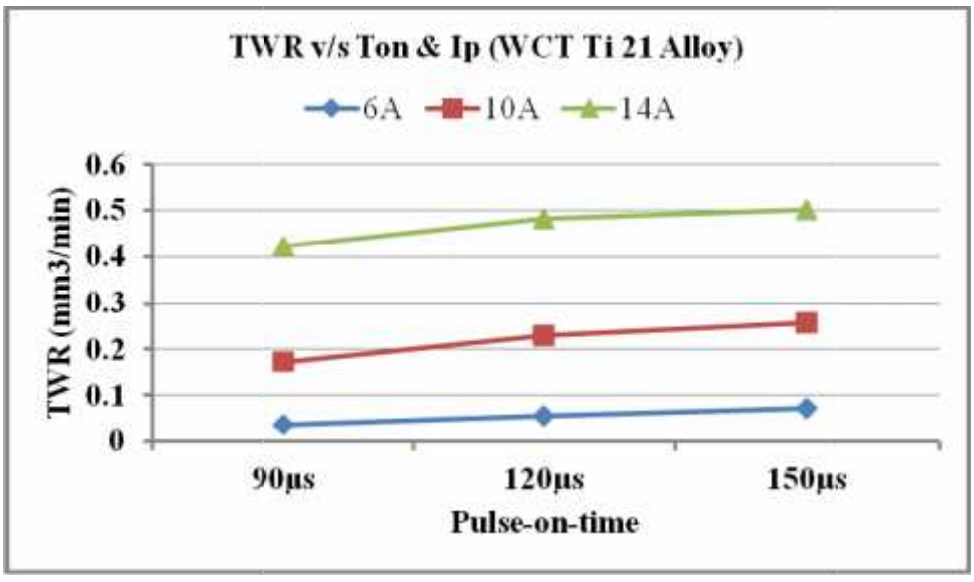

(Figure 6.4 a, WCT Ti 21 Alloy)

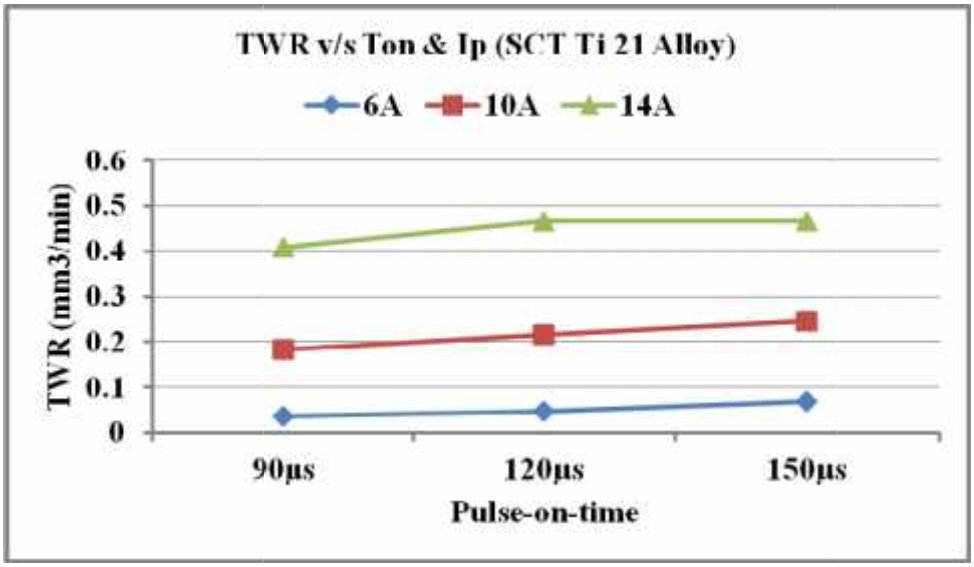

(Figure 6.4 b, SCT Ti 21 Alloy)

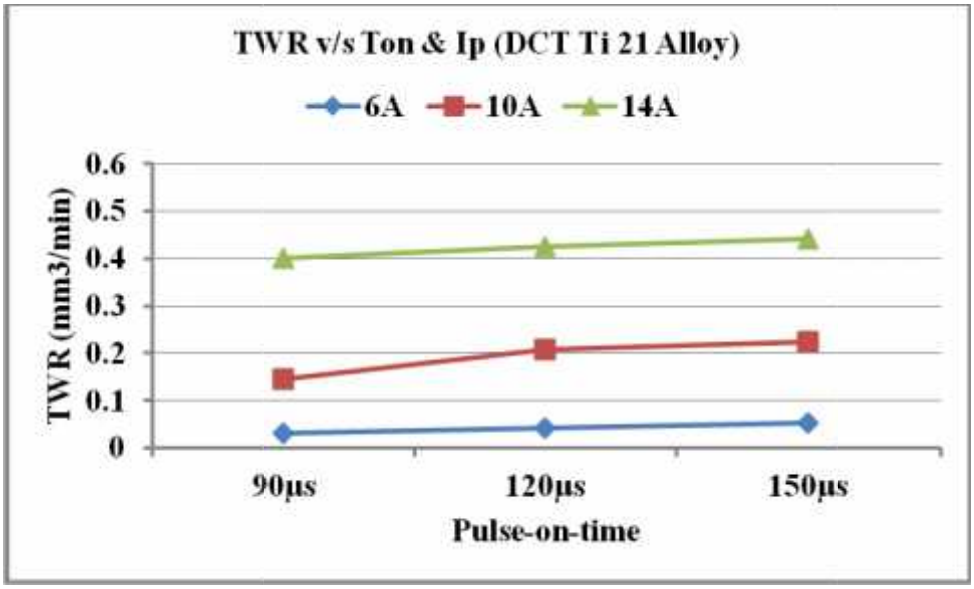

(Figure 6.4 c, DCT Ti 21 Alloy)

Figure 6.4: TWR v/s Pulse-on-time and Current (WCT, SCT, DCT) Ti 21 Alloy

The interaction plots of parameters for TWR variation are shown in Figure 6.4 (a, b, c) for WCT, SCT and DCT workpiece respectively. Figure 6.4 illustrates that TWR increases upon increase in I_p for all values of T_{on}. Higher TWR was obtained at 14A current and lower at low values of peak current, *i.e.* 6A. Thus, it was concluded that low current value is the key factor to increase the life of the tool during the EDM process. A uniform increase in TWR was observed for all values of currents, *i.e.* 6A, 10A and 14A at on-time setting of 90µs, 120µs and 150µs as shown in Figure 6.4 (a, b, c) as compared to 10A and 14A current. However, smaller value of current 6A causes reduction in MRR.

6.2.3 SURFACE ROUGHNESS (SR)

The average values of three observations of SR are presented in Table 6.2 for WCT, SCT and DCT titanium alloys and also plotted in graphical form (see Figure 6.5). By observing the graphical presentation, it can be clearly understood that low values of the SR were observed in case of DCT alloy followed by SCT alloy when compared to WCT alloy. The percentage changes in response SR for the nine experiments are summarized in Table 6.6, which shows the maximum improvement of 19.58% for DCT material of experiment number 4 and 14.60% for SCT material of experiment number 7. As removal of heat from the machining zone was increased in case of DCT alloys due to higher thermal conductivity, it contributes in a better surface finish than non-treated alloys. However, the increase in SR was also observed in both the cases, *i.e.* trial 2 SCT alloy and trial 3 DCT alloy.

Table 6.6: Percentage Gain/Loss in Surface Roughness

	Experiment Number								
	1	**2**	**3**	**4**	**5**	**6**	**7**	**8**	**9**
SCT	-4.88	1.5	-4.07	-8.62	-8.08	5.03	-14.60	-4.33	-8.85
DCT	-10.06	-9.83	3.42	-19.58	-12.93	-8.52	-8.50	-11.33	-13.70

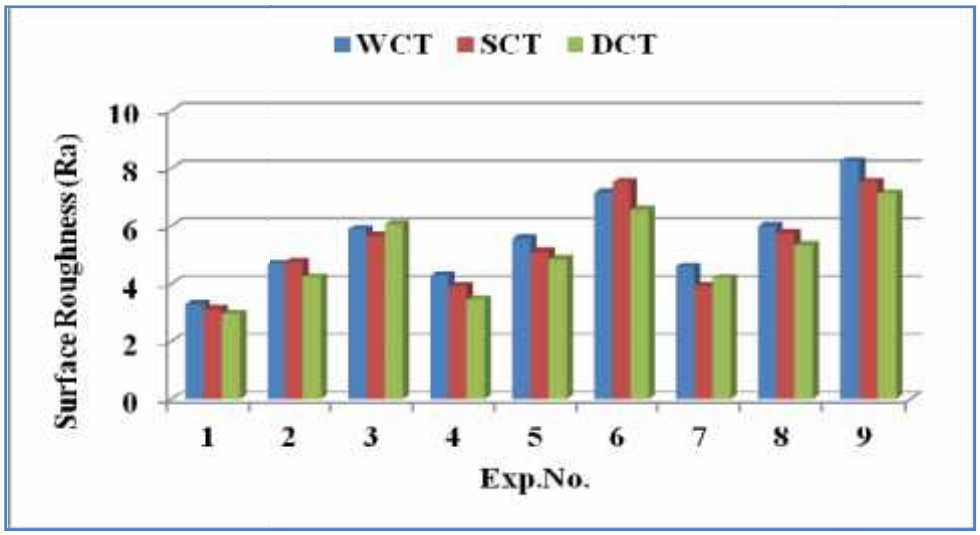

Figure 6.5: Comparison of SR in between WCT, SCT and DCT Ti 21Alloy

Peak-current was observed to be the most significant electrical parameter that affected SR as shown in ANOVA results (see Table 6.4). The variation in SR values against the input parameters (I_p & T_{on}) for WCT, SCT and DCT are presented in Figures 6.6 (a, b, c) respectively for current 6A, 10A and 14A. From Figure 6.6, it was observed that surface

finish gradually decreases, as the value of the current increases. Higher current increases the thermal energy in the spark zone, thus, increasing the melting rate of workpiece material, resulting in larger crater size which causes poor surface texture. Low value of SR was observed at a setting of 6A current and 90µs on-time. This statement indicates that a better surface texture can be obtained only at low current with smaller T_{on} due to low metal erosion. In addition to the influence of current, pulse-on-time also influences the SR in a negative way as expected. But from Figure 6.6, it can be seen that as the duration of pulse-on-time increased, *i.e.* 120 to150µs, the surface finish of the workpiece being slightly improved at current 6A and 10A, because the intensity of generated sparks decreasing on account of the expansion of plasma channel. In EDM process, better surface finish can be obtained only at low values of I_p and T_{on}.

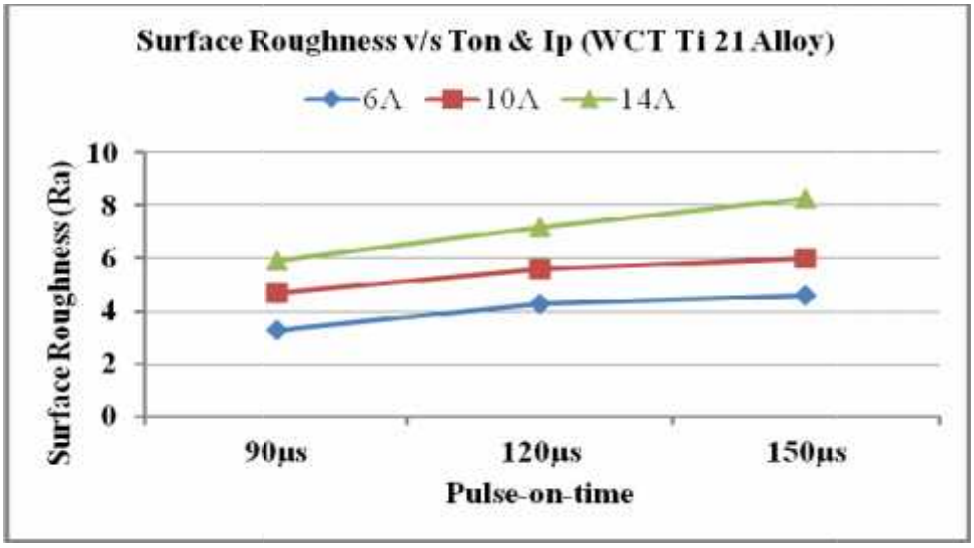

(Figure 6.6a, WCT Ti 21 Alloy)

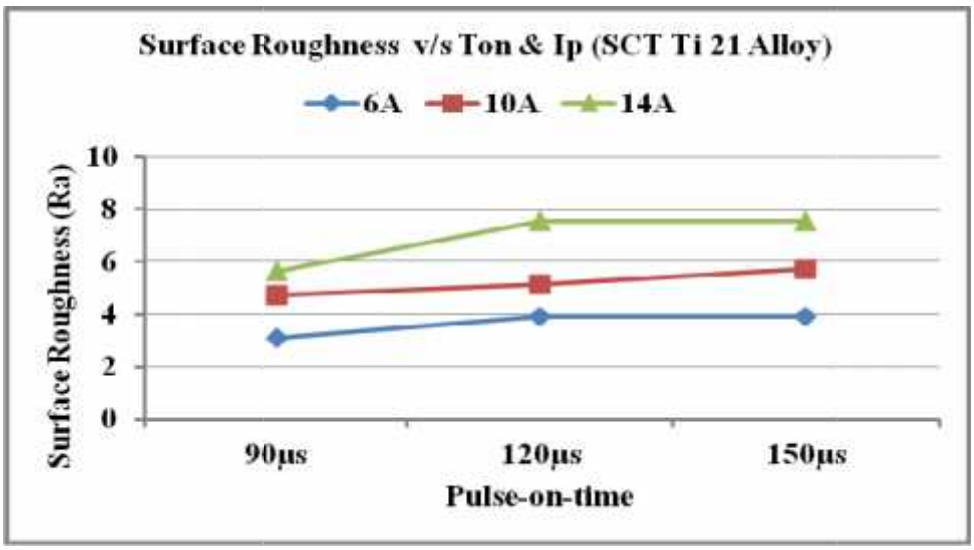

(Figure 6.6 b, SCT Ti 21 Alloy)

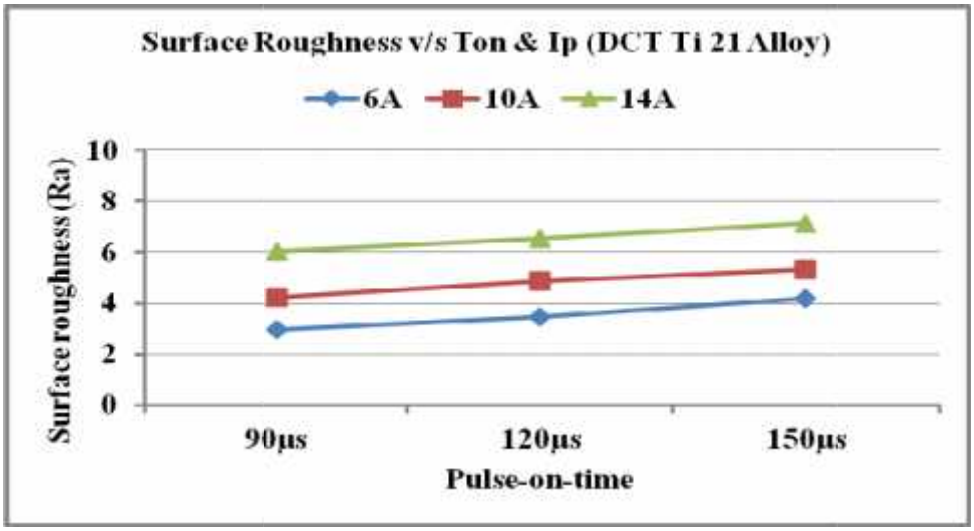

(Figure 6.6 c, DCT Ti 21 Alloy)

Figure 6.6: SR v/s Pulse-on-time and Current (WCT, SCT, DCT) Ti 21 Alloy

6.2.4 MICRO-HARDNESS (MH)

Table 6.2 shows the average values of MH of three different WCT, SCT and DCT workpiece materials of nine experiments. Calculated ANOVA results are also presented in presented in Table 6.4 which shows that I_p is the most significant factor affecting the MH with 62.65%, 59.15% and 72.85% for WCT, SCT and DCT work materials respectively. Machine parameter T_{on} also significantly affected the response as shown in Table 6.4. The comparison between the micro-hardness for WCT, SCT and DCT has been made based on the experimental results which are presented in the form of column graphs (see Figure 6.7).

An increase in micro-hardness was observed for both SCT and DCT alloy except for experiment number 1 for SCT alloy and 4 for DCT alloy where it was reduced. The micro-hardness, increased in the range 2.25% to 7.20% for SCT and 6.90% to 17.30% for DCT alloy. Percentage gain or loss in micro-hardness for SCT and DCT treated alloys are listed in Table 6.7.

Significant increase in micro-hardness was observed in case of DCT alloys than SCT or WCT alloys. Micro-hardness of the machined surface was increased with the increase in current as highlighted in Figures 6.8 (a, b, c). From the results, it was noticed that the highest value of MH was obtained when a Ti-5Al-2.5Sn alloy workpiece was machined at a setting of I_p 14A and T_{on} 150µs. The average value 320 HVN of Ti-5Al-2.5Sn specimen before machining was observed. The maximum value 479.33HV was observed at I_p 14A and T_{on} 150µs. The

maximum improvement (49.78%) in surface hardness was observed during trial number 9 after machining.

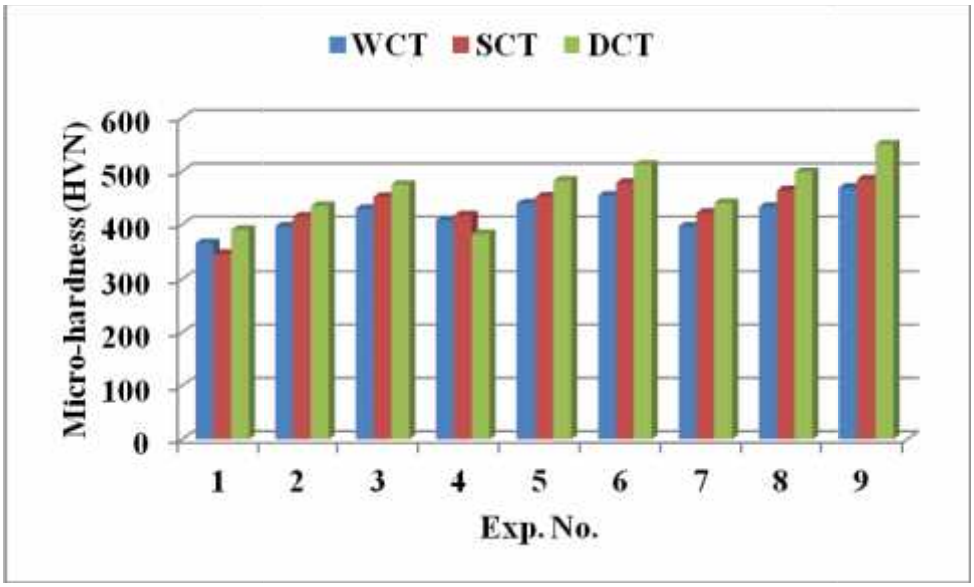

Figure 6.7: Comparison of MH in between WCT, SCT and DCT Ti 21Alloy

Table 6.7: Percentage Gain/Loss in Micro-hardness

Cryogenic Treatment	Experiment Number								
	1	2	3	4	5	6	7	8	9
SCT	-5.50	4.66	5.16	2.25	2.86	5.21	6.55	7.20	3.41
DCT	6.90	9.71	10.51	-6.32	9.66	12.72	11.02	15.07	17.30

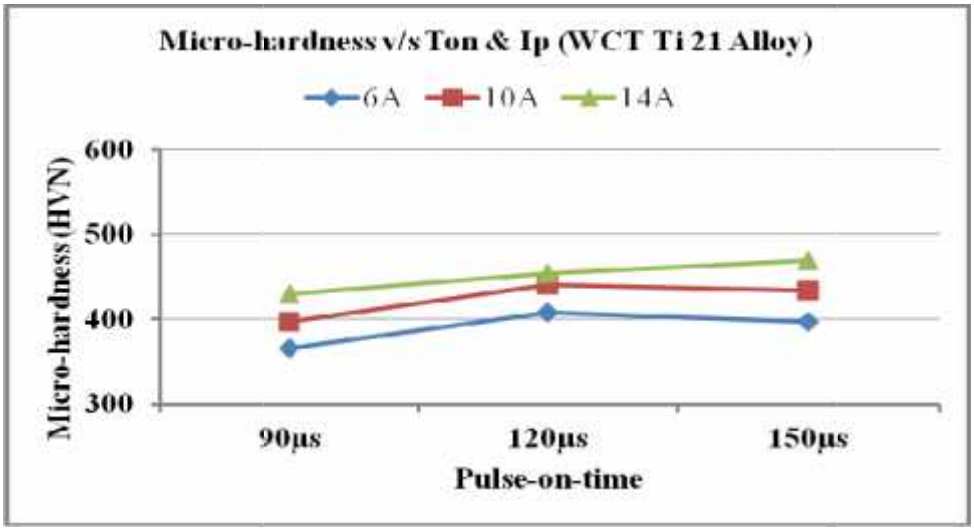

(Figure a, WCT Ti 21 Alloy)

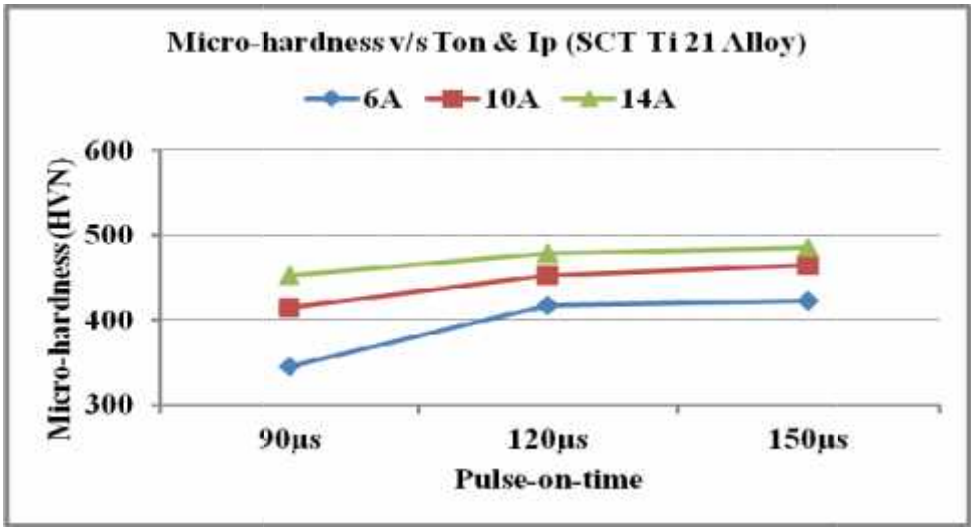

(Figure b, SCT Ti 21 Alloy)

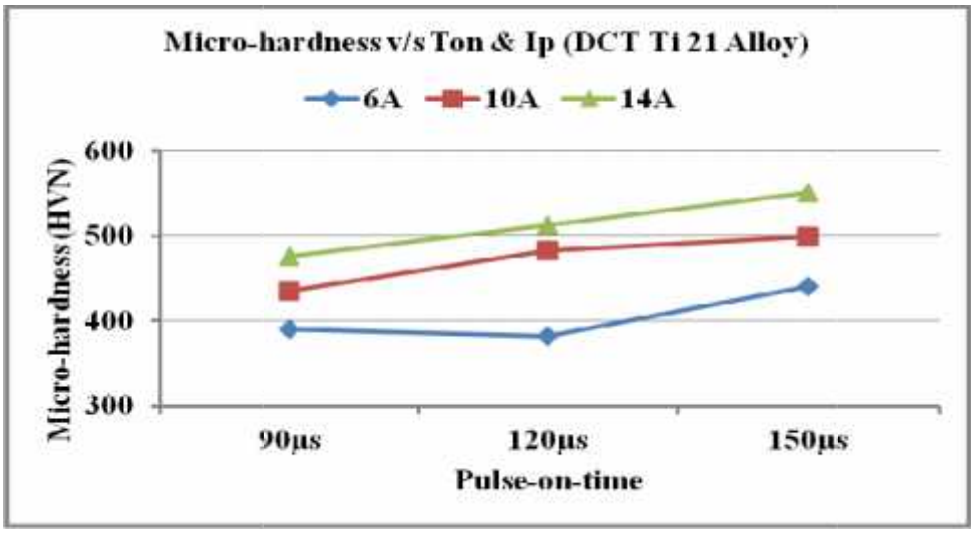

(Figure c, DCT Ti 21 Alloy)

Figure 6.8: MH v/s Pulse-on-time and Current (WCT, SCT, DCT) Ti 21 Alloy

From Figures 6.8, it was observed that MH increases sharply with the increase in T_{on} from 90 µs to 120 µs for all value of current, after that trend slightly decreases as T_{on} extended up to 150µs except for DCT alloy. At higher values of I_p and T_{on} (14A & 150µs) more discharge energy is applied to the workpiece. As a result more heating and quenching of the machined surface takes place during T_{off} period, resulting in more hardening of the surface [135]. In addition to that, due to generation of high thermal energy during the machining process, carbon decomposes from the dielectric resulting in the penetration of the cracked carbon into the machined surface. Moreover, carbon element interacts with Ti and Al element of Ti-5Al-2.5Sn alloys and forms their carbides such as Titanium- Carbides (TiC) and Aluminum-Titanium-Carbides ($Al_2Ti_4C_2$), thus, increasing the surface hardness. These results also confirm studies by other researchers [26, 53].

6.3 EXPERIMENTATION PHASE-C

During this experimentation, *i.e* Phase-C, three grades of titanium alloys without cryo-treated and deep cryo-treated were used as work material: (i) WCT TITAN 15, (ii) DCT TITAN 15, (iii) WCT TITAN 21, (iv) DCT TITAN 21, (v) WCT TITAN 31 and (vi) DCT TITAN 31. All the six types of titanium alloy were machined with three different WCT, SCT and DCT electrode (Cu, Cu-Cr and Cu-W). The entire experimental work under this phase was performed in Mn powder mixed FERROLAC 3M EDM Oil with a concentration of 10g/liter. After completion of a set of nine experiments, used powder mixed dielectric was replaced with fresh powder mixed dielectric. Four input parameters, namely I_p, T_{on}, electrode material and cryo-treatment of electrode material were varied at three levels to evaluate their effect on machining performances (MRR, TWR, SR and MH). The results are shown in Table 6.8. The value of T_{off} 45 µs was kept constant and machining time for each cut was fixed at 30 minutes. The experiment run conditions after assignment of the control factors in L_9 OA are summarized in Table 6.9. A total 18 sets for each of the nine experiments were conducted.

Table 6.8: Representation of Control Factor with their Levels for Phase-C

Control Factors	**Levels**		
	Level-1	**Level-2**	**Level-3**
Pulse-on-time, T_{on} (µs)	90	120	150
Peak Current, I_p (A)	6	10	14
Electrode Material	Cu	Cu-Cr	Cu-W
Cryogenic of Electrode	WCT	SCT	DCT

Table 6.9: L_9 Experimental Design for Phase-C Experimentation

Experiment	**Control Factors**			
Number	**Pulse-on-time T_{on} (µs)**	**Peak Current I_p (A)**	**Electrode Material**	**Cryo-treatment of Electrode**
1.	90	6	Cu	WCT
2.	90	10	Cu-Cr	SCT
3.	90	14	Cu-W	DCT
4.	120	6	Cu-Cr	DCT
5.	120	10	Cu-W	WCT
6.	120	14	Cu	SCT

7.	150	6	Cu-W	SCT
8.	150	10	Cu	DCT
9.	150	14	Cu-Cr	WCT

The following issues related to Phase-C experimentation have been addressed here:

- The effects of deep cryogenic treatment of Ti 15, Ti 21 and Ti 31 titanium alloys on EDM performance (MRR, TWR, SR and MH) has been investigated by comparing the experimental results with and without cryogenic treatment of titanium alloys.
- The effect of cryogenic treated (SCT and DCT) electrodes has been studied under this experimentation.
- The effect of two significant parameters (I_p and T_{on}) on machining characteristics has been investigated.
- Metallographic analysis of the WCT and DCT selected samples has been performed by using SEM, EDS and XRD techniques.
- Multiple characteristic optimization of WCT and DCT TITAN 15 alloy has been performed by using the grey relational analysis technique.

6.3.1 MATERIAL REMOVAL RATE (MRR)

Based on observed data of MRR as shown in Table 6.10 to 6.12 corresponding ANOVA was performed for all three types of WCT and DCT workpiece and results are summarized in Table 6.13. The main effects plots were derived using Minitab 16 and are presented in Figures 6.9 (a, b) for Ti 15 alloy, 6.10 (a, b) for Ti 21 alloy and 6.11 (a, b) for Ti 31 alloy. Here, Figure (a) shows WCT alloy and (b) shows DCT alloy of all three workpiece materials.

Table 6.10: Observation Table for MRR (WCT & DCT Ti 15 Alloy)

Exp. No	**MRR (WCT TITAN 15) (mm^3/min)**			**S/N Ratio (dB)**	**MRR (DCT TITAN 15) (mm^3/min)**			**S/N Ratio (dB)**
	R1	**R2**	**R3**		**R1**	**R2**	**R3**	
1.	0.545	0.536	0.552	-5.285	0.614	0.624	0.602	-4.248
2.	1.005	1.107	0.985	0.243	1.125	1.132	1.115	1.0148
3.	1.425	1.417	1.435	3.080	1.446	1.462	1.457	3.257
4.	0.903	0.915	0.895	-0.875	1.11	1.124	1.007	0.639
5.	1.315	1.296	1.305	2.314	1.417	1.432	1.395	3.012

6.	1.426	1.445	1.45	3.169	1.527	1.495	1.515	3.592
7.	0.825	0.805	0.815	-1.779	0.752	0.765	0.782	-2.315
8.	1.417	1.435	1.443	3.116	1.475	1.483	1.462	3.366
9.	1.405	1.435	1.396	2.995	1.593	1.605	1.572	4.027

Table 6.11: Observation Table for MRR (WCT & DCT Ti 21 Alloy)

Exp. No	MRR (WCT TITAN 21) (mm^3/min)			S/N Ratio (dB)	MRR (DCT TITAN 21) (mm^3/min)			S/N Ratio (dB)
	R1	R2	R3		R1	R2	R3	
1.	0.627	0.615	0.605	-4.216	0.632	0.625	0.642	-3.974
2.	1.376	1.253	1.363	2.458	1.51	1.495	1.52	3.569
3.	1.537	1.517	1.526	3.675	1.935	1.912	1.957	5.731
4.	1.005	0.987	1.107	0.249	1.12	1.126	1.134	1.036
5.	1.372	1.392	1.382	2.809	1.488	1.475	1.495	3.439
6.	1.689	1.692	1.705	4.585	1.853	1.867	1.847	5.369
7.	0.915	0.897	0.907	-0.855	1.052	0.902	0.917	-0.443
8.	1.487	1.478	1.467	3.389	1.654	1.672	1.668	4.426
9.	1.425	1.436	1.454	3.157	1.5	1.485	1.472	3.438

Table 6.12: Observation Table for MRR (WCT & DCT Ti 31 Alloy)

Exp. No	MRR (WCT TITAN 31) (mm^3/min)			S/N Ratio (dB)	MRR (DCT TITAN 31) (mm^3/min)			S/N Ratio (dB)
	R1	R2	R3		R1	R2	R3	
1.	0.657	0.675	0.662	-3.549	0.752	0.775	0.805	-2.198
2.	1.131	1.145	1.12	1.076	1.222	1.2	1.235	1.7182
3.	1.659	1.672	1.662	4.425	1.825	1.842	1.837	5.271
4.	0.878	0.863	0.865	-1.224	1.057	1.107	1.11	0.753
5.	1.152	1.145	1.167	1.248	1.385	1.392	1.372	2.816
6.	1.787	1.765	1.772	4.982	1.734	1.753	1.724	4.795
7.	0.935	0.926	0.917	-0.668	1.157	1.145	1.14	1.193
8.	1.415	1.433	1.427	3.076	1.505	1.517	1.523	3.608
9.	1.213	1.209	1.225	1.696	1.585	1.575	1.57	3.955

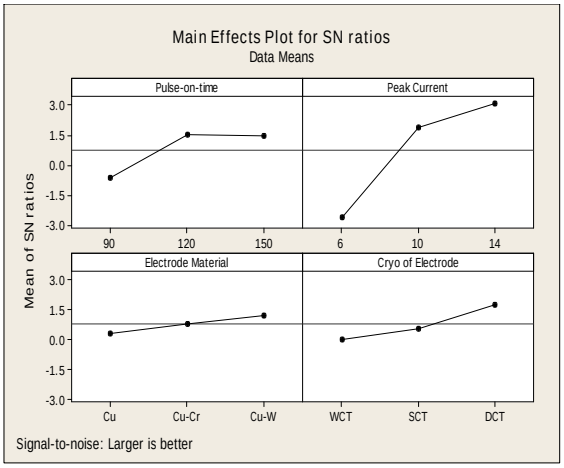

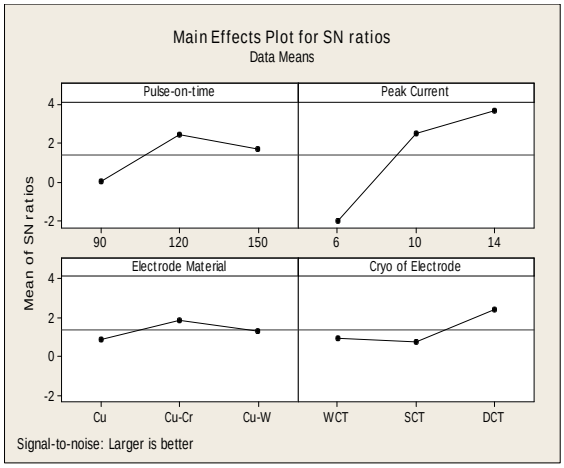

(a- WCT) **(b- DCT)**

Figure 6.9: Main Effect Plots for S/N Ratios of MRR for TITAN 15 Alloys

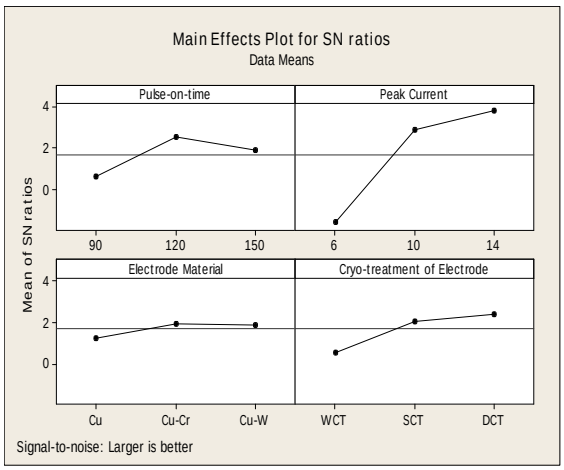

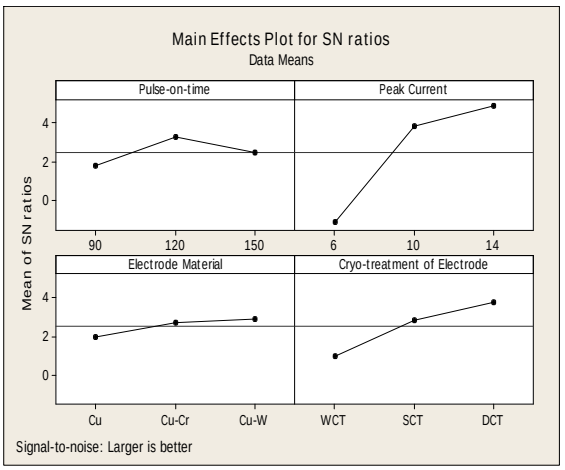

(a- WCT) **(b- DCT)**

Figure 6.10: Main Effect Plots for S/N Ratios of MRR for TITAN 21 Alloys

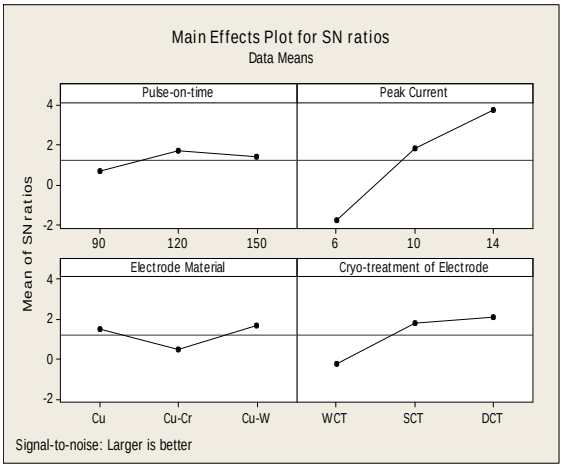

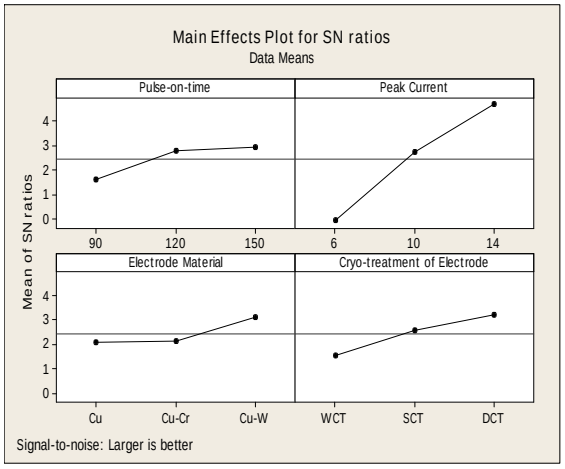

(a- WCT) **(b- DCT)**

Figure 6.11: Main Effect Plots for S/N Ratios of MRR for TITAN 31 Alloys

From Figures 6.9 to 6.11, it can be clearly seen that I_p highly affected the MRR. As current increases from 6A, the MRR sharply increases up to 10A, thereafter, at higher values of current, *i.e.* 14A, MRR start to decrease. The thermal energy in the machining zone increases as current increases up to a certain limit.

Table 6.13: ANOVA Results of S/N Data for MRR

Source of Variation	DoF	Without Cryogenic Treated			Deep Cryogenic Treated		
		Seq. SS	Adj. MS	PC (%)	Seq. SS	Adj. MS	PC (%)
TITAN 15 (ASTM grade II, Ti Alloy)							
C	2	9.206	4.603	13.14	9.152	4.576	13.44
B	2	54.796	27.398	78.21	52.413	26.207	77.02
E	2	1.141	0.5705	1.63	1.486	0.743	2.18
F	2	4.917	2.458	7.02	4.995	2.497	7.36
Total	8	70.06			68.045		
TITAN 21 (ASTM grade VI, Ti-5Al-2.5Sn Alloy)							
C	2	5.651	2.825	9.02	3.409	1.704	4.37
B	2	50.326	25.163	80.36	61.137	30.568	78.38
E	2	0.888	0.444	1.42	1.538	0.769	1.97
F	2	5.767	2.884	9.20	11.916	5.958	15.28
Total	8	62.632			78.00		
TITAN 31 (ASTM grade V, Ti-6Al-4V Alloy)							
C	2	1.643	0.822	2.72	3.182	1.591	7.26
B	2	47.087	23.544	77.95	34.305	17.152	78.33
E	2	2.328	1.164	3.85	1.962	0.981	4.48
F	2	9.343	4.672	15.48	4.346	2.173	9.93
Total	8	60.402			43.795		

C- Pulse-on-time, B – Peak current, E – Electrode material, F - Cryogenic treatment of electrode material

MRR was also affected by T_{on}, because during this period electric energy in the form of current was applied in the spark zone. MRR increases with increase in T_{on} from 90µs to 120µs and at longer pulse duration it decreases. Machining with high current and longer pulse-on-time leads to arcing, resulting in unstable machining, and causing reduction in

volume of metal removal. Further, at high current and longer on-time, more carbon cracked from the dielectric fluid and hard TiC compound is formed on the machined surface, which has a higher melting point than titanium. The developed TiC layer takes more time to melt and vaporize, leading to increase in machining time, thus, reducing the MRR. In addition to carbide compounds, due to oxidation of titanium alloy and other elements, oxide compounds one also be formed on the surface, which reduces the MRR. DCT Cu-W electrode shows higher MRR than Cu and Cu-Cr electrode as shown in Figures 6.9 to 6.11. Overall small effect of electrode material was observed on MRR, as shown in Table 6.13, in the range of 1.42% to 4.48%. But the significant effect of CT of electrodes was observed on MRR as presented in Table 6.13. DCT electrode highly influenced the MRR followed by SCT electrodes. DCT process increased the thermo-electrical properties of the electrode material resulted in less TWR and higher MRR.

From ANOVA presented in Table 6.13 and Figure 6.12, peak current was observed as the most significant factor affecting MRR. The range of contribution of peak current varies between 77.02% to 80.36% for different workpieces. Cryogenic treatment of electrode material was observed as the second significant factor that affected the MRR. The percent contribution of each control factor was determined and plotted in pie-chart as shown in Figure 6.12. The peak current (Factor B) with the largest area is indicative of the highest effect on MRR as compared to other parameters.

The percentage change in MRR after comparing the results for the WCT and DCT alloy are presented in Table 6.14. The maximum gain in MRR was observed to be 19.5%, 26.8% and 29.68% for (i) Ti15alloy, (ii) Ti21 alloy and (iii) 29.68% for Ti31 alloy respectively. The percent change (gain or loss) in response was calculated using following equation (6.1):

$$\% \text{ change} = \frac{\text{MRR of WCT-MRR of DCT}}{\text{MRR of WCT}} \times 100 \quad (6.1)$$

Table 6.14: Percentage Change in MRR for WCT and DCT Titanium Alloys

Workpiece	**Experiment Number**								
Material	**1**	**2**	**3**	**4**	**5**	**6**	**7**	**8**	**9**
TITAN 15	12.68	8.91	2.1	19.5	8.35	4.86	-6.01	2.95	12.6
TITAN 21	2.92	13.53	26.8	9.00	7.52	11.58	5.63	12.67	3.27
TITAN 31	17.02	7.68	10.28	25.7	19.84	-2.08	23.86	6.32	29.68

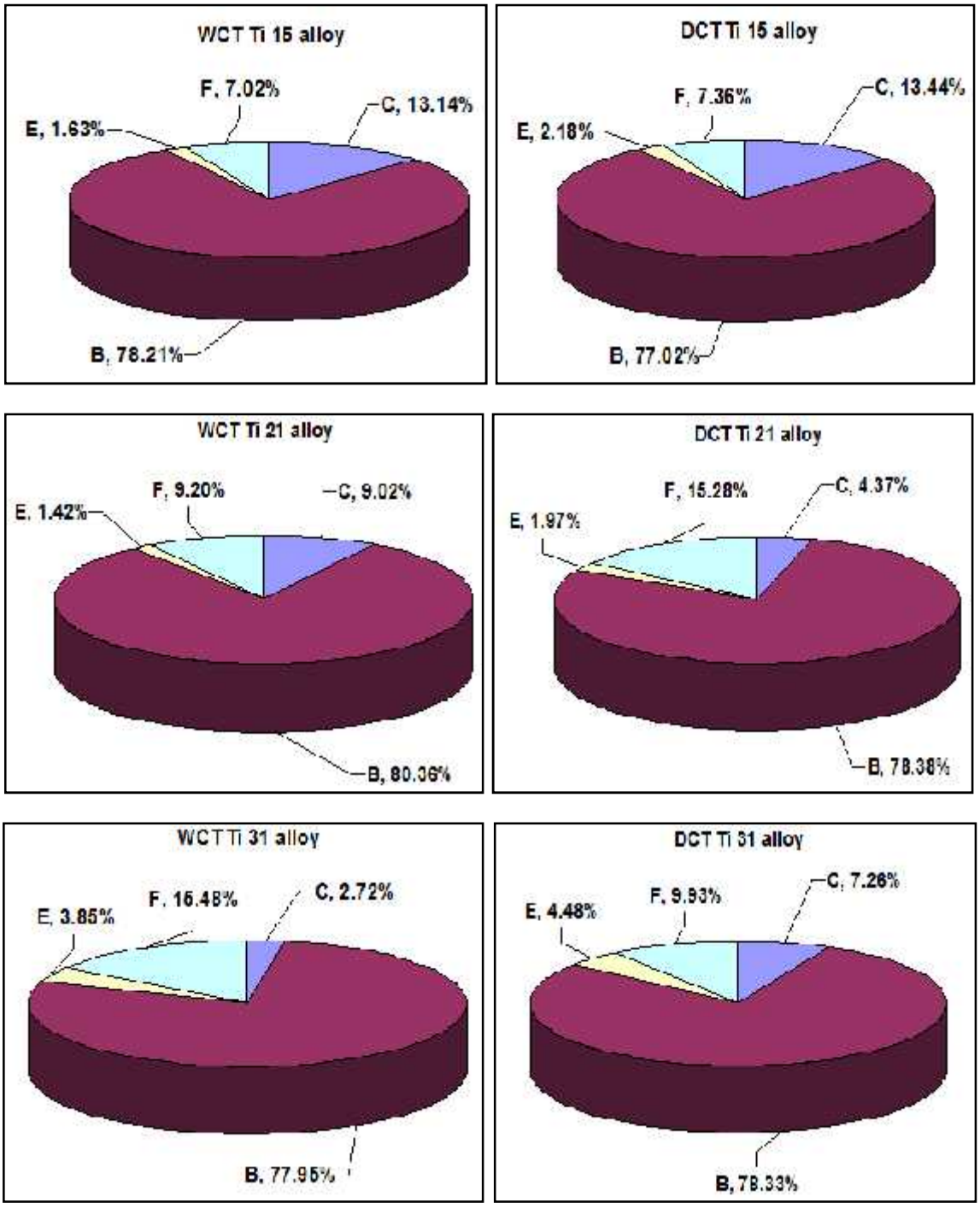

Figure 6.12: Percent Contribution of Control Factors on MRR

The percentage change in MRR (gain/loss) for three materials, namely T1 15, Ti 21 and Ti 31 titanium alloy is presented in graphical form as shown in Figure 6.13. From this Figure it can be clearly seen that significant improvement in MRR was observed after compared the experimental results of the WCT workpiece with DCT workpiece. Figure 6.14 shows the

comparative chart between WCT and DCT titanium alloys drawn based on the observation presented in Table 6.10 to 6.12.

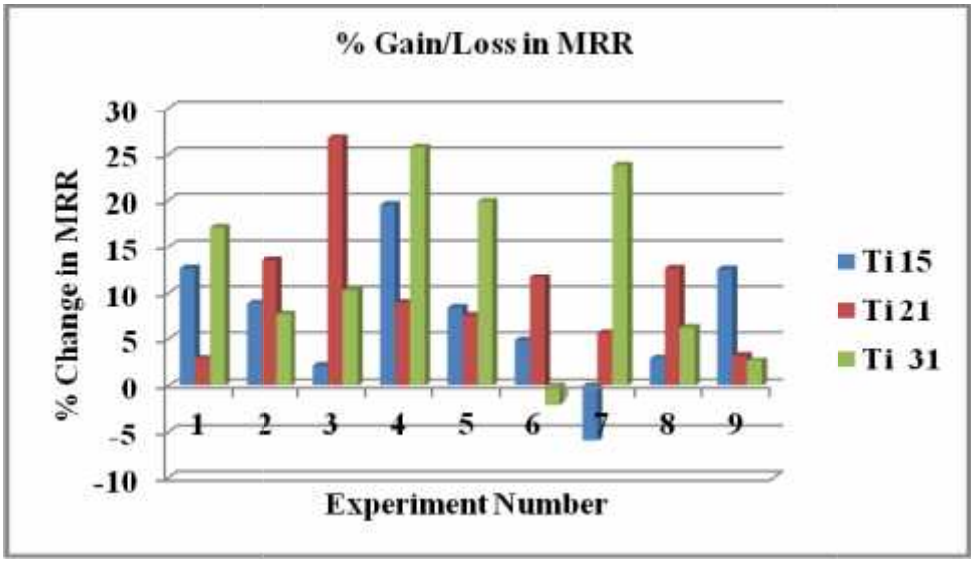

Figure 6.13: %Gain/Loss in MRR

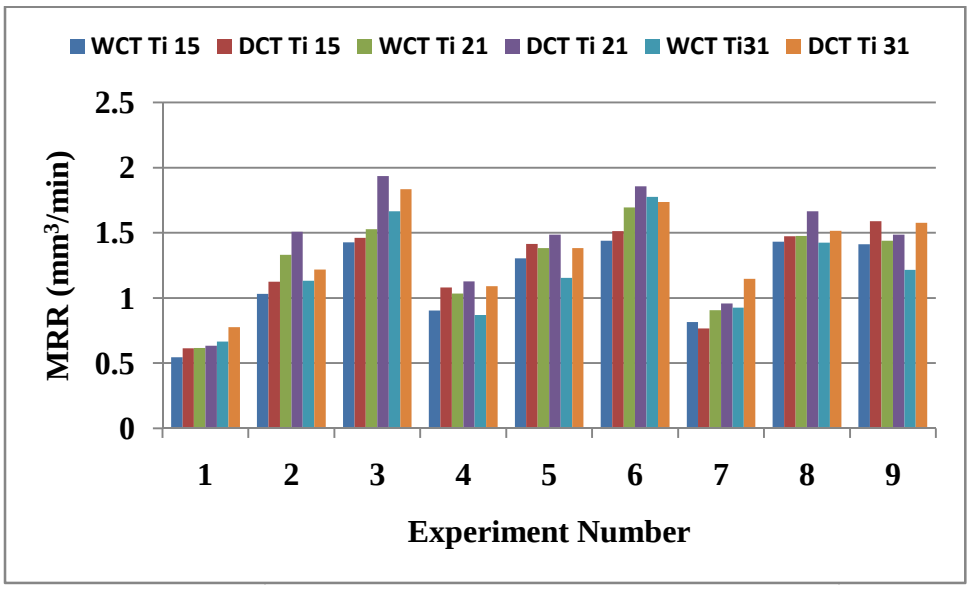

Figure 6.14: MRR comparative chart for WCT and DCT titanium alloys

6.3.2 TOOL WEAR RATE (TWR)

The calculated values of TWR after machining are presented in Table 6.15 to 6.17 for three grades of the WCT and DCT titanium alloys and Figure 6.15 shows the graphical representation of the observed results. Figure 6.15 shows the reduction in TWR in case of DCT alloys as compared to WCT titanium alloys. The main effects plots for S/N ratios of TWR against input parameters are shown in Figures 6.16 to 6.18.

Viewing the contribution of individual process parameter listed in ANOVA presented in Table 6.18, as expected peak current resulted in largest electrode wear rate in the range of 78.46% to 87.65%, followed by the cryogenic treatment of electrode (7.3% to 13.4%). The electrode material and pulse-on-time has little effect on TWR in comparison of other parameters.

It is well known that, in EDM the discharge energy is increased by increasing the amount of I_p and T_{on}. Due to this increased spark energy more metal was removed from the bottom surface of the tool, resulting in higher tool wear. But by observing slope of TWR in Figures 6.16 to 6.18, it can be clearly seen that in the higher range of on-time, less effect on TWR was observed by increasing value of T_{on}, but after 120 µs the trend of curve declines due to the expansion of plasma channel.

Table 6.15: Observation Table for TWR (WCT & DCT Ti 15 Alloy)

Exp. No	TWR (WCT TITAN 15) (mm^3/min)			S/N Ratio (dB)	TWR (DCT TITAN 15) (mm^3/min)			S/N Ratio (dB)
	R1	R2	R3		R1	R2	R3	
1.	0.1156	0.1054	0.1192	18.8962	0.0782	0.0768	0.0805	22.1010
2.	0.2154	0.2342	0.2476	12.6613	0.2162	0.1985	0.2051	13.6920
3.	0.4174	0.3987	0.4097	7.7725	0.3705	0.3585	0.3652	8.7597
4.	0.0746	0.0725	0.0710	22.7675	0.0589	0.0575	0.0595	24.6362
5.	0.3589	0.3675	0.3785	8.6739	0.3895	0.4045	0.3972	8.0217
6.	0.4095	0.4107	0.4124	7.7259	0.3537	0.3472	0.3357	9.2282
7.	0.0478	0.0502	0.0495	26.1648	0.0406	0.0415	0.0427	27.6163
8.	0.1776	0.1682	0.1576	15.4939	0.1245	0.1305	0.1275	17.8882
9.	0.4564	0.4325	0.4267	7.1562	0.4130	0.4176	0.4212	7.5914

Table 6.16: Observation Table for TWR (WCT & DCT Ti 21 Alloy)

Exp. No	TWR (WCT TITAN 21) (mm^3/min)			S/N Ratio (dB)	TWR (DCT TITAN 21) (mm^3/min)			S/N Ratio (dB)
	R1	R2	R3		R1	R2	R3	
1.	0.0835	0.0810	0.0795	21.793	0.056	0.056	0.055	25.087
2.	0.1690	0.1725	0.1805	15.186	0.197	0.187	0.195	14.268
3.	0.4307	0.4202	0.4154	7.491	0.351	0.387	0.367	8.665

4.	0.0393	0.0425	0.0417	27.704	0.024	0.023	0.021	32.754
5.	0.3781	0.3825	0.3745	8.441	0.345	0.321	0.336	9.510
6.	0.5025	0.5125	0.4975	5.948	0.426	0.408	0.416	7.604
7.	0.1125	0.1274	0.1204	18.398	0.067	0.065	0.064	23.629
8.	0.1052	0.0985	0.1107	19.583	0.096	0.093	0.096	20.435
9.	0.5235	0.5247	0.5375	5.537	0.497	0.487	0.475	6.255

Table 6.17: Observation Table for TWR (WCT & DCT Ti 31 Alloy)

Exp. No	TWR (WCT TITAN 31) (mm^3/min)			S/N Ratio (dB)	TWR (DCT TITAN 31) (mm^3/min)			S/N Ratio (dB)
	R1	R2	R3		R1	R2	R3	
1.	0.091	0.089	0.088	20.957	0.077	0.078	0.077	22.214
2.	0.223	0.207	0.215	13.345	0.202	0.213	0.200	13.742
3.	0.345	0.322	0.336	9.511	0.307	0.298	0.316	10.241
4.	0.067	0.065	0.064	23.629	0.044	0.043	0.042	27.248
5.	0.431	0.420	0.415	7.491	0.376	0.365	0.386	8.494
6.	0.456	0.432	0.427	7.156	0.433	0.447	0.436	7.153
7.	0.072	0.070	0.069	23.023	0.056	0.056	0.055	25.108
8.	0.112	0.105	0.110	19.245	0.098	0.098	0.096	20.225
9.	0.502	0.507	0.512	5.895	0.487	0.468	0.472	6.446

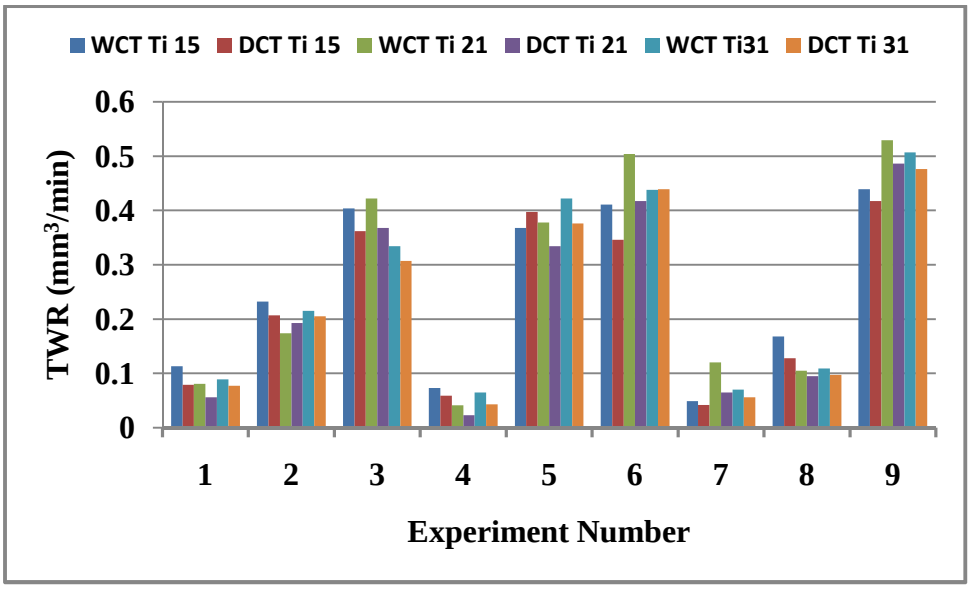

Figure 6.15: TWR comparative chart for WCT and DCT titanium alloys

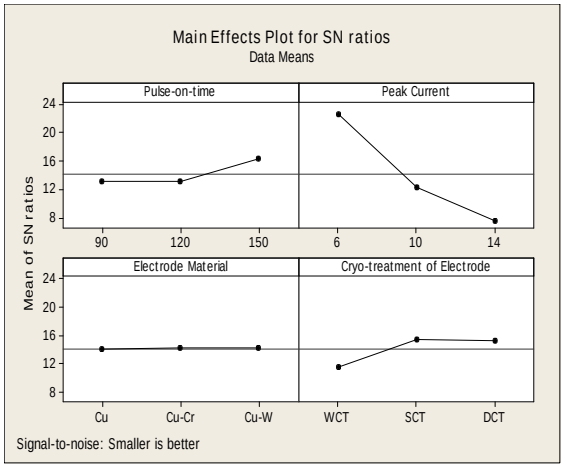

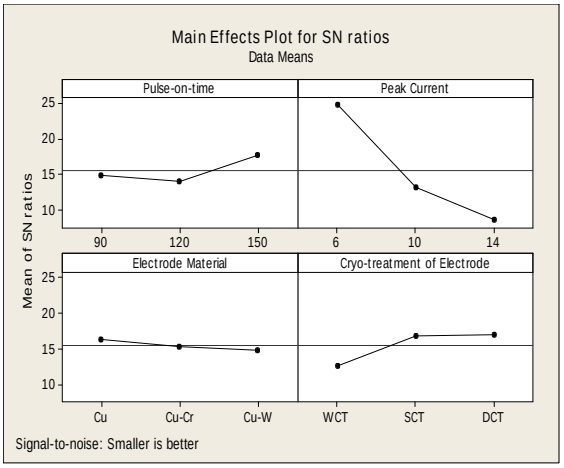

(a- WCT) **(b- DCT)**

Figure 6.16: Main Effect Plots for S/N Ratios of TWR for TITAN 15 Alloys

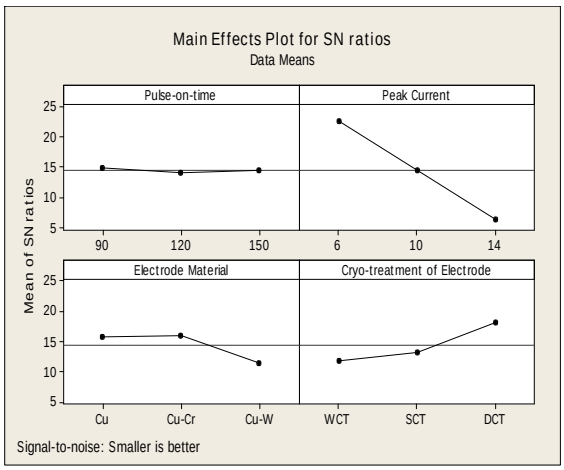

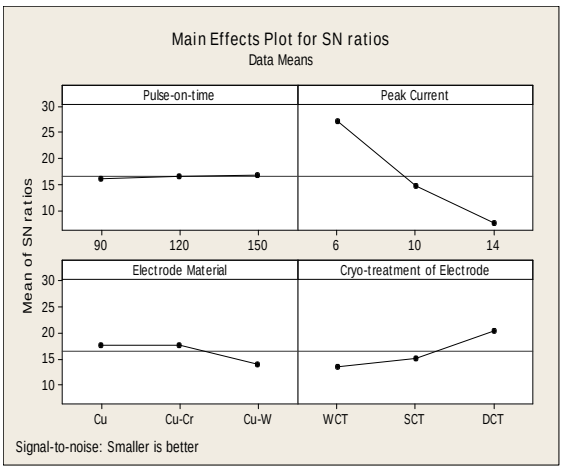

(a- WCT) **(b- DCT)**

Figure 6.17: Main Effect Plots for S/N Ratios of TWR for TITAN 21 Alloys

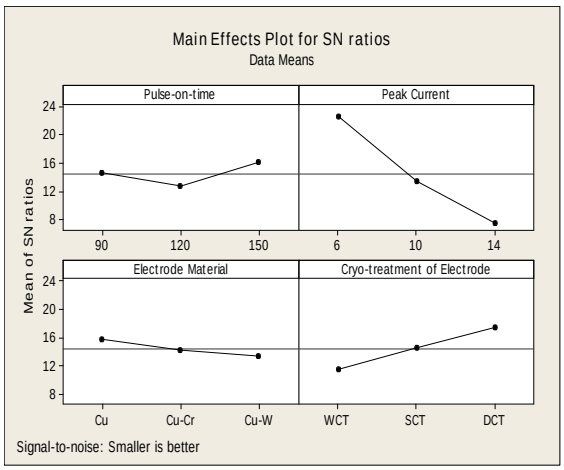

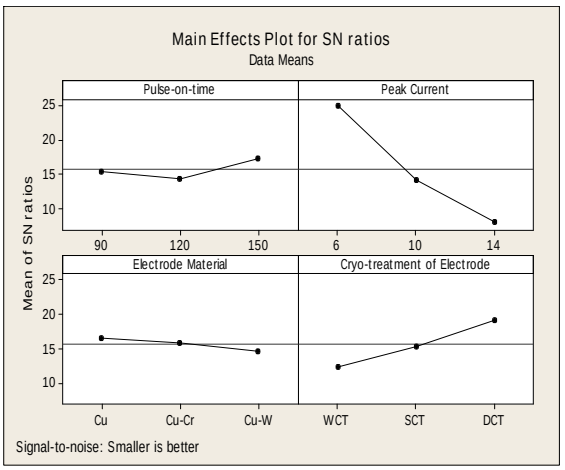

(a- WCT) **(b- DCT)**

Figure 6.18: Main Effect Plots for S/N Ratios of TWR for TITAN 31 Alloys

The S/N response graphs in Figure 6.16 to 6.18 of different WCT and DCT titanium alloys shows that TWR increases upon increasing the value of I_p. It means, low value of I_p, factor (B) was the key factor for low TWR in the EDM process. The mean results of TWR have been compared for different WCT and DCT titanium alloy workpiece and percent change in TWR are listed in Table 6.19 and also plot in graphical form as shown in Figure 6.19.

Table 6.18: ANOVA Results of S/N Data for TWR

Source of Variation	DoF	Without Cryogenic Treated			Deep Cryogenic Treated		
		Seq. SS	Adj. MS	PC (%)	Seq. SS	Adj. MS	PC (%)
TITAN 15 (ASTM grade II, Ti Alloy)							
C	2	20.340	10.170	5.01	22.862	11.431	4.70
B	2	355.839	177.920	87.65	420.358	210.179	86.48
E	2	0.052	0.026	0.01	4.047	2.023	0.84
F	2	29.775	14.888	7.33	38.791	19.395	7.98
Total	8	406.006			486.057		
TITAN 21 (ASTM grade VI, Ti-5Al-2.5Sn Alloy)							
C	2	0.953	0.477	0.20	0.989	0.495	0.15
B	2	398.860	199.430	78.46	592.606	296.303	84.22
E	2	40.976	20.488	8.06	28.873	14.437	4.10
F	2	67.537	33.768	13.28	81.126	40.563	11.53
Total	8	508.326			703.594		
TITAN 31 (ASTM grade V, Ti-6Al-4V Alloy)							
C	2	16.374	8.187	3.87	13.446	6.723	2.54
B	2	343.777	171.187	81.17	439.056	219.528	83.00
E	2	9.117	4.558	2.15	5.623	2.811	1.06
F	2	54.262	27.131	12.81	70.914	35.457	13.4
Total	8	423.530			529.038		

The maximum reduction in TWR was observed 30.77% for TITAN 15, 45.21% for TITAN 21 and 34.05% for TITAN 31. From Figure 6.19, it can be clearly seen that significant reduction or gain in TWR was observed with the DCT workpiece than WCT workpiece. Also, loss or increase in TWR observed for experiment 2 (Ti 21 alloy), experiment 5 (Ti 15 alloy) and experiment 6 (Ti 31 alloy) as shown in Figure 6.19 and Table 6.19.

Table 6.19: Percentage Change in TWR for WCT and DCT Titanium Alloy

Workpiece Material	Experiment Number								
	1	2	3	4	5	6	7	8	9
TITAN 15	30.77	11.1	10.74	19.4	-7.82	15.9	15.45	24.05	4.84
TITAN 21	31.61	-11.15	12.8	44.04	11.74	17.26	45.21	9.26	7.84
TITAN 31	12.85	4.65	7.94	34.05	10.92	-0.076	21.4	10.6	6.11

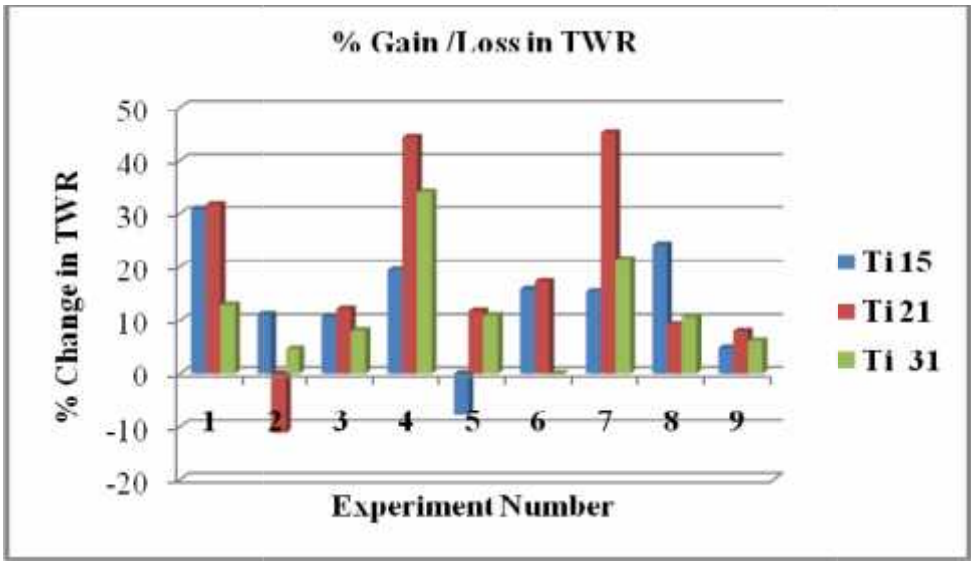

Figure 6.19: % Gain/Loss in TWR

The percent contribution of each process parameter is shown in Figure 6.20 shows the highest effect of peak current. The significant effect of cryo-treatment of the electrode was observed as can be seen in Figure 6.20 and ANOVA Table 6.18. Highest effect of cryo-treatment of electrode material of 13.4% was observed with EDM of DCT Ti-6Al-4V titanium alloy.

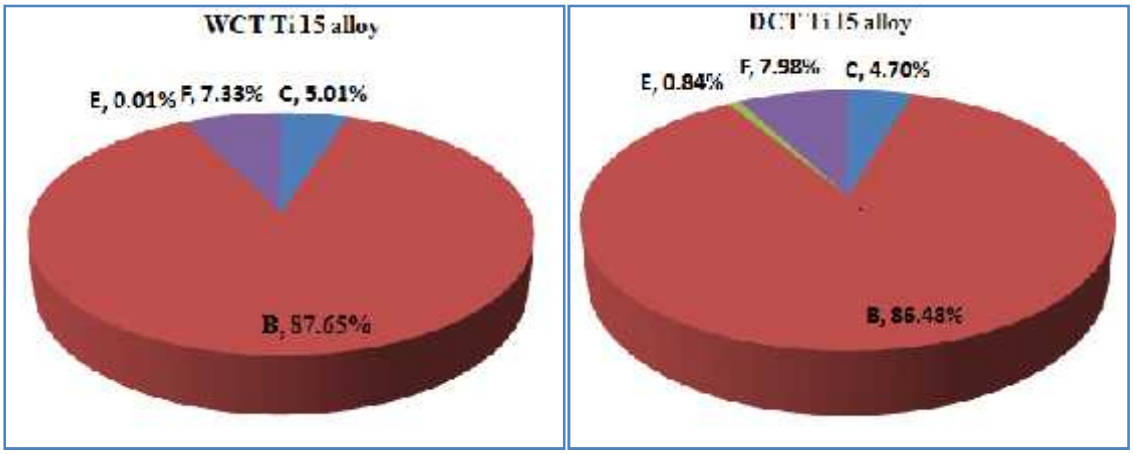

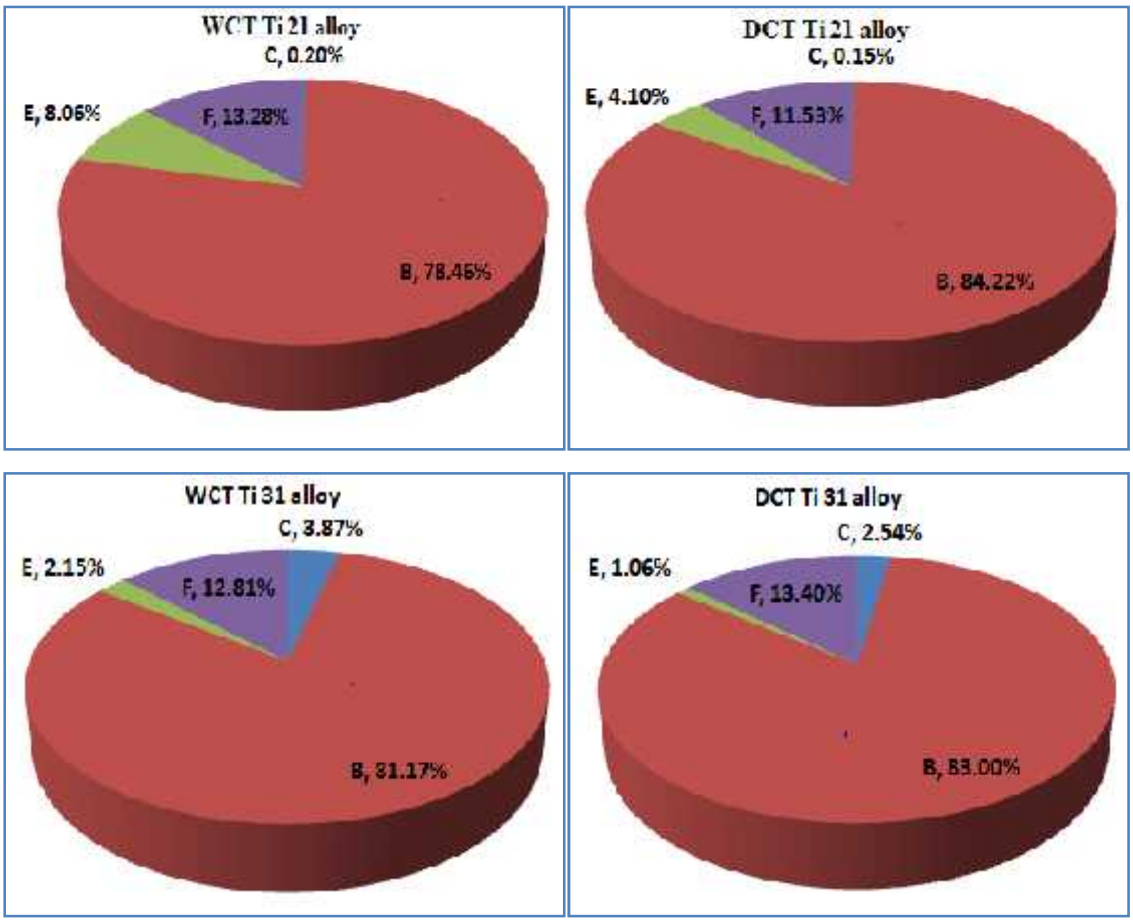

Figure 6.20: Percent Contribution of Control Factors on TWR

6.3.3 SURFACE ROUGHNESS (SR)

The tested values of the SR and their calculated S/N ratios of the machined workpiece samples are given in Table 6.20 to 6.22. ANOVA was performed for all the three grades of the workpiece and the corresponding results are listed in Table 6.23. Figure 6.21 shows the effect of deep cryogenic treatment as compared to WCT titanium alloys on surface roughness. Significant improvement was observed in DCT titanium alloys as compared to untreated alloys. The results of ANOVA table show that peak current followed by DCT of electrode material and T_{on} significantly affect the SR of workpiece samples. Electrode materials show little effect on SR.

Table 6.20: Observation Table for SR (WCT & DCT Ti 15 Alloy)

Exp. No	SR (WCT TITAN 15) (Ra in microns)			S/N Ratio (dB)	SR (DCT TITAN 15) (Ra in microns)			S/N Ratio (dB)
	R1	R2	R3		R1	R2	R3	
1.	3.75	4.45	3.52	-11.880	3.31	3.85	3.15	-10.756

2.	4.91	5.31	4.75	-13.972	3.95	4.25	5.15	-13.024
3.	5.92	5.65	5.63	-15.170	5.54	4.75	4.85	-14.081
4.	3.69	4.12	3.95	-11.874	3.15	3.5	3.92	-10.974
5.	5.69	5.75	5.85	-15.214	5.86	5.62	6.12	-15.373
6.	5.67	5.75	6.25	-15.410	5.52	5.82	5.9	-15.192
7.	4.95	5.05	4.85	-13.893	4.35	4.65	4.65	-13.164
8.	5.15	4.25	4.52	-13.359	4.5	4.65	4.15	-12.944
9.	8.35	7.35	8.75	-18.246	6.5	7.15	6.95	-16.742

Table 6.21: Observation Table for SR (WCT & DCT Ti 21 Alloy)

Exp. No	SR (WCT TITAN 21) (Ra in microns)			S/N Ratio (dB)	SR (DCT TITAN 21) (Ra in microns)			S/N Ratio (dB)
	R1	R2	R3		R1	R2	R3	
1.	4.05	4.35	4.62	-12.762	3.62	4.2	3.85	-11.815
2.	4.32	4.86	4.46	-13.165	4.12	3.92	4.26	-12.261
3.	4.85	4.35	4.95	-13.486	4.45	4.15	4.75	-12.980
4.	4.02	3.2	4.2	-11.667	3.25	3.05	3.52	-10.315
5.	5.45	6.02	5.67	-15.145	4.95	5.22	5.1	-14.136
6.	5.92	6.57	6.15	-15.875	6.25	6.75	6.02	-16.052
7.	4.1	4.07	4.24	-12.334	3.65	4.15	4.07	-11.959
8.	5.02	4.87	5.45	-14.184	4.25	5.07	4.75	-13.446
9.	8.95	8.5	7.92	-18.555	8.5	6.83	7.85	-17.794

Table 6.22: Observation Table for SR (WCT & DCT Ti 31 Alloy)

Exp. No	SR (WCT TITAN 31) (Ra in microns)			S/N Ratio (dB)	SR (DCT TITAN 31) (Ra in microns)			S/N Ratio (dB)
	R1	R2	R3		R1	R2	R3	
1.	4.00	4.35	3.75	-12.129	3.55	3.13	3.45	-10.582
2.	4.60	4.15	4.45	-12.877	3.68	3.85	3.56	-11.361
3.	5.25	6.25	5.10	-14.896	4.25	5.22	4.75	-13.546
4.	3.75	3.62	4.05	-11.621	3.42	3.30	3.65	-10.781
5.	4.85	4.90	5.10	-13.894	5.15	4.68	4.70	-13.712
6.	5.75	6.25	5.95	-15.544	5.12	5.72	5.24	-14.593
7.	4.35	4.25	4.55	-12.839	3.52	3.95	4.05	-11.702

8.	4.45	4.75	4.55	-13.227	4.12	4.25	4.35	-12.549
9.	8.05	8.52	7.95	-18.252	7.85	6.85	8.15	-17.658

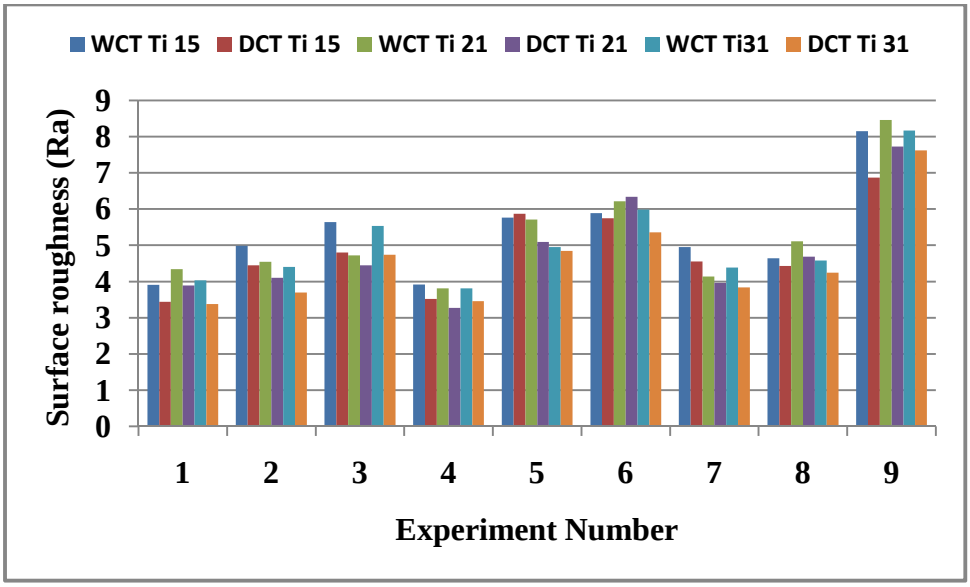

Figure 6.21: SR comparative chart for WCT and DCT titanium alloys

Table 6.23: ANOVA Results of S/N Data for Surface Roughness

Source of Variation	DoF	Without Cryogenic Treated			Deep Cryogenic Treated		
		Seq. SS	Adj. MS	PC (%)	Seq. SS	Adj. MS	PC (%)
TITAN 15 (ASTM grade II, Ti Alloy)							
C	2	3.467	1.733	11.08	4.461	2.230	14.06
B	2	20.933	10.467	66.92	20.788	10.394	65.54
E	2	2.783	1.391	8.90	2.315	1.157	7.30
F	2	4.097	2.049	13.10	4.154	2.077	13.10
Total	8	31.280			31.718		
TITAN 21 (ASTM grade VI, Ti-5Al-2.5Sn Alloy)							
C	2	5.383	2.692	14.88	6.322	3.161	14.90
B	2	20.732	10.366	57.34	27.119	13.559	63.65
E	2	1.069	0.535	2.95	0.840	0.420	1.97
F	2	8.978	4.489	24.83	8.178	4.089	19.48
Total	8	36.161			42.459		
TITAN 31 (ASTM grade V, Ti-6Al-4V Alloy)							
C	2	3.495	1.748	10.40	6.906	3.453	17.10

B	2	25.966	12.983	77.30	27.748	13.874	68.75
E	2	0.578	0.289	1.72	0.726	0.363	1.80
F	2	3.547	1.773	10.58	4.981	2.490	12.35
Total	8	33.587			40.360		

The S/N response plots in Figures 6.22 to 6.24 (a-WCT and b-DCT) shows that SR increases with increase in I_p and T_{on}. From Figures 6.22 to 6.24 (a, b) for Ti 15 and Ti 31 alloy it was observed that DCT Cu electrodes improved the surface finish, whereas DCT Cu-W electrode showed better surface finish for WCT and DCT Ti 21 alloy. The plots indicate that a better surface finish is obtained with low I_p, smaller T_{on} and DCT of electrode material as it comes low power erosion. In other words, EDM with low I_p, shorter T_{on} and DCT electrode material is removed material from surface in smaller size of craters, thereby improving the surface finish.

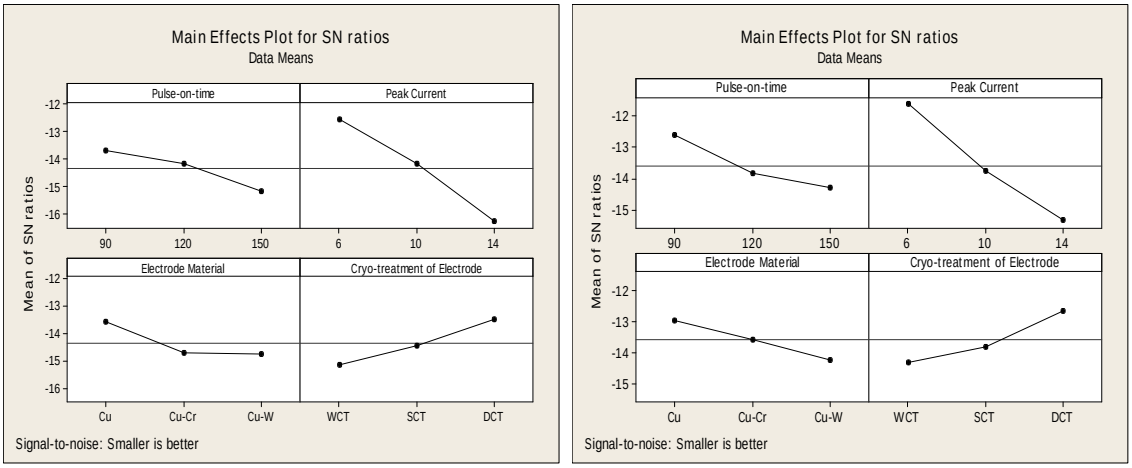

(a- WCT) **(b- DCT)**

Figure 6.22: Main Effect Plots for S/N Ratios of SR for TITAN 15 Alloys

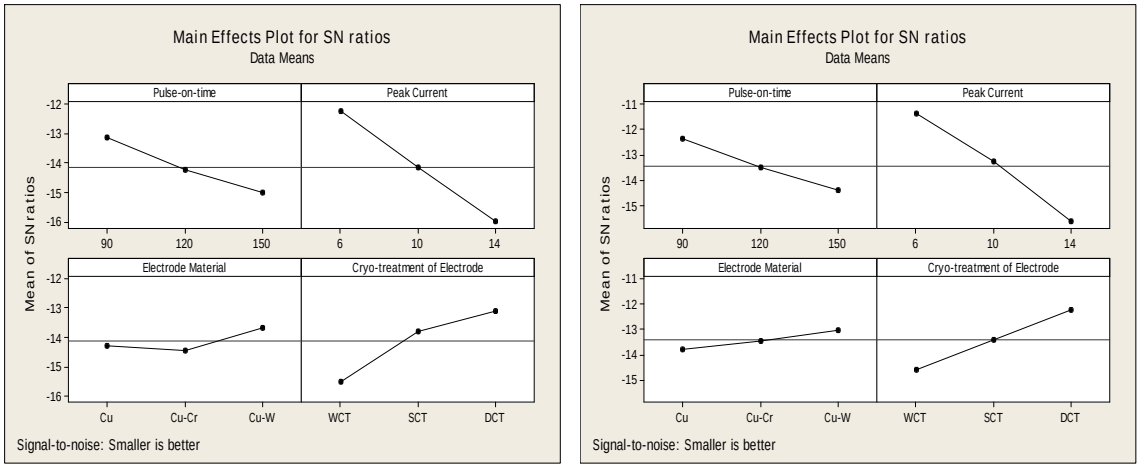

(a- WCT) **(b- DCT)**

Figure 6.23: Main Effect Plots for S/N Ratios of SR for TITAN 21 Alloys

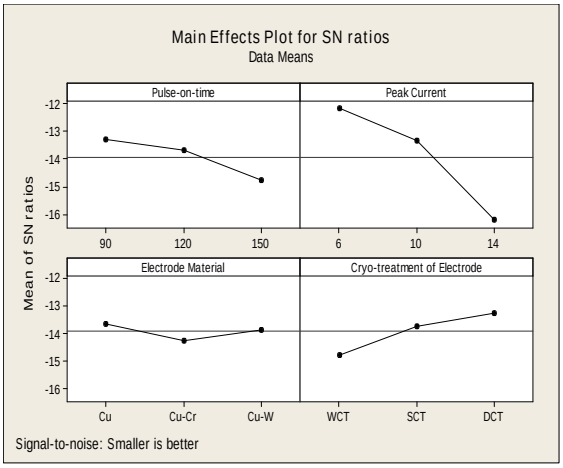

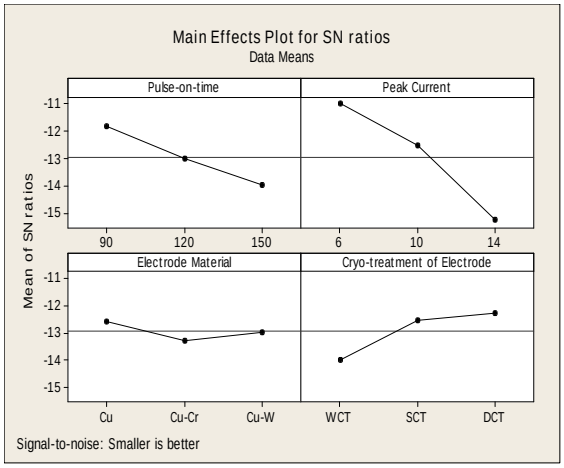

(a- WCT) **(b- DCT)**

Figure 6.24: Main Effect Plots for S/N Ratios of SR for TITAN 31 Alloys

From Table 6.24, the maximum improvement of 16.40% in SR was observed for trial number 1 for DCT Ti-6Al-4V alloy. Surface finish deteriorated marginally for trial number 6 for DCT Ti-5Al-2.5Sn alloy. Based on the factor contributions, graph was plotted which shows how the selected factors affected the SR of various workpiece samples are shown in Figure 6.25.

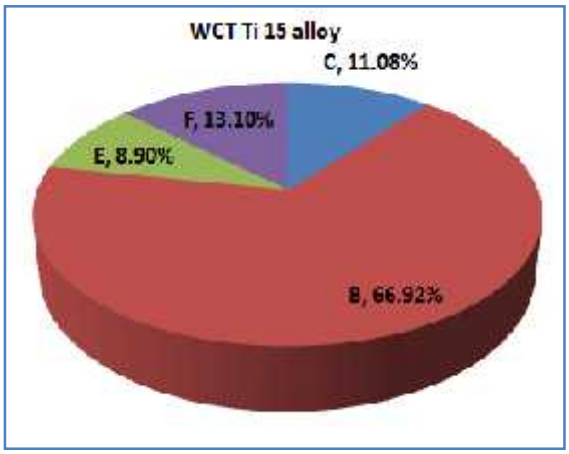

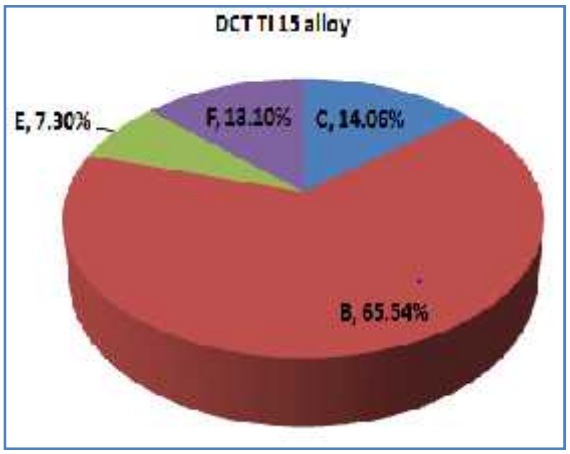

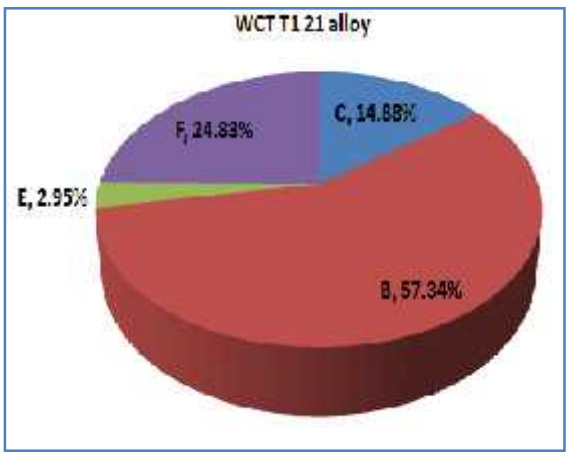

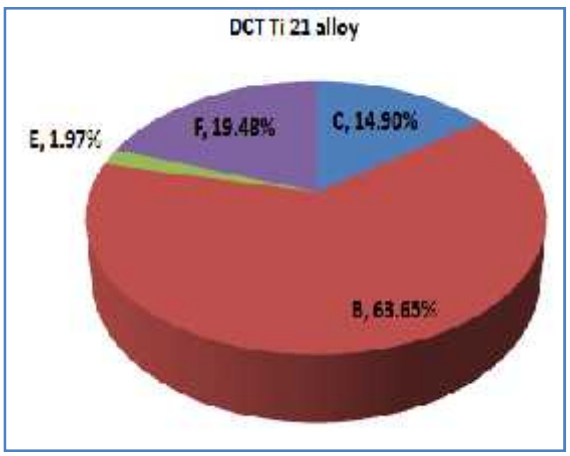

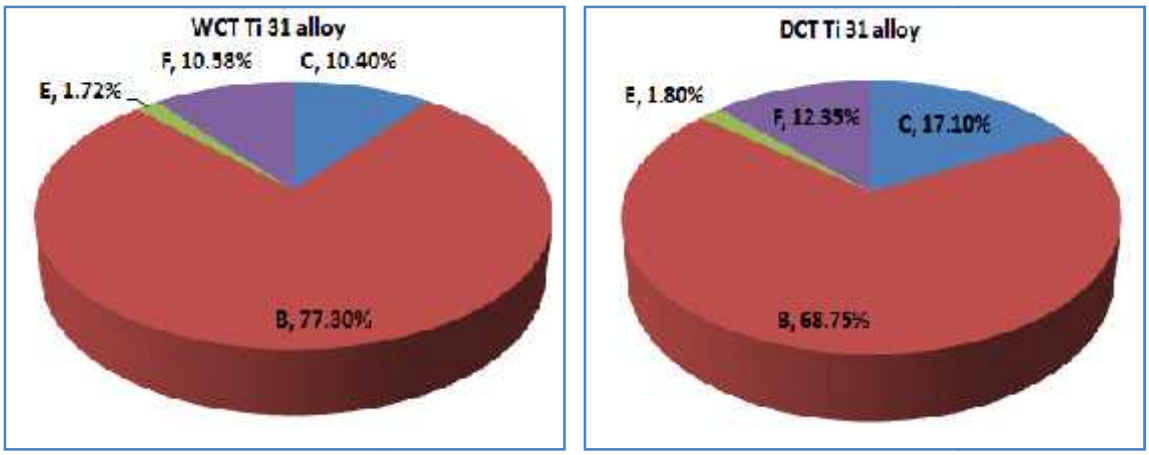

Figure 6.25: Percent Contribution of Control Factors on SR

Table 6.24: Percentage Change in SR for WCT and DCT Titanium Alloys

Workpiece Material	Experiment Number								
	1	2	3	4	5	6	7	8	9
TITAN 15	12.30	10.82	12.04	10.20	-1.74	2.54	8.10	4.52	15.82
TITAN 21	10.37	9.90	5.72	14.17	10.85	-2.10	4.35	8.22	8.65
TITAN 31	16.40	16.00	14.28	9.20	2.22	10.36	12.33	7.42	6.85

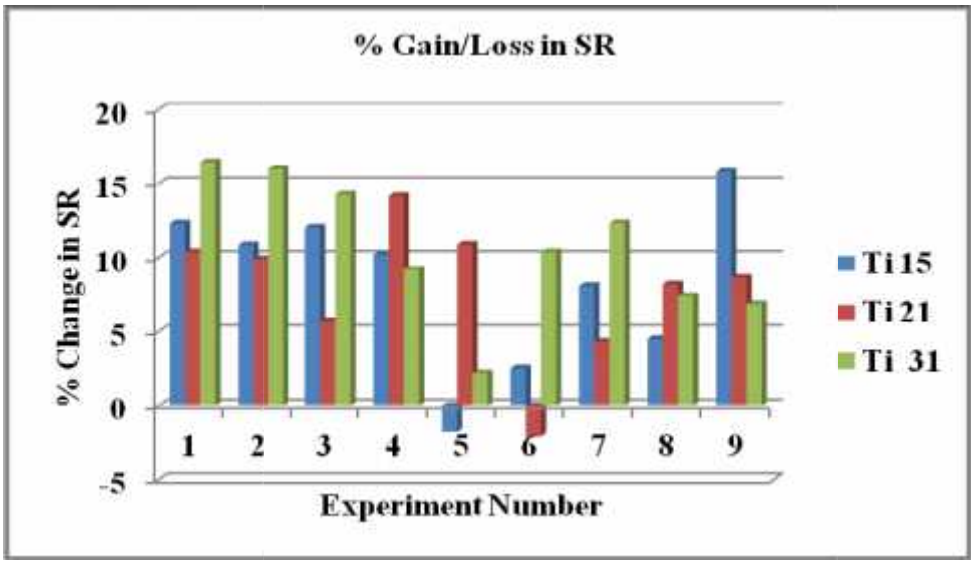

Figure 6.26: % Gain/Loss in Surface Roughness

The percentage change in SR (gain/loss) is shown in Figure 6.26, which shows significant reduction or gain in SR in case of DCT workpiece than WCT workpiece. Also, loss or increase in SR was observed for experiment 5 (Ti 15 alloy) and experiment 6 (Ti 21 alloy) as shown in Figure 6.26 and Table 6.24.

6.3.4 Micro-hardness (MH)

The micro-hardness of three grades of WCT and DCT titanium alloys for each of the nine trials with two repetitions is listed in Tables 6.25 to 6.27. The ANOVA based on the "*larger the better*" response characteristic was completed using Minitab 16 and is tabulated in Table 6.28. As expected, I_p and T_{on} were observed to be the key factors affecting micro-hardness. Also, electrode material and their cryogenic treatment were observed to be other significant factors.

Table 6.25: Observation Table for MH (WCT & DCT Ti 15 Alloy)

Exp. No	MH (WCT TITAN 15) (HVN)			S/N Ratio (dB)	MH (DCT TITAN 15) (HVN)			S/N Ratio (dB)
	R1	R2	R3		R1	R2	R3	
1.	350	335	315	50.434	365	345	392	51.266
2.	435	480	468	53.252	462	496	470	53.540
3.	564	505	492	54.281	570	590	586	55.295
4.	410	432	445	52.634	402	445	452	52.694
5.	486	465	495	53.652	470	524	500	53.919
6.	545	575	564	54.978	535	542	510	54.460
7.	455	474	440	53.174	472	485	465	53.512
8.	505	495	542	54.199	595	557	580	55.219
9.	535	545	490	54.348	545	520	568	54.700

Table 6.26: Observation Table for MH (WCT & DCT Ti 21 Alloy)

Exp. No	MH (WCT TITAN 21) (HVN)			S/N Ratio (dB)	MH (DCT TITAN 21) (HVN)			S/N Ratio (dB)
	R1	R2	R3		R1	R2	R3	
1.	402	375	390	51.788	412	394	436	52.318
2.	438	470	445	53.072	464	472	484	53.499
3.	592	580	602	55.434	620	615	590	55.677
4.	430	425	445	52.732	442	478	458	53.229
5.	502	515	532	54.251	562	570	584	55.145

6.	520	502	572	54.468	585	610	578	55.425
7.	482	474	454	53.434	470	488	494	53.691
8.	542	592	580	55.119	610	602	595	55.596
9.	535	584	562	54.952	590	565	570	55.188

Table 6.27: Observation Table for MH (WCT & DCT Ti 31 Alloy)

Exp. No	MH (WCT TITAN 31) (HVN)			S/N Ratio	MH (DCT TITAN 31) (HVN)			S/N Ratio
	R1	R2	R3	(dB)	R1	R2	R3	(dB)
1.	400	390	406	52.009	380	408	385	51.832
2.	480	492	475	53.664	502	520	536	54.299
3.	590	605	580	55.438	602	632	612	55.777
4.	464	456	475	53.345	480	495	472	53.661
5.	549	552	590	55.007	565	576	592	55.229
6.	562	585	602	55.303	588	605	610	55.574
7.	487	472	480	53.617	482	487	524	53.921
8.	576	602	588	55.393	580	615	600	55.531
9.	625	592	602	55.647	631	620	604	55.820

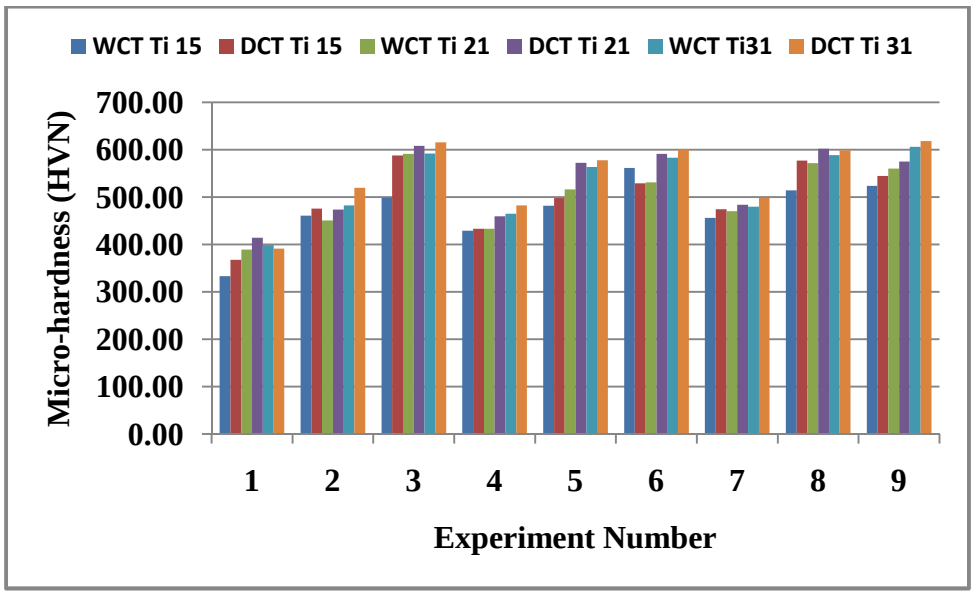

Figure 6.27: MH comparative chart for WCT and DCT titanium alloys

Figure 6.27 shows the effect of deep cryogenic treatment as compared to WCT titanium alloys on micro-hardness. Significant increase in micro-hardness was observed in DCT titanium alloys as compared to untreated alloys.

The plot of main effects for S/N ratios for the control factors of the WCT and DCT workpiece are shown in Figures 6.28 to 6.30. The micro-hardness of work samples increases with increase in value of I_p followed by T_{on}. From the ANOVA results and main effects plot (refer Figure 6.28 to 6.30); it was observed that DCT copper-tungsten electrode also contributes in higher micro-hardness. Therefore, from the results it was concluded that the highest micro-hardness was observed when the three grades of titanium alloy work samples were machined with I_p 14A, T_{on} 150µs and DCT Cu-W electrode.

Table 6.28: ANOVA Results of S/N Data for Micro-hardness

Source of Variation	DoF	Without Cryogenic Treated			Deep Cryogenic Treated		
		Seq. SS	Adj. MS	PC (%)	Seq. SS	Adj. MS	PC (%)
TITAN 15 (ASTM grade II, Ti Alloy)							
C	2	2.800	1.400	19.56	1.954	0.977	14.70
B	2	9.349	4.675	65.32	8.783	4.392	66.10
E	2	0.3761	0.188	2.63	0.709	0.354	5.33
F	2	1.789	0.894	12.49	1.842	0.921	13.87
Total	8	14.314			13.288		
TITAN 21 (ASTM grade VI, Ti-5Al-2.5Sn Alloy)							
C	2	1.763	0.882	14.55	1.629	0.814	13.24
B	2	8.175	4.088	67.47	8.773	4.386	71.32
E	2	1.001	0.500	8.26	1.126	0.563	9.15
F	2	1.177	0.589	9.72	0.776	0.388	6.29
Total	8	12.116			12.303		
TITAN 31 (ASTM grade V, Ti-6Al-4V Alloy)							
C	2	2.229	1.115	17.44	2.057	1.028	14.53
B	2	9.596	4.798	75.08	10.723	5.362	75.61
E	2	0.424	0.212	3.32	0.665	0.332	4.75
F	2	0.537	0.268	4.16	0.732	0.366	5.11
Total	8	12.785			14.178		

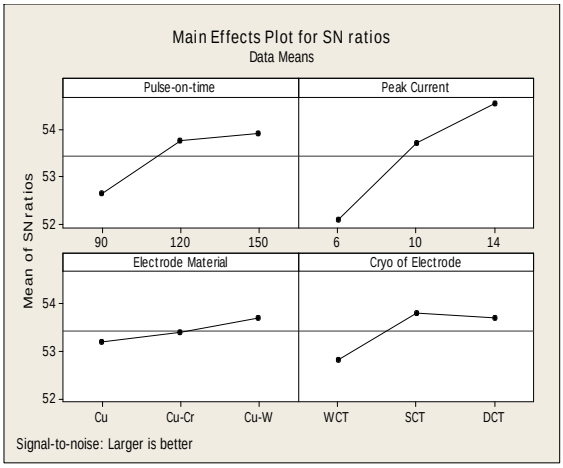

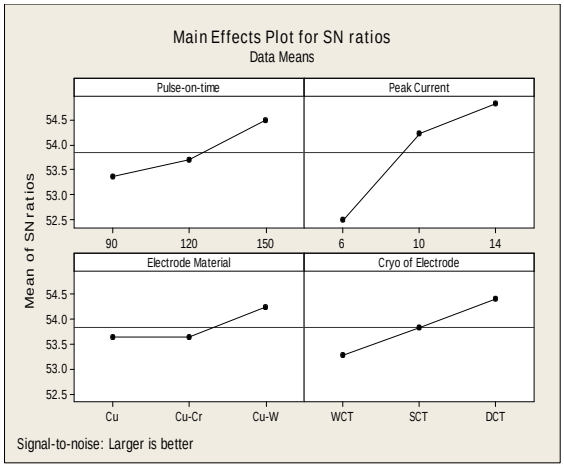

(a- WCT) **(b- DCT)**

Figure 6.28: Main Effect Plots for S/N Ratios of MH for TITAN 15 Alloys

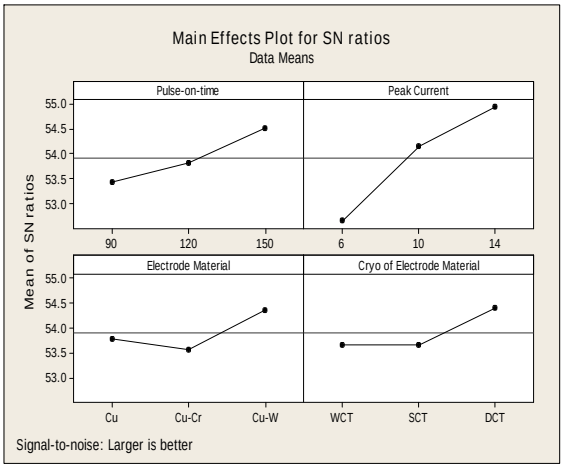

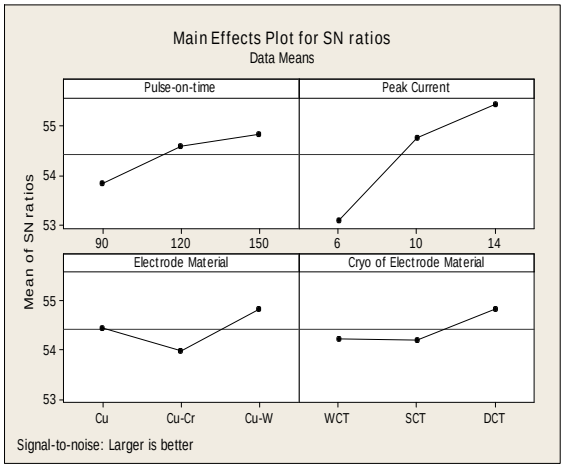

(a- WCT) **(b- DCT)**

Figure 6.29: Main Effect Plots for S/N Ratios of MH for TITAN 21 Alloys

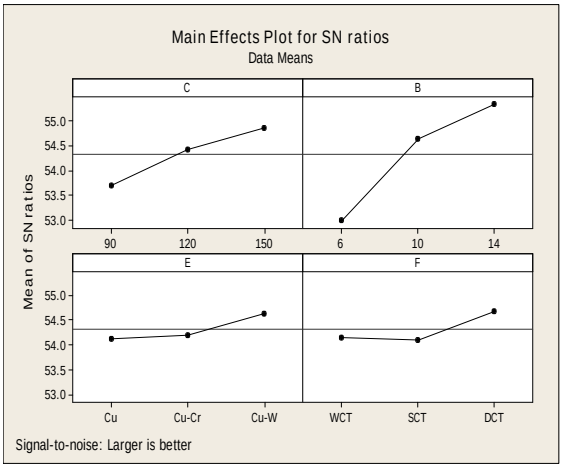

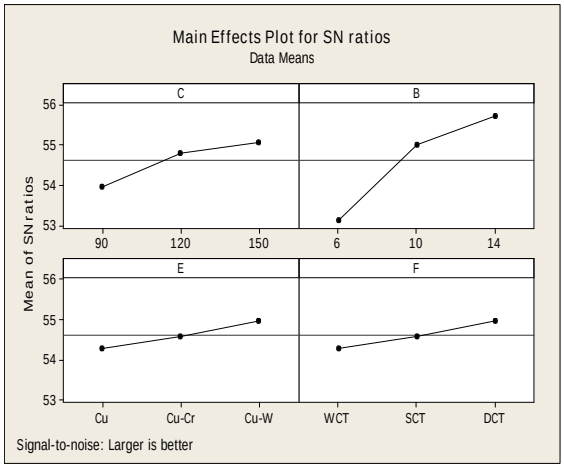

(a- WCT) **(b- DCT)**

Figure 6.30: Main Effect Plots for S/N Ratios of MH for TITAN 31 Alloys

As compared to micro-hardness of base material of the WCT and DCT titanium alloys as indicated in Table 6.29, significant improvement in MH of 68.85% to 107.78% was observed in samples machined using Mn powder mixed with dielectric fluid. The maximum hardness 618HVN was observed for DCT Ti-6Al-4V alloy. The comparative values of percentage change in micro-hardness of Ti 15, Ti 21 and Ti 31 alloy are listed in Table 6.30. The maximum percent gain 11.24% for Ti 21 alloy, 12.32% for Ti 15 alloy and 7.68% for Ti 31 was observed. The percent contribution of each control factors on the micro-hardness is shown in Figure 6.31. Peak current had the most effect on the micro-hardness, followed by pulse-on-time.

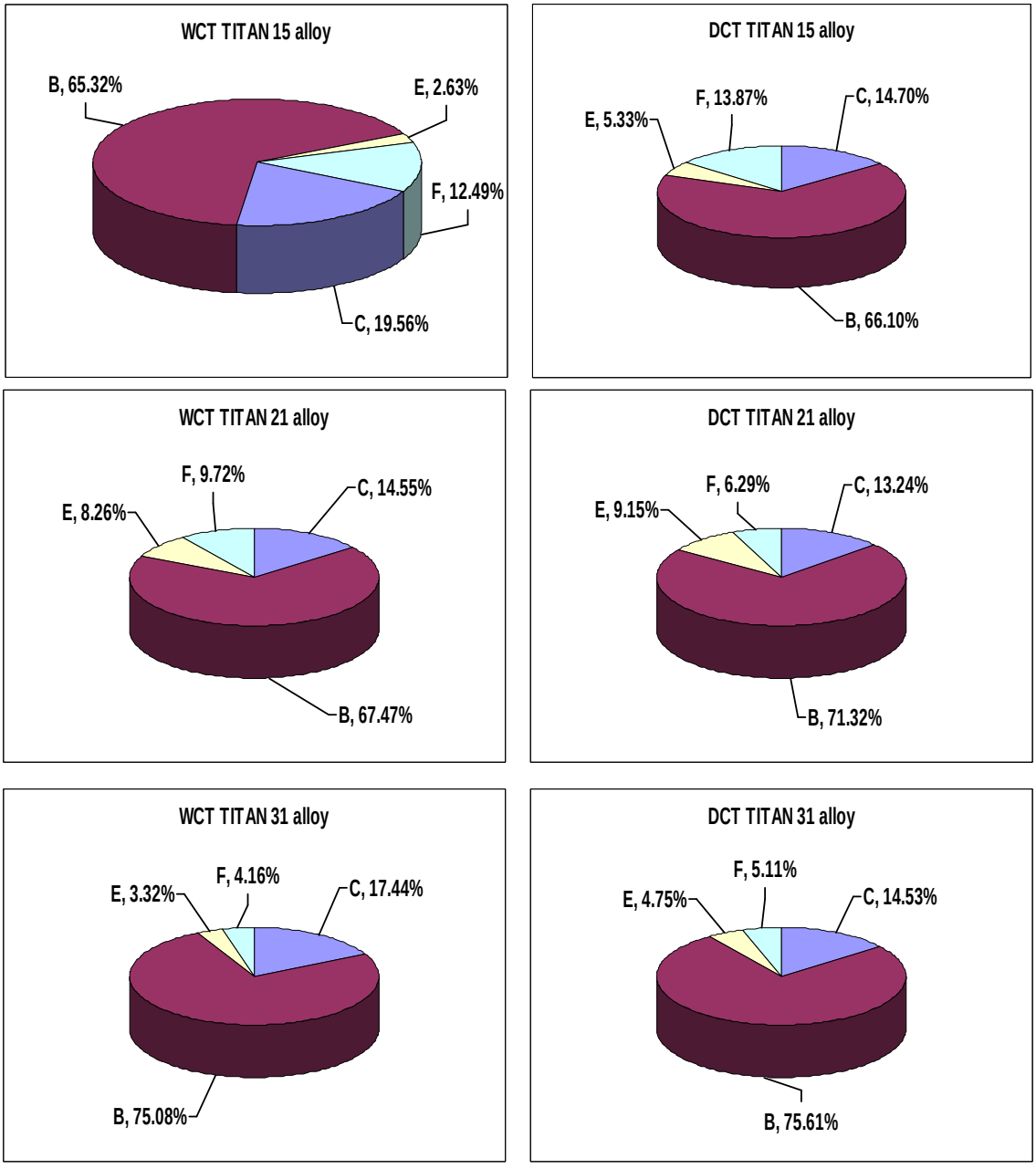

Figure 6.31: Percent Contribution of Control Factors on Micro-hardness

Table 6.29: Micro-hardness of WCT and DCT Titanium Alloys Specimen

Micro-hardness	TITAN 15		TITAN 21		TITAN 31	
(HVN)	WCT	DCT	WCT	DCT	WCT	DCT
Before EDM	270	287	305	320	315	366
After PMEDM	561	582	591	608	606	618
Improvement (%)	107.78	102.78	93.77	90.00	92.38	68.85

Table 6.30: Percentage Change in MH for WCT and DCT Titanium Alloys

Workpiece	Experiment Number								
Material	1	2	3	4	5	6	7	8	9
TITAN 15	10.21	3.25	11.85	0.93	3.32	-5.75	3.95	12.32	4.05
TITAN 21	6.43	4.95	2.88	6.00	10.08	11.24	2.98	5.43	2.62
TITAN 31	-1.92	7.68	4.00	3.65	2.48	3.08	3.75	1.70	1.98

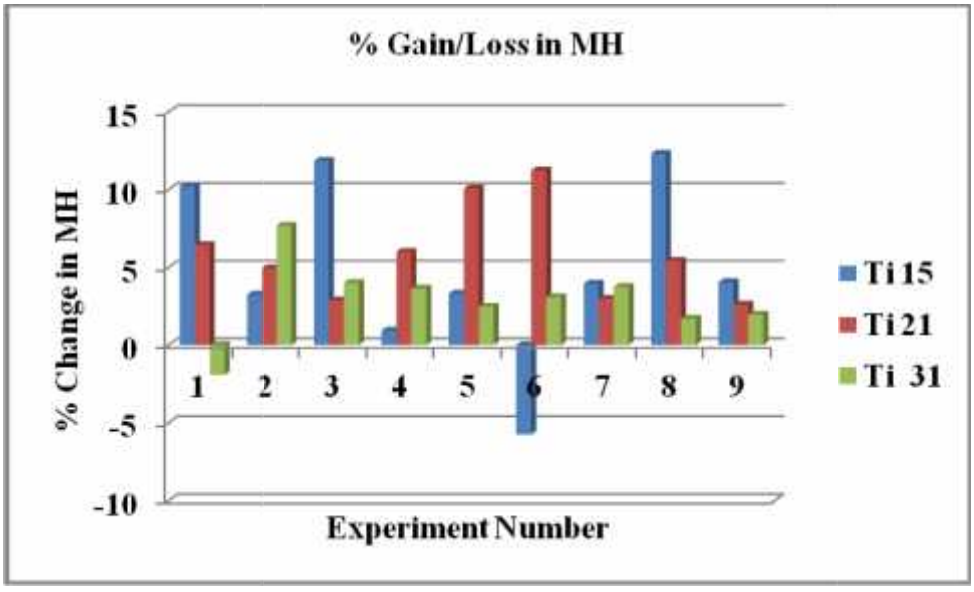

Figure 6.32: % Gain/Loss in Surface Roughness

The percentage changes in MH (gain/loss) are shown in Figure 6.32, which shows significant gain in MH in case of DCT workpiece than WCT workpiece. Also, loss in MH was observed during experiment 1 (Ti 31 alloy) and experiment 6 (Ti 15 alloy) and is shown in Figure 6.32 and Table 6.30.

6.4 GREY RELATIONAL ANALYSIS (GRA): A MULTIPLE OPTIMIZATION CASE STUDY

GRA technique can be effectively used to optimize the multiple performance characteristics. In GRA, the systems which have a lack of information are referred to as grey system. This study uses GRA to establish Grey Relational Grade (GRG) which is a ranking scheme that ranks the order of the grey relationship among dependent and independent factors [142-143].

For multi-response optimization, MRR, TWR, SR and MH were considered as the response parameters. The objective is to maximize the MRR and MH; while minimizing TWR and SR. In other words, multi optimization of response parameters is entirely different from single optimization of response. Here, it is not possible that the higher S/N ratio for one output may correspond to higher for the other response parameter; it may be lower for another response. For this reason, evaluation of the S/N ratio of all the response parameters is required. Thus, the GRA approach for multi response optimization has been applied [26].

In this study, MRR and MH are considered as "*higher-the-better*" quality characteristics, whereas TWR and SR are "*lower-the-better*" type characteristics. Therefore, improvement in one response may lead to degradation of other response. By applying GRA theory with Taguchi method, multiple optimization type of problem can be efficiently solved [54,142-143].

During the study, if the expectation is *larger-the-better* (e.g., MRR and MH), it can be expressed by equation (6.2):

$$x_i^*(k) = \frac{x_i^0(k) - \min x_i^0(k)}{\max x_i^0(k) - \min x_i^0(k)} \tag{6.2}$$

If the expectation is *smaller-the-better* (e.g., TWR and SR), it can be expressed by equation (6.3):

$$x_i^*(k) = \frac{\max x_i^0(k) - x_i^0(k)}{\max x_i^0(k) - \min x_i^0(k)} \tag{6.3}$$

Where

$x_i^*(k)$ is the value after grey relational generation

$\min x_i^0(k)$ is the smallest value of $x_i^0(k)$;

$\max x_i^0(k)$ is the largest value of $x_i^0(k)$.

The grey relational coefficient [$¶_i(k)$] can be calculated by using following equation (6.4):

$$¶_i(k) = \frac{\Delta_{\min} + s\Delta_{\max}}{\Delta_{0i}(k) + s\Delta_{\max}} \quad (6.4)$$

Where

$x_i^*(k)$ denotes the reference sequence;

$x_j^*(k)$ denotes the comparability sequence;

$s \in [0-1]$ is the distinguishing coefficient, 0.5 is widely accepted;

$\Delta_{0i} = \left\| x_0^*(k) - x_i^*(k) \right\|$ is the difference in absolute value between $x_0^*(k)$ and $x_i^*(k)$;

$\Delta_{\min} = \min_{\forall j \in i} \min_{\forall k} \left\| x_0^*(k) - x_j^*(k) \right\|$ is the smallest value of Δ_{0i};

$\Delta_{\max} = \max_{\forall j \in i} \max_{\forall k} \left\| x_0^*(k) - x_j^*(k) \right\|$ is the largest value of Δ_{0i}.

6.4.1 MULTI RESPONSE OPTIMIZATION USING GRA FOR WCT TITAN 15 ALLOY

The steps followed in GRA are as given below:

STEP-1: From the original results, the values of S/N ratios were determined for quality characteristics. The calculated S/N ratios for different responses are listed in Table 6.31. The maximum value, minimum value and the difference between maximum and minimum were calculated.

STEP-2: In this step, normalization of the data sequence in the range between zero and one was performed by using data preprocessing methodology. The normalized value for MRR/MH and TWR/SR were calculated using equation (6.2) and (6.3) respectively. The normalized S/N data are summarized in the first half of Table 6.32.

STEP-3: In this step, the deviation sequence was calculated by subtracting respective normalized value from one, and is listed in the second half of Table 6.32.

STEP-4: In this step, the grey relational coefficient was determined using equation (6.4). The calculated grey relational coefficient is summarized in Table 6.33 for each response.

Table 6.31 Signal-to-noise Ratios of Response Values (WCT Ti 15 Alloy)

Experiment Number	S/N ratios (dB)			
	MRR	TWR	SR	MH
1.	-5.2846	18.8962	-11.8804	50.4332
2.	0.2429	12.6613	-13.9717	53.2512
3.	3.0800	7.7725	-15.1705	54.2806
4.	-0.8745	22.7675	-11.8745	52.6342
5.	2.3140	8.6739	-15.2140	53.6519
6.	3.1686	7.7259	-15.4105	54.9780
7.	-1.7782	26.1648	-13.8933	53.1736
8.	3.1161	15.4939	-13.3589	54.1997
9.	2.9949	7.1562	-18.2458	54.3473
Maximum	3.1686	26.1648	-11.8745	54.9780
Minimum	-5.2846	7.1562	-18.2458	50.4332
Difference	8.4532	19.0085	6.3713	4.5448

Table 6.32: Normalization and Deviation Sequence of S/N Ratio (WCT Ti 15 Alloy)

Exp. No.	Normalized S/N ratio				Deviation Sequence			
	MRR	TWR	SR	MH	MRR	TWR	SR	MH
1.	0.0000	0.3823	0.0009	0.0000	1.0000	0.6171	0.9991	1.0000
2.	0.6539	0.7104	0.3292	0.6200	0.3461	0.2896	0.6708	0.3800
3.	0.9895	0.9676	0.5173	0.8465	0.0105	0.0324	0.4827	0.1535
4.	0.5217	0.1787	0.0000	0.4843	0.4783	0.8213	1.0000	0.5157
5.	0.8989	0.9202	0.5241	0.7082	0.1011	0.0798	0.4759	0.2918
6.	1.0000	0.9700	0.5550	1.0000	0.0000	0.0300	0.4450	0.0000
7.	0.4148	0.0000	0.3168	0.6030	0.5852	1.0000	0.6832	0.3970
8.	0.9938	0.5614	0.2330	0.8287	0.0062	0.4386	0.7670	0.1713
9.	0.9795	1.0000	1.0000	0.8612	0.0205	0.0000	0.0000	0.1388

STEP-5: GRG was determined by taking the average value of the grey relational coefficient for each response, as can be seen in Table 6.33 and were thereafter ranked from 1 to 9. The highest GRG which corresponds to the optimal levels of experiments were chosen. GRG with rank/order of all the nine experiments is presented in Table 6.33.

Table 6.33: Grey Relational Coefficient, Grade and Order (WCT Ti 15 Alloy)

Exp.	Control Factors				Grey Relational Coefficient				GRG	Order
No.	C	B	E	F	MRR	TWR	SR	MH		
1.	C1	B1	E1	F1	0.3333	0.4473	0.3335	0.3333	0.3618	9
2.	C1	B2	E2	F2	0.5909	0.6332	0.4270	0.5682	0.5549	6
3.	C1	B3	E3	F3	0.9795	0.9391	0.5088	0.7652	0.7981	3
4.	C2	B1	E2	F3	0.5111	0.3784	0.3333	0.4923	0.4288	8
5.	C2	B2	E3	F1	0.8318	0.8623	0.5124	0.6315	0.7095	4
6.	C2	B3	E1	F2	1.0000	0.9434	0.5291	1.0000	0.8681	2
7.	C3	B1	E3	F2	0.4607	0.3333	0.4226	0.5574	0.4435	7
8.	C3	B2	E1	F3	0.9877	0.5327	0.3946	0.7449	0.6650	5
9.	**C3**	**B3**	**E2**	**F1**	**0.9605**	**1.0000**	**1.0000**	**0.7827**	**0.9358**	**1**

6.4.2 MULTI RESPONSE OPTIMIZATION USING GRA FOR DCT TITAN 15 ALLOY

By following the same steps, multi response optimization of performance characteristics was completed for DCT TITAN 15 titanium alloy. The calculated S/N ratios for responses are given in Table 6.34. Table 6.35 shows the calculated normalized values and deviation sequence for the each response which was used to find the grey relation coefficient (see Table 6.35). The GRC, grade and order were listed in Table 6.36 and the highest grade 0.8251(first rank) corresponds to the optimal setting of parameters.

Table 6.34 Signal-to-noise Ratios of Response Values (DCT Ti 15 Alloy)

Experiment Number	S/N ratio (dB)			
	MRR	TWR	SR	MH
1.	-4.2489	22.1010	3.4367	51.2657
2.	1.0148	13.6920	4.4500	53.5403
3.	3.2570	8.7597	5.0467	55.2956
4.	0.6394	24.6362	3.5233	52.6942
5.	3.0116	8.0217	5.8667	53.9187

6.	3.5920	9.2282	5.7467	54.4601
7.	-2.3150	27.6163	4.5500	53.5116
8.	3.3656	17.8882	4.4333	55.2189
9.	4.0270	7.5914	6.8667	54.7003
Maximum	4.0270	27.6163	6.8667	55.2956
Minimum	-4.2489	7.5914	3.4367	51.2657
Difference	8.2759	20.0248	3.4300	4.0298

Table 6.35: Normalization and Deviation Sequence of S/N Ratio (DCT Ti 15 Alloy)

Exp.	Normalized S/N ratio				Deviation Sequence			
No.	MRR	TWR	SR	MH	MRR	TWR	SR	MH
1.	0.0000	0.2754	1.0000	0.0000	1.0000	0.7246	0.0000	1.0000
2.	0.6360	0.6954	0.7046	0.5644	0.3640	0.3046	0.2954	0.4356
3.	0.9070	0.9417	0.5306	1.0000	0.0930	0.0583	0.4694	0.0000
4.	0.5907	0.1488	0.9747	0.3545	0.4093	0.8512	0.0253	0.6455
5.	0.8773	0.9785	0.2915	0.6583	0.1227	0.0215	0.7085	0.3417
6.	0.9474	0.9183	0.3265	0.7927	0.0526	0.0817	0.6735	0.2073
7.	0.2337	0.0000	0.6754	0.5573	0.7663	1.0000	0.3246	0.4427
8.	0.9201	0.4858	0.7094	0.9810	0.0799	0.5142	0.2906	0.0190
9.	1.0000	1.0000	0.0000	0.8523	0.0000	0.0000	1.0000	0.1477

Table 6.36: Grey Relational Coefficient, Grade and Order (DCT Ti 15 Alloy)

Exp.	Control Factors				Grey Relational Coefficient				GRG	Order
No.	C	B	E	F	MRR	TWR	SR	MH		
1.	C1	B1	E1	F1	0.3333	0.2754	1.0000	0.3333	0.4855	8
2.	C1	B2	E2	F2	0.6360	0.6954	0.6286	0.5344	0.6236	6
3.	**C1**	**B3**	**E3**	**F3**	**0.8431**	**0.9417**	**0.5158**	**1.0000**	**0.8251**	**1**
4.	C2	B1	E2	F3	0.5499	0.1488	0.9519	0.4365	0.5218	7
5.	C2	B2	E3	F1	0.8030	0.9785	0.4138	0.5941	0.6973	5
6.	C2	B3	E1	F2	0.9049	0.9183	0.4261	0.7069	0.7390	3
7.	C3	B1	E3	F2	0.3948	0.0000	0.6064	0.5304	0.3829	9
8.	C3	B2	E1	F3	0.8622	0.4858	0.6325	0.9633	0.7359	4
9.	C3	B3	E2	F1	1.0000	1.0000	0.3333	0.7720	0.7763	2

Table 6.37: Details of experiments with better performance

Workpiece Material	Exp. No.	Control Factors				Response Parameters				Grade
		C	B	E	F	MRR	TWR	SR	MH	
WCT Ti 15	9	150µs	14A	Cu-Cr	WCT	1.412	0.439	8.15	523.33	0.9358
DCT Ti 15	3	90µs	14A	Cu-W	DCT	1.455	0.365	5.05	582.00	0.8251

The GRG with highest rank corresponds to the optimal level of experiments. The experiments with highest GRG value for WCT and DCT Ti 15 alloy were extracted and are summarized in Table 6.37. Experiment 9 shows the highest GRG of 0.9358 for WCT material, showing the optimal setting of control factors (T_{on} 150µs, I_p 14A, and WCT Cu-Cr electrode ($C_3B_3E_2F_1$)). Experiment 3 shows the highest GRG of 0.8251 for DCT material, showing the optimal setting of control factors (T_{on} 90µs, I_p 14A, and DCT Cu-W electrode ($C_1B_3E_3F_3$)).

Table 6.38 Response Table for the Grey Relational Grade (WCT TITAN 15 Alloy)

Symbol	Process Parameter	Grey Relational Grade				
		Level-1	Level-2	Level-3	Max-min	Rank
C	Pulse-on-time (µs)	0.5716	0.6688	0.6814*	0.1098	2
B	Peak Current (Ip)	0.4114	0.6431	0.8673*	0.4560	1
E	Electrode Material	0.6316	0.6398	0.6504*	0.0187	4
F	Cryogenic of Electrode	0.6690*	0.6222	0.6306	0.0469	3

*** Highest value**

Table 6.39 Response Table for the Grey Relational Grade (DCT TITAN 15 Alloy)

Symbol	Process Parameter	Grey Relational Grade				
		Level-1	Level-2	Level-3	Max-min	Rank
C	Pulse-on-time (µs)	0.6447	0.6527*	0.6317	0.0210	3
B	Peak Current (Ip)	0.4634	0.6856	0.7801*	0.3167	1
E	Electrode Material	0.6535*	0.6406	0.6351	0.0184	4
F	Cryogenic of Electrode	0.6530	0.5818	0.6943*	0.1124	2

*** Highest value**

The mean of the GRG for each input parameter according their respective levels were determined by calculating the simple arithmetic average and are summarized in Table 6.38 for WCT TITAN 15 alloy and in Table 6.39 for DCT TITAN 15 alloy. The optimal

combination of process parameter for WCT TITAN 15 titanium was found to be as C_3 (T_{on}, 150 µs), B_3 (I_p, 14A), E_3 (electrode material, Cu-W) and F_1 (cryogenic treatment of electrode, WCT). For DCT TITAN 15 alloy, Table 6.39 lists the optimal combination of parameters as C_2 (T_{on}, 120 µs), B_3 (I_p, 14A), E_1 (electrode material, Cu) and F_3 (cryogenic treatment of electrode, DCT).

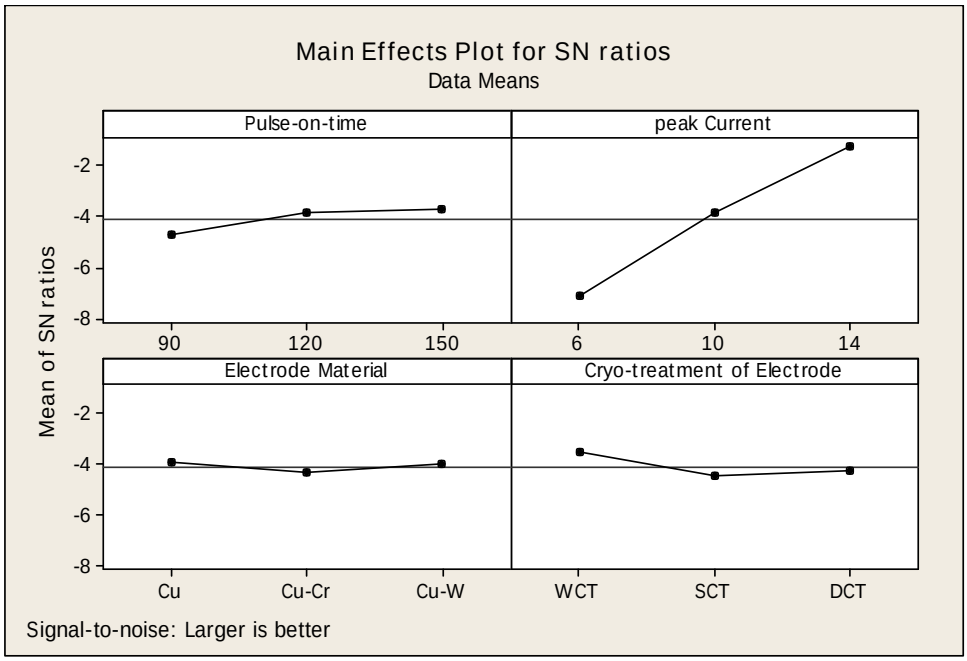

(a- WCT)

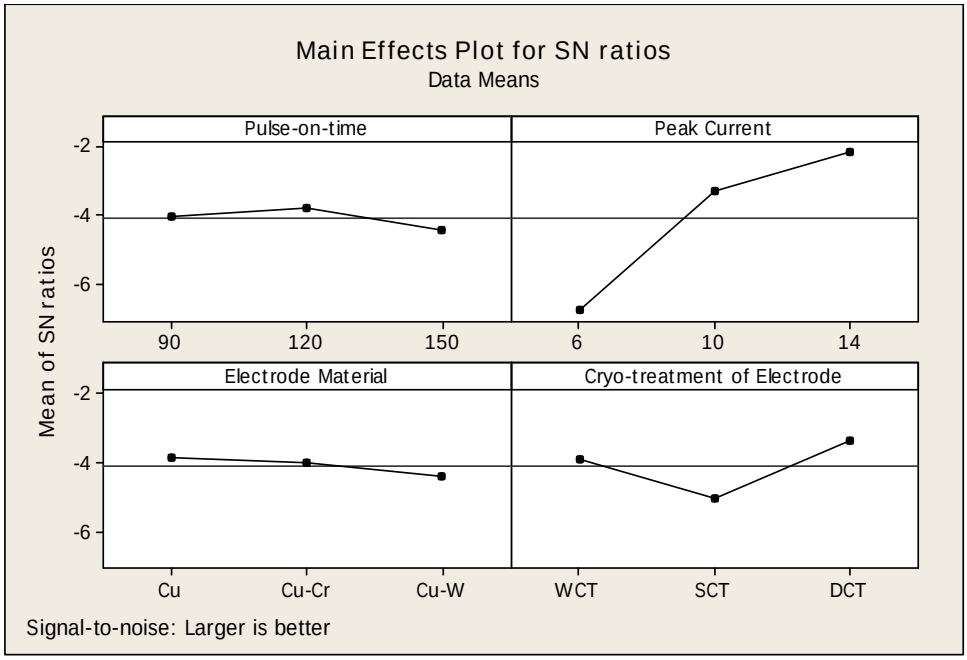

(b- DCT)

Figure 6.33: Grey Relational Grade Graph for WCT & DCT TITAN 15 Alloy

Table 6.40: Performance Results using the Initial Orthogonal Array and Optimal Grey Predicted Process Parameter

Response	Optimal Process Parameters					
	WCT TITAN 15 alloy			DCT TITAN 15 alloy		
	Orthogonal Array	Grey Theory Prediction	Experimental	Orthogonal Array	Grey Theory Prediction	Experimental
Level	$C_3B_3E_2F_1$	$C_3B_3E_1F_1$	$C_3B_3E_1F_1$	$C_1B_3E_3F_3$	$C_2B_3E_1F_3$	$C_2B_3E_1F_3$
MRR	1.412	1.477	1.485	1.455	1.715	1.625
TWR	0.439	0.467	0.452	0.365	0.334	0.325
SR	8.150	7.945	7.750	5.047	5.165	4.950
MH	523.333	578.83	590.500	582.000	566.775	586.50

Table 6.40 shows the comparative results using of the initial results from the Table 6.33 ($C_3B_3E_2F_1$ for WCT, trial 9 and $C_1B_3E_3F_3$ for DCT, trial 3) and grey theory optimal design ($C_3B_3E_3F_1$ for WCT, and $C_2B_3E_1F_3$ for DCT) process parameters in EDM of WCT and DCT TITAN 15 workpiece material. The main effects plot for a grey relational grade of WCT and DCT Ti 15 alloy is shown in Figure 6.33. The grey relational predicted value for optimal combination ($C_3B_3E_2F_1$ for WCT and $C_1B_3E_3F_3$ for DCT) for each response was obtained by using the following equation:

Predicted value = Avg. of C3 + Avg. of B3 + Avg. of E1 + Avg. of F1 – 3×Overall average of response

The predicted value and OA of each response are given in Table 9.40, and the results are within the acceptable limit.

Chapter 7

METALLOGRAPHIC ANALYSIS

7.1 INTRODUCTION

In EDM process, continuous heating and cooling takes place at both terminals, *i.e.* workpiece and electrode which affect the micro-structural properties. I_p, T_{on} and T_{off} are the three important EDM parameters which significantly affect the surface properties in terms of surface topography and metallurgical characteristics. Dielectric type, powder suspended dielectric fluid also influences the micro-structural properties of the machined specimen. Elements of a workpiece and tool material are transferred into each other's surface. Elements also migrate from dielectric fluid on to both the electrodes. These migrated elements interact with the base elements of workpiece and tool metal and form various types of phases. For this reason, metallurgical and surface properties of electrode and the workpiece are known to change. Hence, it was most important to conduct the metallographic analysis of the titanium alloys machined samples, to observe changes in the surface properties after machining.

This chapter discusses and summarizes surface properties of the machined workpiece samples and electrode samples at different settings of the input process parameters.

7.2 METALLOGRAPHIC PROCESS

The microscopic study is based on micrographs and EDAX data for different machining conditions. After the completion of machining, the samples were first cut to size 6 mm x 18 mm using CNC wire-EDM machine (model Sprincut 734, Electronica) as shown in Figure 7.1 (a). Figure 7.1 (b) shows the original ED-machined workpiece sample from which metallographic samples using wire EDM were cut. Thereafter, all the specimen were cleaned with acetone solution and dried in air. The samples were then etched with Kroll's reagent solution of 5% hydrofluoric acid, 10% nitric acid and 85% distilled water and dried in air. Also, samples from all the 18 tool-electrode surfaces after were cut to 3 mm thickness using wire-EDM machine as shown in Figure 7.1 (c). The SEM, EDAX and XRD analysis of workpiece samples and tool-electrode samples were examined for microstructural characterization [164].

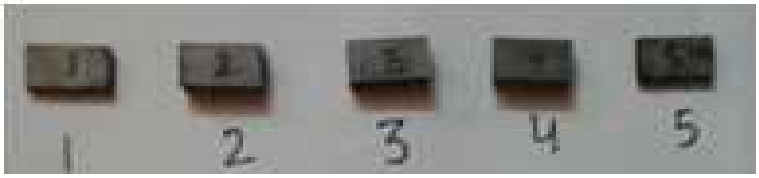

Fig. (a)

Fig. (c)

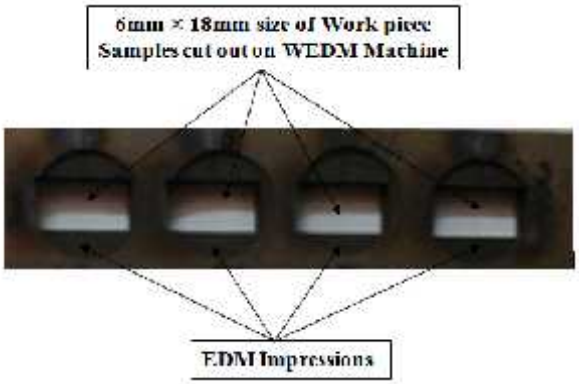

Fig. (b)

Figure 7.1 (a) Workpiece cut out Samples, (b) Original Workpiece Sheet and (c) Electrode cut out Samples

Micro-structural analysis was carried out on a Scanning Electron Microscopy (SEM) analyzer (JEOL, JSM-6610LV, JAPAN) to examine the surface characteristics. SEM micrographs were obtained from the electrically discharged machined surface at magnifications of ×100, ×500 and ×1000. The weight percentages of various chemical elements were measured using Energy Dispersive Spectroscopy (EDS) / Energy Dispersive X-ray analysis (EDX) analyzer. To investigate the possibility of formation of various compounds on the machined workpiece surface, X-Ray Diffraction (XRD) analysis was performed using PANALYTICAL X- ray diffractometers, Netherlands along with X'Pert High Score Plus and Origin Pro 8 software. (*Courtesy; IIT Ropar*)

7.3 METALLOGRAPHIC ANALYSIS OF TITANIUM ALLOY WORKPIECES FOR PHASE-A (MAIN EXPERIMENTATION)

7.3.1 MICROSTRUCTURE ANALYSIS USING SEM

The microstructure of the titanium alloy machined surface was analyzed using SEM micrographs. SEM micrographs for each of workpiece were prepared and are presented in Figures 7.2 to 7.19 for all the 18 experiments. From the micrographs, it can be seen that the process produces irregular surface texture and also defects such as globules of debris, pinholes, and spherical particles with craters of varying sizes, crater rims, micro-cracks, pock

marks, spherical nodules, protruding particles, recast layer, pull out materials. Thus, the machined surface generally has an uneven surface profile. The current was observed to be the most significant factor, which increases the available discharge energy, causing deeper craters, which results in large quantity of molten and floating metal suspended in the inter electrode gap resulting in deep and overlapping craters. The SEM images are in agreement with the results reported by Hascalik and Caydas [19].

A very high temperature of about 8000^0C to 12000^0C or sometimes even up to 20000^0C is obtained at the spot due to the hitting of highly energetic electrons on the workpiece surface [1-2]. At such high temperature, workpiece material melts and vaporizes, leaving a crater on machined surfaces. Though, under the influence of dielectric fluid small amount of molten material cools quickly. I_p and T_{on} were observed to be the two most principal factors which influence the surface morphology.

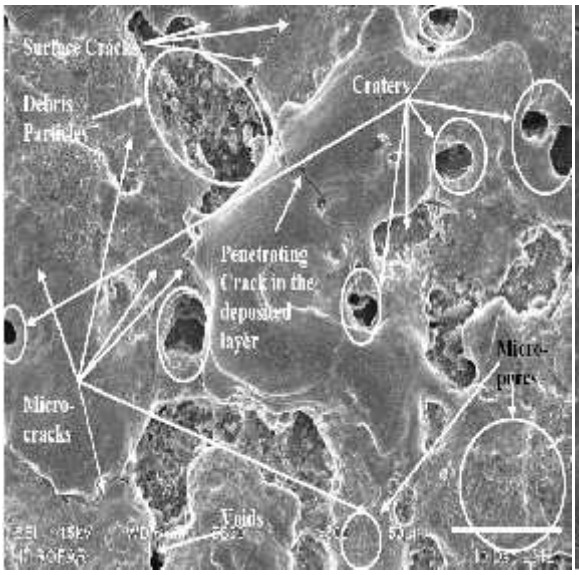

Figure 7.2: SEM Micrograph of WCT Ti Alloy Machined with WCT Cu Electrode in EDM Oil Dielectric (I_p 6A, T_{on}90 µs, T_{off} 30 µs) for Exp. No. 1

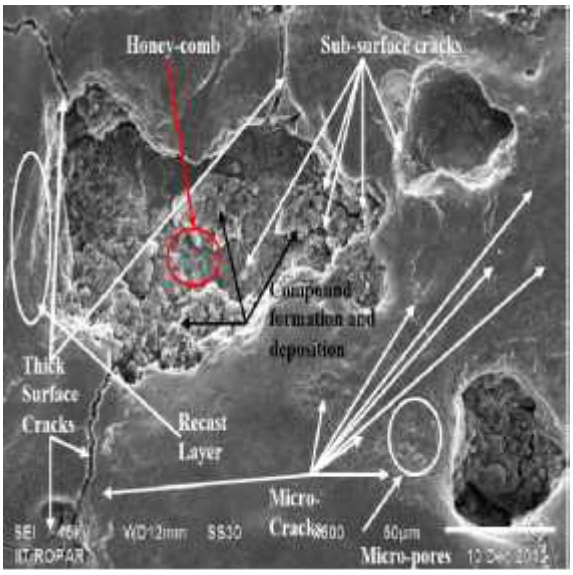

Figure 7.3: SEM Micrograph of SCT Ti-5Al-2.5Sn Alloy Machined with SCT Cu-Cr Electrode in Mn Powder Mixed Dielectric (I_p 6A, T_{on} 120 µs, T_{off} 30 µs) for Exp. No. 2

The SEM micrographs of machined surface at I_p 6A, T_{off} 30µs for various T_{on} (90µs, 120µs, 150µs) under the experimental conditions corresponds to experiment number 1, 2 and 3 at a magnification of 500X as shown in Figures 7.2-7.4. Due to the low discharge energy at 6A current, small craters with low depth were formed. Micro-cracks, micro-pores were also

noticed on the surface. As T_{on} increases (120µs, 150µs) the surface cracks become wider because discharge energy is supplied for longer pulse duration as shown in Figures 7.3 and 7.4. The formation of a recast layer on the machined surface is also clearly seen in the micrographs (refer Figure 7.3 and 7.4).

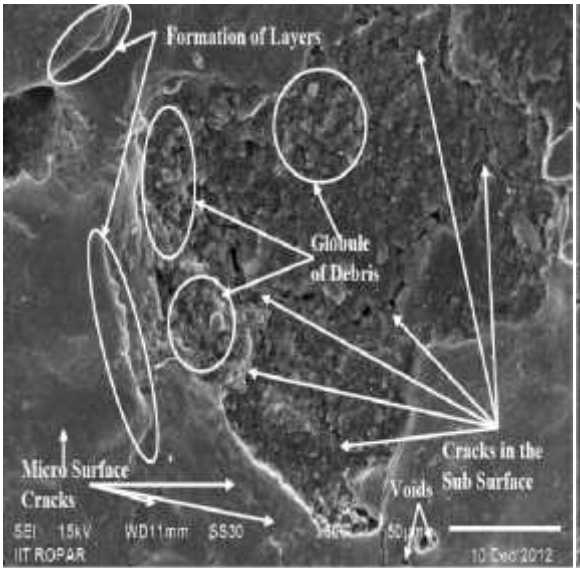

Figure 7.4: SEM Micrograph of DCT Ti-6Al-4V Alloy Machined with DCT Cu-W Electrode in W Powder Mixed Dielectric (I_p 6A, T_{on} 150 µs, T_{off} 30 µs) for Exp. No. 3

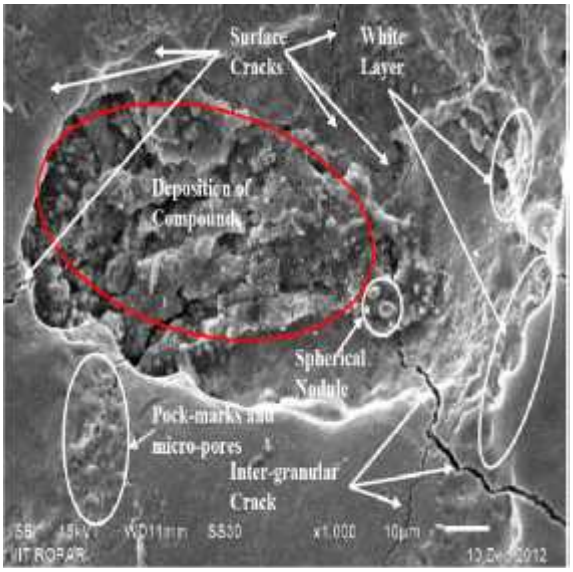

Figure 7.5: SEM Micrograph of DCT Ti-6Al-4V Alloy Machined with SCT Cu-Cr Electrode in EDM Oil Dielectric (I_p 10A, T_{on} 90µs, T_{off} 30µs) for Exp. No. 4

Figures 7.5 to 7.7 correspond to trials conducted at I_p 10A, T_{off} 30µs for various T_{on} (90µs, 120µs and 150µs) and corresponds to experiment number 4, 5 and 6. The surface irregularities increase with an increase in I_p. EDM at high I_p 10A resulted in deeper and larger discharge craters on the machined surface because of high discharge energy in the spark zone. This leads to increase in MRR and micro-hardness, but reduced the surface finish and tool life. It was observed that some part of the molten material was carried away by the dielectric fluid and the remaining melted metal re-solidified to form lumps of debris on the machined surface. Rate of cracking of carbon from dielectric fluid also increased which precipitated on the surface in layer form called recast layer [149]. Wider surface crack was observed at T_{on} 150µs for experiment 6 (refer Figure 7.7), because discharge energy was supplied for longer time. Lumps of debris can be clearly seen in Figures 7.6 and 7.7.

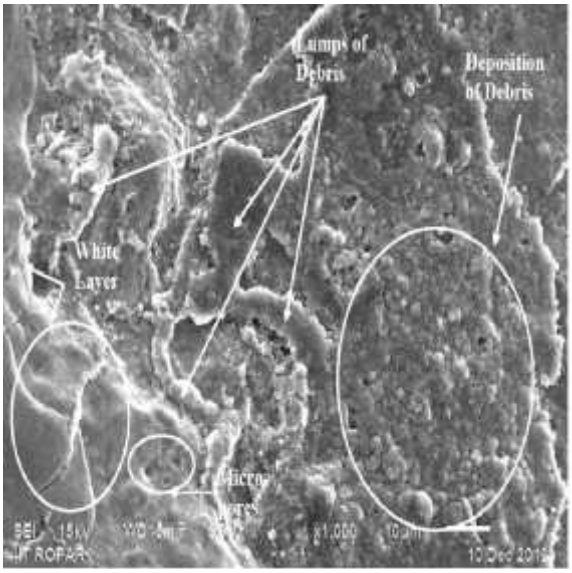

Figure 7.6: SEM Micrograph of WCT Ti Alloy Machined with DCT Cu-W Electrode in Mn Powder Mixed Dielectric (I_p 10A, T_{on} 120µs, T_{off} 30µs) for Exp. No. 5

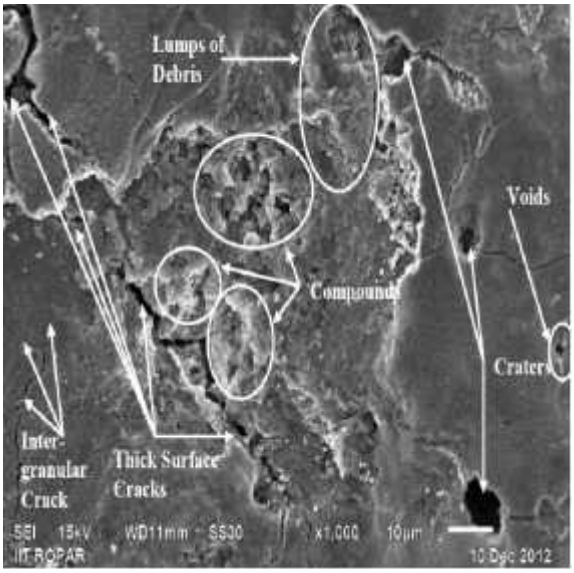

Figure 7.7: SEM Micrograph of SCT Ti-5Al-2.5Sn Alloy Machined with WCT Cu Electrode in W Powder Mixed Dielectric (I_p 10A, T_{on} 150µs, T_{off} 30µs) for Exp. No. 6

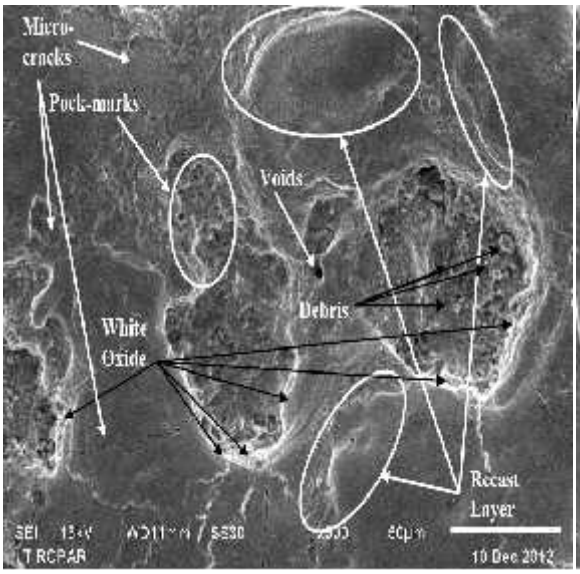

Figure 7.8: SEM Micrograph of DCT Ti-5Al-2.5Sn Alloy Machined with DCT Cu Electrode in Mn Powder Mixed Dielectric (I_p 14A, T_{on} 90µs, T_{off} 30µs) for Exp. No 7

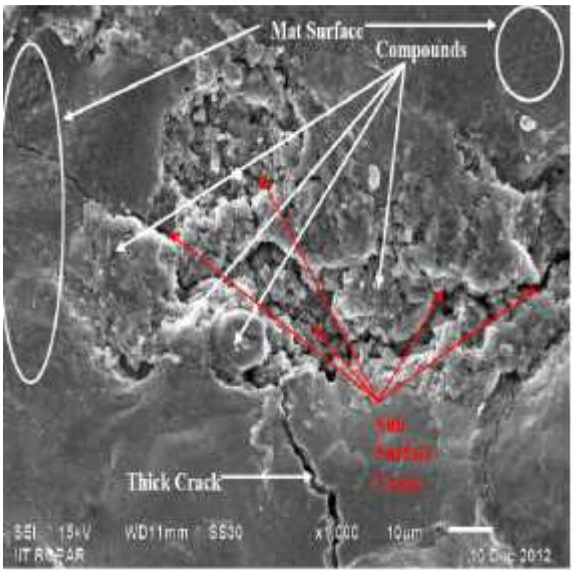

Figure 7.9: SEM Micrograph of WCT Ti-6Al-4V Alloy Machined with WCT Cu-Cr Electrode in W Powder Mixed Dielectric (I_p 14A, T_{on} 120µs, T_{off} 30µs) for Exp. No 8

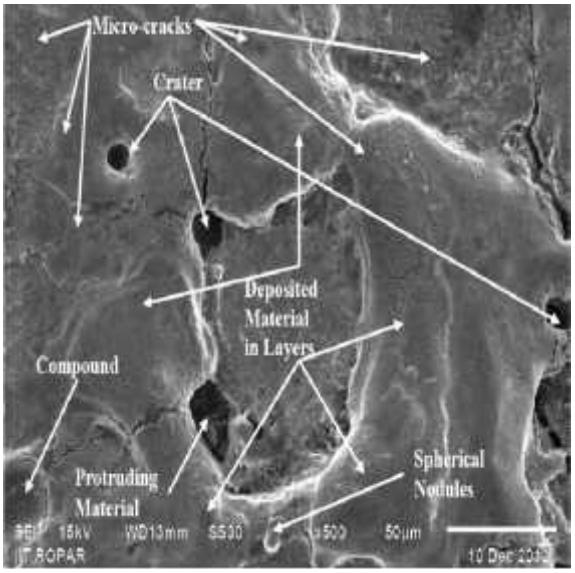

Figure 7.10: SEM Micrograph of SCT Ti Alloy Machined with SCT Cu-W Electrode in EDM Oil Dielectric for (I_p 14A, T_{on} 150µs, T_{off} 30µs) Exp. No. 9

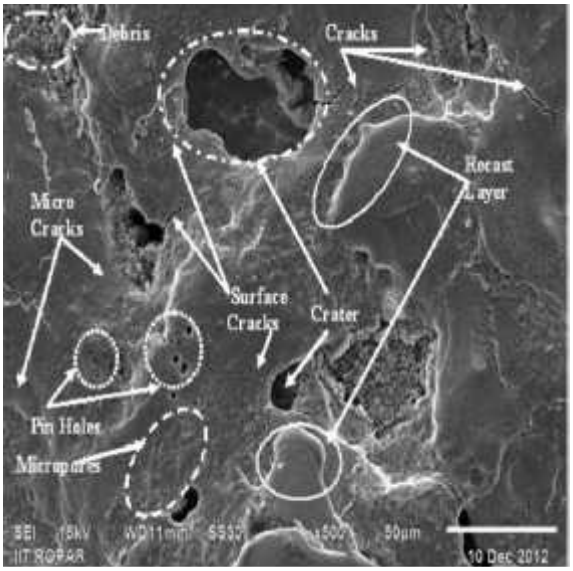

Figure 7.11: SEM Micrograph of WCT Ti-5Al-2.5Sn Alloy Machined with SCT Cu-W Electrode in W Powder Mixed Dielectric (I_p 6A, T_{on} 90 µs, T_{off} 45µs) for Exp. No. 10

The SEM micrographs of the ED- machined work pieces at an I_p of 14A for various T_{on} 90µs, 120µs, 150µs and T_{off} 30µs are shown in Figures 7.8 to 7.10 for experiment number 7, 8 and 9. The regular cracking of dielectric occurred causing more melts expulsions resulting in a higher density of globules accumulation in close vicinity and more residual stresses due to high heat energy of machining zone and, hence, increased surface roughness. These developed stresses resulted in wider and deeper surface cracks and had a higher MRR and poorer finish. A few spherical shaped particles were observed on the surface due to surface tension of molten material. During EDM at high I_p and low T_{off}, debris in the spark gap increased leading to abnormal arcing. The abnormal arcing decreased the discharge rate, thus, lowering the MRR, surface finish, increasing the TWR and also reduced the dielectric strength resulting in poor machining efficiency [146]. Deeper and wider surface cracks can be clearly seen in Figures 7.9 and 7.10 for experiment 8 and 9 due to high current 14A and longer on-time, *i.e.* 120µs and 150µs. Moreover, due to high spark energy, more number of crack, sub surface crack were observed on the machined surface as can be seen in Figure 7.9.

The SEM micrographs of Ti 15, Ti 21 and Ti 31 titanium alloy machined at I_p 6A, T_{off} 45µs for different T_{on} (90µs, 120µs, 150µs) corresponds to experiments 10, 11 and 12 as shown in Figures 7.11 to 7.13. Due to the low spark energy at 6A current and higher value of T_{off}, *i.e.* 45µs shallow craters, micro-cracks were observed on the machined surface as shown in

Figures 7.12 and 7.13. The formation of a recast layer is also noticed on the surface. Inter-granular micro-cracks, compound formations, mat surface and void can be clearly seen in Figure 7.13. In SEM image (Figure 7.12) pin holes were observed on SCT Ti-6Al-4V alloy. Due to increase in T_{off} from 30 to 45 µs, the surface inequalities improve in terms of lesser and shallow craters, reduction in the formation of surface cracks with lesser width than at 30 µs T_{off}. Due to this issue surface finish is improved, but the material removal rate decreased.

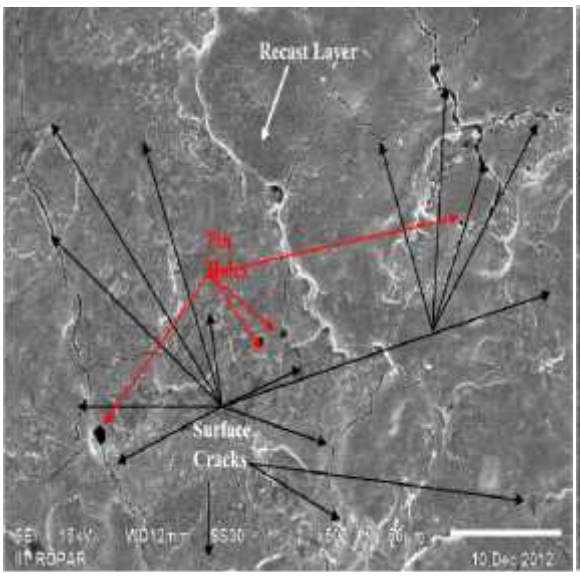

Figure 7.12: SEM Micrograph of SCT Ti-6Al-4V Alloy Machined with DCT Cu Electrode in EDM Oil Dielectric (I_p 6A, T_{on} 120µs, T_{off} 45µs) for Exp. No. 11

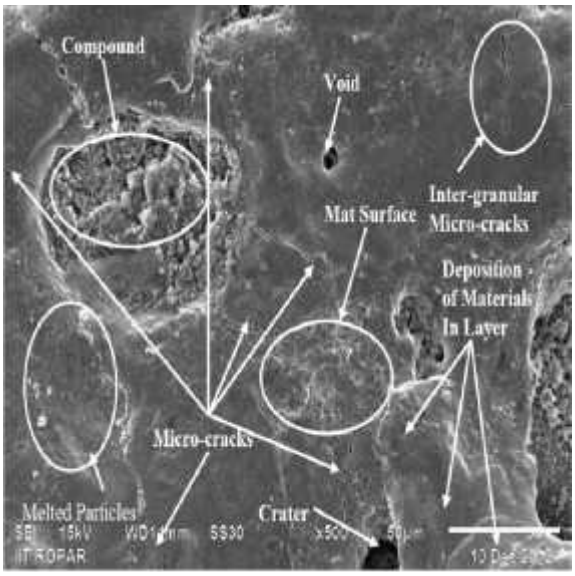

Figure 7.13: SEM Micrograph of DCT Ti Alloy Machined with WCT Cu-Cr Electrode in Mn Powder Mixed Dielectric (I_p 6A, T_{on} 150µs, T_{off} 45µs) for Exp. No. 12

Figures 7.14 to 7.16 show micrographs for experiment numbers 13, 14 & 15 at I_p 10A, T_{off} 45µs for different T_{on} 90µs, 120µs and 150µs. The surface defects increase due to the higher value of I_p. EDM at high I_p 10A resulted in formation of bigger craters on the machined surface because the amount of thermal energy increased in the spark zone as shown in Figure 7.16 for trial 15. This reduced the surface finish and tool life. A number of spherical nodules can be seen in SEM micrograph (see Figure 7.14). Thick and deeper cracks in subsurface were observed due to higher energy as shown in Figure 7.15 for experiment 14. Increase in T_{off}, *i.e.* from 30 to 45 µs led to deposition of molten metal in compound form, thus improving the surface hardness.

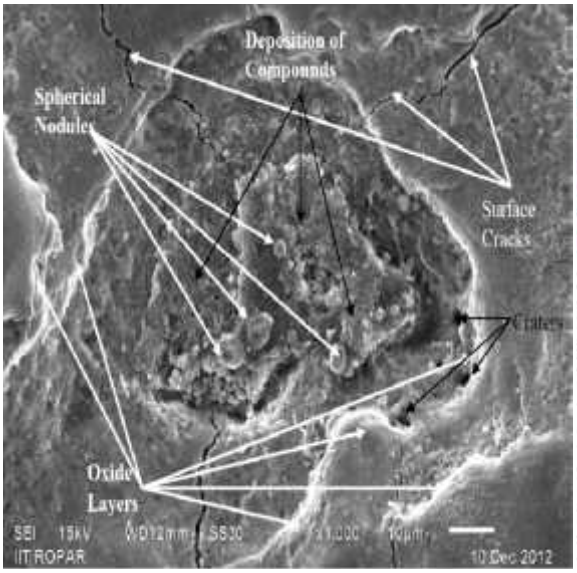

Figure 7.14: SEM Micrograph of SCT Ti-6Al-4V Alloy Machined with WCT Cu-W Electrode in Mn Powder Mixed Dielectric (I_p 10A, T_{on} 90µs, T_{off} 45µs) for Exp. No. 13

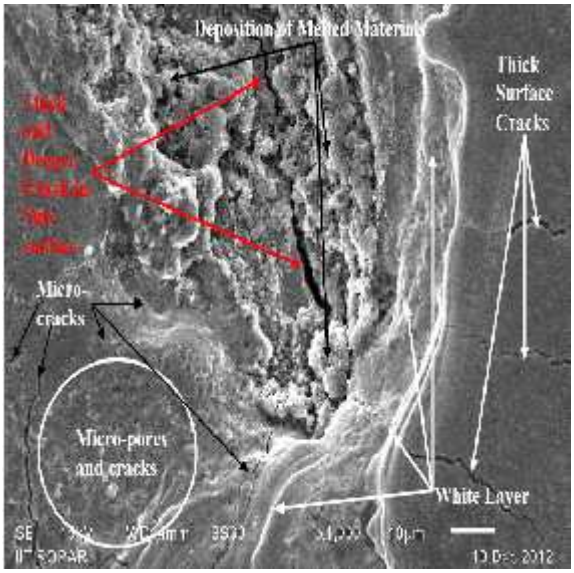

Figure 7.15: SEM Micrograph of DCT Ti Alloy Machined with SCT Cu Electrode in W Powder Mixed Dielectric (I_p 10A, T_{on} 120µs, T_{off} 45µs) for Exp. No. 14

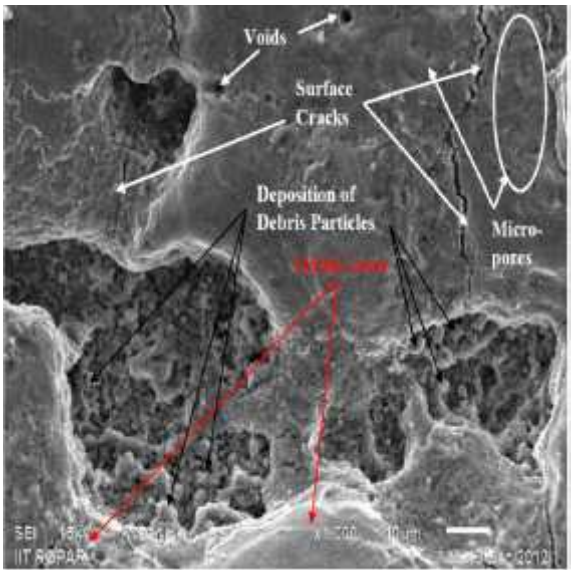

Figure 7.16: SEM Micrograph of WCT Ti-5Al-2.5Sn Alloy Machined with DCT Cu-Cr Electrode in EDM Oil Dielectric (I_p 10A, T_{on} 150µs, T_{off} 45µs) for Exp. No. 15

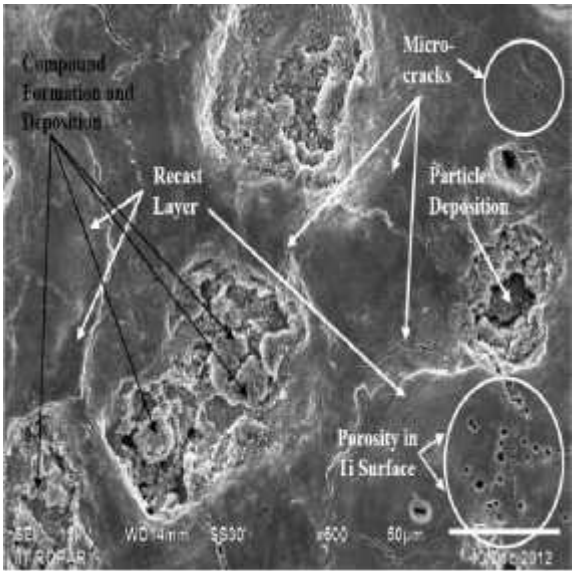

Figure 7.17: SEM Micrograph of SCT Ti Alloy Machined with DCT Cu-Cr Electrode in W Powder Mixed Dielectric (I_p 14A, T_{on} 90µs, T_{off} 45µs) for Exp. No. 16

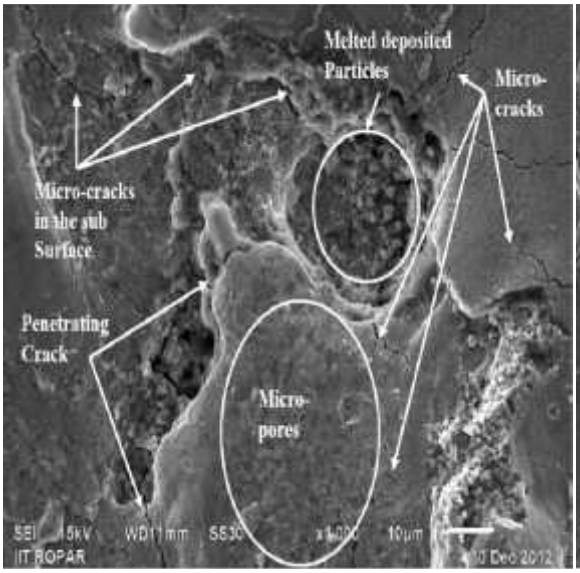

Figure 7.18: SEM Micrograph of DCT Ti-5Al-2.5Sn Alloy Machined with WCT Cu-W Electrode in EDM Oil Dielectric (I_p 14A, T_{on} 120 µs, T_{off} 45 µs) for Exp.No. 17

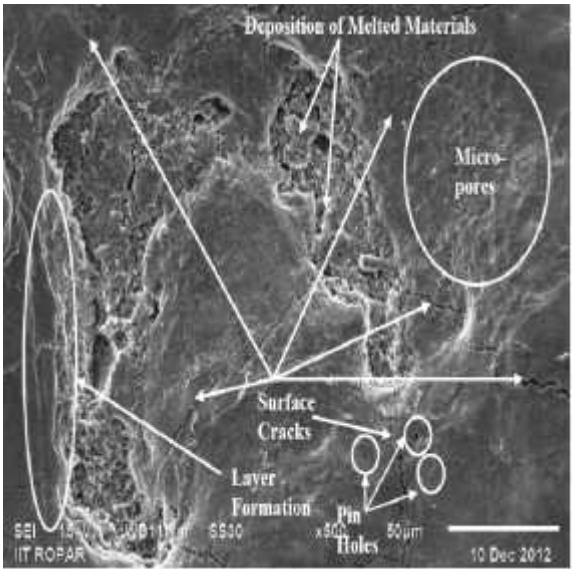

Figure 7.19: SEM Micrograph of WCT Ti-6Al-2.4V Alloy Machined with SCT Cu Electrode in Mn Powder Mixed Dielectric (I_p 14A, T_{on} 150 µs, T_{off} 45 µs) for Exp.No. 18

The SEM micrographs of machined specimen at an I_p of 14A for various T_{on} 90µs, 120µs, 150µs and T_{off} 45µs are shown in Figures 7.17 to 7.19 (experiment number 16, 17 and 18). Porosity on SCT Ti machined surface was observed (see Figure 7.17). The surface irregularities increase with an increase in current and on-time. Further, it can be seen that T_{on} also affected the surface characteristics. From the SEM images it is clear that surface irregularities and unevenness on machined surfaces increases with an increase in T_{on} at the same setting of I_p. This may be happening when T_{on} increases the plasma channel expands. This issue expands the area of contact zone of discharge and consequently reducing energy density and the impulsive force [150-151]. As a result, the melted debris particles were not completely removed from the machining gap and forms an apparent globule like recast layer to weaken the surface of machined components. Besides this surface defect, other defects namely micro-pores, pock mark, voids, pinholes, etc. also form which attributes to further degrade in surface finish with an increase in T_{on} [109].

- ***Recast layer***

In the EDM process, due to generation of high temperature melting and vaporization of the material take place. Out of the total melted material some of the molten material was not

flushed away from the inter electrode gap and re-solidifies on the surface of machined samples in the layer form that is known as recast layer. This developed recast layer can be clearly seen at the cross section as well as on the top surface of the machined parts. The thickness of this layer very much depends on the I_p. The thickness of recast layer was increased with increase of I_p and T_{on}. In addition, to decrease in surface finish, it also weakens the machined parts due to its brittleness and reduces the machining efficiency in terms of low MRR and high TWR. Formation of micro-cracks in the recast layer were also observed in the SEM micrographs as seen in Figures 7.2, 7.4, 7.6, 7.8, 7.10, 7.12, 7.14, 7.17, 7.19. The observation of the study was an agreement with Srivastava and Pandey [109].

- ***Formation of Cracks***

During the EDM process, heat energy is applied in the form of bombardment of electrons for each and every discharge pulse. This high temperature between the two electrodes is responsible for developing thermal / residual stresses at the machined surface. Further, when the magnitude of these developed stresses exceeds the ultimate tensile strength of the workpiece materials, cracks are formed on the surface. The continuous heating and cooling of the machined surface contributes to a rapid increase in yield stresses which results in the formation of cracks [19]. During the heating process, the areas of work material which were plastically transformed cannot come to original state, so that developed plane stresses parallel to the surface, leads to crack formation normal to the surface [144]. Additionally, except the machining parameters, different material properties such as tensile strength, thermal conductivity, thermal expansion coefficient and Young modulus [145-146] also affect the formation of micro-cracks. The surface cracks at various experimental conditions are shown in Figures 7.2 to 7.19. From the SEM micrographs, it was observed that the high value of T_{on} and I_p is directly responsible for the crack formations, because these two factors lead to generation of high heat on the work sample. It can be seen from Figures 7.5, 7.7, 7.9, 7.10, 7.14, 7.16, 7.18, and 7.19 that the surface cracks get wider during machining with high value of I_p and T_{on}. This statement was also supported by the other researches [19, 109].

7.3.2 ENERGY DISPERSIVE X-RAY (EDX) ANALYSIS

In addition to the SEM analysis, the composition of the machined surfaces was analyzed by using the EDX analyzer to recognize the elemental chemical composition of the EDMed surface. An EDX spectrum shows the peaks corresponding to the energy levels for which the

most X-rays had been received [39, 146]. Each of these peaks is unique to an atom, and therefore, corresponds to a single element. The height of a peak in a spectrum represents that the element in the specimen is more concentrated [39]. The maximum peak heights of Titanium (Ti) are clearly visible in the EDX spectra followed by carbon (refer Figure 7.20). The EDX results of all the 18 number of samples are shown in Figure 7.20 (a to r) for the three grades of titanium alloys. As expected, the principal elements in chemical composition of machined surface were Titanium (Ti), Aluminum (Al), Vanadium (V), Tin (Sn) which are the constituents of TITAN 15, TITAN 21 and TITAN 31 alloys. The EDX analysis showed residuals of Copper (Cu), Chromium (Cr), Tungsten (W), Tin (Sn), Chromium (Cr), Manganese (Mn), Oxygen (O), Carbon (C) on the machined surfaces. This may be due to material migration during machining, due to melting, vaporization and re-solidification from the electrode, dielectric fluid or the powder. At high temperature, the dielectric decomposes and carbon is deposited on the machined surface. This observation is in agreement with other studies reported in the literature. [19, 44, 53, 147]. Further, the carbon may also stick to the bottom surface of the tool, thus, lowering the discharge efficiency. Moreover, Mn and W powder mixed with the dielectric were also observed on the machined surface. During EDX test, X-rays were focused on the machined surface at five different places to check the element percentage and then the average value was taken for analysis purpose. Table 7.1 shows the average weight % of different elements of parent metal as well as elements transferred from the tool material and/or powder added dielectric.

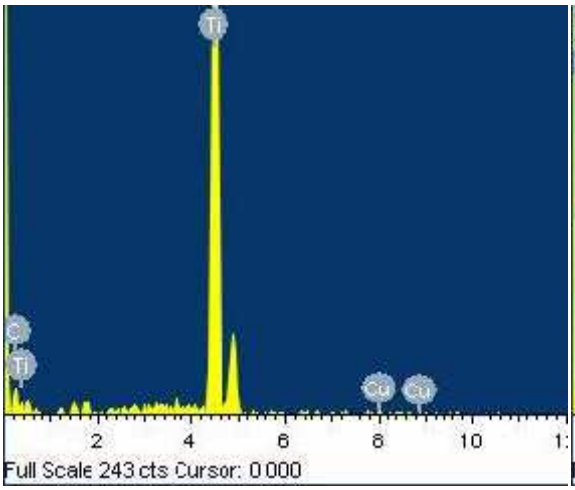

Figure 7.20 (a) Exp. No. 1

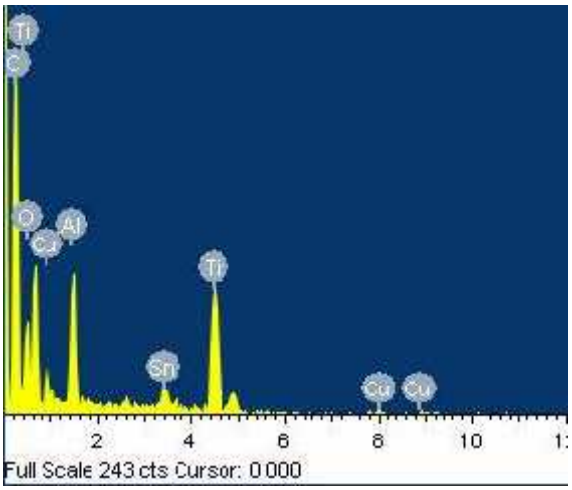

Figure 7.20 (b) Exp. No. 2

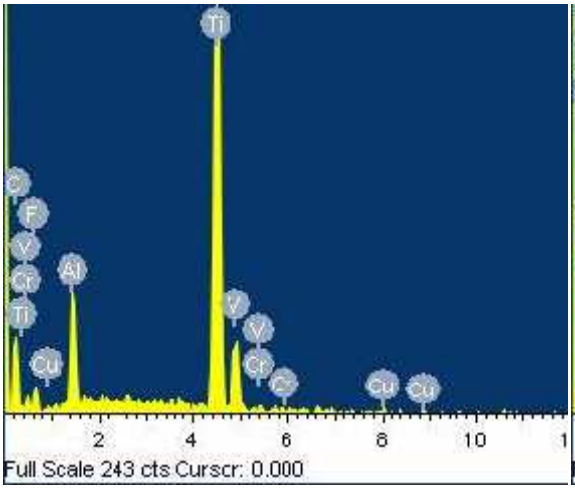

Figure 7.20 I Exp. No. 3

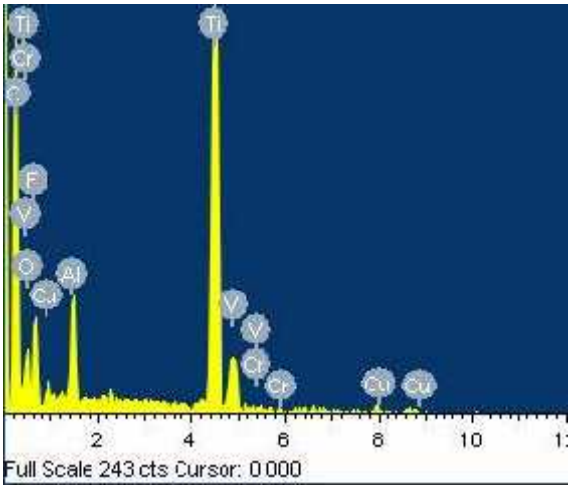

Figure 7.20 (d) Exp. No. 4

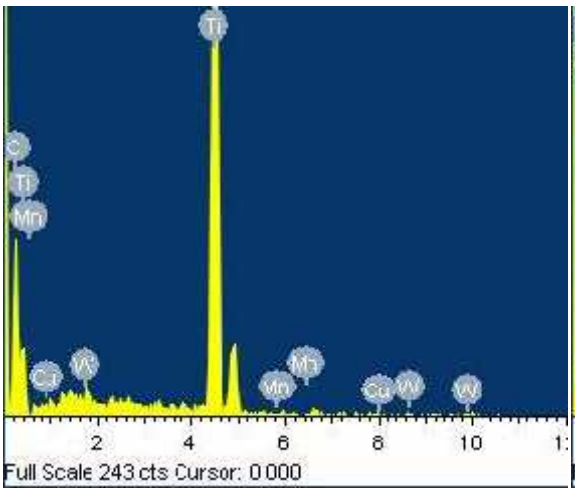

Figure 7.20 (e) Exp. No. 5

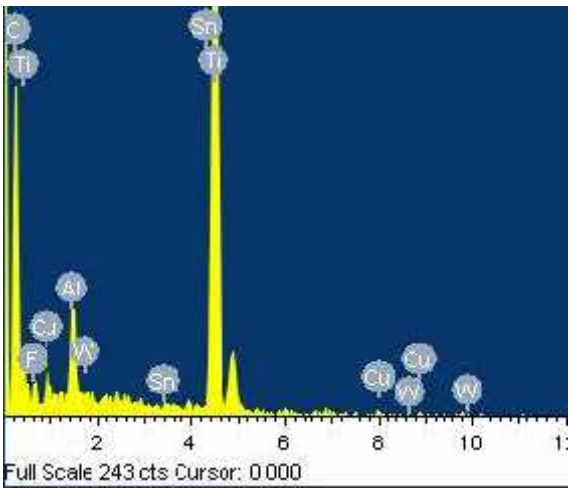

Figure 7.20 (f) Exp. No. 6

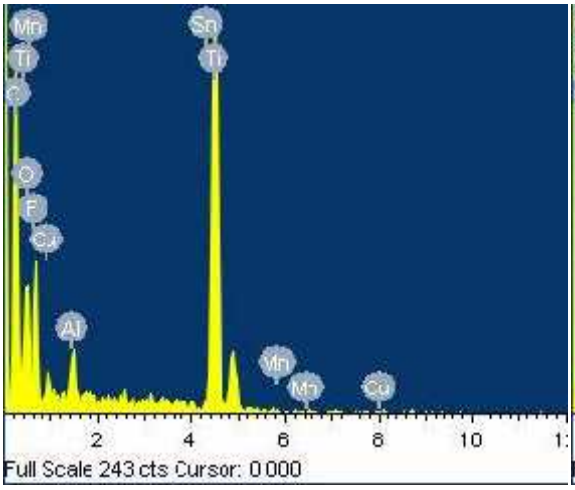

Figure 7.20 (g) Exp. No. 7

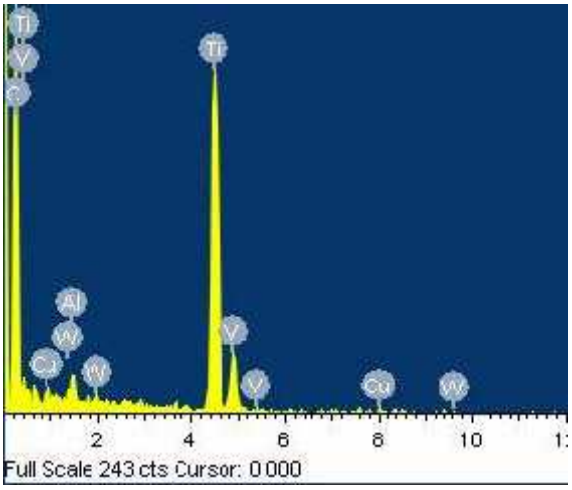

Figure 7.20 (h) Exp. No. 8

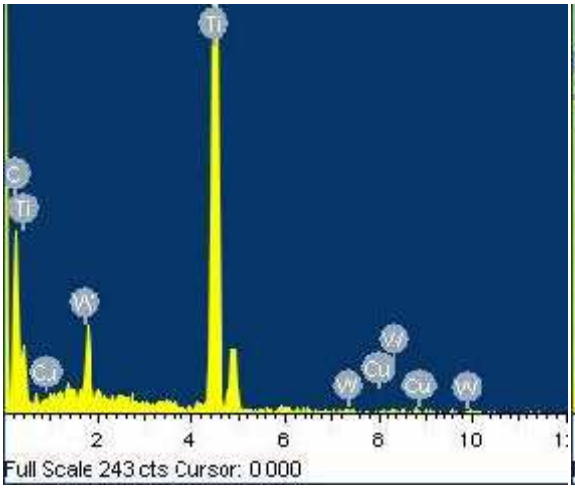

Figure 7.20 (i) Exp. No. 9

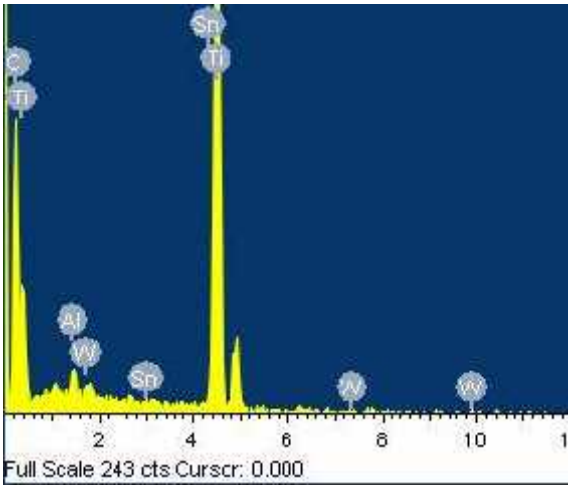

Figure 7.20 (j) Exp. No. 10

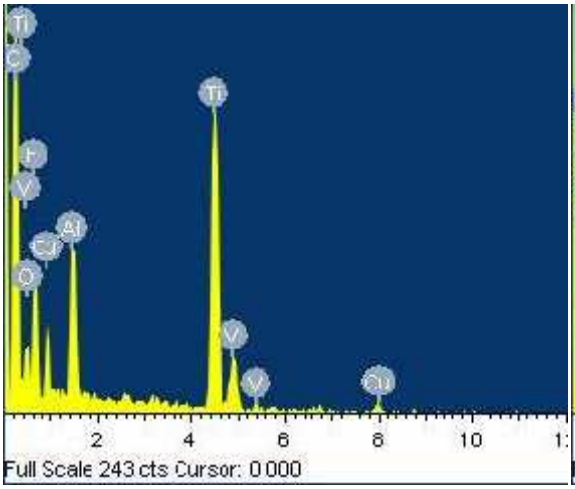

Figure 7.20 (k) Exp. No. 11

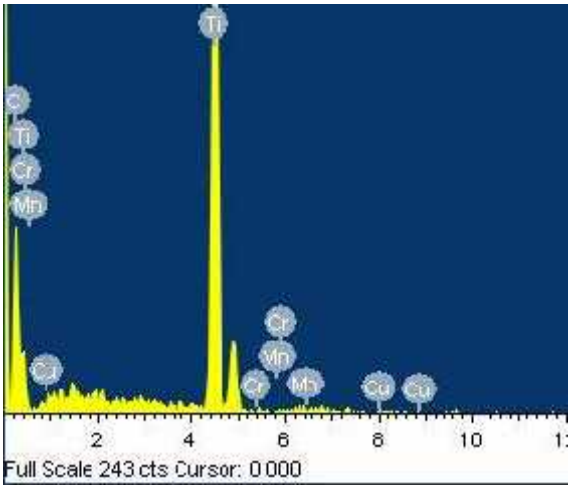

Figure 7.20 (l) Exp. No. 12

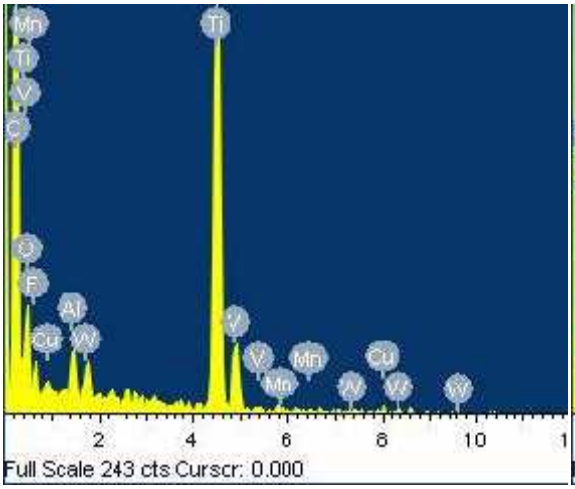

Figure 7.20 (m) Exp. No. 13

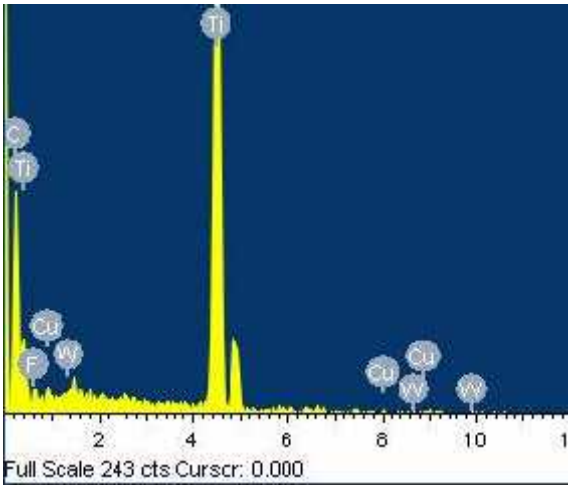

Figure 7.20 (n) Exp. No. 14

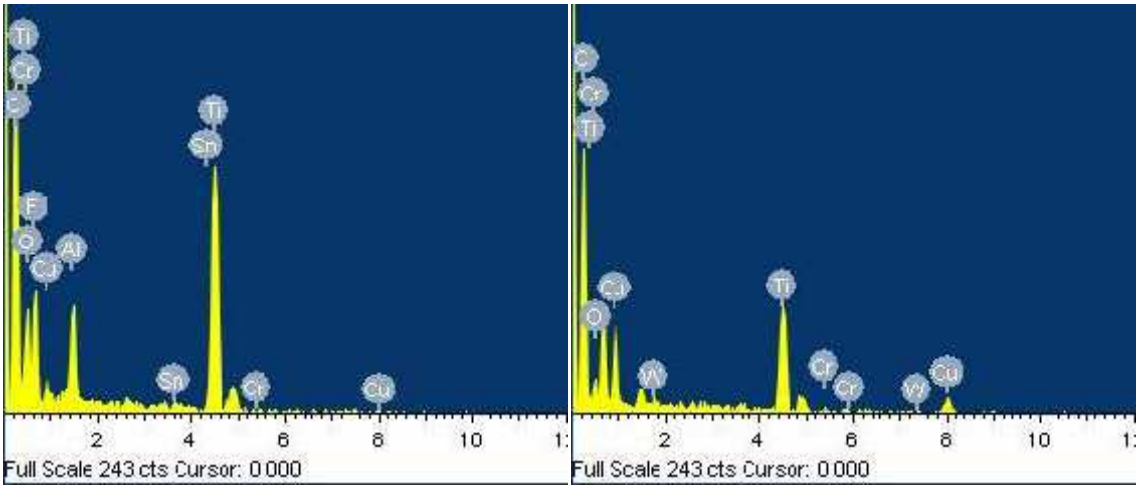

Figure 7.20 (o) Exp. No. 15 **Figure 7.20 (p) Exp. No. 16**

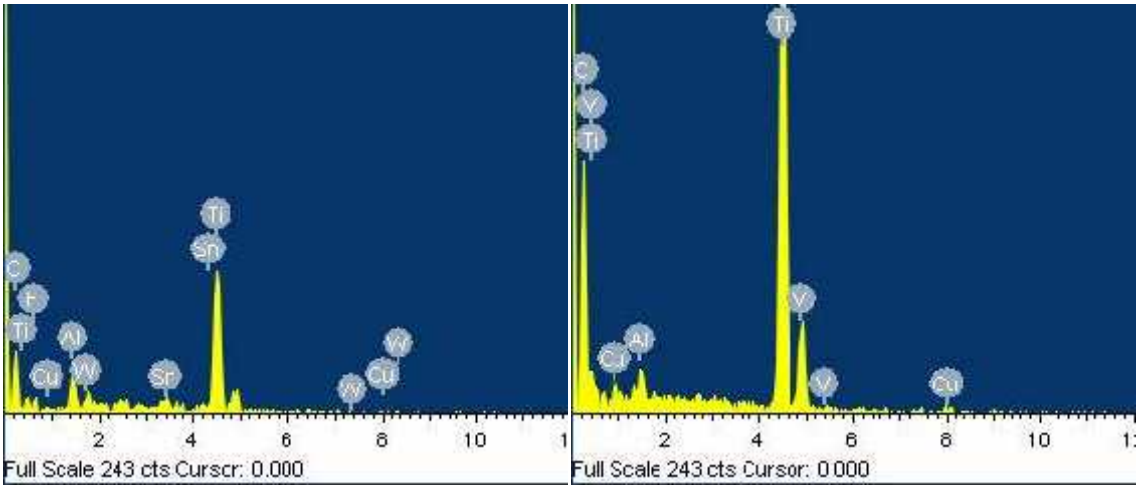

Figure 7.20 (q) Exp. No. 17 **Figure 7.20 I Exp. No. 18**

Figure 7.20 (a to r): EDX Spectrum of Electric Discharge Machined Titanium Alloy Specimens (Experiment Number 1-18)

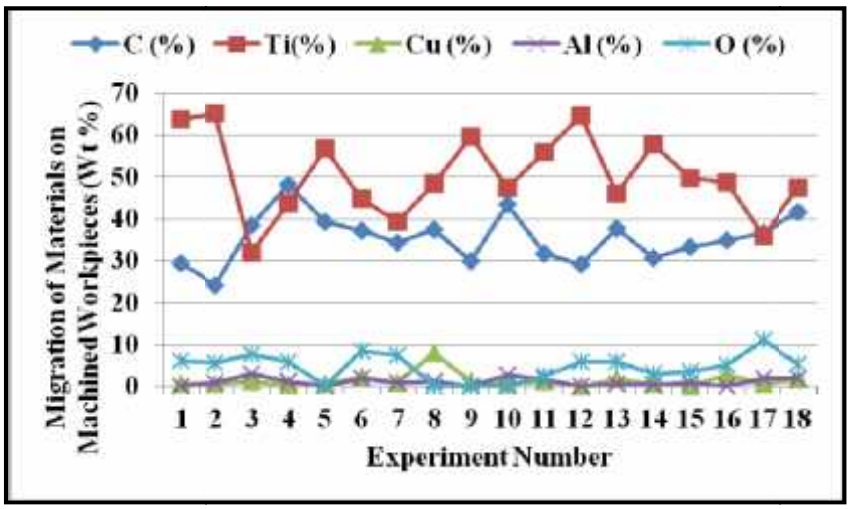

Figure 7.21: Migration of Different Materials on Workpiece Samples

Table 7.1: Observation of Various Elements after Machining of Workpiece Samples

Exp. No.	Average weight (%) of different elements										
	C	O	Ti	Cu	Al	Cr	W	Sn	Mn	V	F
1.	29.44	6.17	63.85	0.54	-----	-----	-----	-----	-----	-----	-----
2.	24.07	5.51	65.10	0.54	0.99	0.016	-----	1.61	-----	-----	2.15
3.	38.39	7.71	31.85	1.20	2.84	0.108	0.81	-----	-----	1.48	15.61
4.	48.14	5.86	43.78	0.24	1.18	0.056	-----	-----	-----	1.45	5.29
5.	39.24	-----	56.73	0.71	-----	-----	1.07	-----	0.108	-----	2.14
6.	37.23	8.33	44.69	2.06	1.98	-----	0.66	1.04	-----	-----	4.00
7.	34.4	7.48	39.34	0.97	0.85	-----		0.84	0.086	-----	16.23
8.	37.45	-----	48.26	7.94	1.02	0.126	0.27	-----	-----	4.94	-----
9.	29.87	-----	59.66	1.17	**----**	-----	4.58	-----	-----	-----	4.72
10.	43.52	-----	47.42	0.66	2.76	-----	0.93	1.17	-----	-----	3.53
11.	31.56	2.46	55.98	1.07	1.55	-----	-----	-----	-----	2.91	4.47
12.	28.98	5.94	64.67	0.07	-----	0.112	-----	-----	0.232	-----	-----
13.	37.64	5.82	46.15	1.64	0.68	-----	1.26	-----	0.306	2.96	3.54
14.	30.54	2.95	57.89	0.73	0.27	-----	0.31	-----	-----	-----	7.31
15.	33.20	3.53	49.81	0.14	0.87	0.164	-----	0.69	-----	-----	11.59
16.	34.88	5.13	48.73	2.72	-----	0.11	0.28	-----	-----	-----	8.15
17.	36.53	11.13	35.95	0.67	1.89	-----	6.61	0.82	-----	-----	6.38
18.	41.47	5.33	47.46	1.70	1.81	0.166	-----	-----	0.036	2.03	-----

From Table 7.1 and EDX analysis, it was observed that Ti base material had the maximum weight %, followed by the migrated C from the dielectric fluid. Furthermore, migration of elements such as Cu, W, and Cr from the electrode materials was also observed in the EDX spectra. Figure 7.21 shows the weight percentage of different materials such as C, Ti, Cu, Al, and O on titanium alloy machined specimens.

7.3.3 X-RAY DIFFRACTION (XRD) ANALYSIS

XRD analyses were conducted on the machined workpiece surface to find out the chemical compounds precisely *i.e.* structural information. X-ray Diffraction (XRD) analysis was done using a Cu-kα source (λ=1.54060 Å) over the 2θ range from 20° to 120°, at temperature of 25°C with step size (2θ) 0.0170 and scan time 20.9550 second on 10 mm specimen length. The XRD pattern confirms the transfer of various elements from tool-electrode material, dielectric fluid (plain or powder mixed) on the machined workpiece surface. Thereafter, these migrated elements interact with the base element of titanium alloys, mainly Ti, Al and then

formed different chemical compounds in carbide form or oxide form, which precipitated on the machined surface.

Titanium is a chemical reactive element and is oxidized during the EDM process forming different chemical compounds of titanium oxides. Also, due to the migration of carbon from the dielectric fluid major chemical compound Titanium-Carbides (TiC) were also formed during the process. To determine the chemical composition and phases on the machined surface exactly, the XRD analysis was completed. The phases were identified in the form of peaks at 2θ scale. The XRD analysis of selected samples was carried out which are described here.

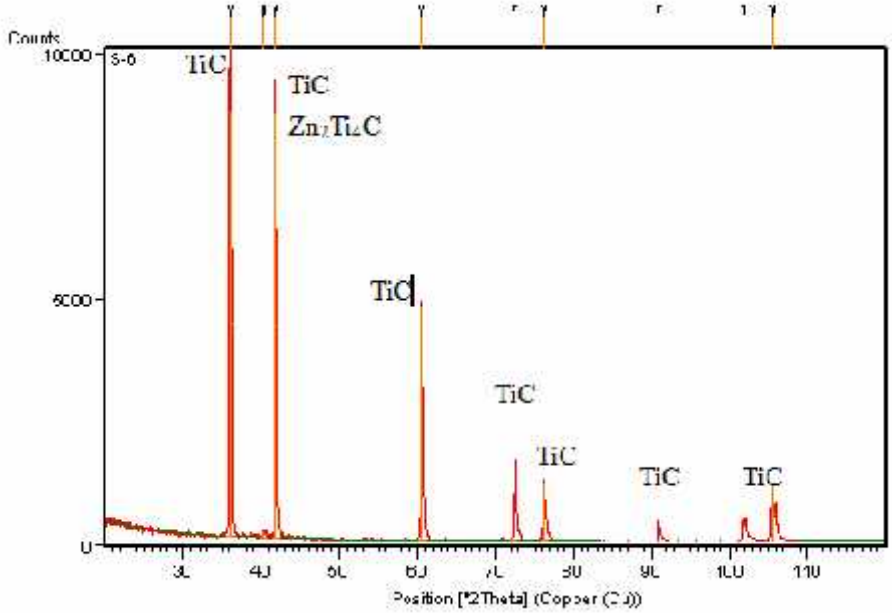

Figure 7.22: XRD Pattern of SCT Ti-5Al-2.5Sn Alloy Machined with WCT Cu Electrode in W Powder Mixed Dielectric (I_p 10A, T_{on} 150µs, T_{off} 30µs) for Exp. No. 6

Figure 7.22 shows the XRD pattern of the of Ti-5Al-2.5Sn alloy machined at I_p of 10A and T_{on} of 150 µs with a Cu electrode in W powder mixed dielectric (experiment 6). Figure 7.22 shows the formation of compounds such as TiC and Zn_2Ti_4C. As carbon was transferred from the dielectric fluid, it interacts with the titanium and forms the hard TiC which was precipitated on the surface. The titanium carbide compounds were observed at the different 2θ positions (36.0526, 41.8467, 60.5795, 72.4777, 76.244, 90.884, 101.842, and 105.570) and Zinc-Titanium-Carbide (Zn_2Ti_4C) at 2θ positions 41.8467.

Zinc was transferred from the copper electrode and formed Zinc-Titanium-Carbide. Some other compounds such as Aluminum-Titanium-Carbide ($Al_2Ti_4C_2$), Germanium- Titanium-

Carbide ($Ge_2Ti_4C_2$), Copper-Titanium-Oxide ($CuTiO_3$), Rutile (TiO_2), Potassium- Titanium-Oxide-Fluoride (K_3TiOF_5), Iron-Titanium-Oxide (FeTiO), Sodium-Iron-Titanium-Oxide ($NaFeTiO_4$), Tin-Titanium-Carbide ($SnTi_2C$), Tin-Titanium-Tungsten-Oxide (Sn_2TiWO_7) were also formed.

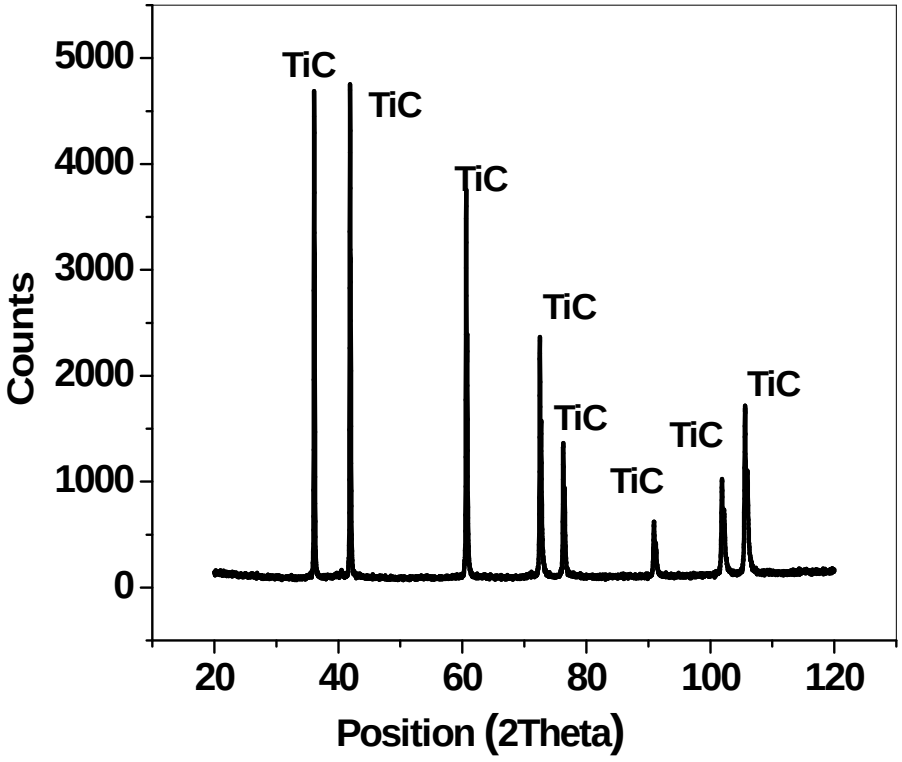

Figure 7.23: XRD pattern of SCT Ti Alloy Machined with SCT Cu-W Electrode in EDM Oil Dielectric for (I_p 14A, T_{on} 150µs, T_{off} 30µs) Exp. No. 9

The outcome of XRD analysis (experiment 9) for machined SCT Ti grade II alloy surface is presented in Figure 7.23. Due to the penetration of carbon on the machined Ti surface, major formation of TiC was noticed on the workpiece surface. The pattern shows the phases of TiC at position-2 theta values 36.100, 41.891, 60.626, 72.521, 76.286, 90.911, 101.843 and 105.605. The highest peak of TiC with maximum counts 4490 was observed at 2θ values 41.891 (Cu K-alpha). The TiC compounds have the highest score of 71. Moreover, some other compounds were also formed such as Germanium-Titanium-Carbide ($Ge_2Ti_4C_2$) and Titanium-Oxide (TiO), but due to a very low score, these compounds are not shown on the XRD plot.

For another case, Figure 7.24 shows the XRD pattern of without cryo-treated Ti-5Al-2.5Sn alloy machined in the presence of W powder mixed dielectric with shallow cryo-treated Cu-

W electrode, 6A I_p, 90µs T_{on} and 45 µs T_{off} (experiment 10). The carbides of titanium were exposed on the XRD pattern at different 2-theta position 36.091, 40.536, 41.874, 60.683, 72.480, 76.263, 90.896, 101.801, 102.246 and 105.615. TiC compound has a maximum peak height with 5002.6 counts obtained at 41.874 2θ position. The other phases of Aluminum-Titanium- Carbide ($Al_2Ti_4C_2$) were also observed at the different 2θ position. The maximum count of $Al_2Ti_4C_2$ was obtained 18.164 at 2θ position 53. 580. The number of counts of $Al_2Ti_4C_2$ was very less as compared to TiC. Further, some other chemical compound also observed such as Tin-Titanium-Carbide ($SnTi_2C$), Tin-Titanium-Tungsten-Oxide (Sn_2TiWO_7), Copper-Titanium-Oxide (Cu_2TiO_3), Gallium-Titanium-Carbide ($Ga_2Ti_4C_2$), Titanium-Zinc –Carbide (Zn_2Ti_4C), Rutile (TiO_2) and Titanium-Oxide (TiO). Due to their very low weightage, these compounds are not shown in the XRD pattern.

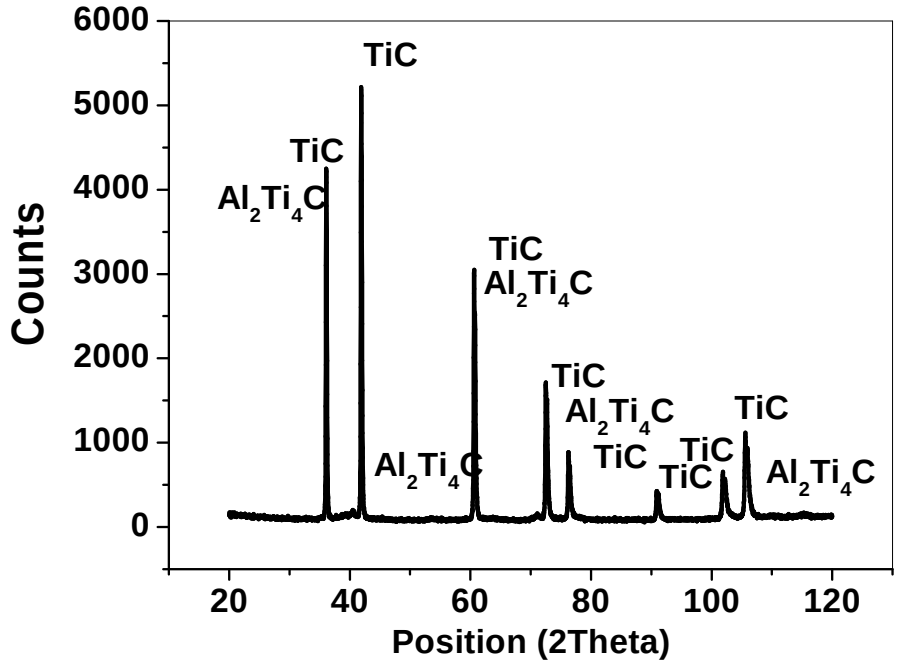

Figure 7.24: XRD pattern of WCT Ti-5Al-2.5Sn Alloy Machined with SCT Cu-W Electrode in W Powder Mixed Dielectric (I_p 6A, T_{on} 90 µs, T_{off} 45µs) for Exp. No. 10

The XRD patterns for the two experiments of Ti alloy machined at different parameters are presented in Figures 7.25 and 7.26 for experiment 12 and 16 respectively. The pattern shows the presence of TiC at 2θ values of 35.88, 41.678, 60.4246, 72.327, 76.0977, 90.749, and 101.727. The highest peak was observed at 2θ values 41.678 (Cu K-alpha). In addition to TiC, TiO phase is also observed on the machined surface at 2θ values 35.88, 41.678, 60.4246,

72.327, 90.749, 101.727, and 105.459. The TiC compounds have the highest score followed by the TiO as shown in Figure 10.25 for experiment 12. Moreover, some other compounds of very low score such as Manganese-Titanium-Oxide (Mn_2TiO_4), Zinc-Titanium-Oxide ($ZnTiO_3$), Titanium-Zinc-Carbide (Zn_2Ti_4C) and Aluminum-Titanium-Carbide ($Al_2Ti_4C_2$) are noticed during the analysis and thus did not show in the XRD plot.

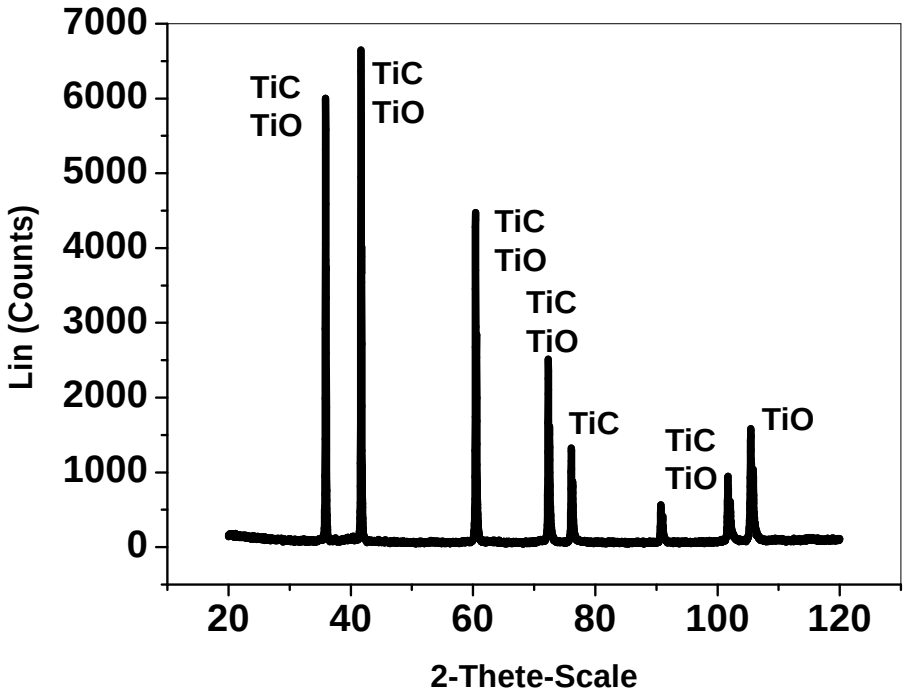

Figure 7.25: XRD pattern of DCT Ti Alloy Machined with WCT Cu-Cr Electrode in Mn Powder Mixed Dielectric (I_p 6A, T_{on} 150µs, T_{off} 45µs) for Exp. No. 12

Figure 7.26 for experiment 16 present the XRD plot of SCT (TI- grade 2) titanium workpiece machined with DCT copper-chromium electrode in tungsten powder mixed dielectric fluid at 14A current. The hard black carbon compound TiC observed in the XRD pattern of maximum score 72 at 2θ position 36.1085, 41.9016, 60.6360, 72.5331, 76.306, 101.938 and 105.649. Another compound Germanium-Titanium-Carbide ($Ge_2Ti_4C_2$) with low score 7 is found at 2θ position 36.1085, 39.95, 41.9016, 60.6360 and 105.649. Further, traces of compounds Nickel-Titanium-Oxide (Ni_3TiO_5), Sodium-Iron- Titanium-Oxide ($NaFeTiO_4$), Sodium-Titanium-Oxide (Na_2TiO_3), Copper-Titanium-Oxide ($CuTiO_3$), Titanium-Zinc-Carbide (Zn_2Ti_4C), Rutile (TiO_2) and Titanium-Oxide (TiO) were observed during the analysis. Due to the low intensity, all these compounds are not seen in XRD analysis.

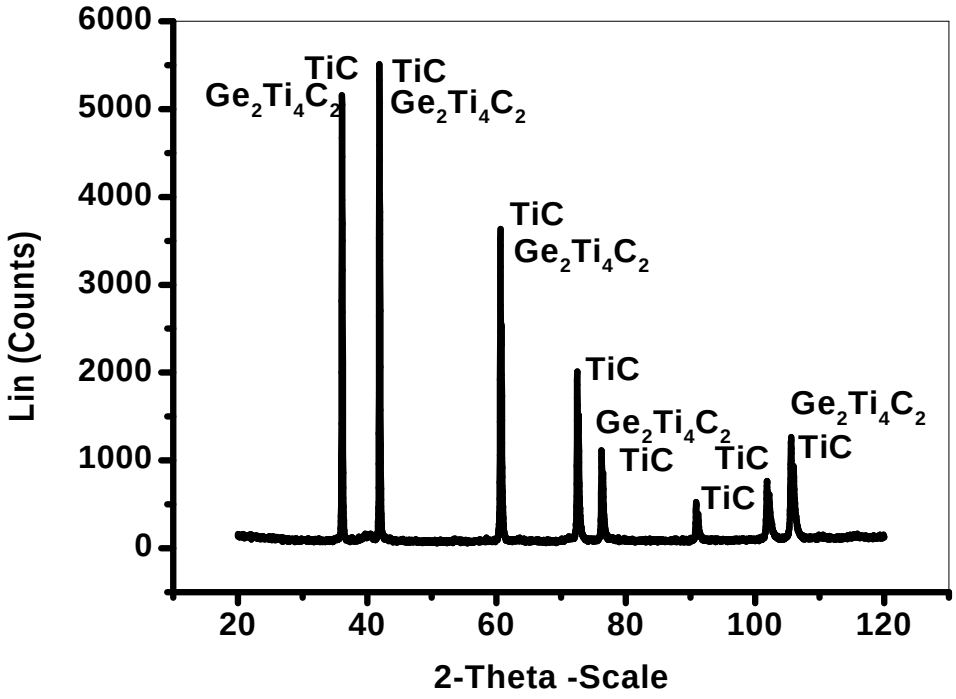

Figure 7.26: XRD pattern of SCT Ti alloy machined with DCT Cu-Cr electrode in W powder mixed dielectric (I_p 14A, T_{on} 90µs, T_{off} 45µs) for Exp. No. 16

The XRD patterns for the two experiment conditions of Ti-5Al-2.5Sn alloy are shown in Figure 7.27 & 7.28 for experiment 2 and 17 respectively. The XRD pattern of SCT Ti-5Al-2.5Sn alloy machined at I_p 6A, T_{on} 120µs and T_{off} 30µs in the presence of suspended manganese powder in dielectric fluid using SCT copper-chromium electrode is shown in Figure 7.27 (experiment 2). The carbides of titanium and manganese-titanium-oxide are seen on the XRD pattern due to the migration of carbon and manganese from dielectric fluid. Irrespective of these two, other compounds such as Hongquite (TiO), Potassium- Titanium-Oxide-Fluoride (K_3TiOF_5), Iron-Titanium-Oxide (FeTiO), Sodium-Iron-Titanium-Oxide ($NaFeTiO_4$), Copper-Titanium-Oxide ($CuTiO_3$), Rutile (TiO_2) and Yttrium- Titanium-Oxide ($Y_2Ti_2O_7$) are noticed during the analysis. Due to the less intensity of these compounds cannot be seen in the XRD plot.

The XRD pattern of DCT Ti-5Al-2.5Sn at machined using copper-tungsten electrode with machining parameters I_p 14A, T_{on} 120µs, and T_{off} 45µs when no powder has been added to the dielectric fluid is presented in Figure 7.28. The XRD pattern indicates the formation of oxide and carbide of titanium (TiO and TiC) after machining. Titanium- carbide of black appearance is formed during the machining which is extremely hard particles similar to tungsten-carbides, which makes the parts more brittle.

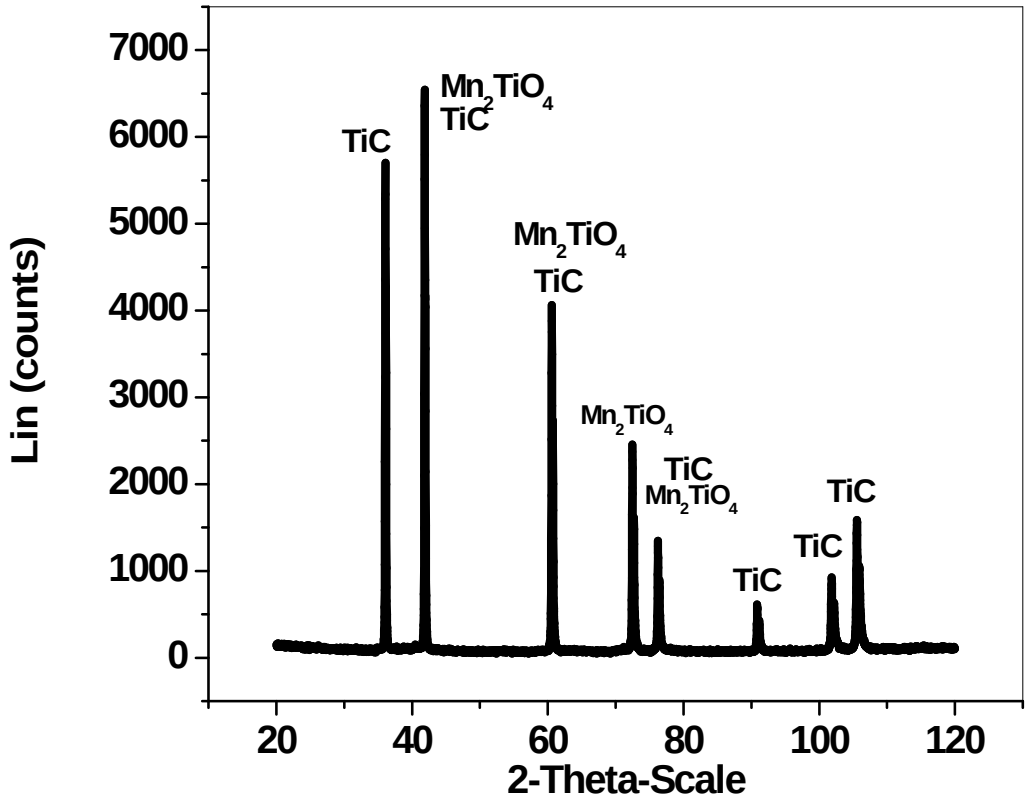

Figure 7.27: XRD pattern of SCT Ti-5Al-2.5Sn Alloy Machined with SCT Cu-Cr Electrode in Mn Powder Mixed Dielectric (I_p 6A, T_{on} 120 µs, T_{off} 30 µs) for Exp. No. 2

The TiC particle is formed by decomposition of carbon present in the dielectric fluid during machining. The decomposed carbon penetrates the machined surface. In addition to TiC compounds, XRD pattern in Figure 7.28, confirm that the titanium oxide (Hongquite) phase occurs with layers dominated by the rutile phase formed on the workpiece surface. Further, it is observed that the white TiO film sticks on the workpiece and does not get removed during machining. This film hinders the flow of current through the two electrodes [148]. In addition to the above compound, some other compounds such as Aluminum-Titanium-Carbide ($Al_2Ti_4C_2$), Tin-Titanium-Carbide ($SnTi_2C$), Manganese-Titanium-Oxide (Mn_2TiO_4), Tin-Titanium-Tungsten-Oxide (Sn_2TiWO_7), Copper- Titanium- Oxide (Cu_2TiO_3) etc., are also observed in small proportion due to the low weight percentage of the elements.

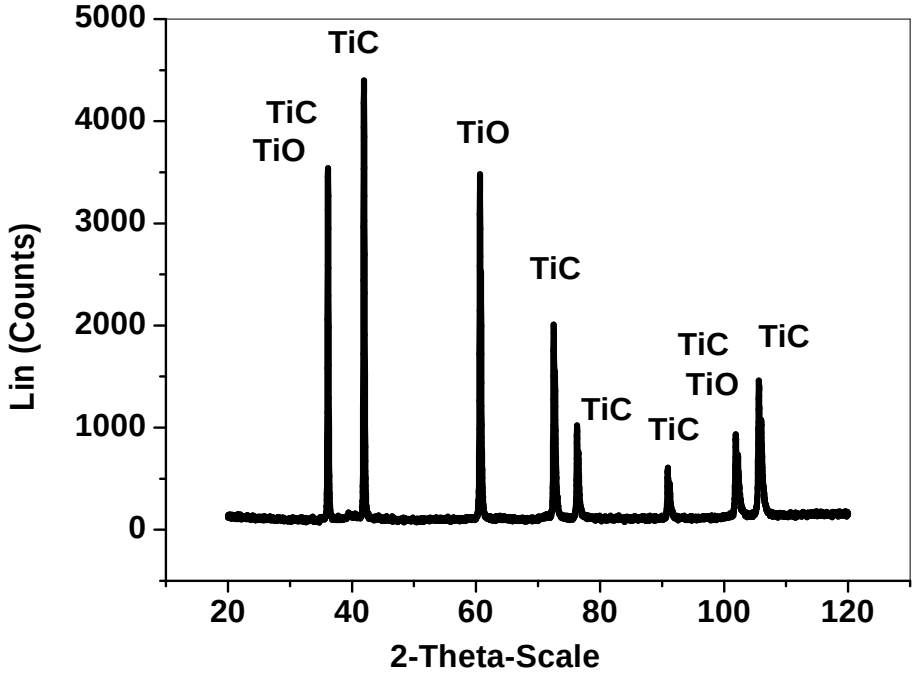

Figure 7.28: XRD pattern of DCT Ti-5Al-2.5Sn Alloy Machined with WCT Cu-W Electrode in EDM Oil Dielectric (I_p 14A, T_{on} 120 µs, T_{off} 45 µs) for Exp.No. 17

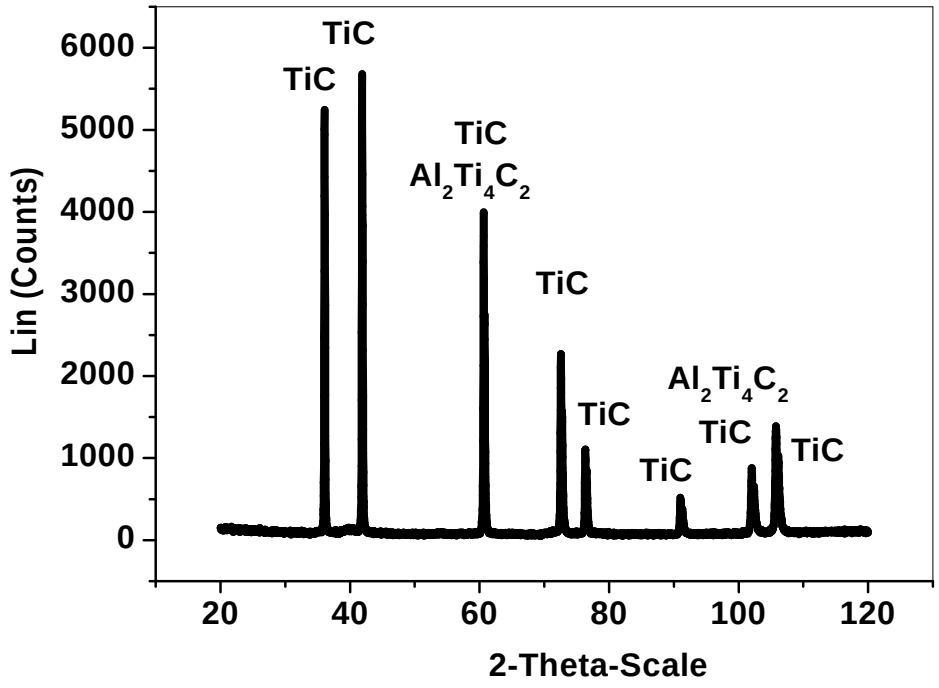

Figure 7.29: XRD Pattern of DCT Ti-6Al-4V Alloy Machined with DCT Cu-W Electrode in W Powder Mixed Dielectric (I_p 6A, T_{on} 150 µs, T_{off} 30 µs) for Exp. No. 3

The XRD pattern for the two trials of Ti-6Al-4V titanium alloy is shown in Figure 7.29 & 7.30 for experiment 3 and 18 respectively. Figure 7.29 shows the XRD pattern of DCT Ti-

6Al-4V alloy was machined using DCT Cu-W tool when W powder added into the dielectric fluid at a 6A I_p, 150µs T_{on} and 30µs T_{off} for experiment 3. The XRD pattern indicates the formation of TiC which is a carbide form of titanium at 2θ positions 36.0653, 41.8732, 60.6512, 72.5821, 76.364, 91.066, 102.024, 105.819 with compound $Al_2Ti_4C_2$ at 60.6512 and 102.024. The other compounds such as Calcite ($CaCO_3$), Nickel- Hydroxide-Methoxide ($C_2H_{10}Ni_3O_6$) and Gallium-Titanium-Carbide ($Ga_2Ti_4C_2$) have been confirmed, but have a very low weightage.

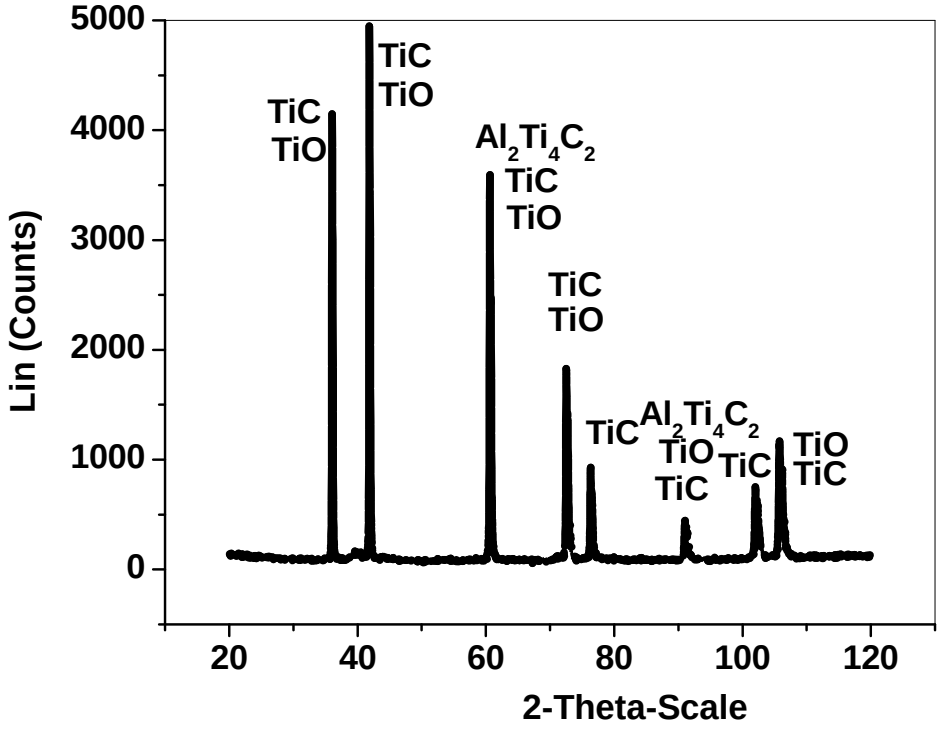

Figure 7.30: XRD Pattern of WCT Ti-6Al-2.4V Alloy Machined with SCT Cu Electrode in Mn Powder Mixed Dielectric (I_p 14A, T_{on} 150 µs, T_{off} 45 µs) for Exp.No. 18

Similarly, Figure 7.30 shows the XRD pattern of Ti-6Al-4V machined at 14A current for experiment 18. The black hard and brittle formation of TiC formed at 2θ positions 36.0512, 41.8612, 60.6404, 72.547, 76.364, 91.085, 102.099, 105.842. Formation of white TiO is observed at 36.0512, 41.8612, 60.6404, 72.547, 76.364, 91.085, 105.842 and $Al_2Ti_4C_2$ at a 2θ angle 60.6404 and 102.099. The low score of other compounds like Zn_2Ti_4C, Mn_2TiO_4, FeTiO, K_3TiOF_5, and Cu_2TiO_3 is noticed in the analysis.

Decomposed carbon from the dielectric EDM Oil due to high temperature; precipitated on the machined surface either in free form or compound form [19, 146]. Different carbide

compounds were observed in the analysis, especially TiC and $Al_2Ti_4C_2$. The migrated carbon also sticks to the bottom surface of electrodes, thus, reducing the discharge efficiency. The melting point and the boiling point of these titanium carbide compounds are approximately 3160^0C (just twice of titanium) and 4820^0C respectively, which increase the time for melting, boiling and evaporation of materials and require the more discharge energy for machining, hence results in a decrease the machining efficiency [148,19]. Moreover, various oxide compounds were also formed during the process, especially TiO, which, act as a barrier between the current flows thus reducing the machining efficiency. The reason of their formation is the interaction of titanium element of base material with soluble oxygen in a dielectric fluid. Due to this reason base material elements interact with the cracked carbon as well as soluble oxygen, respectively; hence various phases / compounds in carbide or oxide form were produced on the machined specimen. This statement is also confirmed by the Jabbaripour et al [53] in their study. Formation of TiC has a large score as compared to the TiO because the percentage of migrated carbon is much more as compared to the oxygen.

The weight % of transferring carbon element is more as compared to the other elements which were transferred from the copper based tool material to the job surface and vice versa. This transferred carbon interacts with the workpiece elements, *e.g.* Ti element, which has large percentage. Due to this phenomenon, TiC compound formed with high score is produced on the machined surface as shown in the XRD patterns. Presence of other low percentage elements in workpiece also forming various compounds on the machined surface.

Since the melting and the boiling points of TiC compounds are very high, the time for melting, boiling and vaporization of materials increases and thus requires higher discharge energy for machining, thus lowering the machining efficiency [19, 42].

The various phases and compounds discussed above were formed on the machined surface due to interaction with the parent metal elements of workpiece and dielectric fluid without powder or with suspended powder particles.

7.4 METALLOGRAPHIC ANALYSIS OF TOOL/ELECTRODE SURFACE AFTER EDM OF TITANIUM ALLOYS

Before conducting the SEM, EDS and XRD analysis, all the 18 tool samples after 18 trials were cleaned properly with acetone solution and then etched with a solution having compositions of 20 ml of Sodium-Hydroxide (NH_4OH), 20ml of Water (H_2O) and 20 ml of Hydrogen-Peroxide (3% H_2O_2).

7.4.1 MICROSTRUCTURE ANALYSIS OF ELECTRODES USING SEM

The SEM micrographs of tools for experiment 1 to 18 after EDM of three grades of titanium alloys at different machining conditions are shown in Figure 7.31 to 7.49. During EDM, high thermal energy is generated between the tool and workpiece due to generation of sparks. Due to high temperature during the process, some material from tool melts and vaporizes from the surface. The molten tool material cools quickly due to circulating dielectric fluid. This continuous heating and cooling alters the surface and metallurgical properties of tool surface.

The SEM micrographs of three different electrode surface namely WCT Cu electrode, SCT Cu-Cr electrode and DCT Cu-W electrode obtained at different experimental conditions I_p 6A, T_{off} 30µs for various T_{on} (90µs, 120µs, 150µs) corresponding to experiment number 1, 2 and 3 at a magnification of 1000X are shown in Figures 7.31 to 7.33. Due to low current, (6A), low spark energy was generated within the spark gap. Small size of craters, micro-cracks, micro-pores and small size of voids were noticed on the electrode surface. As T_{on} increases to 150µs, thick surface cracks were noticed on the DCT Cu-W electrode surface as shown in Figures 7.33. The formation of spherical nodules is clearly seen in the micrographs (refer Figure 7.31 to 7.33). Deposition of melted particles is also clearly seen in the SEM images.

Figures 7.34 to 7.36 represents micrograph of machined samples of tool for experiments 4,5 and 6 at I_p 10A, T_{off} 30µs and T_{on} of 90µs, 120µs and 150µs respectively using different electrode materials. As current increases from 6A to 10A, it results in higher discharge energy, thereby increasing the surface irregularities. Deeper and larger sizes of craters on the electrode surface were noticed due to increase in discharge energy in the spark zone as shown in Figures7.34 to 7.36. This leads to increase in TWR and surface roughness. It was observed that some part of the molten material was carried away by the dielectric fluid and the

remaining melted metal re-solidified to form lumps of debris on the machined surface which can be clearly seen in Figures 7.35. Due to powder mixed dielectric, smoother surface of electrode were observed.

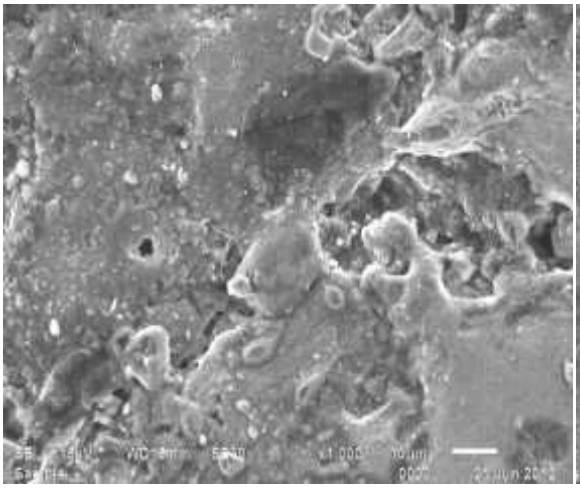

Figure 7.31: SEM Micrograph of WCT Cu Electrode when WCT Ti Alloy Machined in EDM Oil Dielectric (I_p 6A, T_{on}90 µs, T_{off} 30 µs) for Exp. No. 1

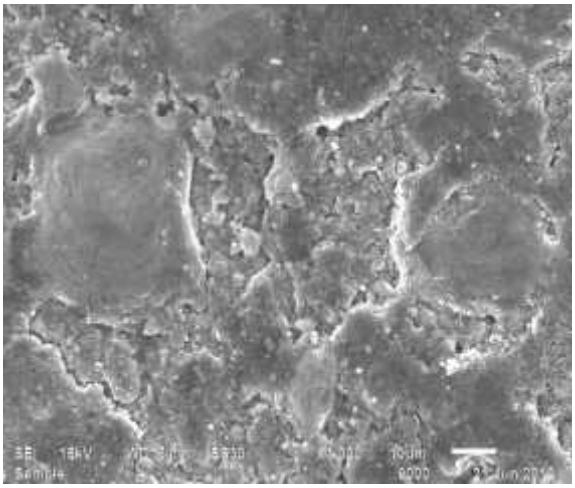

Figure 7.32: SEM Micrograph of SCT Cu-Cr Electrode when SCT Ti-5Al-2.5Sn Alloy Machined in Mn Powder Mixed Dielectric (I_p 6A, T_{on} 120 µs, T_{off} 30 µs) for Exp. No. 2

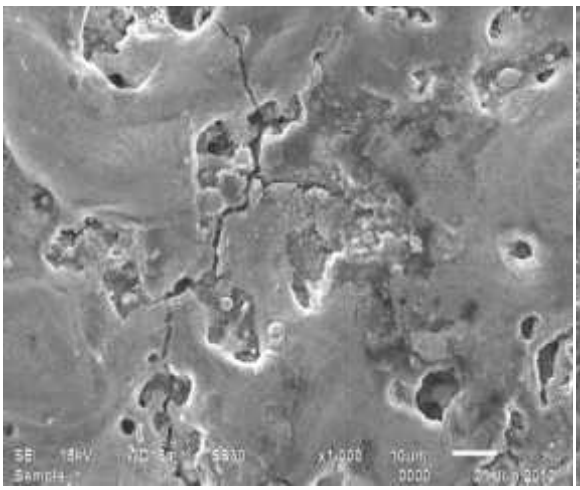

Figure 7.33: SEM Micrograph of DCT Cu-W Electrode when DCT Ti-6Al-4V Alloy Machined in W Powder Mixed Dielectric (I_p 6A, T_{on} 150 µs, T_{off} 30 µs) for Exp. No. 3

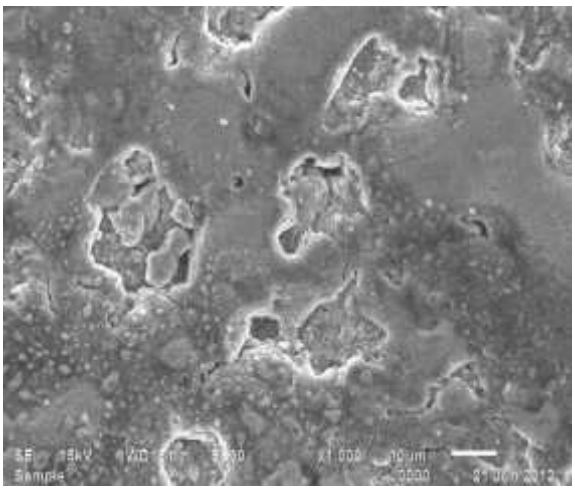

Figure 7.34: SEM Micrograph of SCT Cu-Cr Electrode when DCT Ti-6Al-4V Alloy Machined in EDM Oil Dielectric (I_p 10A, T_{on} 90µs, T_{off} 30µs) for Exp. No. 4

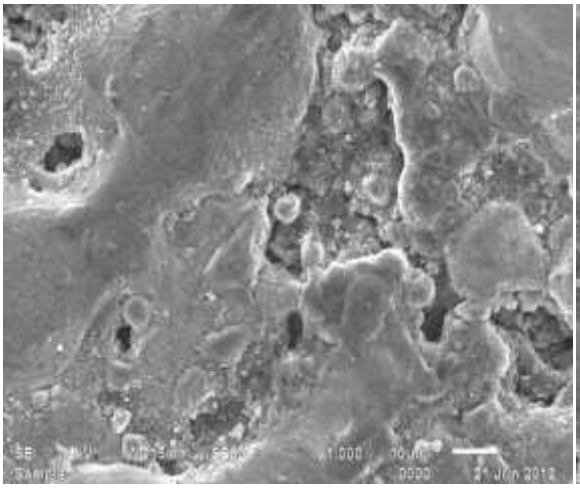

Figure 7.35: SEM Micrograph of DCT Cu-W Electrode when WCT Ti Alloy Machined in Mn Powder Mixed Dielectric (I_p 10A, T_{on} 120µs, T_{off} 30µs) for Exp. No. 5

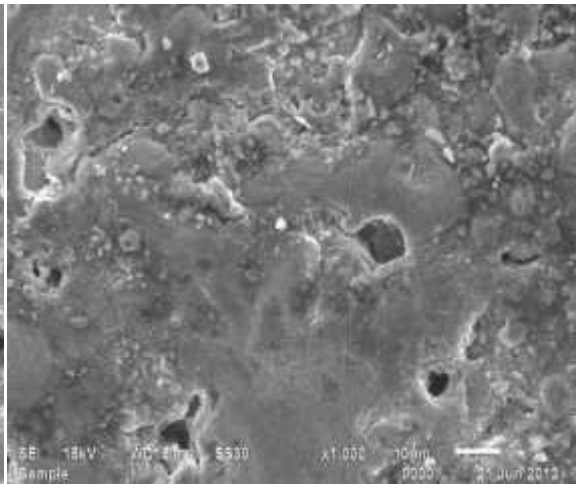

Figure 7.36: SEM Micrograph of WCT Cu Electrode when SCT Ti-5Al-2.5Sn Alloy Machined in W Powder Mixed Dielectric (I_p 10A, T_{on} 150µs, T_{off} 30µs) for Exp. No. 6

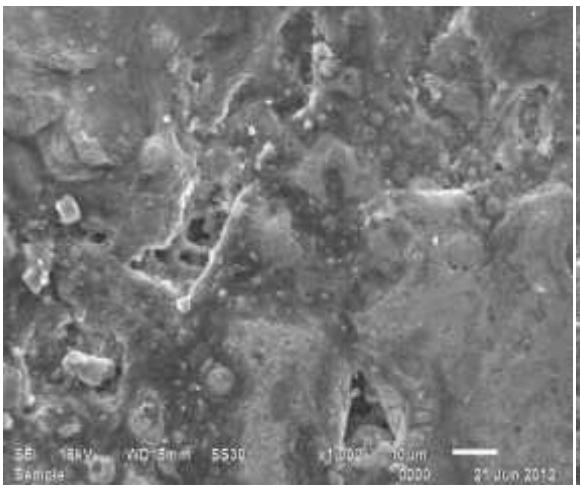

Figure 7.37: SEM Micrograph of DCT Cu Electrode when DCT Ti-5Al-2.5Sn Alloy Machined in Mn Powder Mixed Dielectric (I_p 14A, T_{on} 90µs, T_{off} 30µs) for Exp. No 7

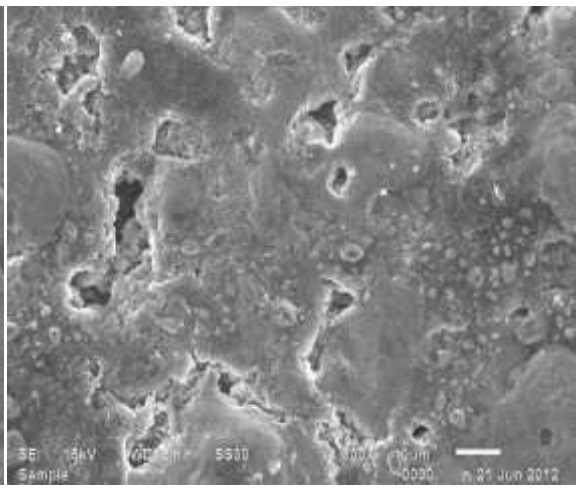

Figure 7.38: SEM Micrograph of WCT Cu-Cr Electrode when WCT Ti-6Al-4V Alloy Machined in W Powder Mixed Dielectric (I_p 14A, T_{on} 120µs, T_{off} 30µs) for Exp. No 8

The SEM micrograph for experiments 7,8 and 9 shown in Figures 7.37 to 7.39 of the electrodes obtained after machining of different grades of titanium alloys at I_p of 14A machined at T_{on} 90µs, 120µs, 150µs respectively. Due to high heat energy (I_p14A and T_{on} 150µs), wider and deeper surface cracks were observed on SCT Cu-W electrode and had a

higher TWR and poor electrode finish. A number of spherical shaped particles were observed on the electrode surface as shown in Figure 7.37 and 7.38 for experiment number 7 and 8.

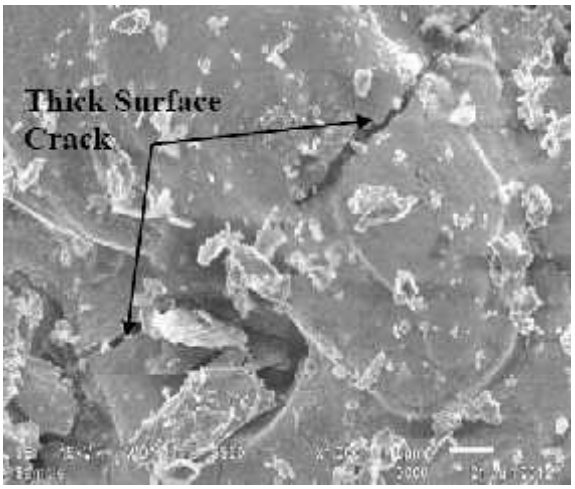

Figure 7.39: SEM Micrograph of SCT Cu-W Electrode when SCT Ti Alloy Machined in EDM Oil Dielectric for (I_p 14A, T_{on} 150µs, T_{off} 30µs) Exp. No. 9

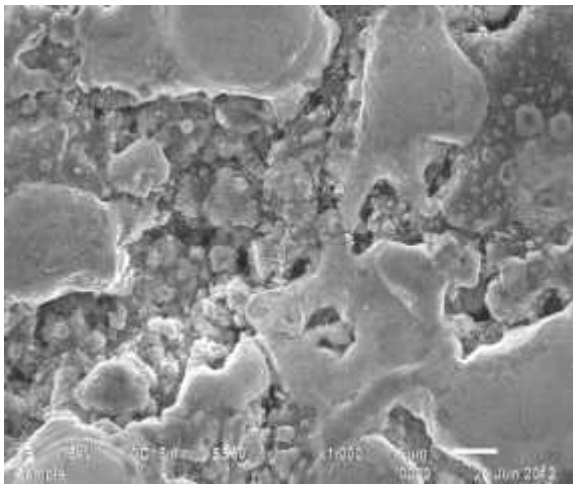

Figure 7.40: SEM Micrograph of SCT Cu-W Electrode when WCT Ti-5Al-2.5Sn Alloy Machined in W Powder Mixed Dielectric (I_p 6A, T_{on} 90 µs, T_{off} 45µs) for Exp. No. 10

The SEM micrograph of SCT Cu-W, DCT Cu and WCT Cu-Cr electrode observed after machining of Ti alloys at I_p 6A, T_{off} 45µs for different T_{on} (90µs, 120µs, 150µs) corresponding to experiments 10, 11 and 12 are shown in Figures 7.40 to 7.42. Small size of craters, lumps of debris, deposition of melted particles, sub surface crack (Figure 7.41) were observed on the electrode surface as also seen in Figures 7.40 and 7.42.

At a lower value of current 6A, the amount of generated thermal energy is less, thus, material was removed from the tool surface in the form of small craters. Moreover, intensity of developed thermal stresses due to low heat energy was reduced, thus reducing the number of surface cracks or micro cracks on the surface of tool material. The thickness of recast layer was also reduced. At higher T_{off} 45µs sufficient time was available for cooling and flushing of melted particles. The wear of Cu-Cr electrode for the same current setting was less than copper electrode, because of the presence of Cr as an alloying element in the copper, which increases its hardenability, wear and abrasion resistance. Thus, its surface characteristics were less affected than copper electrode. The SR of Cu-Cr electrode was observed to be better as compared to the Cu or Cu-W electrode at the same current setting (see Table 4.36, Chapter 4).

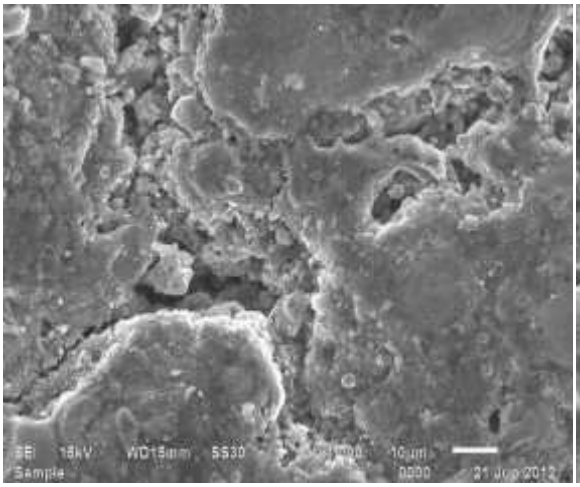

Figure 7.41: SEM Micrograph of DCT Cu Electrode when SCT Ti-6Al-4V Alloy Machined in EDM Oil Dielectric (I_p 6A, T_{on} 120µs, T_{off} 45µs) for Exp. No. 11

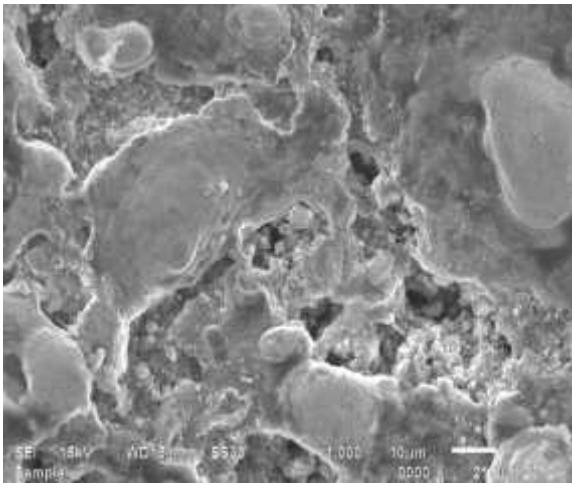

Figure 7.42: SEM Micrograph of WCT Cu-Cr Electrode when DCT Ti Alloy Machined in Mn Powder Mixed Dielectric (I_p 6A, T_{on} 150µs, T_{off} 45µs) for Exp. No. 12

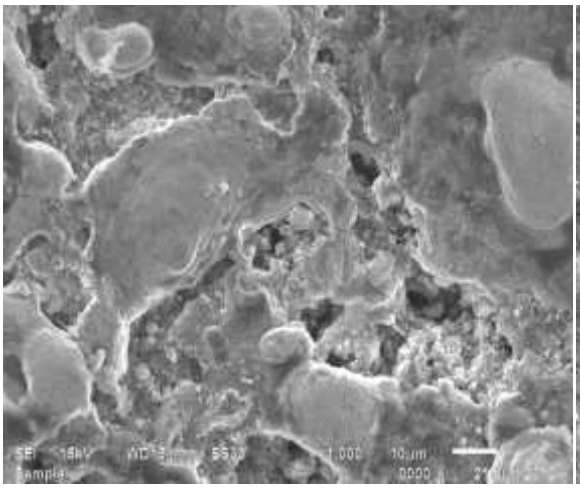

Figure 7.43: SEM Micrograph of WCT Cu-W Electrode when SCT Ti-6Al-4V Alloy Machined in Mn Powder Mixed Dielectric (I_p 10A, T_{on} 90µs, T_{off} 45µs) for Exp. No. 13

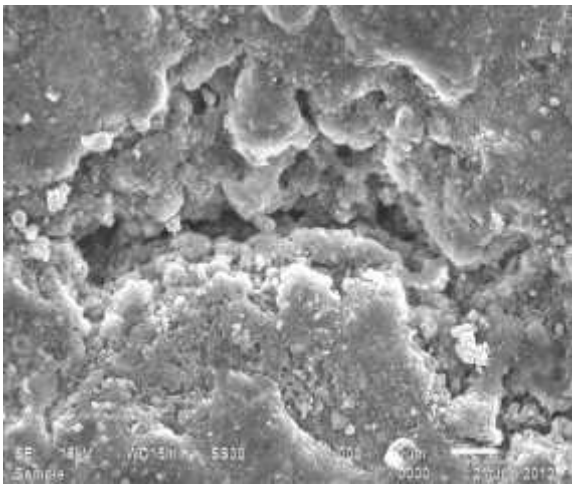

Figure 7.44: SEM Micrograph of SCT Cu Electrode when DCT Ti Alloy Machined in W Powder Mixed Dielectric (I_p 10A, T_{on} 120µs, T_{off} 45µs) for Exp. No. 14

Figures 7.43 to 7.45 represent the micrograph for experiments 13, 14 and 15 completed at I_p 10A, T_{off} 45µs for different T_{on} 90µs, 120µs and 150µs respectively using different electrodes. Due to the higher I_p, surface defects on electrode surface increased as shown in Figures 7.43 to 7.45. A number of spherical particles can be seen in SEM micrographs. Further, it was also

observed that slight increase in T_{off} from 30 to 45 µs, deposition of molten metal in compound form increased, thereby improving the surface finish of the electrode surface.

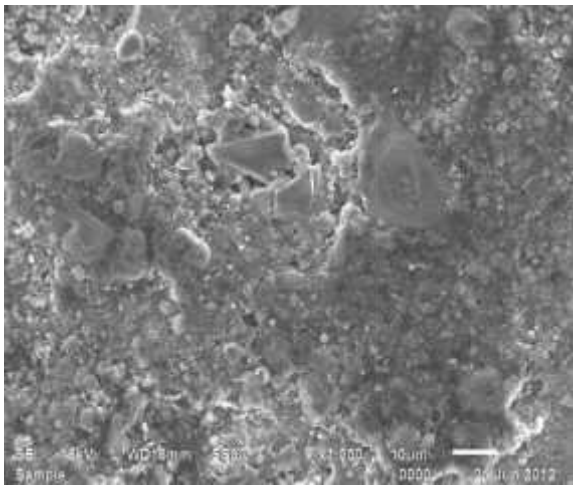

Figure 7.45: SEM Micrograph of DCT Cu-Cr Electrode when WCT Ti-5Al-2.5Sn Alloy Machined in EDM Oil Dielectric (I_p 10A, T_{on} 150µs, T_{off} 45µs) for Exp. No. 15

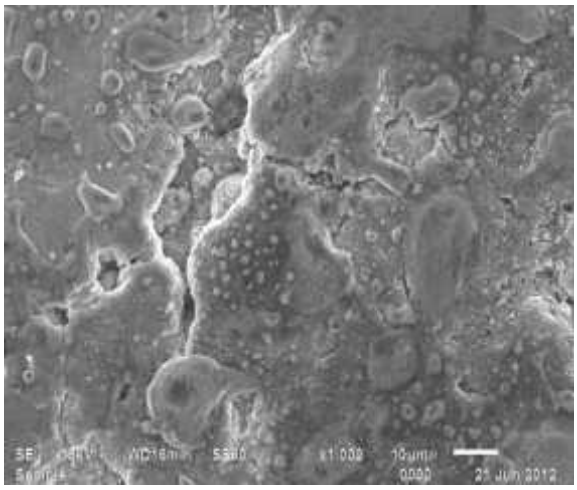

Figure 7.46: SEM Micrograph of DCT Cu-Cr Electrode when SCT Ti Alloy Machined in W Powder Mixed Dielectric (I_p 14A, T_{on} 90µs, T_{off} 45µs) for Exp. No. 16

The SEM micrographs of the three electrode surfaces obtained after machining of work pieces at I_p 14A for various T_{on} 90µs, 120µs, 150µs respectively and T_{off} 45µs are shown in Figures 7.46 to 7.48 respectively. The micrograph corresponds to experiment number 16, 17 and18 of the main experiment. SEM images showed a rough surface at high I_p of 14A. For trial 18, maximum SR of electrode surface (Ra 5.09) was observed during machining WCT Ti-6Al-4V alloy work material with an SCT Cu electrode. Due to the high value of current more discharge energy was available in the spark zone, resulting in the formation of deeper and larger size of craters on the bottom surface of the electrode. The tool's surface finish was affected. The bigger size of spherical globule particles can be clearly seen in the SEM pictures for experiments 16 to 18 as shown in Figures 7.46 to 7.48. On account of high discharge energy, thermal stresses were developed on the surface of tool material due to continuous heating and cooling of the material. As a result, cracks were produced on the tool surface, resulting in the poor surface finish.

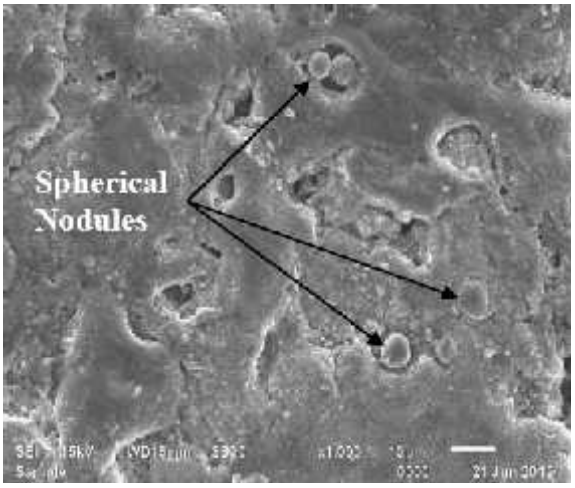

Figure 7.47: SEM Micrograph of WCT Cu-W Electrode when DCT Ti-5Al-2.5Sn Alloy Machined in EDM Oil Dielectric (I_p 14A, T_{on} 120 µs, T_{off} 45 µs) for Exp.No. 17

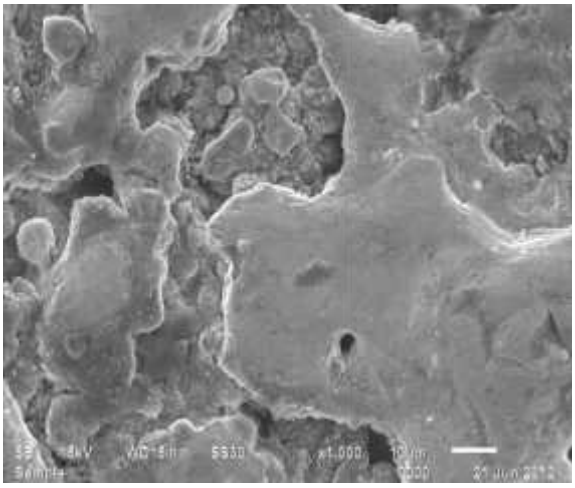

Figure 7.48: SEM Micrograph of SCT Cu Electrode when WCT Ti-6Al-2.4V Alloy Machined in Mn Powder Mixed Dielectric (I_p 14A, T_{on} 150 µs, T_{off} 45 µs) for Exp.No. 18

Further, it was observed that the overall micro structure of samples is heterogeneous which consist of the larger size of spherical carbides because of higher temperature on the workpiece as well as tool surfaces. In addition to that, the formation of martensite structure was observed on the tool surface due to the rapid quenching of tool material in dielectric media. However, area which was affected by the high temperature/heat due to high peak current 14A was deeper in the case of Cu-W electrode for experiment 17), for WCT Cu-Cr electrode of experiment 12 and for SCT copper electrode of experiment 18. Whereas, it was less deep at 6A current in case of WCT Cu-Cr tool for experiment 12. Due to the re-solidification of melted materials which was not carried away by the dielectric, lumps of debris were observed on the tool surfaces for experiments 10, 12, 13, 16, 17.

7.4.2 EDX ANALYSIS OF ELECTRODE SURFACE

Figure 7.49 (a to r) shows the EDX spectrums of different tool electrode materials for experiment number 1-18 to determine the chemical composition of the tool surface. Due to high thermal energy generated in the spark zone, the materials was also removed from the surface of the electrode, but significantly lower than what is eroded from the surface of workpiece surface. Carbon was decomposed from dielectric and produced in the form of hard carbides of titanium (TiC), deposited back on the lower surface of tool. The other

elements such as: oxygen, aluminum, manganese and tungsten were also observed on the tool surface.

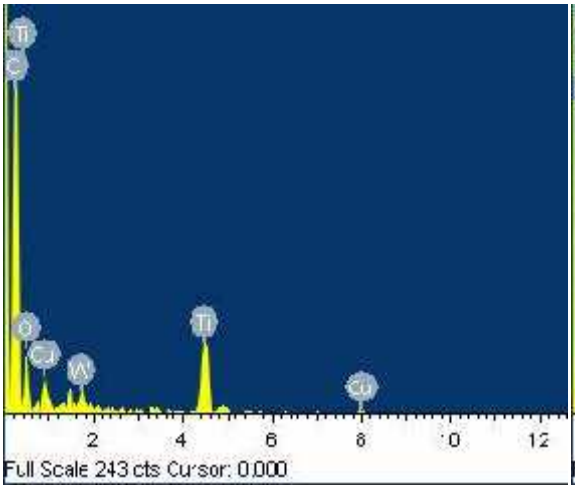

Figure 7.49 (a) Exp. No. 1

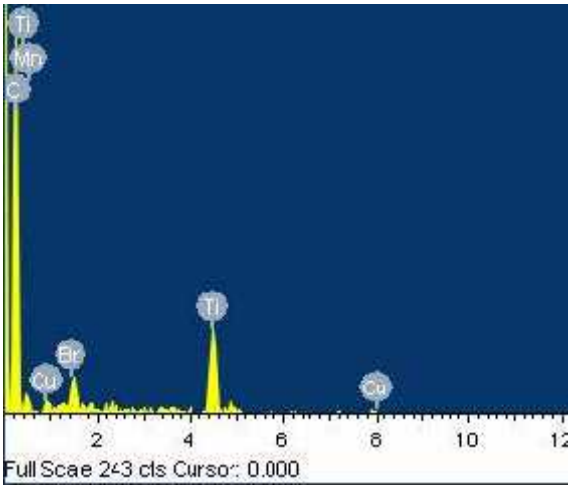

Figure 7.49 (b) Exp. No. 2

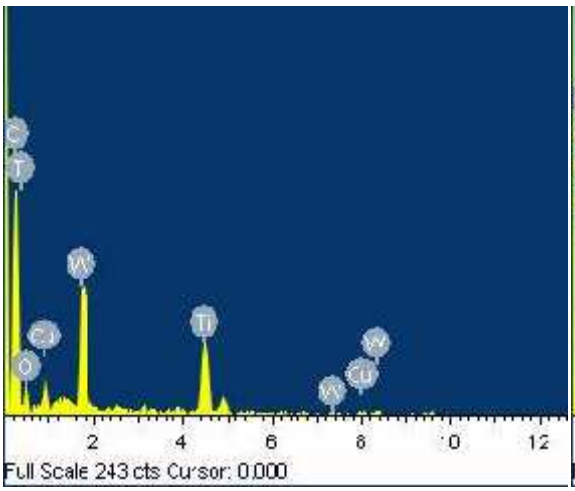

Figure 7.49 (c) Exp. No. 3

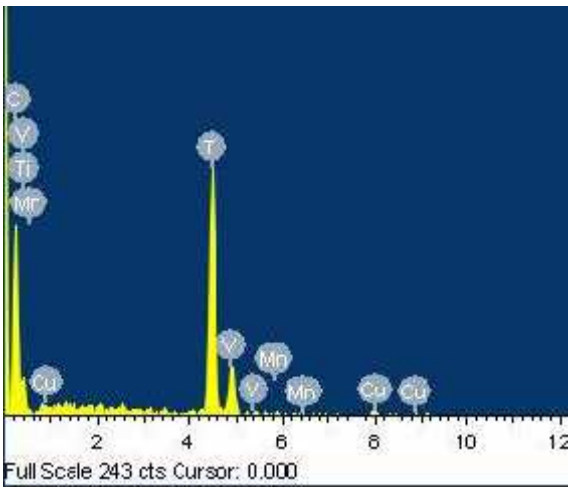

Figure 7.49 (d) Exp. No. 4

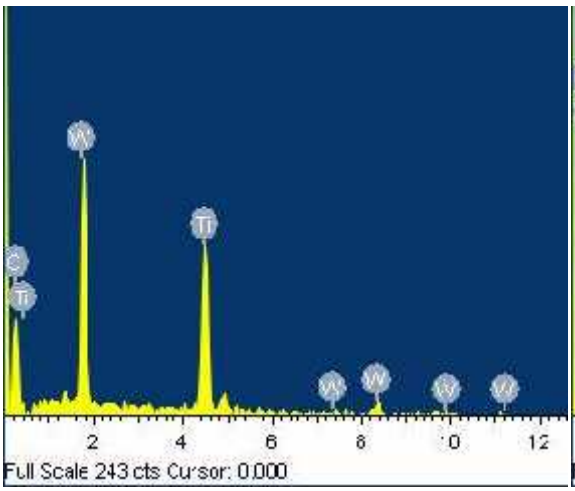

Figure 7.49 (e) Exp. No. 5

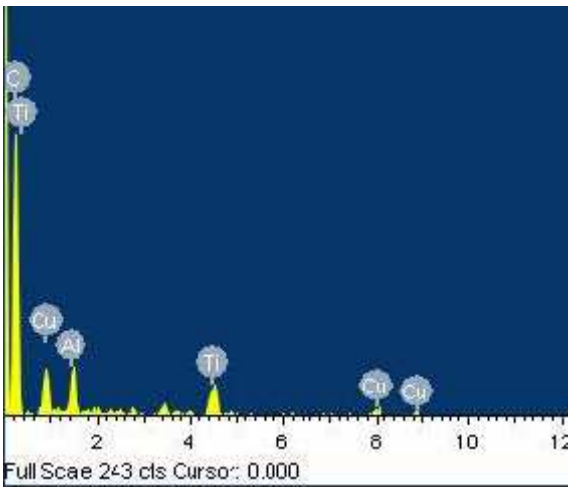

Figure 7.49 (f) Exp. No. 6

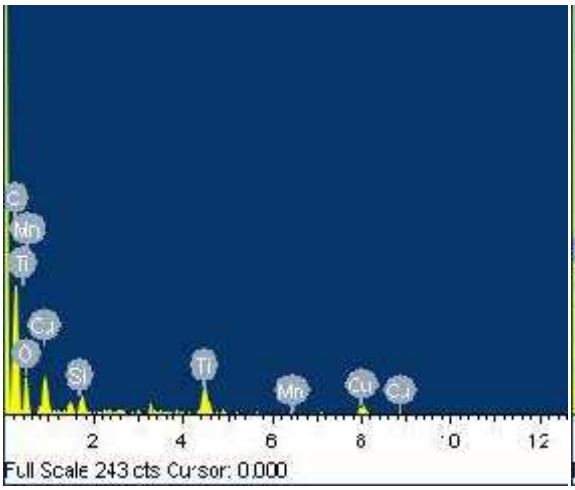

Figure 7.49 (g) Exp. No. 7

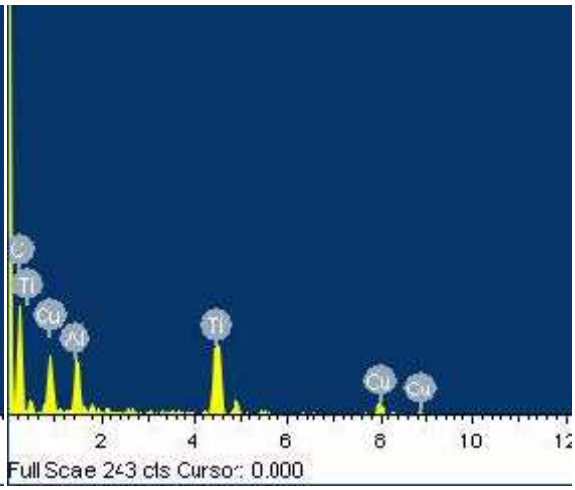

Figure 7.49 (h) Exp. No. 8

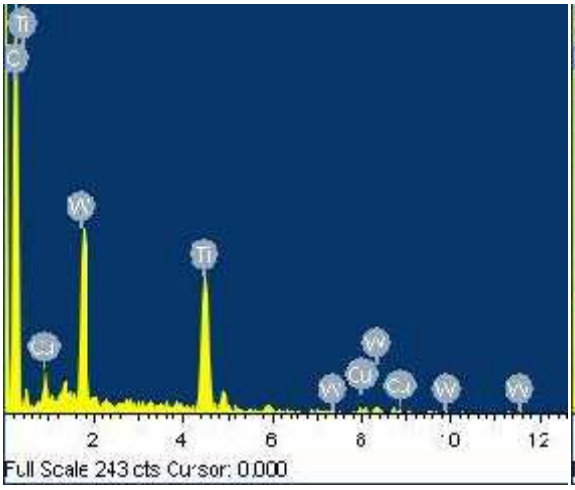

Figure 7.49 (i) Exp. No. 9

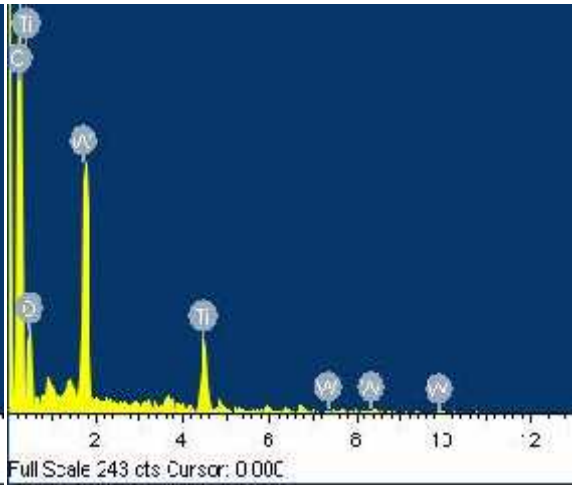

Figure 7.49 (j) Exp. No. 10

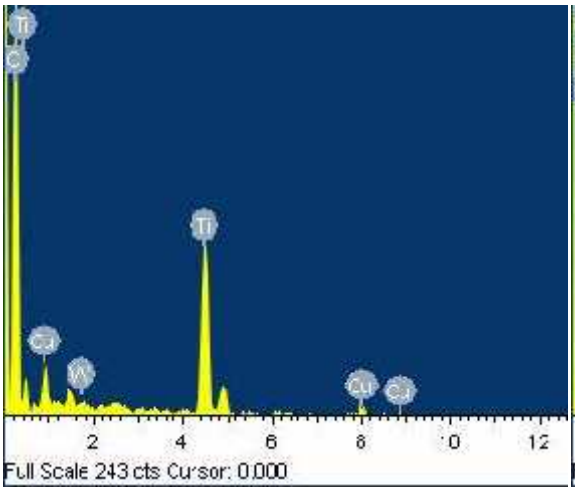

Figure 7.49 (k) Exp. No. 11

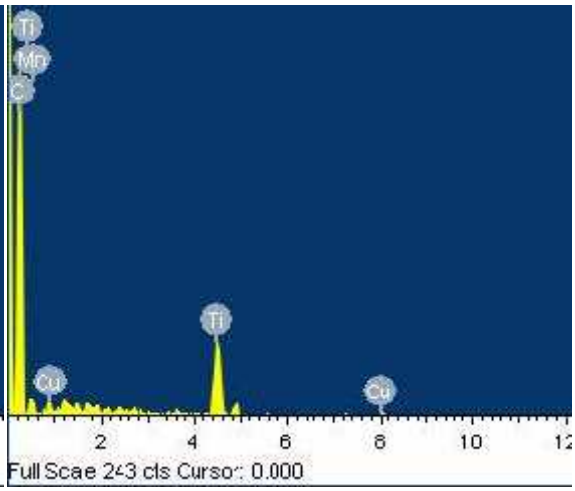

Figure 7.49 (l) Exp. No. 12

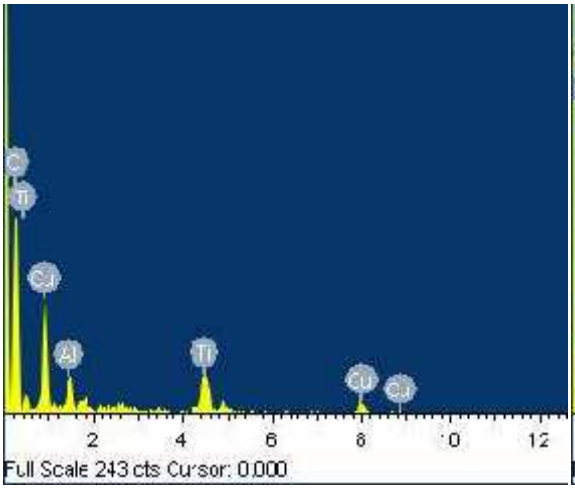

Figure 7.49 (m) Exp. No. 13

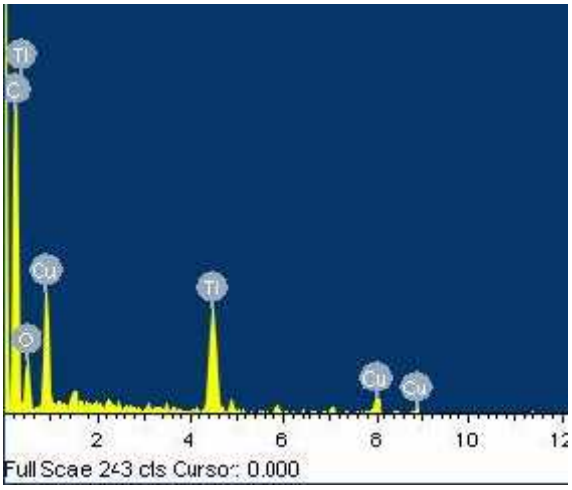

Figure 7.49 (n) Exp. No. 14

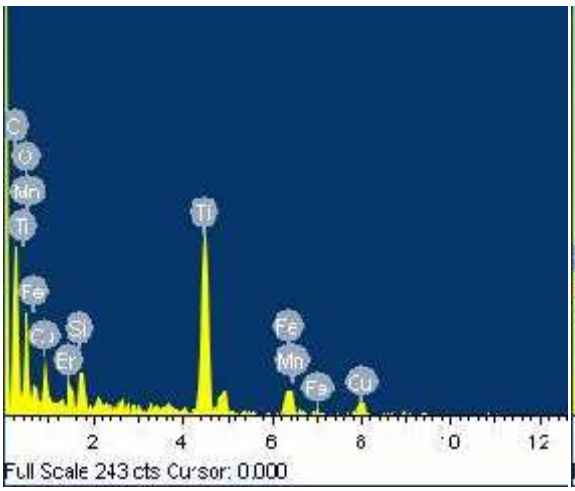

Figure 7.49 (o) Exp. No. 15

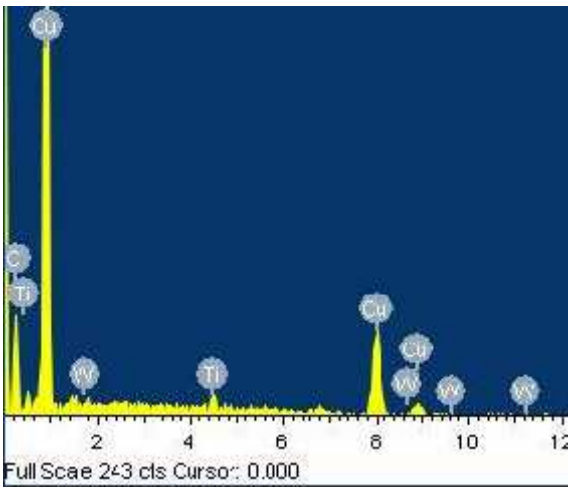

Figure 7.49 (p) Exp. No. 16

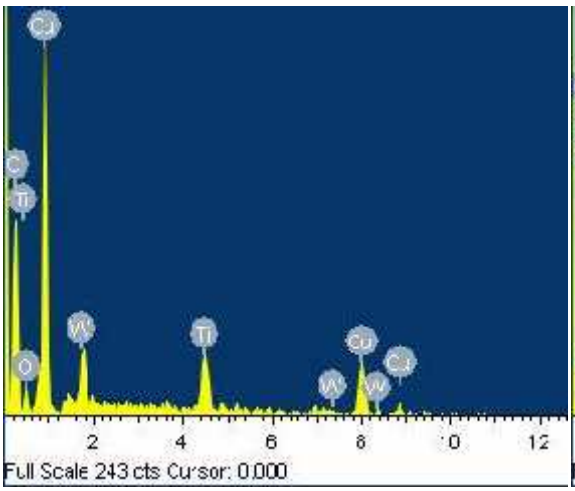

Figure 7.49 (q) Exp. No. 17

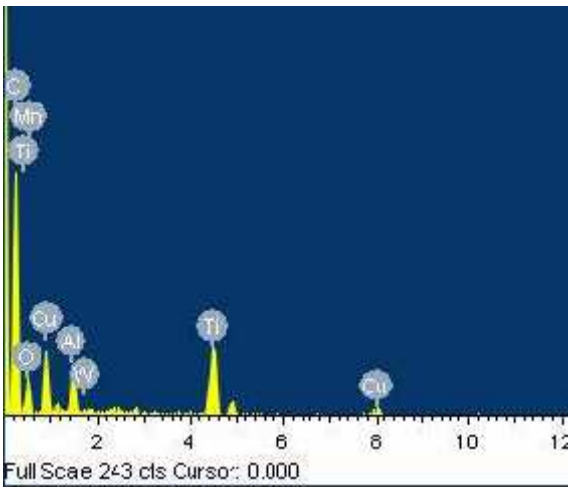

Figure 7.49 I Exp. No. 18

Figure 7.49 (a to r): EDX Spectrum of Different Tool Materials (Exp.No. 1-18)

The weight percentage of migrated Ti and C elements were higher as compared to other elements seen on tool surface as shown in Figures 7.49 (a to r) corresponding to experiments 1-18. The different migrated elements can be seen in the EDS spectra in the form of peaks. From the EDX analysis, it was concluded that high peaks indicates the higher value of elements present in the tool material. Thus, different chemical phases were formed due to the transfer of different materials, as indicated on the XRD patterns. A summary of different migrated elements observed on the tool surface is presented in Table 7.2, and Figure 7.50 shows the graphical representation of various elements

Table 7.2: Summary of Different Elements Observed on Tool Surfaces

Experiment	Equivalent weight (%) of different elements							
Number	C	O	Ti	Cu	Mn	W	Al	Other Elements
1	55.31	24.52	13.84	4.07	0.08	0.80	-----	Fe = 1.38
2	67.23	9.15	14.51	5.16	0.03	-----	3.06	Br = 0.90
3	60.56	11.20	11.90	1.40	0.20	13.20	0.70	Br = 0.87
4	60.92	4.95	20.50	9.94	0.14	0.51	2.21	V = 0.85
5	57.31	4.55	20.43	0.25	-----	16.79	0.70	
6	63.30	10.13	20.69	2.27	-----	-----	1.10	Ca =2.12, Si =0.38
7	55.86	26.59	5.62	10.36	0.29	-----	0.50	K = 0.4, Si = 0.38
8	60.42	6.45	27.43	3.63	-----	0.50	1.39	Cr = 0.19
9	44.53	4.11	8.00	9.33	-----	15.61	0.24	Mg = 18.2
10	48.86	5.14	6.39	1.17	-----	38.45	-----	
11	64.86	10.17	23.64	0.71	0.10	0.30	-----	Si = 0.24
12	61.92	-----	35.72	1.23	0.40	0.30	0.44	
13	66.54	-----	5.34	4.61	-----	22.80	0.71	
14	66.26	19.45	10.35	3.04	-----	-----	-----	K=0.2,S=0.3,Si=0.4
15	44.73	8.08	13.60	16.04	0.05	2.45	0.60	Fe = 13.4, Si = 0.37
16	57.30	2.56	15.50	23.78	0.39	0.22	0.23	
17	53.10	6.97	9.13	5.38	-----	25.48	-----	
18	55.30	16.15	12.58	14.55	0.09	0.30	1.03	

C = Carbon, O = Oxygen, Ti = Titanium, Cu =Copper, Mn = Manganese, W = Tungsten, Al = Aluminum, Fe = Ferrous, Ca = Calcium, Cr = Chromium, K = Potassium, Mg = Magnesium, Si = Silicon, S = Sulphur, V = Vanadium, Br = Beryllium

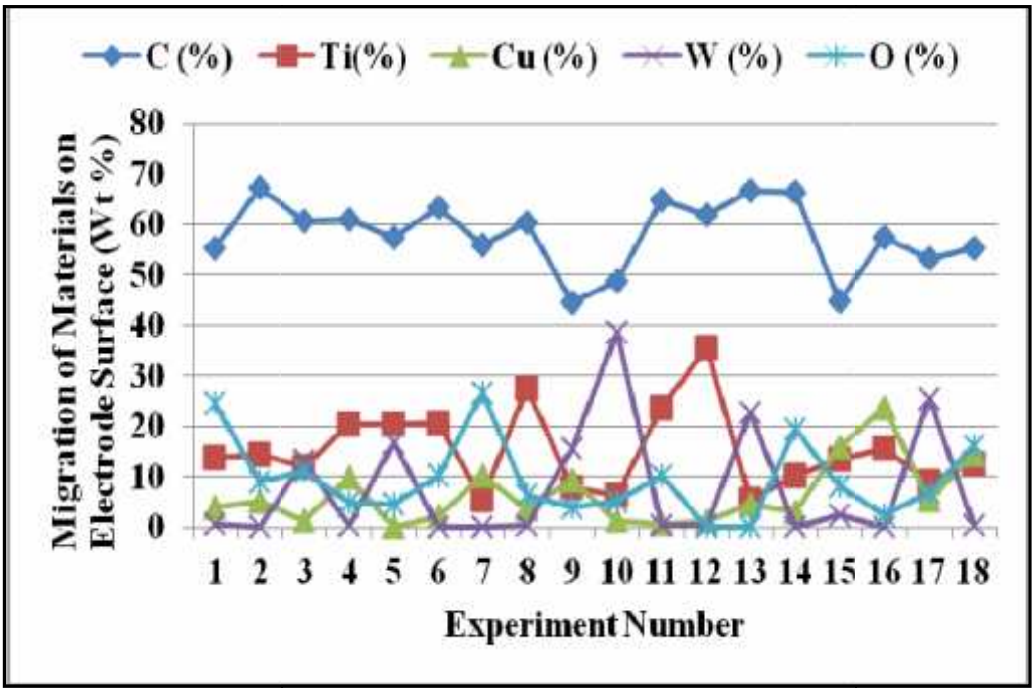

Figure 7.50: Migration of Different Materials on Surface of Different Electrodes

7.4.3 XRD ANALYSIS OF ELECTRODE

In order to confirm the formation of different chemical compounds and phases, XRD analysis was performed on selected tool samples. Before XRD analysis, all the tool samples were properly cleaned using acetone solution. XRD analysis confirmed the migration of different elements from workpiece and powder mixed dielectric on tool surface and then interaction with the parent elements in copper based tool materials (Cu, Cr, and W) and then produced various compounds or phases in carbide form or oxide form, which deposited on the tool surface. Figure 7.51 shows the XRD pattern of the WCT Cu-Cr electrode observed after EDM of DCT Ti 15 titanium machined at current of 6A, T_{on} of 150µs, T_{off} of 45µs in Mn powder added dielectric (experiment 12). The XRD pattern shows the formation of compounds such as TiC also called Hongquiite, Nickel-Aluminum-Titanium-Carbide (Al0.5Cni$_3$Ti0.5), and Aluminum-Titanium-Oxide (Al_2TiO_5) at different 2θ scale. Elements Ti and Al were transferred from the work material and C from dielectric.

The hard TiC compounds were observed in the pattern at different 2-theta angles 36.0, 41.790, 60.528, 72.436, 74.207, 101.896, and 105.517 as shown in Figure 7.51. The highest peak of TiC was observed at 74.207 2-theta angle with maximum counts 15306. Nickel-Aluminum-Titanium-Carbide *(Al0.5Cni3Ti0.5)* was also observed with count 12693 at 2-

theta position 43.41. Small traces of Aluminum-Titanium-Oxide (Al_2TiO_5) with low score can also be seen in the XRD pattern at the different 2θ angles 26.22, 41.79, 50.66, 60.53, 74.21, 76.18, 101.78, 105.52. Moreover, the formation of some other low score compounds such as Magnesium-Aluminum-Titanium-Oxide ($Mg_2Al_6Ti_7O_{25}$), Sodium-Iron-Titanium-Oxide ($NaFeTiO_4$), Copper-Chromium-Manganese-Oxide, Chromium-Titanium-Oxide (Cr_4Ti_4O) were also observed during the analysis.

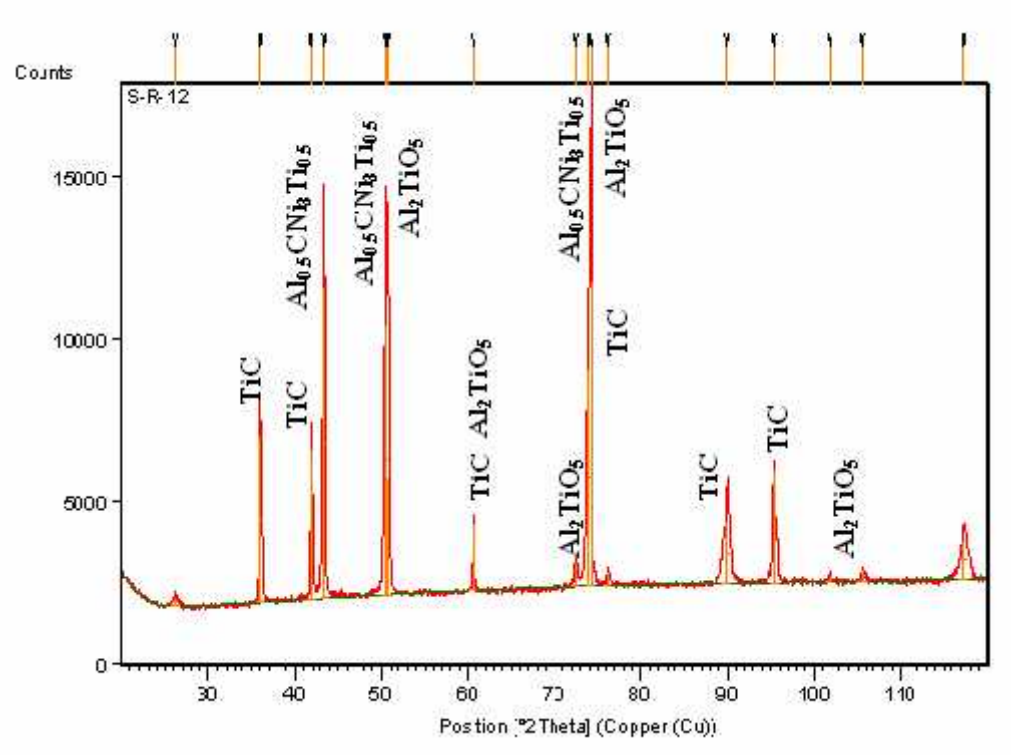

Figure 7.51: XRD Pattern of Cu-Cr Electrode (WCT) after the Machining of Ti (DCT) for Exp. No. 12 ($A_2B_1C_3D_2E_2F_1G_1H_3$)

Another case shown in Figure 7.52 shows the XRD pattern of WCT Cu-Cr electrode obtained after machining of DCT Ti-5Al-2.5Sn titanium alloy in a simple dielectric (without powder) at (I_p of 14A, T_{on} of 120µs and T_{off} of 45 µs). Titanium-Carbide (TiC), Aluminum-Titanium-Carbide ($Al_2Ti_4C_2$), Tin-Titanium-Carbide ($SnTi_2C$), Nickel-Aluminum-Titanium-Carbide (Al0.5Cni$_3$Ti0.5), Titanium-Tungsten-Carbide (WtiC) were observed at different 2-theta positions from 34.70 to 114.94 as shown in Figure 7.52. Moreover, the formation of some other low score compounds were also observed such as Titanium-Zinc-Carbide (Zn_2Ti_4C), Zinc-Iron-Titanium-Oxide ($ZnFeTiO_4$), but due to a very low value, these compounds are not shown on the XRD pattern.

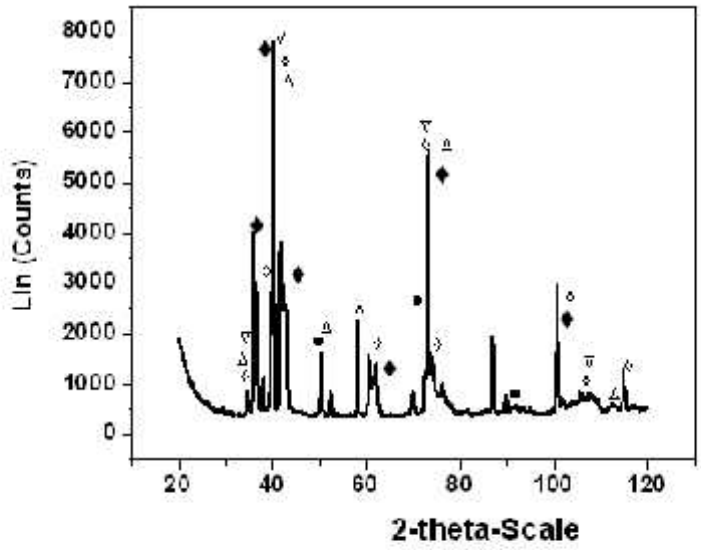

▽ - Aluminum Titanium Carbide, Δ - Tu. Titanium Carbide, ● - Nickel Aluminum Titanium Carbide, ▽ Titanium Tungsten Carbide, ♦ - Titanium Carbide

Figure 7.52: XRD Pattern of Cu-W Electrode (WCT) after the Machining of Ti-5Al-2.5Sn Alloy (DCT) for Exp.No. 17 ($A_2B_3C_2D_1E_3F_1G_2H_3$.)

Figure 7.53 for experiment 18 shows the XRD pattern of SCT copper electrode observed during the machining of WCT Ti-6Al-4V alloy at I_p 14A, T_{on} 150 µs, T_{off} 45 µs with Mn powder mixed dielectric. The presence of different elements, namely Ti, C, O, Mn, and Al were observed on the copper electrode surface due to migration from workpiece surface and Mn powder mixed dielectric. These migrated elements formed different compounds such as Titanium-Carbide, Nickel-Aluminum-Titanium-Carbide, Manganese-Titanium-Oxide, and Copper-Titanium-Oxide at different 2-theta position, which are shown in the XRD pattern. From Figure 7.53, it can be seen that hard black compound TiC with high score observed in the XRD pattern at 2θ positions 36.02, 41.83, 72.53, 74.12, 76.30, and 102.01. Other low weightage compounds were also formed such as Manganese-Titanium-Oxide (Mn_2TiO_4) noticed at 2θ angle 36.015, 60.61; Nickel-Aluminum-Titanium-Carbide (Al0.5Cni$_3$Ti0.5) at 2θ angle 43.32, 50.4671 and Copper-Titanium-Oxide (Cu_2TiO_3) at 2θ angle 43.32. The highest peak of Nickel-Aluminum-Titanium-Carbide ($Al_{0.5}Cni_3Ti_{0.5}$) with maximum counts 56506 was observed at 2θ position 50.472. Moreover, traces of white compound of Titanium-Oxide (TiO) were noticed at the different 2θ position with maximum count of 5068 observed at 2θ value 41.825.

Further, some other compounds were also observed such as Manganese-Titanium-Oxide (Mn_2TiO_4), Sodium-Iron-Titanium-Oxide ($NaFeTiO_4$), Copper-Titanium-Oxide (Cu_2TiO_3), Honguiite (TiO), Iron-Titanium-Oxide (FeTiO), Rutile (TiO_2), Aluminum-Titanium-Oxide (Al_2TiO_5), Nickel-Titanium-Oxide (Ni_5TiO_7). But, due to their very low weightage, these precipitated compounds are not shown in the XRD pattern.

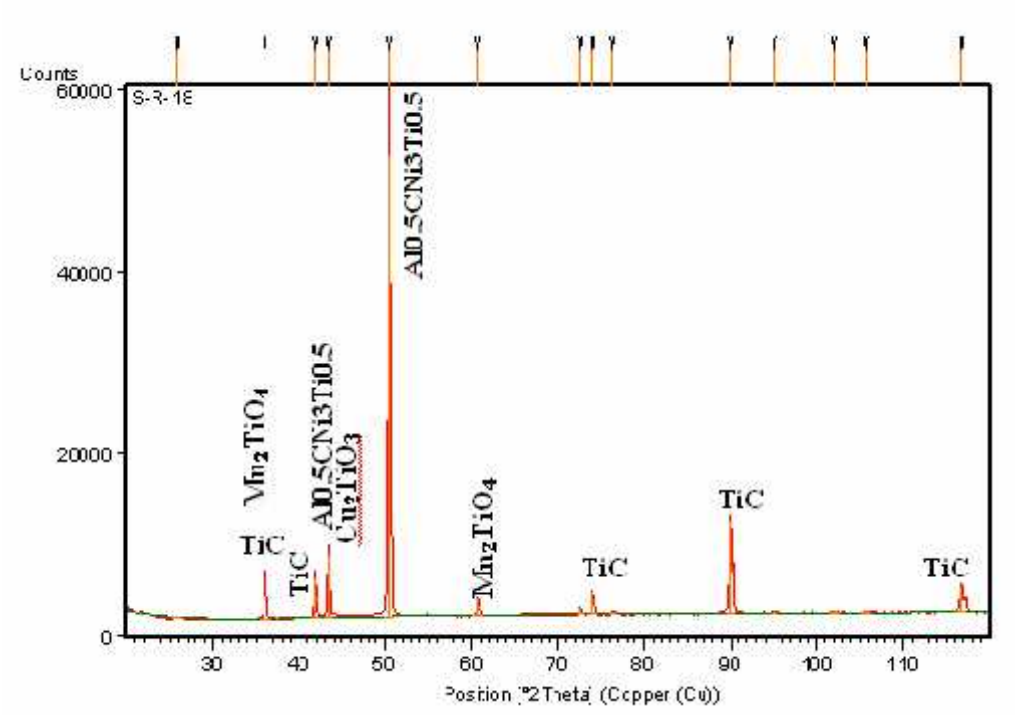

Figure 7.53: XRD Pattern of Cu Electrode (SCT) after the Machining of Ti-6Al-4V Alloy (WCT) for Exp.No. 18 ($A_2B_3C_3D_2E_1F_2G_3H_1$)

7.5 METALLOGRAPHIC ANALYSIS OF TITANIUM ALLOY WORKPIECES FOR PHASE-C EXPERIMENTATION

During Phase-C, the metallographic analysis of the WCT and DCT selected samples were analyzed by using SEM, EDX and XRD analyzer.

7.5.1 MICROSTRUCTURE ANALYSIS

The micro structural analysis of selected WCT and DCT titanium alloy (Ti, Ti-5Al-2.5Sn, Ti-6Al-4V) samples after PMEDM were studied by using SEM micrographs (×500 and 1000) magnification and is shown in Figures 7.54 to 7.58. From the literature and experimental

results, it was concluded that I_p and T_{on} are the key factors which highly affected the quality of the machined surface. The SEM images for the WCT and DCT titanium alloy, showed much damaged surface due to the formation of various surface defects such as micro-cracks, surface cracks, voids, craters of different sizes, pockmarks, melted drops, globules of debris. All these surface defects were responsible for poor surface finish represented by an uneven surface profile. The experimental results are also in line with this observation.

TITAN 15: SEM image of two samples corresponding to experiment-1 during machining of TITAN 15 at I_p 6A, T_{on} 90 µs, T_{off} 45 µs for both WCT and DCT of workpiece with an untreated copper electrode in Mn powder suspended dielectric is shown in Figures 7.54 (a & b). Due to low spark energy at 6A current, fewer micro cracks and small size of pin holes were observed on the surface. Traces of white oxide (TiO) can also be seen on the machined surface due to the oxidation of Ti in the dielectric. Due to low spark energy, a small quantity of cracked carbon from dielectric medium was transferred on the machined surface. This leads to deposition of carbon on machined surface either in free form or compound form (TiC). Transfer of Cu, Zn from copper electrode and Mn from powder mixed dielectric took place resulting in the formation of their chemical compound as shown in XRD analysis.

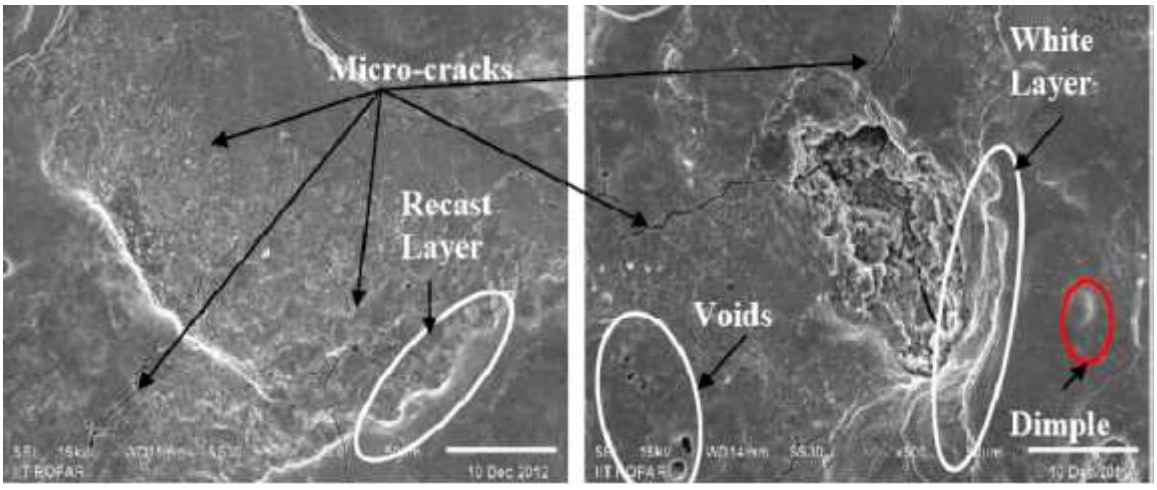

(a) WCT TITAN 15 (b) DCT TITAN 15

Figure 7.54: SEM Image of TITAN 15 Alloys for Experiment-1 (I_p =6A, T_{on}= 90µs, T_{off} =45µs and Electrode= WCT Cu)

Figure 7.55 (a & b) represent the ED-machining at I_p 14A, T_{on} 150 µs, T_{off} 45 µs with WCT Cu-Cr electrode. Due to high current and pulse-on-time, the level of spark energy is increased very high as compared to 6A and 90µs T_{on}, resulting in rough and unequal machined surface (see Figure 7.55). Due to high spark energy available at 14A current, more surface cracks

were observed in the SEM images. The large size of craters and appendages were observed in WCT Ti15 than DCT Ti15 alloy for the same experimental condition as shown in Figure7.55. The micrographs show a number of thick cracks around the region with compounds deposition due to high thermal energy. Lumps of deposited compounds more clearly visible indicated by the red circle in the untreated SEM photograph than DCT picture. The details of the compound formation are presented in XRD analysis. The average SR for WCT and DCT was observed as 7.49 Ra and 7.18 Ra respectively, for experiment 9 which shows the improvement in surface characteristics.

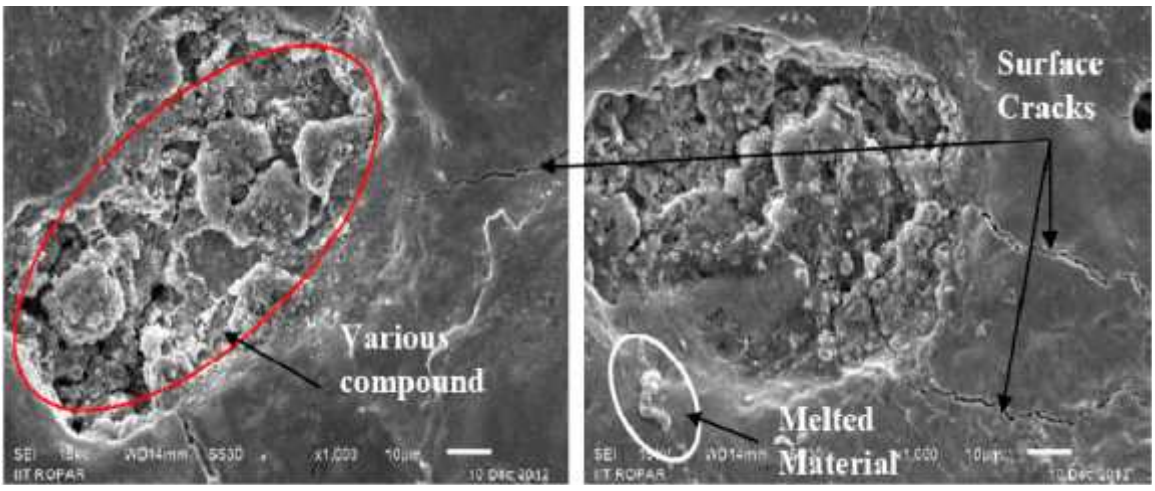

(a) WCT TITAN 15 (b) DCT TITAN 15

Figure 7.55: SEM Image of TITAN 15 Alloys for Experiment-9
(I_p =14A, T_{on}= 150µs, T_{off} =45µs and Electrode= WCT Cu-Cr)

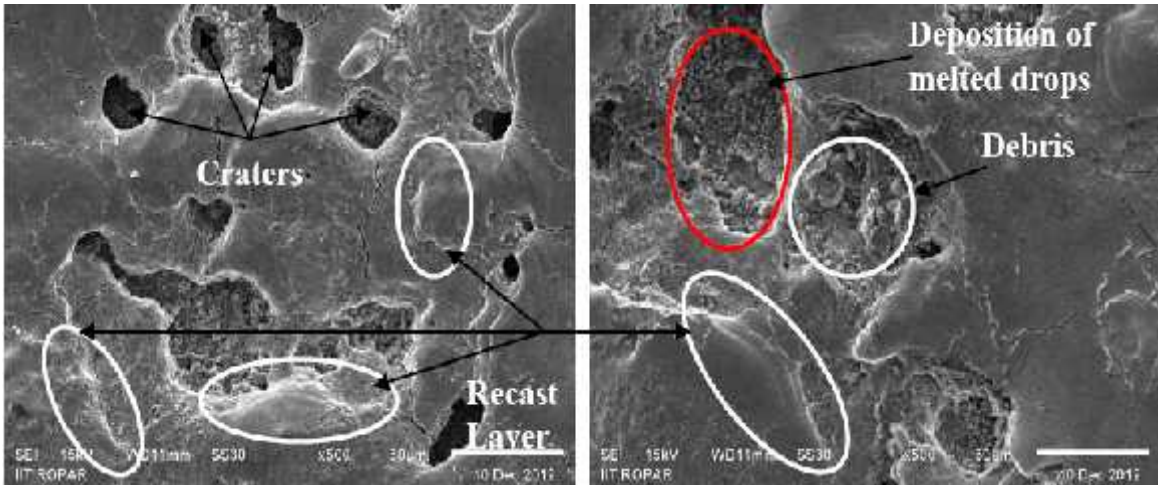

(a) WCT TITAN 21 (b) DCT TITAN 21

Figure 7.56: SEM Image of TITAN 21 (Ti-5Al-2.5Sn) Alloys for Experiment-9
(I_p =14A, T_{on}= 150µs, T_{off} =45µs and Electrode= WCT Cu-Cr)

TITAN 21: The SEM micrographs of the WCT and DCT Ti-5Al-2.5Sn titanium alloy are shown in Figure 7.56 (a & b) for experiment 9. WCT Cu-Cr electrode was used to machine the samples at I_p 14A, T_{on} 150µs, T_{off} 45µs with Mn powder added dielectric. Due to high I_p 14A, large number of big craters of bigger can be seen in the SEM image (Figure 7.56 a) than DCT alloy, resulting in higher MRR and poor surface finish. Comparatively thinner and less numbers of cracks were observed on the DCT Ti-5Al-2.5Sn alloy. Due to high I_p 14A and longer T_{on} 150µs recast layer with cracks was observed on the machined specimen. Smoother surface was observed in case of DCT alloy than WCT alloy.

***TITAN 31*:** The SEM micrographs of the WCT and DCT Ti-6Al-4V titanium alloy are shown in Figure 7.57 for experiment 5. The machining conditions of experiment 5 is I_p =10A, T_{on}= 120µs, T_{off} =45µs and electrode material = WCT Cu-W. The FERROLAC 3M EDM Oil with Mn powder was used as a dielectric medium for the machining. While comparing SEM micrographs of the WCT and DCT, significant changes can be observed after machining. High number of voids can be clearly seen in SEM micrograph of WCT Ti-6Al-4V (Figure 7.57a) due to poor thermal/electrical conductivity of work materials than DCT material. On both the surfaces, thicker cracks were observed due to high thermal energy and cooling by dielectric. Thicker recast layer was observed in case of DCT alloy. Overall smoother surface texture was observed in DCT alloy as can be seen in Figure 7.57b.

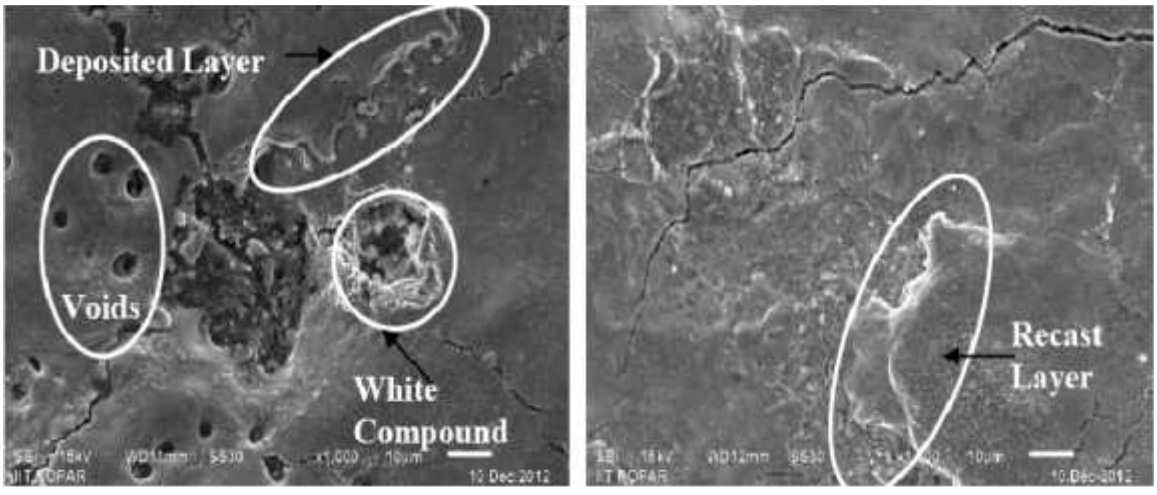

(a) WCT TITAN 31 (b) DCT TITAN 31

Figure 7.57: SEM Image of TITAN 31 (Ti-6Al-4V) Alloys for Experiment-5 (I_p =10A, T_{on}= 120µs, T_{off} =45µs and Electrode= WCT Cu-W)

Figure 7.58 (a & b) shows the SEM image of WCT and DCT Ti-6Al-4V machined at (I_p =14A, T_{on}= 150µs, T_{off} =45µs) with Cu-Cr electrode in Mn powder mixed dielectric. The

comparatively much damaged surface was observed in case of machining of WCT alloy than DCT alloy (see in Figure 7.58 a & b). In both micrographs bigger/deeper size of craters were clearly visible, resulted in higher MRR with poor surface texture. Compounds of TiC and $Al_2Ti_4C_2$ were also observed on the machined surface. In addition to TiC and $Al_2Ti_4C_2$ other different compounds were also formed during the EDM process. Due to the continuous excessive heating and rapid cooling a distorted layer of martensitic structure can be seen. Due to the oxidizing of Ti-6Al-4V, a white layer (TiO) was formed on the surface which can be clearly visible in the SEM micrographs. The thickness of this white layer can be controlled by proper setting of input parameters, because it was in direct contact with the atmosphere. Due to the formation of these carbide and oxide compounds or layers, machining efficiency of process was reduced, because these layers take more time to melt and vaporize, but the micro-hardness of machined surface was increased.

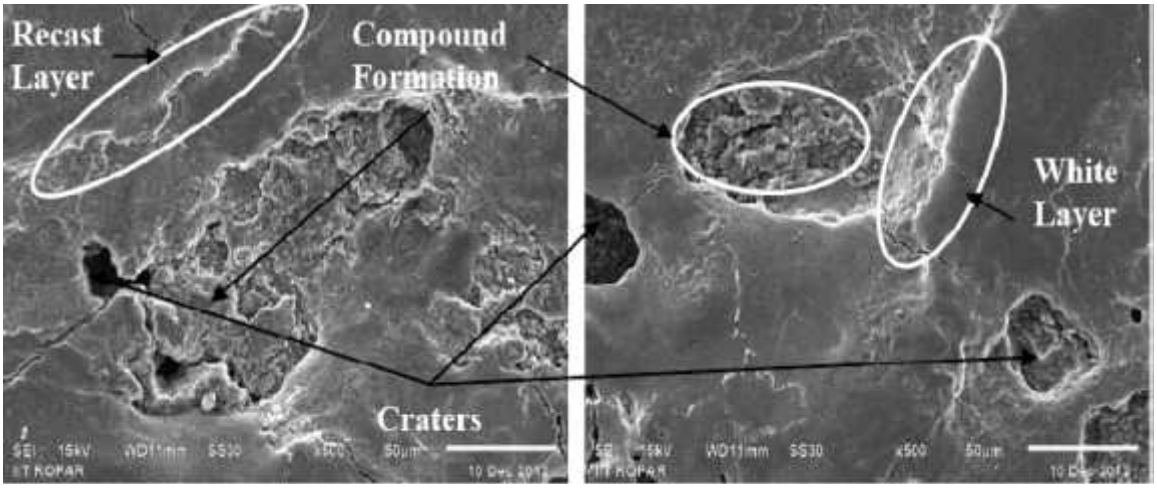

(a) WCT TITAN 31 (b) DCT TITAN 31

Figure 7.58: SEM Image of TITAN 31 (Ti-6Al-4V) Alloys for Experiment-9 (I_p =14A, T_{on}= 150µs, T_{off} =45µs and Electrode= WCT Cu-Cr)

7.5.2 EDX ANALYSIS

The results of the EDX analysis of the selected samples are shown in Figures 7.59 to 7.63. The key elements in chemical composition of the PMEDM surface were Ti, Al, V, Sn, which are the constituent of the base metal such as Ti 15, Ti 21 and Ti 31 titanium alloys. Further, presence of residuals of C, O, Mn, Cu, W, and Cr were also noticed on the machined surface in layers form or compounds form. Carbon was the major element precipitated on the machined surface either in free form or compound due to its decomposition. The elements of electrode material can also be seen in the EDX images due to their transfer at high temperature. The weight percentage of chemical elemental compositions depended on the machining conditions.

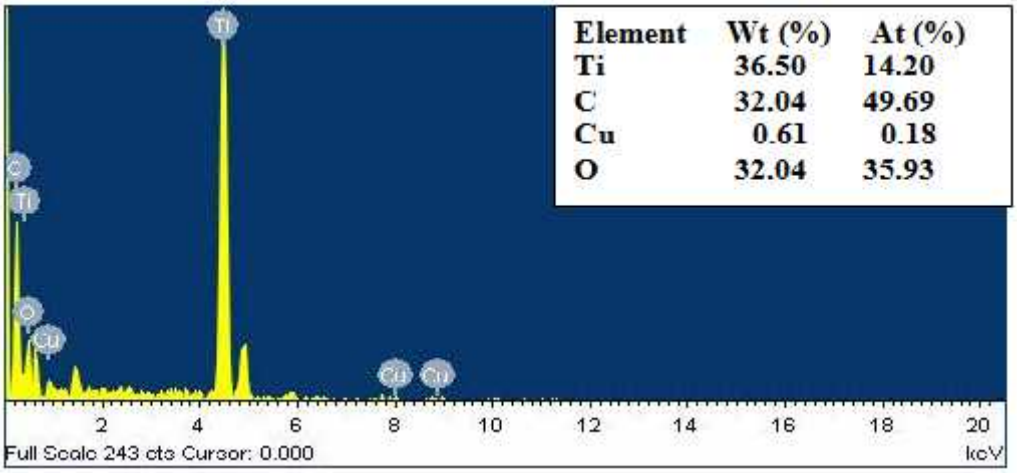

Figure 7.59: EDX Analysis on Machined Surface of DCT TITAN 15 Sample (I_p =6A, T_{on}= 90µs, T_{off} =45µs and Electrode= WCT Cu)

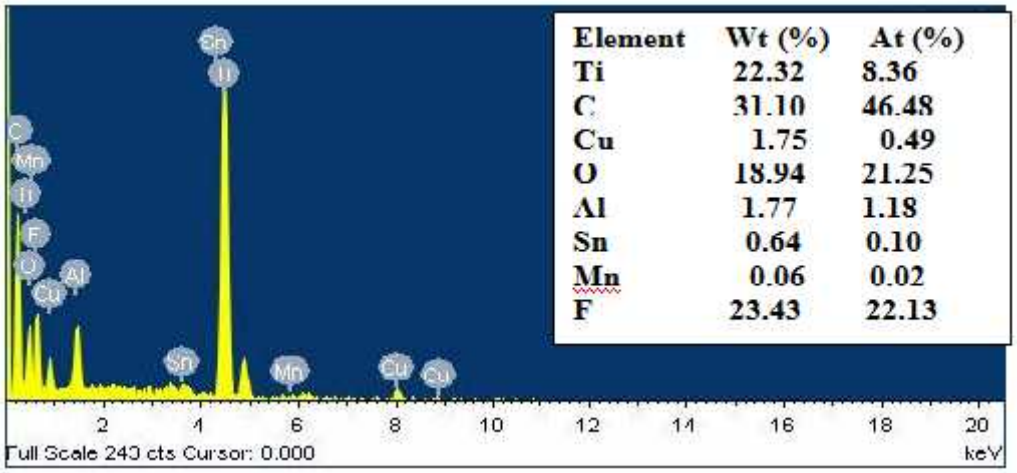

Figure 7.60: EDX Analysis on Machined Surface of WCT Ti-5Al-2.5Sn Sample (I_p =14A, T_{on}= 150µs, T_{off} =45µs and Electrode= WCT Cu-Cr)

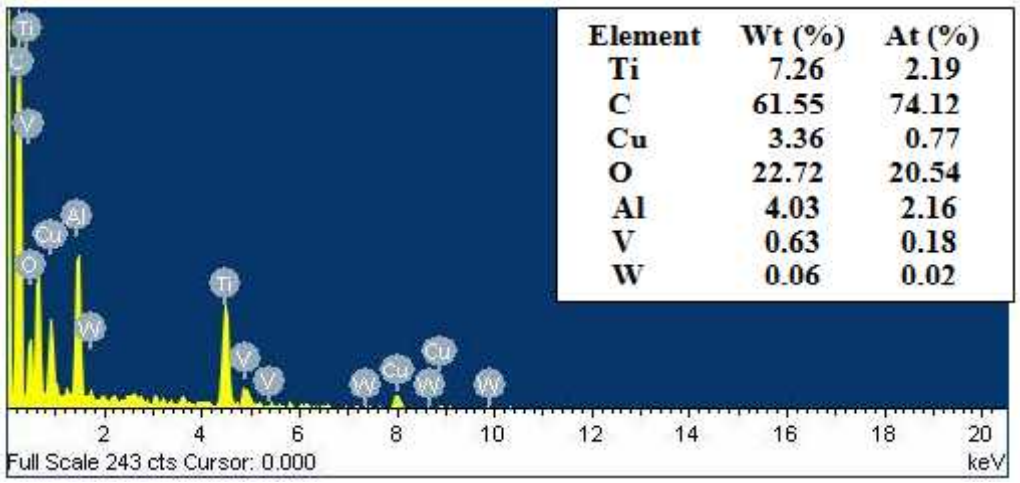

Figure 7.61: EDX Analysis on Machined Surface of WCT Ti-6Al-4V Sample (I_p =10A, T_{on}= 120µs, T_{off} =45µs and Electrode= WCT Cu-W)

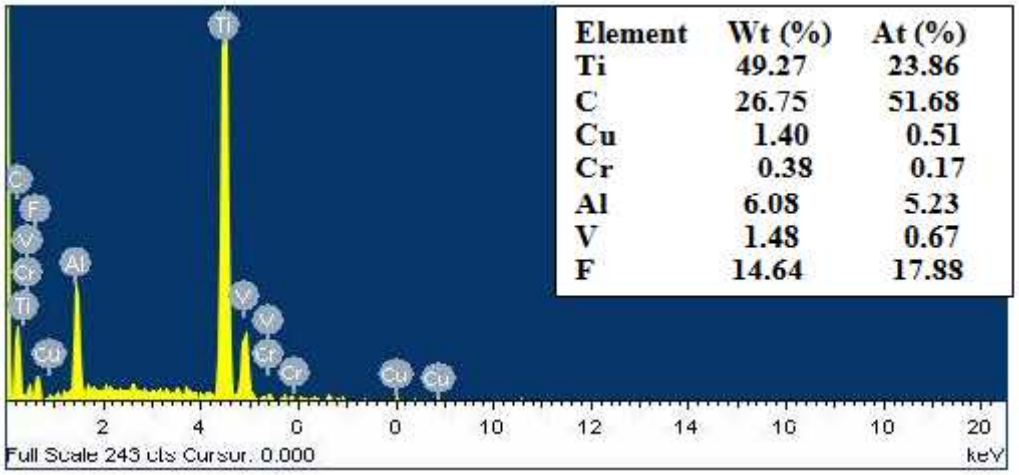

Figure 7.62: EDX Analysis on Machined Surface WCT Ti-6Al-4V Sample (I_p =14A, T_{on}= 150µs, T_{off} =45µs and Electrode= WCT Cu-Cr)

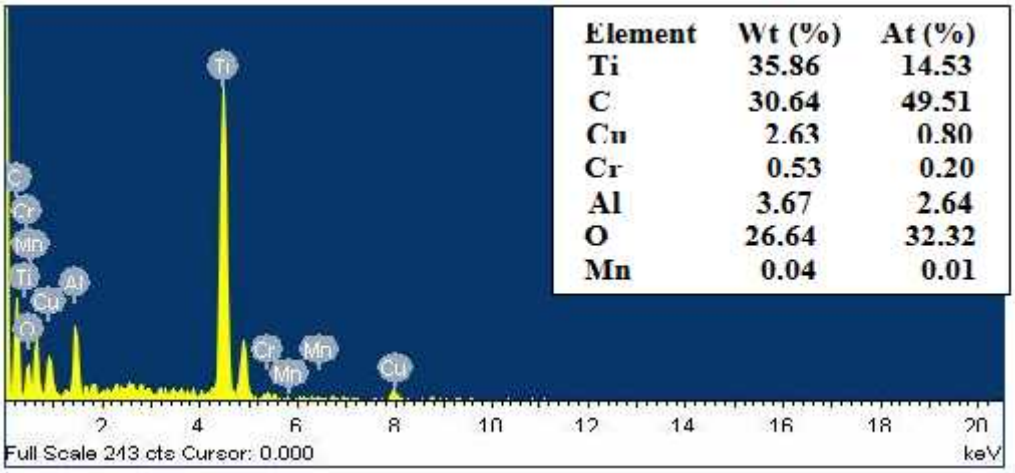

Figure 7.63: EDX Analysis on Machined Surface of DCT Ti-6Al-4V Sample (I_p =14A, T_{on}= 150µs, T_{off} =45µs and Electrode= WCT Cu-Cr)

7.5.3 XRD ANALYSIS

The XRD analyses of some selected samples were conducted which are explained in the following section:

TITAN 15: Figure 7.64 shows the XRD analysis of the DCT Ti 15 titanium alloy machined at parameters setting of I_p 6A, T_{on} 90µs, T_{off} 45µs and WCT Cu electrode in Mn powder added dielectric (Trial 1). The plot shows the formation of main compound TiC at the various 2θ positions (36.07, 41.87, 60.61, 72.64, 76.24, 90.94, 101.95, and 105.57). The traces of Manganese-Titanium-Oxide (Mn_2TiO_4) were also observed due to transfer of Mn powder from dielectric as shown in Figure 7.64. The other compounds were also formed on machined

surface such as Titanium-Carbide-Sulphide ($Ti_4C_2S_2$), Zinc-Titanium-Carbide (Zn2Ti4C) and Copper-Titanium-Oxide (Cu_3Ti_3O), but due to low weightage, these compounds are not shown on the XRD pattern

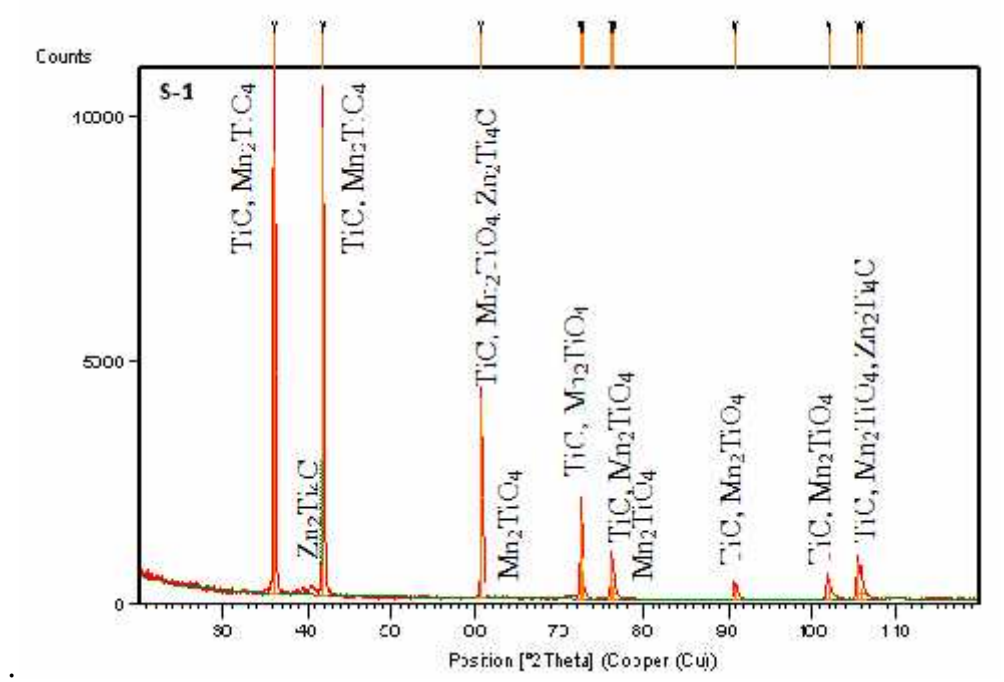

Figure 7.64: XRD Analysis on Machined Surface of DCT TITAN 15 Sample (I_p =6A, T_{on}= 90µs, T_{off} =45µs and Electrode= WCT Cu)

TITAN 21: The outcome of XRD analysis (experiment 9) for EDMed WCT TITAN 21 (Ti-5Al-2.5Sn) work sample is presented in Figure 7.65, machined at I_p 14A, T_{on}=150µs, T_{off} 45µs with WCT Cu-Cr electrode in Mn powder added dielectric. Three major compounds were formed during the process which is shown in the XRD pattern (see Figure 7.65). The highest sorcing chemical compound Titanium-Carbide (Ti_8C_5) was observed at various 2θ values 36.01, 41.81, 60.54, 72.43, and 76.20. The other Carbon-Titanium (TiC) compound was observed at different 2θ positions 36.01, 41.81, 60.54, 72.43, 76.20, 90.85, and 101.81. The traces of Aluminum-Titanium-Carbide ($Al_2Ti_4C_2$) can also be seen at various 2θ angles 40.39, 60.54, 72.43, 76.20, 101.81 and 105.54. The weight of $Al_2Ti_4C_2$ is very less as compared to Ti_8C_5 and TiC compound. Further, in addition to the above said compounds, some other compound such as Titanium-Carbide-Sulphide ($Ti_4C_2S_2$), Copper-Titanium-Oxide (Cu_3Ti_3O), Titanium-Carbide-Nitride ($C_{0.7}N_{0.3}Ti$), Tin-Titanium-Carbide ($SnTi_2C$), Manganese-Titanium-Oxide (Mn_2TiO_4) and Copper-Titanium-Oxide (Cu_3Ti_3O) were also

formed, but due to low weight percentage these are not presented in XRD pattern (Figure 7.65).

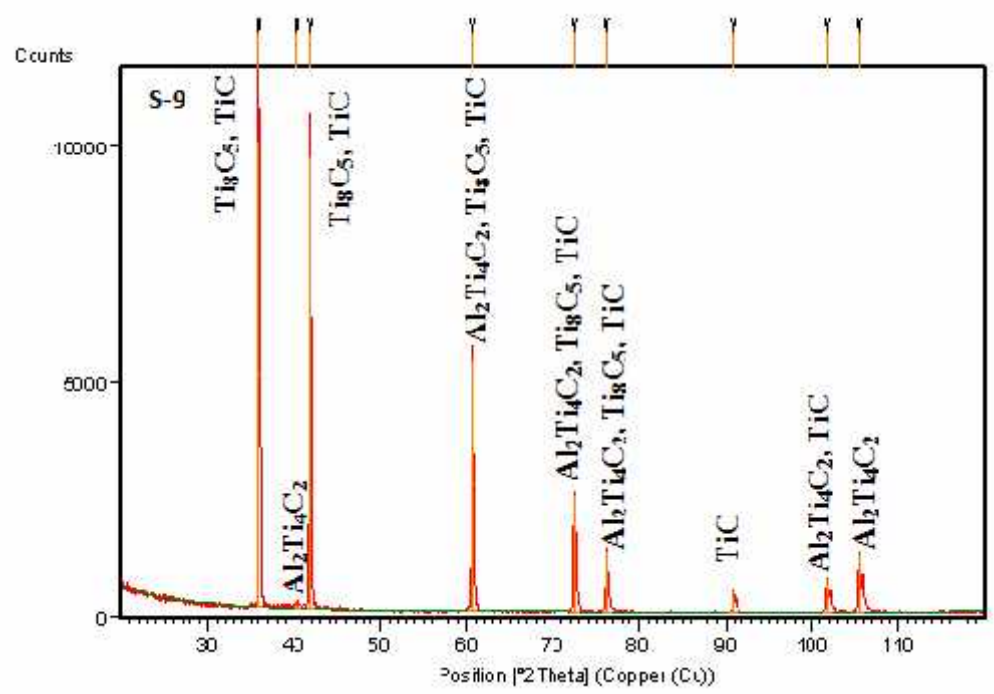

Figure 7.65: XRD Analysis on Machined Surface of WCT TITAN 21 Sample (I_p =14A, T_{on}= 150µs, T_{off} =45µs and Electrode= WCT Cu-Cr)

TITAN 31: The XRD pattern for the trial conditions of untreated TITAN 31 (Ti-6Al-4V) machined with Cu-W tool in Mn powder blended dielectric at a setting of I_p 10A, *Ton* 120µs and T_{off} 45µs for experiment 5 is shown in Figure 7.66. The XRD pattern shows the formation of TiC, $Al_2Ti_4C_2$ at various 2θ angles. TiC compound was observed at 2θ positions 36.13, 41.94, 60.73, 72.76, 76.45, 91.15, and 102.17. The other compound $Al_2Ti_4C_2$ was noticed at 39.86, 60.73, 102.17 and 106.09. Traces of some other compounds, namely Titanium-Vanadium-Carbide ($Ti_{0.11}V_{0.89}C_{0.50}$), Titanium-Carbide-Nitride ($C_{0.7}N_{0.3}Ti$), Titanium-Carbide-Nitride-Hydrite ($TiC_{0.3}N_{0.6}H_{0.08}$), Manganese-Titanium-Oxide (Mn_2TiO_4) and Copper-Titanium-Oxide (Cu_3Ti_3O), Titanium-Tungsten-Oxide ($Ti_{0.54}W_{0.46}O_2$), Titanium-Vanadium-Oxide ($TiVO_4$), Copper-Nickel-Titanium-Oxide ($CuNi_{0.5}Ti_{0.5}O_2$) were observed, but due to their low weightage these are not seen in the XRD pattern.

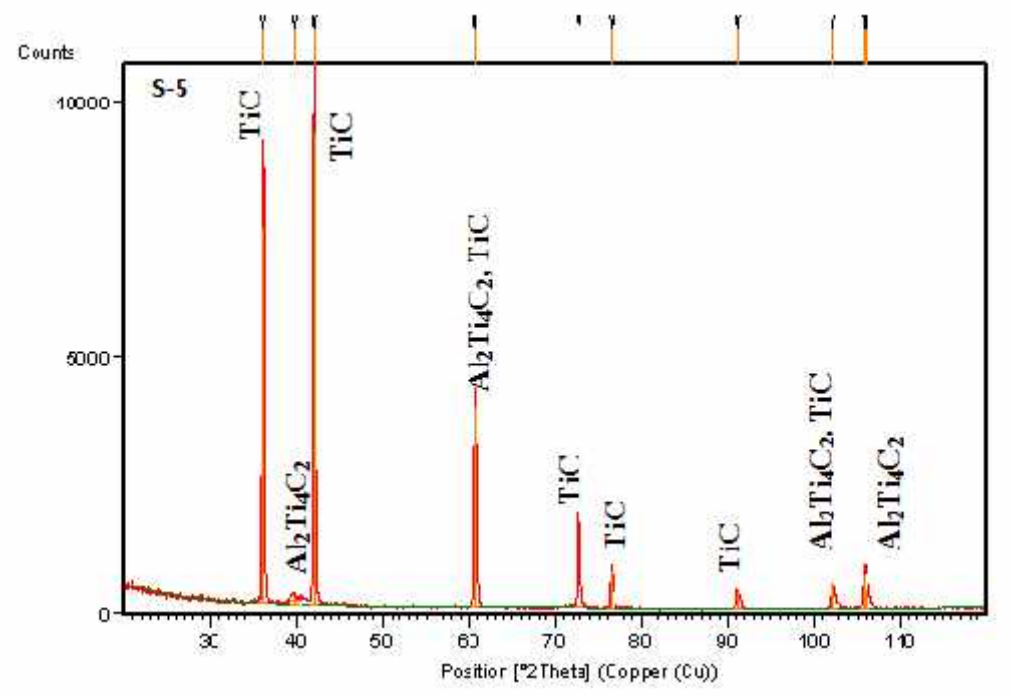

Figure 7.66: XRD Analysis on Machined Surface of WCT Ti-6Al-4V Sample (I_p =10A, T_{on}= 120µs, T_{off} =45µs and Electrode= WCT Cu-W)

Chapter 8

CONCLUSIONS AND SCOPE FOR FUTURE WORK

8.1 CONCLUSIONS

This chapter presents a summary of the experimentation, results thereof, the conclusions drawn from the research work and recommendations for future work. Experimental investigation has been carried out on various grades of titanium alloy by using an EDM process with different set of parameters. The study covers the experimentation, statistical evaluation and metallographic analysis. The information obtained from the experimental results and statistical analysis by observing the values and plots of the response characteristics versus machining input parameters and their contribution showed that I_p is the most significant machining parameter that highly affected the machining performance followed by T_{on}.

After summarizing the key aspects of the experimental observed results, the following conclusions may be drawn:

8.1.1 CONCLUSIONS FOR MAIN EXPERIMENTATION (PHASE-A)

In Phase-A main experimentation, three grades of titanium alloys (Ti 15, Ti 21 and Ti 31) were machined with Cu, Cu-Cr and Cu-W electrodes. The cryogenic treatment (shallow and deep) was applied on both workpiece and tool materials. Two types of powders Mn and W were mixed with the dielectric liquid. The machining performance was measured in terms MRR, TWR, SR and micro-hardness. From the experimental results, the following conclusions have been drawn:

1. During the EDM process spark energy increases as the value of I_p and T_{on} increases, which affect the machining performance *i.e* MRR, TWR, SR, micro-hardness and surface integrity of machined samples. Higher MRR was observed at high value of I_p (14A) and T_{on} (150µs) at the cost of higher TWR and poor surface finish.
2. Though T_{off} has no effect on MRR and TWR, but it has a significant effect on surface roughness and micro-hardness. Longer T_{off} duration, *i.e.* 45µs reduces the MRR, but improves the surface finish and micro-hardness of the machined parts.

3. Arcing on workpiece or electrode surface was noticed at higher I_p value (14A), longer duration of T_{on} (150µs) and smaller duration of T_{off} (30µs). Due to arcing the machining efficiency was reduced in terms of low MRR, poor surface finish, higher TWR and more deposition of carbon on the machined surface.
4. Cu-Cr electrode gives a higher MRR, low TWR, better surface finish than Cu and Cu-W material.
5. Cu-W tool improves the surface hardness, but its wear rate is high as compared with the other two electrodes.
6. The addition of powders (Mn & W) with the dielectric liquid had smaller effects on the response characteristics such as MRR (1.26%), TWR (1.62%), surface finish (3.03%) and micro-hardness (1.06%).
7. The workpiece properties and machining parameters highly affected the machining characteristics. The Ti-6Al-4V and Ti-5Al-2.5Sn titanium alloy significantly affected the MRR, SR and micro-hardness than Ti 15 alloy. Workpiece contributes on MRR, SR and MH was 8.2 %, 7.59 % and 5.48 % respectively.
8. The TWR was highly affected by the properties of tool material. From the study, it was concluded that tool material has 19.30 % contribution on TWR.
9. A mathematical model considering the significant machine parameters and the thermo-physical properties of the workpiece and electrode materials was developed for predicting MRR and TWR using dimensional analysis approach. A third- degree polynomial equation was found to be the best fit curve after experimental validation with a high coefficient of correlation. The developed mathematical model shows good agreement when compared to the observed experimental results.
10. In EDM process, the various thermo-electric properties of the workpiece and tool materials have performed an important role on the response characteristics.
11. Peak current was observed as the most significant factor, followed by T_{on} and T_{off} and workpiece material that affect the surface roughness.
12. The structural design of Artificial Neural Network (ANN) was selected, trained, validated, tested and then used for simulation to optimize the surface roughness and micro-hardness. Experimental results and ANN predicted results showed good agreement. The maximum percentage relative error of 2.346% and a minimum of 0.006 % were obtained for surface roughness.

13. Micro-hardness of the machined surfaces was highly affected by current followed by pulse-off-time, type of workpiece material, pulse-on-time and types of electrode material.
14. AHP was used for optimizing all the four performance measures, namely MRR, TWR, SR and micro-hardness globally. The final results of the solution should be used only as indicator to what may be the best answer. Although the search for better result never ends.
15. Metallographic analyses were carried out by using SEM, EDX and XRD equipment of the selected samples. The discharge energy in the form of I_p and T_{on} highly affected the surface topography of the machined samples.
16. The SEM micrographs show that high discharge energy ($I_p \times T_{on}$) was responsible for producing the surface defects such as; surface or thermal cracks, craters, thick recast layer, micro pores, pin holes, residual stresses and debris.
17. Migration of different chemical elements from the electrode and dielectric media was observed on the machined surface and electrode surface as confirmed by the EDX spectrums. The presence of a large percentage of carbon was noticed in EDX analysis due to decomposition of dielectric at high temperature.
18. XRD results show the major formation of Titanium-Carbide (TiC) compound which got precipitated on the machined surface and formed a hard layer. The study provides an insight into the migration of different elements from the tool and the powder mixed dielectric fluid onto the machined surface thereby improving the surface properties.
19. High melting temperature of TiC layer, *i.e.* approx twice of titanium reduced the machining efficiency especially MRR.
20. The surface properties of tool materials were highly affected by the tool material (66.82%) followed by the current (21.68%) and on-time (9.27%).
21. The theoretical predicted values for all the response characteristics were determined by using Taguchi approach. Predicted results have been compared with the confirmatory experimental results and found within the limits of agreeable error.

8.1.2 CONCLUSIONS FOR EXPERIMENTATION (PHASE-B)

Under this Phase-B experimentation, Ti-5Al-2.5Sn alloy was machined using energy of electric spark with Cu-Cr electrode with two input parameters, I_p and T_{on} which were identified as the significant parameters in Phase-I main experimentation. Experimentation

under this plan has been performed in three ways; electric discharge machining of WCT Ti52.5 alloy, SCT Ti52.5 alloy and DCT Ti52.5 alloy. Summarizing the main features of the results, the following conclusions may be drawn:

1. From the study, it was concluded that I_p has the maximum influence on performance characteristics rather than T_{on}. The performance measures were directly proportional to the I_p, but inversely proportional to T_{on}. The likely reason for this is that as the duration of on-time increases frequency of spark occurrence decreases. It means machining performance decreases at extended pulse-on-time.
2. The observed experimental results showed improvements in the performance measures in case of EDM of DCT Ti52.5 titanium alloy as compared to SCT and WCT Ti52.5 titanium alloy.
3. The maximum gain in MRR of 21.84% for DCT and 13.92% for SCT workpiece were observed.
4. The maximum improvement in TWR of 27.40%, and a minimum of 4.96% were observed in case of DCT alloys than non-treated alloys. On the other side, maximum improvement in TWR 14.28%, and a minimum 3.07% was observed in SCT alloys.
5. The maximum reduction in Ra value of 19.58% was observed in DCT alloys while 14.60% in SCT alloys when compared with WCT alloy.
6. The micro-hardness increased in the range 2.25% to 7.20% for SCT and 6.90% to 17.30% for DCT alloy.
7. The major reason of increase in micro-hardness was the migration of cracked carbon from a dielectric medium which formed the hard layer of TiC on the machined surface.
8. The value of micro-hardness increases with increase in I_p and T_{on} and values of TWR and SR also increase at that higher value.
9. Two major compounds TiC and TiO were formed during machining which reduces machining efficiency *i.e.* decreases productivity.

8.1.3 CONCLUSIONS FOR EXPERIMENTATION (PHASE-C)

In Phase-C experimentation, the EDM performance of three variants of titanium alloys without cryogenic treatment and deep cryogenic treatment were compared. Three variants of tool materials (Cu, Cu-Cr and Cu-W) were employed for machining of titanium alloys. Effects of cryogenic treatment of tool materials on the machinability of titanium alloys were

investigated under this experimental work. The entire experiment was conducted in Mn powder suspended dielectric medium. From the experimental results, the main conclusions can be summarized as follows:

1. Peak current was observed as the most critical factor which highly affected the MRR followed by on-time and cryogenic treatment of electrode.
2. Effect of electrode material on MRR was observed to be low. However higher MRR was observed with Cu-W electrode due to presence of tungsten element as compared to Cu and Cu-Cr electrodes.
3. Higher MRR was observed with DCT electrode as compared to WCT and SCT electrode.
4. Significant increase in MRR of 19.5%, 26.8% and 29.68% for deep cryogenically treated TITAN 15, TITAN 21 and TITAN 31, respectively was observed.
5. Peak current was observed as the most significant factor, followed by cryogenic treatment of electrode material that affected the TWR.
6. Low TWR was observed with SCT copper electrode during EDM of WCT and DCT TITAN 15, whereas TWR was reduced in the machining of TITAN 21 and 31 alloys with DCT copper electrode.
7. Cryogenically treated electrode material significantly affected the TWR as observed from the ANOVA results (*Table 6.18*).
8. Significant reduction in TWR of 30.77%, 45.21% and 34.05% for DCT TITAN 15, TITAN 21 and TITAN 31, respectively was observed.
9. Peak current was observed as the leading factor that highly affected the SR followed by cryogenic treatment of electrode materials, on-time and electrode material.
10. Improvements in SR of 15.82%, 14.17% and 16.40% for DCT Ti 15, Ti 21 and Ti 31 respectively, was observed.
11. The surface modification of machined surface was measured by its hardness, and experimental result showed that the maximum increase in micro-hardness of 107.78% was noticed during PMEDM of WCT Ti 15 alloy and, 102.78% for DCT Ti 15 alloy.
12. Increase in micro-hardness of 12.32%, 11.24% and 7.68% were observed, when a comparison was made between WCT and DCT TITAN 15, TITAN 21 and TITAN 31 respectively.
13. Current was noticed as the key factor that highly affected the micro-hardness followed by T_{on} and cryogenic treatment of electrode material.

14. DCT Cu-W was found the best electrode material for higher micro-hardness for all the three grades of titanium alloys.
15. Deposition of suspended powder particles and decomposed carbon elements were observed on the machined specimens resulting in the formation of various compounds, especially TiC that significantly increased the surface hardness.
16. Grey Relational Analysis (GRA) with Taguchi's OA was applied to optimize the PMEDM process with multiple characteristics. In this approach multiple response variables were converted into a single grey relational grade and highest grade represents the optimum setting of process parameters, which gives better result. Further, it was concluded that performance characteristics in terms of MRR, TWR, SR and MH can be improved by using the optimum level of input process parameters.

The conclusions indicating the deliverables of the research are summarized as under:

Main Experimentation (Phase-A)

(I)Material Removal Rate

This study was undertaken to study the machining of titanium alloys with EDM and establish a mathematical model considering the significant machine parameters and the thermal–physical properties of work materials on MRR. The peak current was the most dominant factor affecting MRR. Addition of Mn and W powder in dielectric had little effect on MRR. A marginal increase in MRR was noted after DCT, which may be due to increase in thermal and electrical conductivities.

A mathematical model was developed for predicting MRR using dimensional analysis in terms of electrical parameters (peak current) and thermal–physical properties of titanium alloys. A third-degree polynomial equation was found to be the best-fit curve after experimental validation with a high coefficient of correlation. The model showed that the thermal properties of the material such as thermal conductivity, specific heat and boiling point of materials affect the erosion process in EDM. The developed mathematical model shows good agreement when compared to the observed experimental results.

The SEM micrographs show clearly that surface defects such as micro-pores, micro-cracks, holes and spherical globules debris increased with increase in current. Migration of the different elements was noted on the machined surface as confirmed by EDX analysis. Carbon

was transferred from the dielectric after its decomposition. Furthermore, formation of different chemical compounds such as titanium carbide was observed during XRD analysis.

(II) Tool Wear Rate

The results of an experimental study were used to develop a micro-mathematical model for predicting TWR by considering the significant parameters and the thermo-physical properties of tool materials. Buckingham's π-theorem was used to develop this model in terms of peak current, pulse-on-time, dielectric fluid and thermal-physical properties of the tool material. A third- degree polynomial equation was developed which shows good agreement with the results obtained during the experimental trials. The thermal conductivity of tool material (k) was observed as an important property from the mathematical model. Peak current was observed as the most significant factor affecting TWR followed by the tool material and pulse-on-time. Effect of Mn powder in dielectric was noticed to be marginally higher than W powder. Insignificant affect of cryogenic treatment of workpiece and tool-electrode was observed on the TWR. The SEM micrographs of the tool surfaces showed micro-pores, micro-cracks, holes, spherical globules debris, melted drops, pockmarks, etc. which increased with increase in current. Migration of different elements from workpiece and powder added dielectric was observed on the tool surface as confirmed in the EDS analysis. Two major elements titanium from workpiece and carbon from dielectric after its breakdown were transferred to the tool surface, resulting in the formation of different chemical compounds as confirmed in the XRD analysis.

(III) Surface Roughness

The objective function was to study the surface characteristics of three types of cryogenically treated titanium alloys. A total of eight factors were considered for studying their impact on surface roughness. A combination of optimum input parameters for minimizing surface roughness were identified using Taguchi approach. ANOVA analysis has been conducted to know the impact of each parameter on SR. Peak current was the most significant factor followed by pulse-on- time and pulse-off -time and workpiece material. The contribution of dielectric fluid (Mn and W powder), electrode material and their cryogenic treatment was observed as less significant. The effect of cryogenic treatment of workpiece material was found to be negligible. The structural design of neural network was selected, trained, validated, tested and then used for simulation to optimize the surface roughness. Experimental results and ANN predicted results showed good agreement. The maximum

percentage relative error of 2.346% and a minimum of 0.006% were obtained. Surface topography analysis was carried out using SEM, EDS and XRD on two grades of titanium material. The SEM pictures show that high discharge energy was responsible for the surface defects such as; surface or thermal cracks, craters, thick recast layer, micro pores, pin holes, residual stresses and debris. Migration of different chemical elements from electrode and dielectric media were observed in EDS spectrum. Presence of large % of carbon was noticed in EDS analysis. XRD results shows major formation of TiC compound which precipitated on the machined surface. The study provides an insight into the migration of different elements from the tool and the powder mixed dielectric fluid on to the machined surface thereby improving the surface properties.

(IV) Micro-hardness

This study has added more insight in the surface modification of different grades of titanium alloy through material transfer mechanism by EDM which is still in the state of research. Surface modification of machined parts was measured in terms of micro-hardness. From the experimental results, it has been found that significant amount of different materials transfer on the machined surface from the powder added dielectric liquid as well as from the electrode material under different machining conditions which modify the chemistry of the machined surface and increased hardness of machined surface. In this study, the percentage of carbon is significantly increased which resulted in the formation of various carbide compounds, resulted in an improvement in micro-hardness. In addition to carbon, migration of other elements such as oxygen, copper, manganese, tungsten, chromium were also observed in the EDX spectrum, which further resulted in the formation of different types of chemical compounds on the machined surface. The experimental results showed that micro-hardness, increased up to 94.85%. The SEM images show the various surface defects such as micro-cracks, micro-pores, tiny holes, craters of different size, globules of debris, recast layer on the machined specimens. At lower current and pulse-on-time better surface characteristics may be obtained as compared with higher current and pulse-on-time, due to low discharge energy for less pulse duration. The maximum micro-hardness 635.67HVN was observed at the optimum setting of parameters. The artificial neural network was selected and then used for simulation to optimize the micro-hardness. Experimental results and ANN predicted results showed good agreement.

Experimentation (Phase-B)

The effect of CT on the machining performance of Ti-5Al-2.5Sn titanium alloy during EDM was investigated for SCT and DCT workpieces. The DCT of Ti-5Al-2.5Sn alloy significantly improves the MRR, TWR, SR, and micro-hardness during EDM in comparison to SCT of the same material which in turn shows improvements when compared to untreated material of the same alloy. The maximum improvement of up to 21.84% for MRR, 27.40% for TWR, 19.58% for SR, and 17.30% for micro-hardness was observed in DCT alloy when compared to the non-treated alloy of the same material. For SCT material, the percentage improvement in machinability, though better than in untreated material, was lower than in the DCT material. In some cases, especially with SCT the machinability did not increase or increased only marginally. Other than the cryogenic effect, peak current along with pulse-on-time also affected the machinability of titanium alloy. For higher current and pulse duration setting, the MRR and micro-hardness improved but also exhibited higher TWR and poor surface finish. Carbon was the major element that was transferred on to the machined surface from the dielectric upon its decomposition.

Experimentation (Phase-C)

The effect of deep cryogenic treatment of three grades of titanium alloy (Ti, Ti-5Al-2.5Sn and Ti-6Al-4V) on machining performance during EDM has been investigated by comparing the experimental results with un-treated titanium alloys. Both type of titanium alloy *i.e.* DCT and un-treated were machined with WCT, SCT and DCT electrodes. The DCT of three grades of titanium alloy (Ti 15, Ti 21 and Ti 31) significantly improves the machinability in comparison to un-treated (WCT) in terms of increasing the MRR and micro-hardness and reducing the TWR and SR. Other than the cryogenic effect of titanium alloys, cryogenic treatment of electrode material was also greatly improved the EDM performance. Electrode material had less influence on machining performance as compared to its cryogenic treatment. Peak current largely affected the machining performance as compared to pulse-on-time.

.

8.2 SCOPE FOR FUTURE WORK

The results presented in this study can be used for effective and economical machining of titanium alloys. A few research directions related to electric discharge machining have been drawn here:

1. In the present investigation, three grades (ASTM Grade 2, 5, & 6) of titanium alloys were considered as work materials. The investigation can be extended to other grades of titanium alloys also. Study can be extended to die and tool steel materials such as molybdenum high speed tool steels, water hardening die steels, tungsten hot work die steels etc. for investigating the machining characteristics. Ceramic materials, advanced materials like MMC's, shape memory alloys, nickel alloys, Inconel alloys would be considered for further investigations.
2. The present study focused on to study the machining characteristics in terms of MRR, TWR, SR and micro-hardness. The other response characteristic, *i.e* residual stress can be investigated by using the EDM process.
3. In this study FERROLAC 3M EDM oil was used as a dielectric medium. The effect of other dielectric fluids on machinability such as transformer oil, paraffin oil, lubricating oil, tap water, some organic liquids, and a mixture of any two hydrocarbon oils can be investigated.
4. In the present study,the concentration of powders (Mn & W) was kept constant during the entire experimental work. Concentration of powder may be varied for further study to investigate its effect on output parameters. Other powders such as titanium, cobalt, boron, chromium, molybdenum, vanadium, etc. can also be used for further study in the future.
5. Under this study, an effort was made to investigate the effect of SCT (-110^0C) and DCT (-184^0C) on the machinability of titanium alloys. However, an insignificant effect of these treatments was observed on machining performances. If an attempt is made in future to use liquid nitrogen directly by a nozzle, the desired results may be obtained.
6. To increase the machining efficiency, multiple electrodes may be used simultaneously for drilling purpose, which would be beneficial from an industry point of view.
7. In the present experimental work, a well known Taguchi's OA was used for optimized the input parameters. However, interaction effect between two parameters was not considered here. Interaction effects may be considered in a future work.
8. The other input process parameters such as voltage, electrode area, flushing pressure, flushing method, electrode polarity, duty cycle, etc. may be considered to study their effect on machining characteristics, in future.

REFERENCES

1. Jain V.K. (2012) Advanced machining processes, 16th edition, *Allied Publishers Pvt. Limited*., New Delhi, ISBN 81-7764-294-4.
2. Pandey P.C. and Shan H.S. (2005) Modern machining processes, 27th edition ,*Tata McGraw-Hill Publishing Company Limited*., New Delhi, , ISBN 0-07-096553-6.
3. Mishra P.K. (2005) Non Conventional Machining, *Narosa Publishing House*New Delhi. ISBN 81-7319-192-1.
4. Weller E.J. (1984) Non-Traditional machining processes, *Society of Manufacturing Engineers*, 15-71.
5. Joshi V. A. (2006) Titanium alloys**:** an Atlas of Structures and Fracture Features, Taylor & Francis Group, USA, ISBN 0-8493-5010-7 (9780849350108).
6. Leyens C. and Peters M. (2003) Titanium and titanium alloys; fundamentals and applications, Willey –VCH Verlag Gmbh& Co. KgaA, Weinheim ISBN: 3-527-30534-3.
7. Sha W. and Malinov S. (2009) Titanium alloys: modeling of microstructure, properties and applications, Woodhead publishing limited, Abington Hall, Granta Park, Great Abington, Cambridge CB21 6AH, UK, ISBN 978-1-84569-375-6.
8. Ezugwu E.O. and Wang Z.M. (1997) Titanium alloys and their machinability – a review, *Journal of Materials Processing Technology*, 68 (1-4):262-274.
9. Dornfeld D.A., Kim J.S., Dechow H., Hewson J. and Chen L.J. (1999) Drilling burr formation in titanium alloy Ti-6Al-4V, *Annals of CIRP*, 48:73-76.
10. Hong H., Riga A. T., Cahoon J. M. and Scott C. G. (1993) Machinability of steels and titanium alloys under lubrication, *Wear* 162-164:34-39.
11. Rahman M., Wong Y.S. and Zareena A.R. (2003) Machinability of titanium alloys, *JSME Int. J. Series C46* :107–115.
12. Veiga C., Davim J.P. and Loureiro A.J.R. (2013) Review on machinability of titanium alloys: The process perspective, Review Advanced Material Science, 34:148-164.

13. Yang X. and Liu C.R. (1999) Machining titanium and its alloys, *Machining Science And Technology*, 3(1):107-139.
14. Siekmann H. J. (1995) How to machine titanium, *Tool Engineer*, 34:78-82.
15. Sreejith P.S. and Nagoi B.K.A. (2000) Dry machining: machining of future, *Journal of Materials Processing Technology*, 101:287-291.
16. Gill S.S., Singh H., Singh R. and Singh J. (2010) Cryoprocessing of cutting tool materials—a review, *International Journal of Advanced Manufacturing Technology*, 48:175-192.
17. Gill S.S. and Singh J. (2010) Effect of deep cryogenic treatment on machinability of titanium alloy (Ti-6246) in electric discharge drilling, *Materials and Manufacturing Processes*, 25:378–385.
18. Jafferson J. M. and Hariharan P. (2013) Machining performance of cryogenically treated electrodes in microelectric discharge machining: A comparative study, *Materials and Manufacturing Processes*, 28:397–402.
19. Hascalik A. and Caydas U. (2007) Electric discharge machining of titanium alloy (Ti-6Al-4V)', *Applied Surface Science*, 253:9007-9016.
20. Webzell S. (2001) That first step into EDM, in: Machinery, 159, (4040) *Findlay Publications Ltd*, Kent, UK, November, 41.
21. Kumar A., Maheshwari S., Sharma C. and Beri N. (2010) Research developments in additives mixed electrical discharge machining (AEDM): A State of Art Review, *Materials and Manufacturing Processes*, 25:1166–1180.
22. Ho K. H. and Newman S. T. (2003) State of the art electrical discharge machining, *International Journal of Machine Tools & Manufacture*, 43:1287-1300.
23. Abbas N. M., Solomon D. G. and Bahari M. F. (2007) A review on current research trends in electrical discharge machining (EDM), *International journal of Machine Tools & Manufacture*, 47:1214-1228.
24. Electric discharge machining, *SME book*, (2001).
25. Houman L. (1983) Total EDM, in: E.C. Jameson (Ed.), Electrical discharge machining: tooling, methods and applications, Society of Manufacturing Engineers, Dearbern, Michigan, 5–19.
26. Lin J.L. and Lin C.L. (2002) The use of the orthogonal array with grey relational analysis to optimize the electrical discharge machining process with

multiple performance characteristics, *International Journal of Machine Tools & Manufacture,* 42:237–244.

27. Schumacher B.M. (2004) After 60 years of EDM the discharge process remains still disputed, *Journal of Material Process technology,* 149:376-381.
28. Kuneida M., Lauwers B., Rajurkar K.P. and Schumacher B.M. (2005) Advancing EDM through fundamental insight into the process, *Annals of CIRP,* 54(2):599–622.
29. Chen Y-F., Chow H-M., Lin Y-C. and Lin C.T. (2008) Surface modification using semi-sintered electrodes on electric discharge machining, *International Journal of Advanced Manufacturing Technology*, 36:490–500.
30. Kansal H.K., Singh S. and Kumar P. (2005) Application of Taguchi method for optimization of powder mixed electric discharge machining, *International Journal of Management and Manufacturing Technology,* 7(2/3/4):329–341.
31. Kansal H.K., Singh S. and Kumar P. (2007) Technology and research developments in powder mixed electric discharge machining (PMEDM), *Journal of Materials Processing Technology,* 184:32-41.
32. Kumar S., Singh R., Singh T.P. and Sethi B.L. (2009) Surface modification by electrical discharge machining: a review, *Journal of Materials Processing Technology*, 209:3675–3687.
33. Kumar S., Batish A., Singh R. and Singh T.P. (2010) Research Developments in Powder Mixed Dielectric Electric Discharge Machining (PMEDM): A review, *2nd International Conference on Production and Industrial Engineering CPIE- 2010*:702-713.
34. Furutani K., Saneto A., Takezawa H., Mohri N. and Miyake H. (2001) Accretion of titanium carbide by electrical discharge machining with powder suspended in working fluid, *Precision Engineering*, 25:138–144.
35. Schumacher B.M. (1990) About the role of debris in the gap during electrical discharge machining. *Ann. CIRP, 39* (1):197–199.
36. Kalia S. (2010) Cryogenic Processing: A Study of Materials at Low Temperatures, *Journal of Low Temperature Physics*, 158:934-945.
37. Carlson E.A. (1991) Cold treating and cryogenic treatment of steel in ASM handbook; Vol. 4, Heat Treating, ASM International , 10 Ed., Metal Park, OH, 203-206.

38. Soni J.S. and Chakraverti G. (1994) Machining characteristics of Titanium with rotary electro-discharge machining, *Wear*, 171:51-58.
39. Soni J.S. (1994) Microanalysis of debris formed during rotary EDM of titanium alloy (Ti-6Al-4V) and die steel (T215 Cr12), *Wear*, 177:71-79.
40. Lin Y.C., Yan B.H. and Chang Y.S. (2000) Machining characteristics of titanium alloy (Ti-6Al-4V) using a combination process of EDM with USM, *Journal of Material Processing Technology*, 104:171–177.
41. Wansheng Z., Zhenlong W., Shichun D., Guanxin C. and Hongyu W. (2002) Ultrasonic and electric discharge machining to deep and small hole on titanium alloy, *Journal of Materials Processing Technology*, 120:101–106.
42. Hascalik A. and Caydas U. (2007) A comparative study of surface integrity of Ti-6Al-4V alloy machined by EDM and AECG, *Journal of Materials Processing Technology*, 190:173–180.
43. Ho S.K., Aspinwall D.K. and Voice W. (2007) Use of powder metallurgy (PM) compacted electrodes for electrical discharge surface alloying/modification of Ti–6Al–4V alloy, *Journal of Materials Processing Technology*, 191:123–126.
44. Fonda P., Wang Z., Yamazaki K. and Akutsu Y. (2008) A fundamental study on Ti–6Al–4V's thermal and electrical properties and their relation to EDM productivity, *Journal of Materials Processing Technology*,202:583–589.
45. Caydas U. and Hascalik A. (2008) Modeling and analysis of electrode wear and white layer thickness in die-sinking EDM process through response surface methodology, *International Journal of Advanced Manufacturing Technology*, 38:1148–1156.
46. Pradhan B. B. and Bhattacharyya B. (2008) Improvement in micro hole machining accuracy by polarity changing technique for micro electrode discharge machining on Ti-6Al-4V, *Proceedings of the Institution of Mechanical Engineers, Part:B , Journal of Engineering Manufacture*, 222 (2):163-173.
47. Pradhan B. B., Masanta M., Sarkar B. R. and Bhattacharyya B. (2009) Investigation of electro-discharge micro-machining of titanium super alloy, *International Journal of Advanced Manufacturing Technology*, 41(11-12):1094-1106.

48. Kao J. Y., Tsao C. C., Wang S. S. and Hsu C. Y. (2010) Optimization of the EDM parameters on machining Ti–6Al–4V with multiple quality characteristics, *International Journal of Advanced Manufacturing Technology*, 47:395-402 .

49. Rahman M.M., Khan M.A.R., Kadirgama K., Noor M.M. and Bakar R.A. (2010) Modeling of Material Removal on Machining of Ti-6Al-4V through EDM using Copper Tungsten Electrode and Positive Polarity, *International Journal of Mechanical and Materials Engineering,* 1(3):135-140.

50. Bao-cheng X., Yu-kui1 W., Zhen-long W. and Wang-sheng Z. (2011) Numerical simulation of titanium alloy machining in electric discharge machining process, *Transactions of Nonferrous Metals Society of China*, 21(2):434-439.

51. Harcuba P., Bacakova L., Strasky J., Bacakova M., Novotna K. and Janecek M. (2012) Surface treatment by electric discharge machining of Ti–6Al–4V alloy for potential application in orthopaedics, *Journal of the Mechanical Behavior of Biomedical Materials,* 7:96-105.

52. Rahman M.M. (2012) Modeling of machining parameters of Ti-6Al-4V for electric discharge machining: A neural network approach, *Scientific Research and Essays*, 7 (8):881-890.

53. Jabbaripour B., Sadeghi M.H., Faridvand S., and Shabgard M.R. (2012) Investigating the effects of EDM parameters on surface integrity, MRR and TWR in machining of Ti–6Al–4V, *Machining Science and Technology*,16:419-444.

54. Meena V.K. and Azad M.S. (2012) Grey relational analysis of micro-EDM machining of Ti-6Al-4V alloy, *Materials and Manufacturing Processes*, 27:973–977.

55. Tang L. and Du Y. T. (2014) Experimental study on green electrical discharge machining in tap water of Ti–6Al–4V and parameters optimization, *International Journal of Advanced Manufacturing Technology*, 70:469-475.

56. Porwal R.K., Yadava V. and Ramkumar J. (2014) Modeling and multi-response optimization of hole sinking electrical discharge micromachining of titanium alloy thin sheet, *Journal of Mechanical Science and Technology*, 28(2):653-661.

57. Shen Y., Liu Y., Zhang Y., Tan B., Ji R., Cai B. and Zhang C. (2014) Determining the energy distribution during electric discharge machining of Ti–6Al–4V, *International Journal of Advanced Manufacturing Technology*, 70(1-4):11-17.

58. Khan M.A.R., Rahman M.M. and Kadirgama K. (2015) An experimental investigation on surface finish in die-sinking EDM of Ti-5Al-2.5Sn, *The International Journal of Advanced Manufacturing Technology*, 77:1727–1740.

59. Chow H.M., Yan B.H., Huang F.Y. and Hung J.C. (2000) Study of added powder in kerosene for the micro-slit machining of Titanium alloy using electro-discharge machining, *Journal of material Processing Technology*,101:95-103.

60. Yan B. H., Tsai H. C. and Huang F. Y. (2005) The effect in EDM of a dielectric of a urea solution in water on modifying the surface of titanium, *International Journal of Machine Tools & Manufacture* ,45:194–200.

61. Chow H.M., Yang L.D., Lin C.T., Chen Y.F. (2008) The use of SiC powder in water as dielectric for micro-slit EDM machining, *Journal of Materials Processing Technology*, 195:160–170.

62. Kibria G., Sarkar B. R., Pradhan B. B. and Bhattacharyya B. (2010) Comparative study of different dielectrics for micro-EDM performance during micro hole machining of Ti-6Al-4V alloy, *International Journal of Advanced Manufacturing Technology*, 48:557-570.

63. Pandey P. C. and Jilani S. T. (1987) Electrical machining characteristics of cemented carbides, *Wear*, 116:77-88.

64. Mohri N., Saito N. and Tsunekawa Y. (1993) Metal Surface modification by electrical discharge machining with composite electrodes, *Annals of the CIRP*, 42 (1):219-222.

65. Tsai K.M. and Wang P.J. (2001) Semi-empirical model of surface finish on electrical discharge machining, *International Journal of Machine Tools & Manufacture*, 41:1455–1477.

66. Lee J.W. (2003) Microstructural evaluation and phase transformation of recast layers in electrical discharge machined dual phase Fe-Mn-Al alloy, *Journal of Materials Science*, 38:1679-1687.

67. Singh S., Maheshwari S. and Pandey P.C. (2004) Some investigations into the

electric discharge machining of hardened tool steel using different electrode materials, *Journal of Materials Processing Technology* ,149:272–277.

68. Ramasawamy H., Blunt L. and Rajurkar K.P. (2005) Investigation of the relationship between the white layer thickness and 3D surface texture parameters in the die sinking EDM process, *Precision Engineering*, 29:479–490.
69. Lin Y.C., Cheng C.H., Su B.L., and Hwang L.R. (2006) Machining Characteristics and Optimization of Machining Parameters of SKH 57 High-Speed Steel Using Electrical-Discharge Machining Based on Taguchi Method, *Materials and Manufacturing Processes*, 21:922–929.
70. Marafona J. (2007) Black layer 234odeling234ion234234on and electrode wear ratio in electrical discharge machining (EDM), *Journal of Materials Processing Technology*, 184:27-31.
71. Marafona J.D. (2009) Black layer affects the thermal conductivity of the surface of copper–tungsten electrode, *International Journal of Advanced Manufacturing Technology*, 42:482-488.
72. Chiang K.T. and Tsai D.C. (2008) Effect of silicon particles on the rapidly resolidified layer of Al-Si alloys in the electro discharge machining process, *International Journal of Advanced Manufacturing Technology*, 36:707–714.
73. Dvivedi A., Kumar P. and Singh I. (2008) Experimental investigation and 234odeling234ion in EDM of Al 6063 SiCp metal matrix composite, *International Journal of Machining and Machinability of Materials*, 3(3):293-308.
74. Dvivedi A., Kumar P. and Singh I. (2010) Effect of EDM process parameters on surface quality of Al 6063 SiCp metal matrix composite, International Journal of Materials and Product Technology, 39 (3-4-3):357-377.
75. Rao G.K.M., Rangajanardhaa G., Rao D.H. and Rao M.S. (2009) Development of hybrid model and optimization of surface roughness in electric discharge machining using artificial neural networks and genetic algorithm, *journal of materials processing technology*, 209:1512-1520.
76. Garg R.K., Singh K. K., Sachdeva A., Sharma V. S., Ojha K. and Singh S. (2010) Review of research work in sinking EDM and WEDM on metal matrix composite materials, *International Journal of Advanced Manufacturing*

Technology, 50:611–624.

77. Patel K.M., Pandey P.M. and Rao P.V. (2010) Optimisation of process parameters for multi-performance characteristics in EDM of Al2O3 ceramic composite, *International Journal of Advanced Manufacturing Technology,*47 (9-12):1137-1147.
78. Rahman M.M., Khan M.A.R., Kadirgama K., Noor M.M. and Bakar R.A. (2011) Experimental investigation into electric discharge machining of stainless steel 304, *Journal of Applied Sciences*, 11(3):549-554.
79. Patel K.M., Pandey P.M. and Rao P.V. (2011) Study on 235odeling235ion235 of Al2O3 ceramic composite in EDM using response surface methodology, *ASME Transactions: Journal Engineering Materials and Technology,*133 (2):272-281.
80. Zhang Y., Liu Y., Ji R., Cai B. and Shen Y. (2013) Sinking EDM in water-in-Oil emulsion, *International Journal of Advanced Manufacturing Technology*,65:705-716.
81. Singh A., Kumar P. and Singh I. (2013) Electric discharge drilling of metal matrix composites with different tool geometries, *Proceedings of the Institution of Mechanical Engineers Part B: Journal of Engineering Manufacturer*, 227 (8):1245-1249.
82. Mohanty A., Talla G. and Gangopadhyay S. (2014) Experimental investigation and analysis of EDM characteristics of Inconel 825, *Materials and Manufacturing Processes*, 29 (5):540-549.
83. Jeswani M.L. (1981) Effects of the addition of graphite powder to kerosene used as the dielectric fluid in electrical discharge machining, *Wear*, 70:133–139.
84. Mohri N., Saito N. and Higashi M. (1991) A new process of finish machining on free surface by EDM methods, Ann *CIRP*, 40(1):207–210.
85. Mohri N., Saito N. and Suzuki M. (1988) Surface modification by EDM, *In: ASME (ed) Proc Winter Annual Meeting of the ASME- Research and Technological Development in Nontraditional Machining, Chicago,* 34:21-30.
86. Narumiya H., Mohri N., Saito N., Ootake H., Tsunekawa Y ., Takawashi T .and Kobayashi K. (1989) EDM by powder suspended working fluid, *In: EDM Technology Transfer (ed) Proc 9th International Symposium for Electro*

*machining – ISEM IX, Nagoya,*5-8.

87. Ming Q.Y. and He L.Y. (1995) Powder-suspension dielectric fluid for EDM, *Journal of Materials Processing Technology*, 52:44-33.
88. Furutani K., Saneto A., Takezawa H., Mohri N. and Miyake H. (2001) Accretion of titanium carbide by electrical discharge machining with powder suspended in working fluid, *Precision Engineering*, 25:138–144.
89. Uno Y., Okada A. and Cetin S. (2001) Surface Modification of EDMed Surface with Powder Mixed Fluid, 2nd *International Conference on Design and production of Dies and Molds*.
90. Pecas P. and Henriques E. (2003) Influence of silicon powder-mixed dielectric on conventional electrical discharge machining, *International Journal of Machine Tools & Manufacture,* 43:1465–1471.
91. Wu K. L., Yan B. H., Huang F. Y. and Chen S. C. (2005) Improvement of surface finish on SKD steel using electro-discharge machining with aluminum and surfactant added dielectric, *International Journal of Machine Tools & Manufacture,* 45:1195–1201.
92. Kansal H.K., Singh S. and Kumar P. (2006) Performance parameters optimization (multi-characteristics) of powder mixed electric discharge machining (PMEDM) through Taguchi's method and utility concept, *Indian Journal of Engineering & Materials Sciences,* 13:209-216.
93. Kansal H.K., Singh S. and Kumar P. (2005) Parametric optimization of powder mixed electrical discharge machining by response surface methodology, *Journal of Materials Processing Technology,* 169 (3):427–436.
94. Pecas P. and Henriques E. (2008,a) Effect of the powder concentration and dielectric flow in the surface morphology in electrical discharge machining with powder-mixed dielectric (PMD-EDM), *International Journal of Advanced Manufacturing Technology*, 37:1120–1132.
95. Pecas P. and Henriques E. (2008,b) Electrical discharge machining using simple and powder-mixed dielectric: The effect of the electrode area in the surface roughness and topography, *Journal of Materials Processing Technology*, 200:250–258.
96. Furutani K., Sato H. and Suzuki M. (2009) Influence of electrical conditions on performance of electrical discharge machining with powder suspended in

working Oil for titanium carbide deposition process, *International Journal of Advanced Manufacturing Technology*, 40:1093-1101.

97. Kumar S. and Singh R. (2010) Investigating surface properties of OHNS die steel after electrical discharge machining with manganese powder mixed in the dielectric, *International Journal of Advanced Manufacturing Technology*, 50:625–633.

98. Kumar A., Maheshwari S., Sharma C. and Beri N. (2010) A study of multiobjective parametric optimization of silicon abrasive mixed electrical discharge machining of tool steel, *Materials and Manufacturing Processes*, 25:1041–1047.

99. Kumar H. and Davim J. P. (2011) Role of Powder in the Machining of Al-10%Sic_p Metal Matrix Composites by Powder Mixed Electric Discharge Machining, *Journal of Composite Materials January* , 45(2):133-151.

100. Ojha K., Garg R.K. and Singh K. K. (2011) Experimental investigation and modeling of PMEDM process with chromium powder suspended dielectric, *International Journal of Applied Science and Engineering*, 9(2):65-81.

101. Batish A., Bhattacharya A., Singla V. K. and Singh G. (2012) Study of material transfer mechanism in die steels using powder mixed electric discharge machining, *Materials and Manufacturing Processes*, 27:449-456.

102. Bhattacharya A., Batish A., Singh G., and Singla V. K. (2012) Optimal parameter settings for rough and finish machining of die steels in powder-mixed EDM, *International Journal of Advanced Manufacturing Technology*, 61:537-548.

103. Zhisheng W., Ping S., Jinrui L. and Shengsum H. (2003) Effect of deep cryogenic treatment on electrode life and microstructure for spot welding hot dip galvanized steel, *Materials and Design*, 24:687-692.

104. Yildiz Y. and Nalbant M. (2008) A review of cryogenic cooling in machining processes, *International Journal of Machine Tools & Manufacture*,48:947–964.

105. Abdulkareem S., Khan A. A. and Konneh M. (2009) Reducing electrode wear ratio using cryogenic cooling during electrical discharge machining, *International Journal of Advanced Manufacturing Technology*, 45:1146-1151.

106. Yildiz Y., Sundaram M.M., Rajurkar K.P. and Nalbant M. (2011) The effects

of cold and cryogenic treatments on the machinability of beryllium-copper alloy in electro discharge machining, 44th CIRP Conference.

107. Srivastava V. and Pandey P. M. (2011) Performance evaluation of EDM process using cryogenically cooled electrode, *Materials and Manufacturing Processes*, 27 (6):683-688.
108. Singh R. and Singh B. (2011) Comparison of cryo treatment effect on machining characteristics of titanium in electric discharge machining, *International Journal of Automotive and Mechanical Engineering,* 3:239-248.
109. Srivastava V. and Pandey P. M. (2012) Effect of process parameters on the performances of EDM process with ultrasonic assisted cryogenically cooled electrode, *Journal of Manufacturing Processes,* 14 (3):393-402.
110. Kumar A., Maheshwari S. and Sharma C. (2012) Effect of cryogenically treated electrode during Aedm of nickel based super alloy 718 for surface quality improvement, *Advanced Materials Research,* 410:236-239.
111. Anawa E.M., Olabi A.G. and Hashmi M.S.J. (2008) Application of Taguchi method to 238odeling dissimilarlaser welded components, *International Journal of Manufacturing Technology and Management,* 15(2):219-227.
112. Wang K., Gelgele H. L., Wang Y., Yuan Q. and Fang M. (2003) A hybrid intelligent method for 238odeling the EDM process, *The International Journal of Machine Tools & Manufacture*, 43:995-999.
113. Bharti P. S., Maheshwari S. and Sharma C. (2012) Multi-objective optimization of electric-discharge machining process using controlled elitist NSGA-II, *Journal of Mechanical Science and Technology,* 26 (6):1875-1883.
114. Kao J.Y. and Tarng Y.S. (1997) A neutral-network approach for the online monitoring of the electrical discharge machining process, *Journal of Material Processing Technology,* 69(1-3):112-119.
115. Tzeng Y., and Chen F. (2007) Multi-objective 238odeling238ion of high-speed electrical discharge machining process using a Taguchi fuzzy-based approach, *Material Design,* 28:1159-1168.
116. Assarzadeh S. and Ghoreishi M. (2008) Neural-network-based modeling and optimization of the electro-discharge machining process, *The International Journal of Advanced Manufacturing Technology*, 39:488-500.
117. Markopoulos A.P., Manolakos D.E. and Vaxevanidis N.M. (2008) Artificial

neural network models for the prediction of surface roughness in electrical discharge machining, *Journal of Intelligent Manufacturing*, 19:283-292.

118. Tzeng C.J. and Chen R.Y. (2013) Optimization of Electric Discharge Machining Process Using the Response Surface Methodology and Genetic Algorithm Approach, *International Journal of Precession Engineering and Manufacturing*, 14 (5):709-717.
119. Sidhu S.S., Batish A. and Kumar S. (2013) Neural-Network-Based modeling to predict residual stresses during electric discharge machining of Al/SiC-MMCs. *Proceedings of the Institution of Mechanical Engineers, Part:B , Journal of Engineering Manufacture*, 227(11):1679-1692.
120. Muthukrishnan N. and Davim J.P. (2009) Optimization of machining parameters of Al/SiC-MMC with ANOVA and ANN analysis, *Journal of Material Processing Technology*, 209:225-232.
121. Olabi A.G., Casalino G., Benyounis K.Y. and Hashmi M.S.J. (2006) An ANN and Taguchi algorithms integrated approach to the optimization of CO_2 laser welding, *Advances in Engineering Software*, 37 (10) (2006) 643-648.
122. Sidhu S.S., Batish A. and Kumar S. (2013) EDM of metal matrix composite for parameter design using lexicographic goal programming, *Materials and Manufacturing Processes*, 28:495-500.
123. Jeswani M.L. (1979) Dimensional analysis of tool wear in electric discharge machining, *Wear*, 55:153-161.
124. Yahya A. and Manning C.D. (2004) Determination of material removal rate of an electro-discharge machining using dimensional analysis, *Phys D:Appl Phys*, 37:1467-1471.
125. Ganpatrao P. N. and Brahmankar P.K. (2010) Determination of material removal rate in wire electro-discharge machining of metal matrix composites using dimensional analysis, *International Journal of Machine Tools & Manufacture*, 51:599-610.
126. Singh R. and Khamba J.S. (2009) Mathematical modeling of tool wear rate in ultrasonic machining of titanium, *The International Journal of Advanced Manufacturing Technology*, 43 (5-6):573-580.
127. Singh R. and Khamba J.S. (2009) Mathematical modeling of surface roughness in ultrasonic machining of titanium using Buckingham-Π approach: a review,

International Journal of Abrasive Technology, 2(1):3-24.

128. Kumar J. and Khamba J.S. (2010) Modeling the material removal rate in ultrasonic machining of titanium using dimensional analysis, *The International Journal of Advanced Manufacturing Technology*, 48 (1-4):103-119.
129. Kiyak M., Aldemir B.E. and Alten E. (2015) Effects of discharge energy density on wear rate and surface roughness in EDM, *The International Journal of Advanced Manufacturing Technology*,79 (1-4):513-518.
130. Ross P.J. (1988) Taguchi technique for quality engineering, *McGraw Hill Book Company, New York*, ISBN 0-07-053866-2.
131. Phadke M.S. (1989) Quality Engineering using robust design, AT & T Bell Laboratories, PTR Printence-Hall Inc., U.S.A, ISBN 0-13-745167-9.
132. Gill S.S., Singh R., Singh H. and Singh J. (2008) Wear 240odeling of cryogenically treated tungsten carbide inserts under dry and wet turning conditions, *International Journal of Machine Tools and Manufacturing*, 49(3-4):256-260.
133. Ndaliman M.B., Hazza M. , Khan A.A. and Ali M.Y. (2012) Development of a new model for predicting EDM properties of Cu-TaC compact electrodes based on artificial neural network method, *Australian Journal of Basic and Applied Sciences*, 6 (13):192-199.
134. Patowari P.K., Saha P. and Mishra P.K., (2010) Artificial neural network model in surface modification by EDM using tungsten-copper powder metallurgy sintered electrodes, *The International Journal of Advanced Manufacturing Technology*,51:627-638.
135. Kumar S. (2009) Surface alloying of OHNS die steel by EDM process using Inconel electrode, *International Journal of Machining of Machinability of Materials*,6(3/4):176-193.
136. Roy R. K. (1990) A primer on the Taguchi method", Van Nostrand Reinhold, New York, USA, ISBN 0-442-23729-4.
137. Satty T. L. (2008) Relative measurement and its generalization in decision making: Why pair wise comparisons are central in mathematics for the measurement of intangible factors-The Analytic Hierarchy/ Network Process. *Review of the Royal Academy of Exact, Physical and Natural Sciences, Series A: Mathematics (RACASAM)*, 102(2): 251-318.

138. Satty T. L. (2008) Decision making for leaders: The Analytical Hierarchy process for Decision in a Complex World. *Pittsburg, Pennsulvania: RWS Publications*, ISBN 0-9620317-8-X.
139. Das S. and Chattopadhyay A.B. (2003) Application of the analytic hierarchy process for estimating the state of tool wear, *International Journal of Machine Tools and Manufacturing* 43:1-6.
140. Chakraborty S. and Dey S. (2006) Design of an analytical hierarchy process based expert system for non-traditional machining process selection, *The International Journal of Advanced Manufacturing Technology*, 31:490-500.
141. Satty T. L. (1994) How to make a decision: Analytical hierarchy process, Interfaces, 24 (6):19-43.
142. Deng J. (1982) Control problem of grey system, *System and Control Letters*, 1:288-294.
143. Deng J. (1989) Introduction to grey system, *Journal of Grey System*, 1:1-24.
144. Theisen W., Schuermann A. (2004) Electro discharge machining of nickel–titanium shape memory alloys, *Material Science Engineering A*, 348:200-204.
145. Tiley J., Searles T., Lee E., Kar S., Banerjee R., Russ J.C. and Fraser H.L. (2004) Quantification of Microstructural Features in Alpha/Beta Titanium Alloys, *Material Science Engineering*, A372:191-198.
146. Kumar A., Kumar V. and Kumar J. (2013) Investigation of microstructure and element migration for rough cut surface of pure titanium after WEDM, *international Journal of Microstructure and Materials Properties*,8(4/5):343-356.
147. S.L. Chen, B.H. Yan and F.Y. Huang, Influence of kerosene and distilled water as dielectrics on the electric discharge machining characteristics of Ti-6Al-4V, *Journal of Material Processing Technology* , 87 (1999) 107-111.
148. Yan B.H., Chang G. W., Chang J.H., and Hsu R.T. (2004) Improving Electrical Discharge Machined Surfaces Using Magnetic Abrasive Finishing, *Machining Science and Technology*, 8 (1):103-118.
149. Mehta B. (2002) Response surface methodology of die-sink electro-discharge machined surfaces, *Master of Science Degree Thesis*, Kate Gleason College of Engineering Rochester Institute of Technology, Rochester, New York.
150. Bhattacharyya B., Gangopadhyay S. and Sarkarc B.R. (2007) Modelling and

analysis of EDMED job surface integrity, *Journal of Materials Processing Technology*, 189:169-177.

151. Dijck F.S. V. and Dutre W.L. (1974) Heat conduction model for the calculation of the volume of molten metal in electrical discharges, *Journal of Physics D: Applied Physics*, 7:899-910.
152. Kumar S. (2014) Simultaneous improvement of micro-hardness and surface finish in die steels by powder-mixed EDM process, *ASME 2014 International Mechanical Engineering Congress and Exposition*, doi: 10.1115/IMECE2014-37890.
153. Palanisamy A., Rekha R., Sivasankaran S. and Narayanan C.S. (2014) Multi-objective optimization of EDM parameters using grey relational analysis for titanium alloy (Ti–6Al–4V), *Applied Mechanics and Materials*,592-594:540-544.
154. Jatti V.K.S. and Singh T.P. (2014) Effect of deep cryogenic treatment on machinability of NiTi shape memory alloys in electro discharge machining, *Applied Mechanics and Materials*, 592-594:197-201.
155. Kuriachen B. and Mathew J. (2015) Effect of powder mixed dielectric on material removal and surface modification in micro electric discharge machining of TI-6AL-4V, **DOI:** 10.1080/10426914.2015.1004705.
156. Singh B. , Kumar J. and Kumar S. (2015) Influences of process parameters on MRR improvement in simple and powder-mixed EDM of AA6061/10%SIC composite, *Materials and Manufacturing Processes*, 30 (3):303-312.
157. Lutjering G. and Williams J.C. Titanium, Iind edition, *Springer Berlin Heidelberg New York*, ISBN 978-3-540-71397-5
158. Garg Dixit, Luthra S. and Haleem A. (2014) Ranking of performance measures of GSCM towards sustainability: Using Analytical Hierarchy Process, *International Journal of Social Behaviour, Educational, Economic and Management Engineering*, 8(3):756-762.
159. Yarlagadda P.K.D.V., Christodoulou P. and Subramanian V.S. (1999) Feasibility studies on the production of electro-discharge machining electrodes with rapid prototyping and the electroforming process, *Journal of Materials Processing Technology*, 89-90:231-237.
160. Muller F. and Monaghan J. (2000) Non-conventional machining of particle

reinforced metal matrix composite, *International Journal of Machine Tools and Manufacturing* 40(9):1351-1366.

161. Dobrzanski L.A., Staszuk M. and Honysz R. (2012) Application of artificial neural networks in properties 243modeling of PVD and CVD coatings, *Archives of Materials Science and Engineering*, 58(2):152-157.
162. Kumar S., Batish A., Singh R. and Singh T.P. (2014) A hybrid Taguchi-artificial neural network approach to predict surface roughness during electric discharge machining of titanium alloys, *Journal of Mechanical Science and Technology*, 28(7):2831-2844.
163. Kumar S., Batish A., Singh R. and Singh T.P. (2015) A mathematical model to predict material removal rate during electric discharge machining of cryogenically treated titanium alloys, *Proceedings of Institutions of Mechanical Engineering, Part B: Journal of Engineering Manufacture*, 229(2):214-228.
164. Mahesh R.A., Jayaganthan R. and Prakash S. (2009) Microstructural characterization and hardness evaluation of HVOF sprayed Ni-5Al coating on Ni-and Fe-based superalloys, *Journal of Materials Processing Technology*, 209(7):3501-3510.
165. Upadhyay V., Jain P.K. and Mehta N.K. (2013) Prediction of surface roughness using cutting parameters and vibration signals in minimum quantity coolant assisted turning of Ti-6Al-4V alloy, *International Journal of Manufacturing Technology and Management*, 27(1/2/3):33-46.
166. Sangwan K.S., Saxena S. and Kant G. (2015) Optimization of machining parameters to minimize surface roughness using integrated ANN-GA approach, *Procedia CIRP*, 29:305-310.
167. Khanna N. and Sangwan K.S. (2013) Machinability analysis of heat treated Ti64, Ti54M and Ti10.2.3 titanium alloys, *International Journal of Precision Engineering and Manufacturing*, 14(5):719-724.
168. Franco P., Estrems M. and Faura F. (2004) Influence of radial and axial runouts on surface roughness in face milling with round insert cutting tools, *International Journal of Machine Tools and Manufacturer*,44(15):1555-1565.

Appendix-A

A 1 PROPERTIES OF TITANIUM ALLOYS

Table A 1: Important Properties of Titanium Alloys

Description	**TITAN 15 (Grade II)**	**TITAN 21 (Grade VI)**	**TITAN 31 (Grade V)**
Density (gm/cm^3)	4.54	4.48	4.42
Hardness (HVN)	270	305	315
Ultimate Tensile Strength (MPa)	344	861	950
Yield Tensile Strength (MPa)	275-410	827	880
Elongation (%)	20	15	10
Poisson' ratio	0.37	0.31	0.342
Fracture Toughness	66	96	75
Modulus of Elasticity (GPa)	105	110-125	113.8
Melting Point (^0C)	1668 ± 10^0C	1571 ± 15^0C	1649 ± 15^0C
Electrical Resistivity (ohm-cm)	5.2e-005	0.00016	0.000178
Specific Heat Capacity ($J/g-^0C$)	0.52	0.53	0.5263
Beta Transus (^0C)	913	1040-1090	999 ± 15^0C
Thermal Conductivity (W/m-k)	16.3	7.8	7.2
Coefficient of Thermal Expansion, Linear ($0\text{-}100^0C$) ($\mu m/m^0C$)	8.41	9.40	8.6

A 2 DIELECTRIC FLUID

FERROLAC 3M EDM Oil was used as dielectric fluid in this study. FERROLAC 3M is a unique product which has very narrow boiling range, low viscosity, and a high flash point making it a safe substitute for kerosene Oil. It is ideally suited for the electric discharge machining operation. It's very high breakdown voltage makes it ideally suited as a dielectric fluid. It has following performance benefits:

- Good Dielectric strength-Safe to use.

- Are non-corrosive and extend the life of the electrode.
- Safe to use as it has high flash points.
- Less topping up required.

The detailed specifications of FERROLAC 3M Oil are listed in Table A 2

Table A 2: Specifications of FERROLAC 3M EDM Oil

Properties	**Test Method**	**Typical Values**
Appearance	Visual	Bright & Clear
Color	ASTM D 1500	<0.5
Specific Gravity @ 29.5^{0}C	ASTM D 1298	0.8250
Kinematics Viscosity @ 40^{0}C	ASTM D 445	3.0cSt
Flash Point	ASTM D 93	100^{0}C
Pour Point	ASTM D 97	-12^{0}C
Break Down Voltage (BDV)	IS: 6792	70KV (rms)
Dielectric Constant	IS:6262	2.2
Copper Corrosion	ASTM D 130	<1

A 3 DETAILED TECHNICAL SPECIFICATION OF EDM MACHINE

Table A 3: Detailed Technical Specifications of OSCARMAX S 645 EDM Machine

1. Power Supply Unit	
Supply Volts	415 V, 3 Ø, 50 Hz
Power Input (Max.)	4.5 KVA
Open Gap Output Voltage	135 ± 5 % V
Machine Current (Max.)	60 A
2. Machine Tool	
Electrode Weight (Max.)	250 Kg.
Workpiece Weight (Max.)	2000 Kg
Servo Travel	400 mm
Reading Accuracy of the Dial Gauge	0.01 mm
2.1. Work Tank	
Length	1500 mm
Width	940 mm
Height	520 mm

2.2. Work Table (Mounting Surface)	
Length	1000 mm
Width	600 mm
2.3. Table Travel	
Longitudinal Travel (X-axis)	600 mm
Transverse Travel (Y-axis)	450 mm
3. Dielectric Unit	
Capacity	1200 Liters
Weight Without Dielectric Fluid	350 Kg.
Filter Elements Type	Paper
Filter Number	02
Filter Rating	Below 20 microns
Outside Dimension (L x W x H)	2200 x 1300 x 580
The standard accessories are: X, Y axis double nut ball screw, 14 inches CRT, Servotransverse on X, Y axis.	